Universitat Autònoma de Barcelona

Progresses in new carbon platforms: graphene and carbon dots. Application to electrochemical sensors and (bio)electronic tongues

Marta Bonet San Emeterio

Universitat Autònoma de Barcelona

Progresses in new carbon platforms: graphene and carbon dots.

Application to electrochemical sensors and (bio)electronic tongues

Marta Bonet San Emeterio

Doctoral Thesis

Doctoral Studies in Chemistry

Director: Prof. Manel del Valle Zafra

Departament de Química

Unitat de Química Analítca

Facultat de Ciències

Març 2022

No creas que estoy huyendo, si me ves retroceder, ¡espera!, que estoy cogiendo carrera.

Robe Iniesta

Memòria presentada per aspirar al Grau de Doctor per la Marta Bonet San Emeterio

MARTA BONET SAN EMETERIO - DNI 47982323E

Firmado digitalmente por MARTA BONET SAN EMETERIO - DNI 47982323E
Fecha: 2022.03.02 18:15:12 +01'00'

Marta Bonet San Emeterio

Vist i plau

MANEL DEL VALLE ZAFRA

Firmado digitalmente por MANEL DEL VALLE ZAFRA
Fecha: 2022.03.02 19:01:15 +01'00'

Dr. Manel del Valle Zafra

Catedràtic de la Universitat Autònoma de Barcelona

Professor de Química Analítica

Bellaterra, 04 de març del 2022

Funding Support

The present dissertation has been developed at the laboratories of the Group of Sensors and Biosensors of the Chemistry Department from Universitat Autònoma de Barcelona, thanks to:

- Ministerio de Ciencia e Innovación (MICINN) for the projects titled “Electronic tongue fingerprinting: aplicaciones en el campo alimentario y de Seguridad” (CTQ2013-41577), “Lenguas bioelectrónicas con transducción electroquímica. Explorando nuevas aplicaciones” (CTQ2016-80170), and “Lenguas electrónicas con sistemas de reconocimiento mejorados” (PID2019-107102RB-C21).
- Secretaria d'Universitats i Recerca del Departament d'Empresa i Coneixement de la Generalitat de Catalunya, and to Fons Social Europeu from the European Union for the predoctoral fellowship FI-2017.
- Universitat Autònoma de Barcelona for the predoctoral fellowship.
- Program Erasmus+ of the European Union for the mobility fellowship tilted Estudis per a la Mobilitat d’Estudiants de Doctorat (KA103).

Grup de Sensors i Biosensors

Gobierno de España

Generalitat de Catalunya

Unió Europea. Fons Social Europeu

Universitat Autònoma de Barcelona

Unió Europea. Erasmus+

Publications

The research caried out during this thesis has produced the following publications:

- Publications included in the thesis dissertation

1. **Artificial Neural Networks for the Resolution of Dopamine and Serotonin Complex Mixtures Using a Graphene-Modified Carbon Electrode.**

   M. Bonet-San-Emeterio, A. González-Calabuig, and M. del Valle

   Electroanalysis, 2019, 31(2), pp.390-397

2. **Graphene for the building of electroanalytical enzyme-based biosensors. Application to the inhibitory detection of emerging pollutants.**

   M. Bonet-San-Emeterio, N. F. Montiel, and M. del Valle

   Nanomaterials, 2021, 11(8), 2094

3. **Modification of electrodes with N-and S-doped carbon dots. Evaluation of the electrochemical response.**

   M. Bonet-San-Emeterio, M. Algarra, M. Petković, and M. del Valle

   Talanta, 2020, 212, 120806

4. **Bioelectronic tongue based on phenol oxidases modified graphene electrodes for the detection of Brettanomyces defect in wine.**

   M. Bonet-San-Emeterio, A. González-Calabuig, and M. del Valle

   (not published)

- Publications made during the thesis project but not included in the dissertation

1. **Voltammetric electronic tongues. Study case, detection of biogenic amines.**

   M. Bonet-San-Emeterio, X. Cetó, and M. del Valle

2. **Voltammetric Electronic Tongue Based on Carbon Paste Electrodes Modified with Biochar for Phenolic Compounds Stripping Detection.**

   C. Kalinke, P. R. de Oliveira, M. Bonet-San-Emeterio, A. González-Calabuig, M. del Valle, A. Salvio Mangrich, L. Humberto Marcolino Junior, M. F. Bergamini

   Electroanalysis, 2019, 31 (11), 2238-2245

3. **Simultaneous voltammetric determination of acetaminophen, ascorbic acid and uric acid by use of integrated array of screen-printed electrodes and chemometric tools.**

   D. Ortiz-Aguayo, M. Bonet-San-Emeterio, M. del Valle

   Sensors, 2019, 19 (15), 3286

Acknowledgements

Doncs ha arribat el moment en que l'aventura a la UAB ha acabat. Després de 10 anys en el campus de la universitat, d'excel·lència que no se'ns oblidi, he de tancar les portes i començar una nova etapa. Però no sense abans agrair a totes aquelles persones que han fet possible que pogués arribar a ser i on soc ara. En aquests anys no he après només ciència, sinó a conviure, a compartir i a sobreviure, per això us dono a tots les gràcies.

Primer de tot m'agradaria agrair al Manel tot el suport que he rebut, com ja sap i t'hem dit moltes vegades, ets el nostre pare científic. Vull donar-te les gràcies per donar-me l'oportunitat de poder realitzar el meu doctorat, perdonar-me que no volgués fer el màster d'investigació i tornar-me a acollir quan m'ho vaig repensar. Gràcies per entendre'm, ensenyar-me noves coses, per les aventures i la confiança.

Vorrei anche ringraziare il professor Franco Mazzei per avermi permesso di stare nel suo laboratorio e avermi accolto a braccia aperte. Grazie mille per tutto quello che ho vissuto e imparato lì.

Vull agrair també als meus companys de lab, Andreu, Inma, Xavi, Anna, Dioni, Noelia (estic superorgullosa de tu, has sigut el millor pollet que he tingut!), Elena, Munmi, Qing, Mingyue, Cris, Joao, Francisco, Ede, Francesca i Valeria. Gràcies, grazie, per tots els riures i moments que hem viscut, sense vosaltres hagués estat totalment diferent. Sobretot vull donar les gràcies a tres persones. Anna, sé que tenim personalitats totalment antagòniques, se que en alguns moments ens hem volgut matar (crec que unes 10 vegades al dia aprox., inclosos festius), però també se que si necessito alguna cosa estaràs allà per ajudar-me i que sempre hi seràs. Elena, moltes gràcies per ser tant bona, sempre m'ajudes a veure els problemes des d'un altre punt de vista. Inma, me hubiese gustado tenerte en el lab hasta el último momento, fuiste y eres un referente para mí, muchas gracias por todo. I Xavi, des del principi vaig connectar molt fàcil amb tu, a vegades fem broma de que em viscut vides paral·lels i que és per ser de Lleida, però de veritat ets una de les persones més boniques que me trobat. Et vull donar les gràcies per ser el meu company de zulo i per ensenyar-me tantíssim. I sobretot per escoltar-me i aguantar-me. A tots, espero no perdre-us mai.

Però la universitat no hagués estat el mateix si no fos per totes aquells projectes de químics amb qui hem vaig trobar el primer dia. Encara recordo quan per casualitat vaig escriure'm amb una noia, la Judit, per patatabrava per anar acompanyades el

primer dia de classe. Doncs des que ens vam trobar a la Plaça Cívica, on ens vam trobar a la Mariona, la Clàudia i la Laura, em anat juntes, i espero que sigui així ¡Hasta el infinito y más allá!, us estimo molt dinosaures. Però no estàvem soles, teníem els nostres nens: el Marc, només fa falta dir que hi porto tants anys com amb la meva parella, el Dani, el meu veí, un dels meus millors amics i guia turístic de Terrassa, l'Arnau, el meu conseller i confident, i el Kevin i el Marcelo, els locos d'ogànica! I que no m'oblida de la Laura Talavera i l'Elia, moltes gràcies pels viatges i aventures viscudes, he tingut sort de trobar-vos ¡Vámonos átomos, que ho petarem!

Però no tot està a la universitat, també vull agrair als meus amics de sempre, als del poble. Moltes gràcies caris per estar incondicionalment al meu costat, per ser-hi en els pitjors i millors moment us estimo molt fort.

També li vull agrair a la meva família. Sense vosaltres no hagués estat possible. Papa i mama, sou el suport més gran que tinc, estic molt orgullosa de vosaltres, del que heu aconseguit i com ens heu educat. Només tinc paraules d'agraïment per vosaltres, per l'esforç que feu constantment, tot per nosaltres. Us estimo infinit. Moltes gràcies Arnau per ser el millor germà que podia tenir, per acompanyar-me i recolzar-me, per riure't de mi quan feia falta i per ser tant generós. Moltes gràcies als meus padrins i a la meva iaia, soc molt afortunada de poder-vos gaudir, m'heu ensenyat tantes lliçons de vida que només us puc tenir que admiració. Moltes gràcies als mes tiets, sogres i cunyats, som una família unida, de la qual estic molt contenta de formar-ne part. Sempre m'heu animat tots a estudiar, a relacionar-me amb la cultura i ajudat a evolucionar com a persona. Sou els millors!

I finalment, el meu pilar de vida, la persona més important de totes. Josep, t'estimo. Se, que sense tu no podria haver arribat fins aquí, dono gràcies a tenir-te al meu costat i a tenir la oportunitat d'haver-te conegut. Ets la millor persona que podia haver escollit com a company de vida. Moltes gràcies per haver-me aguantat en aquest llarg camí, se que em trobes a faltar, però com la Marta ésser escrivent de tesis, t'informo que la teva Marta novia torna aviat.

Evidentment, no podia acabar els agraïments, sense mencionar a l'Euler, el científic no, el meu gos. Tinc la immensa sort de tenir un gran gos, amb el qui he pogut passar grans moments, i també li vull donar les gràcies perquè per ell he estat obligada en els moment més complicats a deixar el món a part i posar-me a jugar i caminar. Junts fem una gran família!

Summary

Summary

In the last few years, different strategies have been developed for the efficient and rapid analysis of numerous samples. In order to improve the current proposals, researchers address the problem from different points of view. Two examples are those that have been followed in this doctoral thesis, the integration of new materials that confer unique properties to the sensors and the use of advanced mathematical tools. Specifically, this project has included in the voltametric sensors, not only new nanomaterials such as graphene and carbon dots, but also biomolecules such as enzymes. A posteriori these sensors have been applied in the framework of electronic tongues, a practice that consists in the use of chemometrics to obtain qualitative or quantitative models. Therefore, this research joins different fields of chemistry such as the science of nanomaterials, the use of electrochemical sensors, and finally, chemometrics, with the aim of improving and, therefore, overcoming problems presented in more classical methods.

The work is divided into two sections, starting with the use of graphene, and then focusing on the integration of carbon dots and modified carbon dots as a key material in sensing platforms. In the first case, graphene, specifically electrochemically reduced graphene oxide has been deposited on an electrode constructed based on a composite of graphite and epoxide resin. Once the electrode is characterized, it is used for the resolution of a complex mixture of ascorbic acid, uric acid, serotonin, and dopamine. In this case, resolution of the mixture and quantification of not only serotonin and dopamine, but also of their two interferents is achieved. Once this electrode is established, it is used as the basis for the creation of two enzymatic biosensors, using laccase and tyrosinase as recognition elements. With the house biosensor, a study of the enzyme kinetics is presented, which is used for the indirect detection of emerging contaminants. Finally, the two biosensors, together with the graphene platform, are included in the electrode array for the multivariate analysis of Brett character in rosé wine.

On the other hand, is presented a first work, based on the incorporation of carbon dots and carbon dots modified with N and S, separately. In this work a first test of the use of carbon dots as electrochemical catalysts is shown. This work shows a first attempt of the use of carbon dots as electrochemical catalysts, which present ideal characteristics to be used as electrode modifiers in the framework of electronic tongues.

Resum

En els últims anys s'han desenvolupat diferents estratègies per l'anàlisi eficaç i ràpid de múltiples mostres. Per tal de millorar les propostes actuals, els investigadors tracten el problema des de diferents punts de vista. Dos exemples són els que s'han seguit en la present tesi doctoral, la integració de nous materials que confereixen propietats úniques als sensors, i l'ús d'eines matemàtiques avançades. Concretament, en aquest projecte s'ha inclòs en sensors voltamètrics, no només nous nanomaterials com el grafè i els punts de carboni, sinó també biomolècules com els enzims. A posteriori, aquests sensors s'han aplicat en el marc de les llengües electròniques, una tàctica que consisteix en l'ús de la quimiometria per tal d'obtenir models qualitatius o quantitatius. Per tant, aquesta investigació uneix diferents camps de la química com són la ciència dels nanomaterials, l'ús de sensors electroquímics, i finalment la quimiometria amb l'objectiu de millorar i, doncs, superar, problemes presentats en mètodes d'un caire més clàssic.

El treball es divideix en dues seccions, primer se centra en l'ús del grafè, i després en la integració de punts de carboni, i punts de carboni modificats com a material clau en les plataformes de sensat. En el primer cas, el grafè, concretament l'òxid de grafè reduït electroquímicament s'ha dipositat en un elèctrode construït en base d'un compòsit de grafit i resina epòxid. Un cop caracteritzat l'elèctrode aquest s'utilitza per a la resolució d'una mescla complexa d'àcid ascòrbic, àcid úric, serotonina i dopamina. En aquest cas, s'aconsegueix la resolució de la mescla i la quantificació de no només la serotonina i la dopamina, sinó també dels seus dos interferents. Un cop establert aquest elèctrode, es fa ús de la mateixa com a base de la creació de dos biosensors enzimàtics, utilitzant com a element de reconeixement la lacasa i la tirosinasa. Amb el biosensor de lacasa es presenta un estudi de la cinètica de l'enzim, la qual s'usa per a la detecció indirecta de contaminants emergents. Finalment, s'inclouen els dos biosensors, juntament amb la plataforma de grafè, en el conjunt d'elèctrodes per l'anàlisi multivariable del caràcter Brett en vi rosat.

Per altra banda, es presenta un primer treball basat en la incorporació dels punts de carboni i els punts de carboni modificats amb N i S, per separat, en elèctrodes de carboni vitri. En aquest treball es mostra una primera provatura de l'ús dels punts de carboni com a catalitzadors electroquímics. Els quals en treballs futurs presenten característiques ideals per ser emprats com a modificadors per elèctrodes en el marc de les llengües electròniques.

Resumen

En los últimos años se han desarrollado distintas estrategias para el análisis eficaz y rápido de múltiples muestras. Para mejorar las propuestas actuales, los investigadores tratan el problema desde distintos puntos de vista. Dos ejemplos son los que se han seguido en la presente tesis doctoral, la integración de nuevos materiales que confieren propiedades únicas a los sensores y el uso de herramientas matemáticas avanzadas. Concretamente, en este proyecto se ha incluido en sensores voltamétricos, no sólo nuevos nanomateriales como el grafeno y los puntos de carbono, sino también biomoléculas como las enzimas. A posteriori estos sensores se han aplicado en el marco de las lenguas electrónicas, una táctica que consiste en el uso de la quimiometría para obtener modelos cualitativos o cuantitativos. Por tanto, esta investigación une diferentes campos de la química como son la ciencia de los nanomateriales, el uso de sensores electroquímicos, y finalmente la quimiometría con el objetivo de mejorar y, pues, superar, problemas presentados en métodos más clásico.

El trabajo se divide en dos secciones, primero se centra en el uso del grafeno, y después en la integración de puntos de carbono, y puntos de carbono modificados como material clave en las plataformas de sensato. En el primer caso, el grafeno, concretamente el óxido de grafeno reducido electroquímicamente se ha depositado en un electrodo construido en base a un composite de grafito y resina epóxido. Una vez caracterizado el electrodo éste se utiliza para la resolución de una mezcla compleja de ácido ascórbico, ácido úrico, serotonina y dopamina. En este caso, se logra la resolución de la mezcla y la cuantificación de no sólo la serotonina y la dopamina, sino también de sus dos interferentes. Una vez establecido el protocolo para la modificación del electrodo, se hace uso de este como base de la creación de dos biosensores enzimáticos, utilizando como elemento de reconocimiento la lacasa y la tirosinasa. Con el biosensor de lacasa se presenta un estudio de la cinética de la enzima, que se usa para la detección indirecta de contaminantes emergentes. Por último, se incluyen los dos biosensores, junto con la plataforma de grafeno, en el conjunto de electrodos por el análisis multivariable del carácter Brett en vino rosado.

Por otro lado, se presenta un primer trabajo basado en la incorporación de los puntos de carbono y los puntos de carbono modificados con N y S, por separado, en electrodos de carbono vítreo. En este trabajo se muestra una primera probatura del uso de los puntos de carbono como catalizadores electroquímicos. Los que en trabajos

futuros presentan características ideales para ser empleados como modificadores por electrodos en el marco de las lenguas electrónicas.

Table of contents

Table of contents

Figures and tables

Figures and tables

Symbols and abbreviations

Symbols and abbreviations

φ	Offset angle
ω	Radial frequency
∆G	Gibbs free energy increment
§	Section
4-EC	4-Ethylcatechol
4-EG	4-Ethylguaiacol
4-EP	4-Ethylphenol
5-HT	Serotonin
AA	Ascorbic Acid
AC	Alternating Current
AFM	Atomic force microscopy
ANN	Artificial neural networks
BA	Biogenic amines
BioET	Bioelectronic tongue
(Bio)sensor	General term to express the group formed by sensors and biosensors.
Biosensor	The sensor that uses a biorecognition element in their receptor part.
C	Capacitor
Ca.	Circa, about
Cat	Catechol
CDs	Carbon dots
CE	Counter or auxiliary electrode
CEC	contaminants of emerging concern
CI	Causal index
CNDs	Carbon nanodots
CPE	Constant Phase Element
CV	Cyclic Voltammetry
CVD	Chemical vapor deposition
CWT	Continuous wavelet transform
CYS	Cysteine
DA	Dopamine
DC	Direct Current
DFT	Discrete Fourier transform
DPV	Differential Pulse Voltammetry
DWT	Discrete wavelet transform
E	Potential
EDAC	1-Ethyl-3-(3-dimethylaminopropyl carbodiimide
EDOT	3,4-Ethylenedioxythiophene

EDTA	Ethylenediaminetetraacetic acid
EE	Electronic eyes
EIS	Electrochemical Impedance Spectroscopy
EN	Electronic nose
ERGO	Electroreduced graphene oxide
ES	Electronic skin
ET	Electronic tongue
F	Faradays
f	Frequency
FFT	Fast Fourier transform
FT	Fourier transforms
GO	Graphene oxide
GQDs	Graphene quantum dots
I	Current
ICH	International Council for Harmonisation of Technical Requirements for Pharmaceuticals for Human Use
Int	Windowed slicing integral method
ISO	International Organization for Standardization
IUPAC	International Union of Pure and Applied Chemistry
Lac	Laccase
LIDAR	Laser imaging detection and ranging
LOD	Limit of detection
LOQ	Limit of quantification
LSV	Linear Sweep Voltammetry
MDOE	Multivariate design of experiments
MIPs	Molecularly Imprinted Polymers
MSE	Mean squared error
MSS	Multisensor systems
N-CDs	Nitrogen Carbon dors
NHS	N-hydroxysulfosuccinimide
NIPALS	Non-linear iterative partial least squares
NRMSE	Normalized root mean square error
PARAFAC	Parallel factor analysis
PC	Principal component
PCA	Principal components analysis
PDs	Polymeric dots
PLS	Partial least squares
PMMA	Poly(methyl methacrylate)
Q	Electric charge
R	Resistance

Ref	Reference electrode
rGO	Reduced graphene oxide
RMSE	Root mean square error
SA	Salicylic acid
SAM	Self-assembled monolayers
S-CDs	Sulfur Carbon dots
SCE	Saturated Calomel Electrode
SIMPLS	Statistically inspired modification of the PLS
SNV	Standard normal variate transform
SVMs	Support vector machines
SWV	Square Wave Voltammetry
T	Time
TEM	Transmission Electron Microscopy
TEOS	Tetraethyl orthosilicate
TS	Taste sensors
Tyr	Tyrosinase
UA	Uric Acid
VOCs	Volatile organic compounds
vs.	Versus
W	Warburg impedance
WE	Working electrode
WT	Wavelet transforms
XPS	X-ray photoelectron spectroscopy
Z	Impedance of a circuit

Chapter I. Introduction

1 INTRODUCTION

1.1 Nanomaterials in (bio)sensors

1.1.1 Graphene

International Union of Pure and Applied Chemistry (IUPAC) defines graphene as "*a single carbon layer of the graphite structure, describing its nature by analogy to a polycyclic aromatic hydrocarbon of quasi-infinite size*", being graphite described as "*modification of the chemical element carbon, in which planar sheets of carbon atoms, each atom bound to three neighbors in a honeycomb-like structure, are stacked in a three-dimensional regular order, it is not correct to use for a single layer a term which includes the term graphite, which would imply a three-dimensional structure. The term graphene should be used only when the reactions, structural relations, or other properties of individual layers are discussed*" [1].

Graphene was insulated and correctly described between 2004 and 2005 by Konstantin Novoselov, Andre Geim, and co-workers, who were Nobel Prize laureated in 2010 [2,3]. Contrary to what can be thought, the graphene concept

was conceived in a pioneering work of Professor P. R. Wallace in 1947, who explored the 3D graphite structure. In this work, the author mentioned that graphite is formed by single hexagonal layers [4]. This was the starting point of the graphene search. During a broad period, the scientific world was trying to synthesize different graphitic forms, some of which are still in use. It must be noted that in those years, all the carbonaceous structures were named indistinctly graphite, although they were working with materials that currently are well distinguished and named. One example is the work of Professor B. C. Brodie, who in 1859 synthetized for the first time graphene oxide (GO). A few years later, in 1898, L. Staudenmaier enhanced his method, and in 1958 W. S. Hummers reported the most famous GO synthetic pathway [5–7].

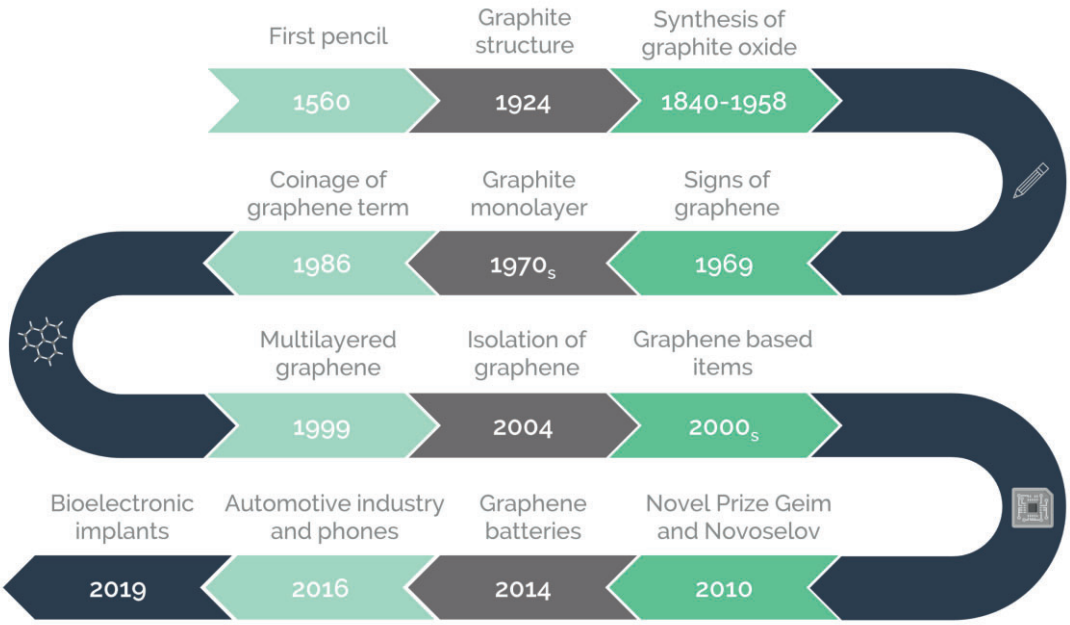

Figure 1.1. Timeline of graphene history [5–17].

It was in 1986 when Professor H. P. Boehm coined the term *"graphene"*, and in 1997 IUPAC reported its current definition. In fact, was he who in 1962 published a paper where it was described the first isolated layer of reduced graphene oxide (rGO), demonstrating hence the existence of individual graphite layers [18], being then, as mentioned in the Nobel Prize documents, and in the work of K. Novoselov and A. Geim, who discovered the first graphene form. Nevertheless, due to the poor quality of the product obtained in that study and consequently, the erroneous extracted conclusions, it was decided to attribute the discovery of graphene to the aforementioned K. Novoselov and A. Geim.

From 2004, graphene forms have been in-depth studied and at present time are commercially available, making possible their application in daily life. For example, these materials are applied in a wide range of products, from sensors and batteries (as electrochemical enhancer) to biological implants [9,16,17,19,20].

1.1.1.1 Structure and properties

From the definition of graphene, this material can be depicted as a flat carbon monolayer with a 2D sp^2 configuration and honeycomb shape (Figure 1.2) [21]. This two-dimensionality is the graphene hallmark when compared with the other graphite derivates. In fact, this material is also known as the mother of all graphitic forms, due to other carbon structures such as carbon nanotubes or fullerenes that can be ideally obtained from it.

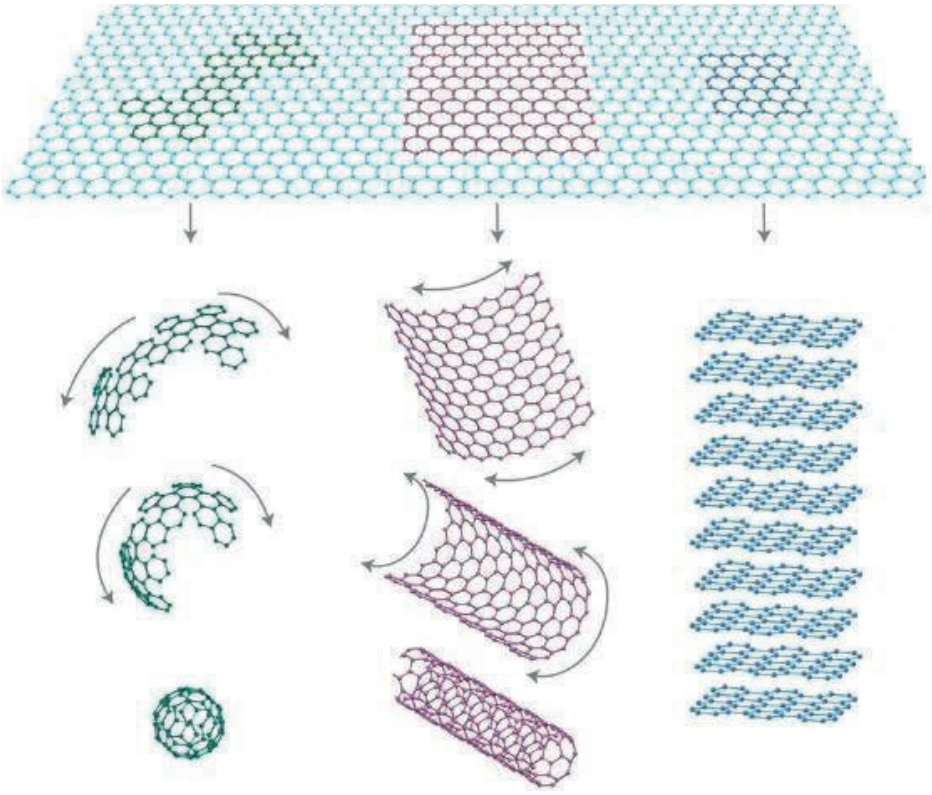

Figure 1.2. Derivation of graphene to other dimensionalities (0D balls, 1D carbon nanotubes, and 3D graphite). Figure reproduced with permission from the Nature Publishing Group from [21].

The abovementioned graphene structure is the one related to the pristine form, but there are multiple variants that differ fundamentally in chemical composition and size. For instance, graphene nanoribbons, described as thin strips [22], or graphene quantum dots, 0D material with less than 100 nm size

[23]. In this direction, graphene derivatives can also be divided by the number of layers, being this a key point. Graphene is defined as a monolayer material, but many of the synthetic routes result in a product that does not meet this condition. This is why, in the bibliography, it can be found articles that define graphene as single, double, few, or multi-layered graphene, graphene-platelets, or graphene flakes. Generally, graphene is distinguished from thin graphite when there are less than 10 layers stacked [21,24].

From the definition of graphene and as a result of the thorough research other derivatives materials such as GO, rGO, and modified graphene were also discovered. All of them are common in the literature, probably due to having a lower cost than the pristine form, being straightforward to manipulate and obtain, and unspecific equipment needed.

GO is an oxidized form of graphene directly originated from the direct synthetic pathway or produced spontaneously from the contact of graphene with air (Figure 1.3). Its concrete structure is still discussed because can vary depending on the obtention process, it is clear that the honeycomb lattice is disrupted by ketone carbonyls, epoxides, alcohols, and carboxylic groups. The differences lie in the concrete presence of oxygenated functional groups and in which quantities those can be found. As it can be expected, these differences will cause variations in their electrochemical characteristics.

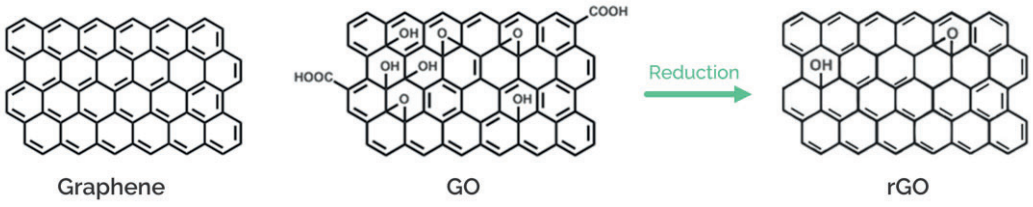

Figure 1.3. Different structures of graphene, GO, and rGO.

Given those oxidized functionalities, GO has advantageous properties such as dispersibility in water, organic solvents, and even in complex matrices. Contrary, it is considered an electrical insulator nanomaterial ($1.64 \cdot 10^4$ Ω·m) due to the abundance of functional groups in the surface which interrupts its sp^2 electrical configuration causing the inhibition of the graphene characteristic electric conductivity [25–27]. In order to overcome this issue, rGO was developed aiming to recover some of the pristine graphene features. The rGO is obtained

from GO via its chemical, thermal, or electrochemical reduction. In this step, GO is turned into a structure similar to conventional graphene by the semi-recovery of the honeycomb lattice. In some specialized studies, like the ones focused on enhancing the electrical properties of graphene, GO is avoided, being rGO of high interest. In fact, in some cases when working with graphene and its derivatives, rGO is rather preferred than pristine graphene because of the unique features that can apport the remaining imperfections. Nevertheless, although GO reduction seems to be a promising and suitable option, it has not yet been possible to obtain graphene that is fully comparable to the obtained with other synthetic processes. It is expected that when the complete reduction of the GO is achieved, this will be the turning point for the use of graphene in industrial processes, and its optimized commercialization on a larger scale.

As discussed until now, graphene and its derivative forms have distinct characteristics. All of them were well studied discovering that in general, despite the worse values obtained for GO and rGO when compared with the pristine form, the features of these materials are still remarkable. Focusing on the pristine graphene, when its properties are contrasted with other more conventional materials such as silicon, the value of this material becomes obvious (reference values in Table 1.1),

Table 1.1. Summary table of some of the graphene properties [28–30].

Characteristic	***Graphene***	***Silicon***
Optical transparency	97.7%	-
Electron mobility	200000 $cm^2 \cdot V^{-1} \cdot s^{-1}$	≤1400 $cm^2 \cdot V^{-1} \cdot s^{-1}$
Thermal conductivity	5000 $Wm^{-1} \cdot K^{-1}$	149 $Wm^{-1} \cdot K^{-1}$
Specific surface area	2630 $m^2 \cdot g^{-1}$	571 $m^2 \cdot g^{-1}$
Tensile Strength	130000 MPa	350MPa
Elastic modulus	250 GPa	150 GPa

In regards to its electrochemical properties, graphene is a winning bet. It is considered a zero-gap semiconductor, in other words, a semi-metal. Its characteristics are given not only for its incredible surface area, being twice that of the carbon nanotubes (1315 $m^2 \cdot g^{-1}$) and *ca.* 200 times greater than that of

graphite (10 $m^2 \cdot g^{-1}$), but also for the conductivity (around 60 times greater than the obtained for carbon nanotubes), and for its electron mobility, which is stable in a broad range of temperatures [2,31].

Besides standing out for its electrical conductive capabilities, graphene also has other surprising mechanical properties. For example, this material and its derivatives present low fracture and high tensile strength, transparency when there are less than 10 layers, thermal conductivity, and chemical stability among others [27].

Regarding the thermal conductivity, graphene and rGO have good in-plane thermal transference, being one of the most remarkable values for the known materials, but as in the case of electric properties, GO presents also lower conductivity [27].

All these promising properties coupled with the potential applications triggered great interest and hope worldwide. In this material, which is evident from e.g. the European projects, and the consequent spin-off based on them.

1.1.1.2 Synthesis

Graphene synthesis is a hot topic in the field because is still the need to find an optimal protocol to achieve a real scalable production. Nowadays procedures are advanced, but despite the progress made in the topic, there are still shortcomings that keep them from reaching as fast as expected goals were set when this material was discovered.

There are multiple pathways to synthesize graphene, being the most common and the preferred summarized in Figure 1.4.

Most of the synthetic routes can be divided into bottom-up or top-down methods. On one side, bottom-up methods have as starting materials simple carbon molecules which are organized to form more complex forms, in this case, pristine graphene. On the other side, top-down methods start from a bigger structure, like graphite, to obtain layered graphene (as depicted in Figure 1.4).

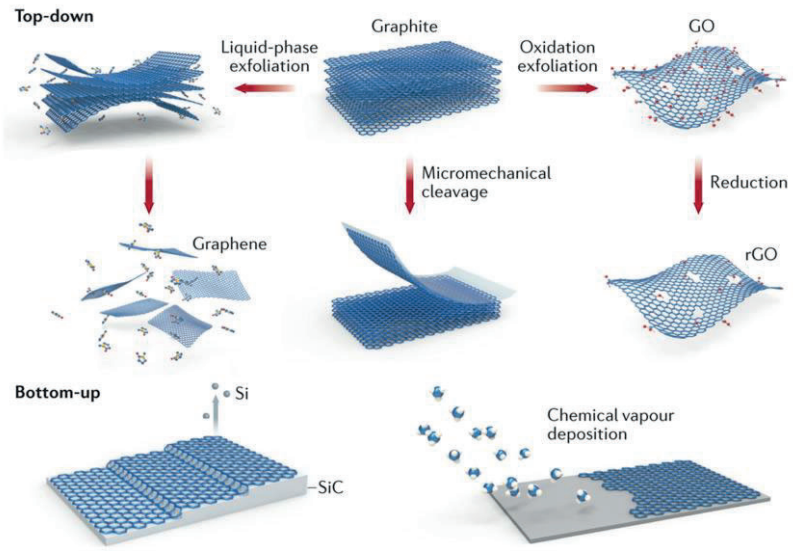

Figure 1.4. Examples of top-down and bottom-up synthesis. Figure reproduced with permission from the Nature Publishing Group from [32].

Table 1.2. Summary table of some of the more common synthetic pathways for the graphene obtention [28].

Method	Description	Advantages	Disadvantages	Ref.
Top-down				
Mechanical exfoliation	HPOG[1] is stripped mechanically. The most famous technique is Scotch® tape.	• Straightforward • High electronic and structural quality • Low cost	• Time-consuming • Poor reproducibility • Non-scalable • Low yield	[21]
Chemical exfoliation	Exfoliation of graphite in organic solvents through surfactants, and sonication, among others.	• Scalable • High yield • Straightforward • Low-cost • User-friendly product	• Low purity • Small size • Time-consuming	[33]
Reduction of GO[2]	GO is obtained from graphite and reduced to rGO. It can be done by different techniques.	• Scalable • High yield • Straightforward • Low cost • User-friendly product	• Low purity • Large number of structural defects • Disruption of sp_2 configuration • Not pristine graphene	[34]

Bottom-up				
Epitaxial growth	Obtention of graphene from hydrocarbon gases. It can be done by different techniques.	• High quality • Large areas • Uniform • Easy tuneable	• Specific materials and equipment • High cost • Needs to be transferred • Variable yield	[35]

[1] **HPOG**: highly ordered pyrolytic graphite. [2] It is referred to as the obtention of rGO, more comparable to graphene in properties terms than GO.

From the different methods described in the table, epitaxial growth is the most extended and promising, being the chemical vapor deposition (CVD) technique the most relevant. The main reasons are the high quality of the resulting product, the industrial adaptation, and the possibility to tune the material given by the technique. Contrary, this method has some drawbacks such as the high cost and complexity of the method, and the material transfer step. Epitaxial growth must be carried out onto metallic substrates, leading to the relocating of the synthesized product from the growth surface to the target substrate when it is required. This process is performed using polymeric films such as poly(methyl methacrylate) (PMMA) (Figure 1.5). As it can be expected during these steps, graphene can suffer damages and contaminations.

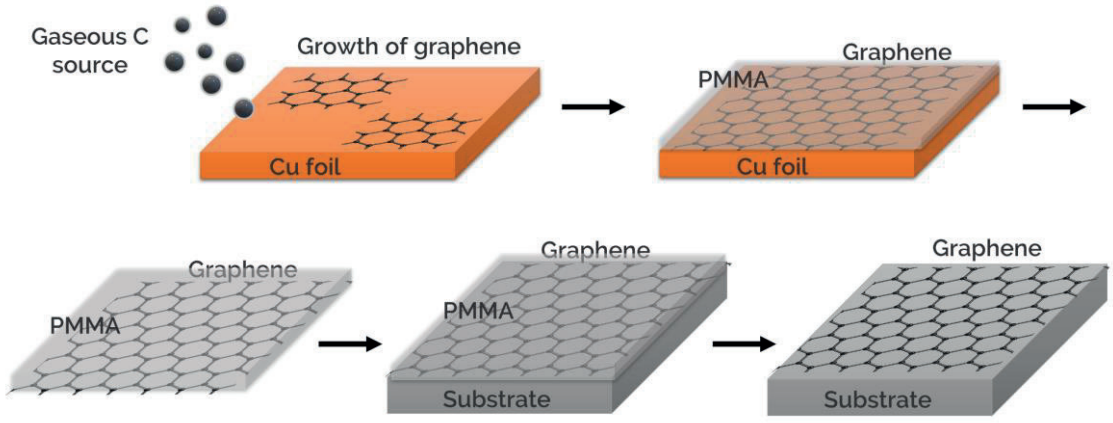

Figure 1.5. Epitaxial CVD synthesis followed by the transferring via polymeric film PMMA of the nanomaterial to the target substrate. Once the material is ready, it is coated with the polymer and then separated from the growth substrate to be cast onto the new surface.

In general, there is no ideal method in which graphene is obtained rapidly, in large quantities, and maintaining perfectly its structural composition. From the

literature, it can be concluded that epitaxial growth is used when high-quality graphene is required, normally when used as part of batteries or electrical components. Oppositely, when other parameters such as the scalability of the final device, the prize, or the user-friendliness are taken into account, researchers consider other options such as the chemical exfoliation or the reduction of GO.

It must be noted that the mentioned fabricating procedures are not the only way to obtain graphene. In this regard, some authors reported that report novel methods such as the electrochemical exfoliation of a pencil lead or the unzipping of carbon nanotubes [36,37].

The synthesis of GO is based on the chemical oxidation of graphite. As aforementioned, Professors B. C. Brodie, L. Staudenmaier, and W. S. Hummers proposed different syntheses to obtain GO, being the latter the more successful. Hummers proposed improvements to the existing pathways to reach a safer procedure. Fort this reason, this method and its evolutions (modified Hummers' methods) are still widely used.

Lastly, rGO is generated from GO via thermal, electrochemical, or chemical reduction. The goal of thermal reduction is to decompose the oxidized functional groups to CO_2 and CO through the application of high temperatures. The electrochemical techniques rely on the use of electron exchange to reduce the functional groups. Finally, the chemical reduction is based on the use of reducing reagents such as hydrazine, amino acids, or fungus.

As expected, depending on the chosen technique, rGO will have different morphological and electrical properties. The key parameters to control are the C/O ratio, the selectivity of the reduction process, and the final chemical and physical properties. The selected reduction process will depend on the system in which it will be applied, the facilities of the laboratory, and may in the use of greener reagents instead use toxic reducers like hydrazine, or hydroquinone [38].

From the explained methods, this thesis dissertation used electroreduced GO obtained from both, commercial and non-commercial GO. The synthesis of GO was carried out by a modified Hummers' method as described in §3.4.

1.1.2 Carbon dots

Carbon dots (CDs) are a novel nanomaterial that was discovered in 2004 by X. Y. Xu and co-workers [39], which is gaining popularity rapidly (Figure 1.6). One example is its use in high-end screen technologies or more recently as fluorescent markers in biological tests.

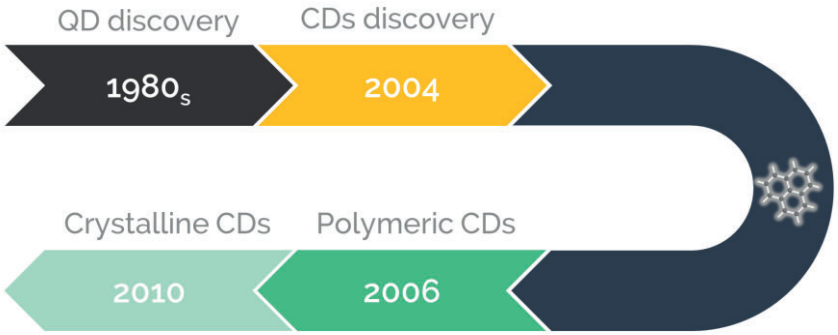

Figure 1.6. Timeline of CDs history [39–42].

As it can be expected, its concept comes from the inorganic quantum dots (QDs), described as semiconductive nanoparticles that have different properties than their bulk precursors. Contrary to the common perception, CDs cannot be named always quantum carbon dots, because not necessarily have a size dependent quantum confinement effect.

CDs can be considered a 0D nanomaterial, of small size (normally around 10 nm), with a carbon-based scaffold and oxygenated functional groups on the surface. CDs are generally classified into three subtypes mainly separated by their structural characteristics: graphene quantum dots (GQDs), carbon nanodots (CNDs), and polymeric dots (PDs). All of them have similar sizes and properties but differ in the core carbon structure and its surface functional groups. GQDs have a single or few graphene layered core, that normally presents high crystallinity and low dimensions. CNDs, are more considered as a spherical shape with an amorphous core, and finally, PDs are named polymeric because they either have a carbon core crosslinked with a polymer, or have a polymeric shell [43].

This nanomaterial presents surprising characteristics, but the most important since now it is their luminescence but is not only the unique property, they are also of small sizes, high conductive, and low toxic.

1.1.2.1 Synthesis

First of all, it must be noted that CDs synthetic methods still have a long way to go. One of the most paradigmatic issues is the study of the tune of precursor reactivity in the in-depth nucleation and growth stages, which are expected to be critical points as in the case of QDs chemistry. These issues together with the complexity of the related organic reactions and their difficult purification and separation hinder the elucidation of standard protocols for its synthesis.

Table 1.3. Summary table of most common CDs synthetic methods.

Method	Description	Advantages	Disadvantages	Ref.
		Top-dow		
Arc discharge	Reorganization of carbon atoms via plasma.	• Simple	• Costly • Large particle size	[39]
Laser irradiation	Laser ablation of the carbo source produces a gas form that crystallizes in a substrate.	• Straightforward • Controlled size • Environment-friendly	• Costly • Intricate	[44]
		Bottom-up		
Microwave pyrolysis	Microwave irradiation of organic carbon sources.	• Well-established • Straightforward • Environment-friendly	• Costly	[45]
Acidic oxidation	Oxidative exfoliation of carbon sources.	• Product tuneability	• Have structural defects	[46]
Hydrothermal synthesis	The precursors are solved and put in a Teflon-lined stainless steel autoclave until carbonization.	• Uniform sizes • Low toxicity • Scalable • Straightforward	• Amorphous product • poorly reproducible	[47]

Electrochemical synthesis	Electrochemical carbonization of carbon sources.	• Straightforward • Non-toxic	• Still in development	[48]

1.2 Sensors and Biosensors

1.2.1 From the beginning until now

Nowadays the word 'sensor' is widely used and familiar for most of us, but some generations ago was difficult to understand this term. During scientific history, scientists have had to overcome new challenges continuously. One of the most relevant problems was the measurement of a phenomenon that can be tangible or not. At this point was when the first sensors appeared. IUPAC defines a sensor as "*a device that transforms chemical information, ranging from the concentration of a specific sample component to total composition analysis, into an analytically useful signal. The chemical information, mentioned above, may originate from a chemical reaction of the analyte or from a physical property of the system investigated*" [49]. Given this broad definition, it is complicated to fix a date for the invention of the sensor, as seen in Figure 1.7, simpler sensors such as the thermometer or the barometer were developed in the first middle of 1600, but it took a few years for the first electrochemical sensors to appear. For instance, the pH glass electrode and the proposal of Leland C. Clark Jnr [50], who developed a device for a persistent problem at that time, the measurement of oxygen in biological fluids. The novelty that highlighted his device was the inclusion of a gas-permeable membrane between the sample and the working electrode [51,52]. A few years later, in 1962, the same investigator presents a coupling for his oxygen sensor based on a glucose oxidase modified membrane which allows the detection of oxygen through the glucose enzymatic oxidation [53]. This system was the first biosensor, defined by IUPAC as "*any device that uses specific biochemical reactions mediated by isolated enzymes, immunosystems, tissues, organelles or whole cells to detect chemical compounds usually by electrical, thermal or optical signals*" [54].

Since then, the (bio)sensors field has been evolving up to the present day, where continuously are appearing improved and novel approaches (Figure 1.7 and Figure 1.8).

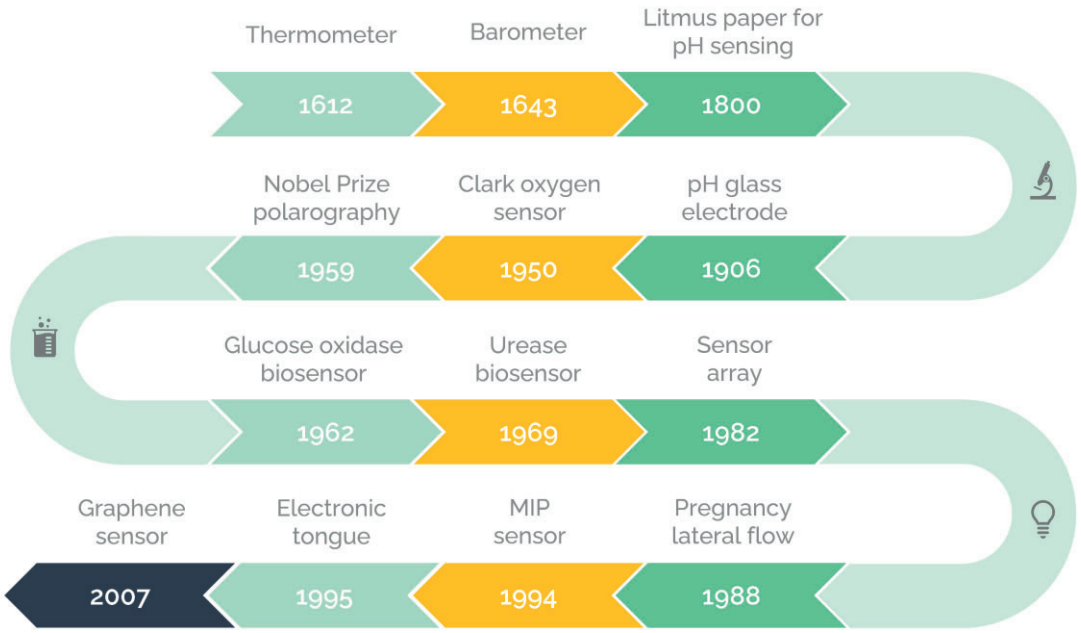

Figure 1.7. Sensor timeline [15,50,53,55–60].

Nowadays the main goals are not only the individual enhancement of the (bio)sensors because the derived problems can be addressed using their synergy with other areas such as chemometrics, nanomaterials, and biotechnology. Thus, there is a need to obtain fast and reliable methods of complex samples.

To demonstrate its continuous progress, Figure 1.8 depicts the number of publications including the words ‘sensor’ or ‘biosensor’ as a keyword showing the increasing trend and the importance of (bio)sensors in investigation projects.

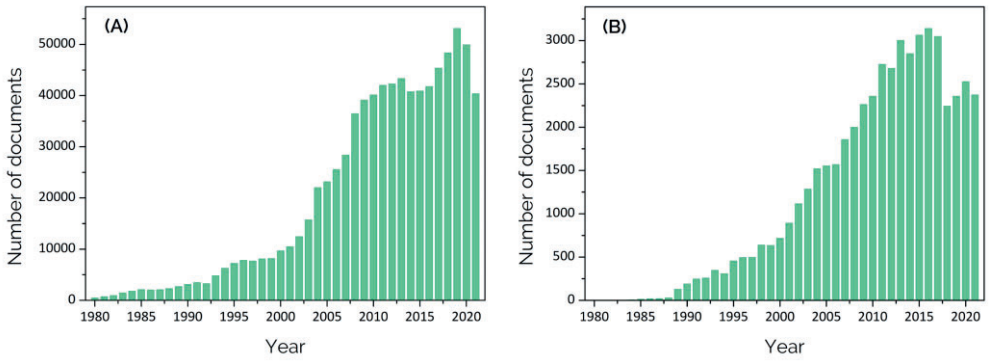

Figure 1.8. Number of publications including as keyword (A) 'sensor' and (B) 'biosensor' from 1980 to 2021 (data acquired from Scopus October 2021).

1.2.2 Description of the ideal (bio)sensor

Based on the general definition of the sensor above mentioned, it can be deduced that the analytical sensor is the one able to carry out a selective measurement of physical, chemical, or biological parameters to give a quantifiable signal. The chemical sensor is formed by two main parts (Figure 1.9): the receptor and the transducer. On the one hand, the receptor is the part of the sensor where the chemical information is transformed into a form of energy that is measured by the transducer; on the other hand, the transducer is the part in charge of the transformation of the received energy into a useful analytical signal. Thus, a primary signal is generated in the receptor that is then transmitted to the transducer, which converts it into a secondary signal, typically of the electric domain. It is important to note that the transducer itself does not confer selectivity to the system [49].

Typically, receptors are classified as physical, chemical, or biochemical depending on the reaction that produces the primary signal. When a chemical reaction is involved, there are classified as chemical, whereas when no chemical reaction takes place are classified as physical. Some examples of the latter are the measurement of absorbance, temperature, pressure, or conductivity. Moreover, there is a third kind of receptor, the biochemical, leading to a biosensor, in which a biochemical process is the source of the signal. Nevertheless, receptors cannot always be categorized into a single class leading to a combination of two of them.

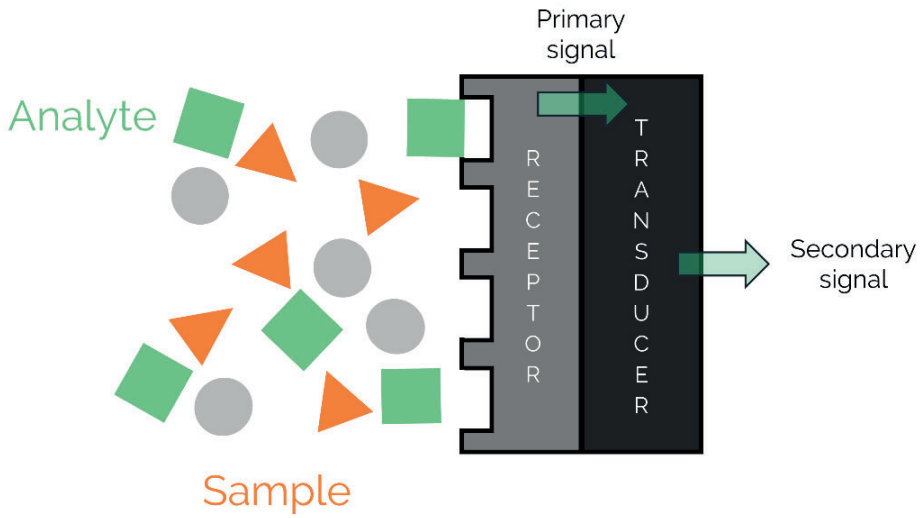

Figure 1.9. Schematic representation of a chemical sensor and its transduction process.

The ideal (bio)sensor is a device that must present the characteristics described in Table 1.4. The information in the table is based on the IUPAC, the international organization for standardization (ISO), and the International Council for Harmonisation of Technical Requirements for Pharmaceuticals for Human Use (ICH) guidelines [61–65].

Some of those terms are generally employed erroneously owing to the conflicts with the same words in other languages and the lack of agreement among different guidelines. Although, it must be noted that the scientific community is making a big effort to standardize these concepts. For this reason, Figure 1.10 shows an explanatory schematic diagram of some of these terms.

Table 1.4. Characteristics of an ideal (bio)sensor

Characteristic	Description
Precision	The closeness between independent test results obtained under stipulated conditions.
Repeatability	Precision under the same operating conditions over a short interval of time. Repeatability is also termed intra-assay precision.
Intermediate Precision	Within-laboratory variations: different days, different analysts, different equipment, etc.
Reproducibility	Precision between laboratories.
Trueness	The closeness between the average value obtained from a large series of test results and an accepted reference value.
Accuracy	The closeness between a quantity value obtained by measurement and the true value. It is considered the sum of trueness and precision.
Sensitivity	The capability of distinguishing between minor variations of the measured quantities.
Limit of detection (LOD)	The lowest concentration of an analyte that can be measured but not necessarily quantitated as an exact value.
Limit of quantification (LOQ)	The smallest concentration of an analyte that can be quantified with suitable precision and accuracy.
Selectivity	The capability of a sensor to distinguish the analyte in the presence of other interferences.

Specificity	Ability to assess unequivocally the analyte in the presence of components that may be expected to be present.
Drift or Operational stability	Long-term stability of the output signal without changing the input. Often induced by humidity, degradation, or temperature among others.
Stability or Storage stability	Capability to generate the same output signal when measuring a standard measurand over a certain period of time.
Response time	The required period of time for the output signal to reach a stable value.
Resolution	The variation of the smallest concentration that can be detected when the concentration is continuously varied.
Reversibility	Ability to return to the stable baseline response after being exposed to a certain amount of analyte.
Hysteresis	The maximum difference in the output signal when the sensor operates first with an increasing and after in a decreasing analyte concentration range.

Moreover, in the present day, some other characteristics must be taken into account when developing a (bio)sensor. For example, the requirements of the final application, a user-friendly design, being low-cost, the materials used in the fabrication process, its impact on the environment, etc.. Considering as positive the usage of biodegradable raw materials and their suitability taking into account their end-use and consumers health [55,66].

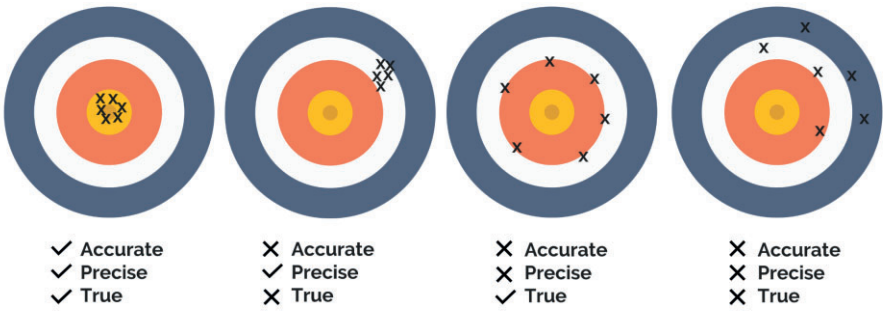

Figure 1.10. Schematic representation of accuracy, precision, and trueness ideal characteristics.

1.2.3 Classification

Sensors can be classified according to different parameters; for example, in the previous section (§1.2.2) those have been sorted by the receptor type, but

they are also classified by the transducer operating process or by the application field, among others. Table 1.5 exposes the classification that recommends the IUPAC considering the principles of signal transduction [49,66,67].

Table 1.5. Sensors classification according to the IUPAC by transducer operating process.

Transducer	Description
Optic	Transforms optical variations produced by the interaction of the analyte with the receptor part.
Electrochemical	Transforms the variation produced by the electrochemical interaction between the analyte and the electrode.
Electrical	Transforms electrical variations produced by the interaction of the analyte, where no electrochemical process takes place.
Mass sensitive	Transforms mass changes caused by the deposition of the analyte onto a surface.
Magnetic	Transforms changes in the paramagnetic properties.
Thermometric	Transforms heat effects from a chemical reaction or adsorption that involve the analyte.
Others	Transform variations of other physical properties, such as radiation.

As mentioned before, other subdivisions can be applied, for instance, it is possible to classify sensors taking into account the method used for the measurement, the final application, or by the analyte that is measured. When a single device combines more than one category is called a multisensor [49].

Lastly, it must be taken into account that biosensors have subclasses, normally divided by the origin of the biorecognition element, for example, enzymes, cells, antibodies, aptamers, or microorganisms.

1.2.4 Arrays of sensors

When developing a sensor, the objective is to achieve the closest to the ideal concept, explained in §1.2.2. From the list (Table 1.4), the most relevant and difficult characteristics are selectivity and sensitivity. Being the other parameters attainable. To overcome the shortcomings of a sensor, normally they used to be developed to work in a specified and controlled sample that does not interfere with the output signal, nevertheless when it is not possible other options

exist. For instance, the pre-treatment of the sample to separate the analyte from the interferences of the matrix, or the use of sensors arrays. From these two, the second option is the one that best suits the fundamental idea of the sensors, which pretends to facilitate and avoid multi-step procedures.

The usage of an array of sensors represents an alternative when the individual sensors are not specific enough. Sensor arrays can consist of redundant, independent, or cross-sensitive sensors, it depends on the main purpose of the experiment. Their description is detailed in Table 1.6 [68]. This kind of approach allows the obtention of multidimensional data that can be processed to obtain information of individual analytes present in complex matrices, resolve compounds mixtures, or find the fingerprint of the target molecules among the interferences. In this manner, the use of advanced mathematical tools and multivariable analysis permits solving problems that classical chemistry cannot easily cope with [52,68].

Arrays of cross-sensitive sensors or unspecific sensors are inspired by the biological recognition systems like animal senses such as taste or smell [69,70].

Table 1.6. Summary table of the different types of sensors arrays that may be used.

Sensor array	Description
Array of redundant sensors	The sensors that form the array are equivalent and so are their output responses. Even though this kind of arrays seems contradictory with the more classical aims, are interesting to solve problems such as failures in the sensors or the entire system. Which helps to increase the precision and stability of the method [71].
Array of independent sensors	The sensors that form the array are selective towards different compounds. This system allows a parallel multi-component analysis. The main advantage of this class is the reduction of analysis time and sample volume [72,73].
Array of cross-sensitive sensors	This array is composed of unspecific (non-correlated) and low selective sensors that present different sensitivities towards the target analytes. The array together with processing tools can deal with the interferents [74–76].

1.2.5 (Bio)sensor modification methods

First of all, it must be pointed out that there are multiple ways described in the bibliography for modification of (bio)sensors. In this section, a brief review of the most common, and herein used, modification techniques will be made.

As it can be expected, the selection of the optimum process will depend on a wide range of factors, such as the type of sensor to be modified, the material to be integrated into the system, or the equipment and facilities available in the laboratory.

Indeed, the immobilization procedure is a key point that can equally inhibit or potentiate the catalytic effect of the material. Thus being the objective to maintain as active as possible both the material and the electrode surface. For this reason, factors such as orientation, interaction, or possible interferences with the supplementary added materials should be taken into account when choosing the modifiers and the way to integrate them into the system [77].

1.2.5.1 Integration of nanomaterials in the sensor

Modification techniques can be classified in many ways, for example, according to the formed bond, to the materials used during the process, to the method used for the modification, or even to the thickness of the new created layer. Regarding the characteristics obtained in each case, the results are different due to the different disposition of the material and then, the different chemical and physical acquired properties.

Table 1.7. Summary table of the most common sensor modifications.

Method	Description	Advantages	Disadvantages	Ref.
Bulk	The modifier is integrated directly into the receptor composite.	• Precise • Surface renewal is not required	• Required a big amount of modifier • Possible reducing of the modifier activity • The modifier is not directly exposed	[74,76,78]

Covalent binding	Formation of covalent bonds between the surface and the modifier.	• More resistant than other modifications • Modifier completely exposed	• Possible reducing of the modifier activity • Difficult to control the final organization • Required concrete functional groups	[79–81]
Non-covalent binding	Inclusion of the modifier to electrode surface via weak forces or adsorption.	• Easy to apply • Modifier completely exposed. • No further treatment is required	• Needs affinity between the surface and the modifier • Low stability • Recurrent renewal of the surface	[34,35,82]
Polymeric films, or entrapment	Formation of a polymeric coat, that contains the modifier, onto the electrode surface.	• Tunable • Easy to adapt	• Needs further steps • The modifier is not completely exposed • Recurrent renewal of the surface	[33,83–85]
3D-printing	Printing of electrodes with modified filaments.	• Similar to bulk modification • On-demand design	• Are not widely described • Complicated to adapt to new cases	[86,87]

When the electrode platform is already prepared, surface modification methods are normally employed, being in the majority of cases a reversible modification. But when the sensor is built manually, the transducer can be directly customized on-demand. Table 1.7 summarizes the most relevant modification processes and some illustrative works that employ them.

In the next paragraphs, some of the abovementioned methods, and the ones employed in our laboratory will be discussed more in detail.

- Bulk

Bulk modification is a direct and easy approach to apply during the building of the electrode. It is one of the most common techniques as it can be found in the literature [74,76,78]. Nevertheless, the scope has been completely

revolutionized by the arrival of printers in laboratories, such as inkjet or 3D. The option to create and print your own electrodes expands the range of choices, being even possible to fabricate complete cells specific to each case. One example is the work of C. Kalinke *et al.* [87].

While the bulk modification is simple to use, it has also some disadvantages. Apart from the fact that the modification of the electrodes has to be made in advance, it requires a significant amount of material, and as also expressed in the examples given, often the surface activation in order to expose the modifier is necessary.

- Non-covalent binding

Non-covalent techniques are based on the formation of coatings that interact via non-bonding interactions (weak forces and adsorptions) with the sensor electrode surface. On one side, this kind of modification method is widespread in the (bio)sensors field. The principal reasons are its simplicity, the well-established protocols, and the promising results. On the other side, since the modifier layer is deposited and kept via weaker interactions than covalent binding or bulk modification, the resulting sensors tend to have shorter operational stability.

The most popular techniques are physical adsorption, such as drop-casting, and self-assembled layers.

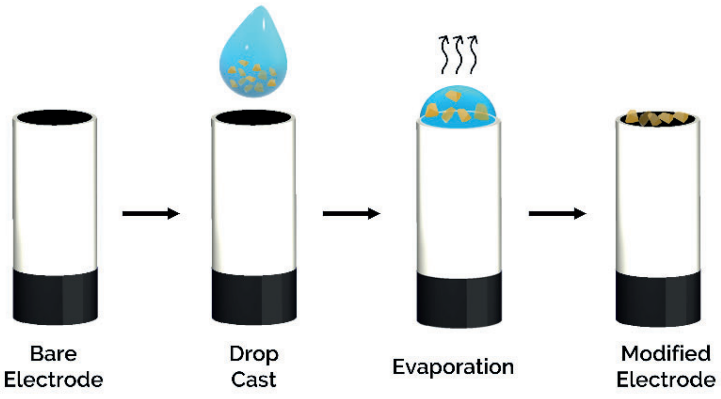

Figure 1.11. Schematic representation of the drop-casting method.

The general steps for the drop-casting are schematized in Figure 1.11. Firstly a suspension of the modifier is prepared in the optimum concentration, afterward, the desired volume is taken and “cast” as a drop onto the electrode,

from where the name of the technique arises. Next, the electrode is left in a saturated environment until all the liquid has evaporated [88]. It must be noted that it can be added as layers as considered to obtain the sought final result. Finally, the modified electrode is obtained. The resulting layer is randomly ordered.

As mentioned, some properties are required to employ drop-casting as a modification technique. One important characteristic is the solubility of the modifier, the material has to be insoluble in the measuring environment in order to maintain the layer over the experimental performance. Additionally, should also be considered the chemical properties of the materials, because the more suitable the structure of the material the more stable the forces created between them.

When applying this technique, it is important to deposit all the volume in the conductive part of the electrode, avoiding the loss of the material. Moreover, strange effects on the distribution of the modifiers can appear due to the different affinities between the different materials. Unwanted distribution can arise also from the hydrophobicity characteristic of the platform material. This will affect the drop shape and the evaporation stage resulting in effects such as the coffee ring effect [88]. As the more hydrophobic the platform is, the bigger the contact angle, giving to a lower capillary flow, hence implying a better distribution of the modifier.

Regarding the evaporation step, is highly recommended to carry it out in a saturated environment, because it allows the controlled evaporation of the solvent and thus a better distribution of the modifier. These issues can be addressed with techniques such as spin-coating, which distributes homogeneously the material onto the surface using the centripetal force.

Another important method is the formation of self-assembled monolayers (SAMs). The goal is the spontaneous guidance of the molecules to form a reversible organized layer onto the electrode surface. To achieve the assembly, it is needed that molecules have one functional group affine with the surface anchoring group and another side that will be organized (spacer and terminal group). A schema of the organization is depicted in Figure 1.12. The terminal groups will define the properties of the sensor and give the opportunity to use it

as reacting point for a posteriori covalent binding, while the other sides anchor the molecules to the substrate. The spacers have weak interactions and keep organized the assembly. Some of the most popular examples are the SAMs formed by thiols on gold surfaces, diazonium salts, or silanes.

The main two strengths of this technique are the accurate control of the resulting coating and the easy tuneability and rearrangement of the layer. Contrary, if the target modifier or substrate is not suitable for the direct application of SAMs, it will need further steps for its preparation, making the entire process more complex.

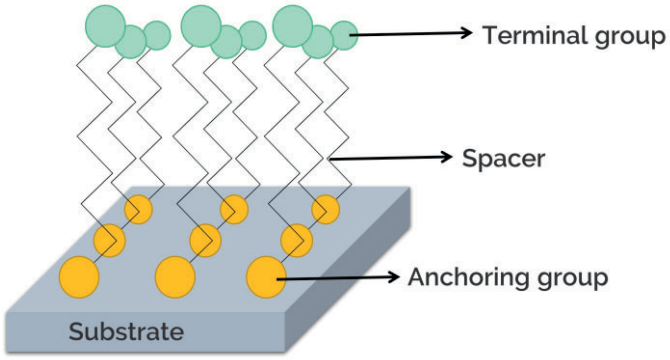

Figure 1.12. Schema of a self-assembly monolayer (SAM).

- Polymeric films

This coating method consists of the creation of a polymeric film that physically entraps the modifier. There are several options to create the polymer, ranging from the use of light to electrochemical polymerization, and it can be directly polymerized on the surface of the electrode or prepared separately and afterward added onto it. Polymeric films can be attached to the surface covalently or not.

Most of the techniques employed to integrate the polymer are like those used in non-covalent modifications, some examples are the drop-casting and spin coating. In these cases, the polymer is suitable solved and deposited on the target platform. For instance, some of the most common polymers are Nafion®, polystyrene, chitosan, agarose, and glutaraldehyde [89–91], which form a membrane, or sol-gel modification that uses an alkoxide precursor such as tetraethyl orthosilicate (TEOS) to form a scaffold with the modifier [84].

Another research line is focused on in situ polymerization. One of the most used methods is electrochemical polymerization. In this case, the monomers are induced by potential or current changes to the polymerization reaction, thus forming a polymer on the surface of the target electrode. In this direction, the modifier is mixed with the monomers solution to be entrapped during the polymerization or alternatively, it is added before. The most popular monomers are 3,4-ethylenedioxythiophene (EDOT) and pyrrole [85,92].

The main advantages of these techniques are the increase of the active area, the high stability of the sensor, and the wide range of materials to be used, which means more versatility when incorporating the modifier and the possibility to entrap more than one material at the same time. On the other side, as in the case of bulk modification, the modifier is not directly exposed, being often necessary an electrode activation step.

1.2.5.2 Immobilization of biorecognition elements in a sensor

When a biosensor is being developed, the choice of the biological recognition element is as important as the method by which it is immobilized. There is a wide range of techniques reported, but Table 1.8 summarizes the most important and commonly used in the biosensors field. The main goal when it is immobilized a biorecognition element in a sensory platform is the maintenance of the biomolecule activity and selectivity, minimizing the leakage of the material, and ensuring a stable environment. As it can be expected, some immobilization methods are common in Table 1.7 and Table 1.8, because they are general concepts that can be applied to any modifier, whether or not it is a biological element. Additionally, more specific methods such as the bioaffinity are detailed.

Table 1.8. Summary table of immobilization techniques.

Method	Description	Advantages	Disadvantages	Ref.
		Reversible		
Non-co-valent binding	Union caused by weak forces.	• Straightforward • Low changes in the conformation • Low cost	• Low stability • Non-controlled orientation	[93]

Bioaffinity	Coupling of the bio-recognition part through a complementary element	• Controlled orientation • Straightforward specific • Selective	• High cost	[94]
Metal-binding	Formation of coordination compounds based on metal ions and biomolecule functional groups.	• Simple	• Low reproducibility	[95]
		Irreversible		
Covalent binding	Formation of covalent bonds between the functional groups of the biomolecule and the platform.	• Low leakage • High stability	• loss of activity due to changes in the conformation • Recurrent renewal of the surface	[96,97]
Cross-linking	Formation of an intermolecular cross-linkage between the enzyme molecules	• Stabilization of the biological elements • High binding strength	• Hinder the mass transference • loss of activity due to changes in the conformation	[20,98]
Polymeric films or entrapment	Capture the bio-recognition element in a polymeric scaffold.	• High applicability • Stable to environmental changes • Low leakage	• Hinders mass transference	[99]

1.3 Electrochemistry

Electrochemistry can be defined as the field of chemistry that studies the interrelation of electrical and chemical effects [100]. There are two main topics, the investigation of chemical processes produced by the application of an electric current (electrolytic cells where Gibbs free energy increases ($\Delta G > 0$), and the investigation of the electric current produced by chemical processes (galvanic cells, $\Delta G < 0$). On the other side, electroanalysis is the application of

electrochemistry to solve real-life analytical problems. This area of chemistry presents advantages such as high sensitivity, or the possibility to perform an in-depth study of the system in a quick and easy way such as reaction kinetics studies, quantification of substances, or identification of compounds [101]. In addition, electrochemical devices present some properties that make them suitable for large-scale production and commercialization. Their main advantages are their low cost, the option to be miniaturized, their compact format, their easy operation, and/or the option to measure in situ.

Electroanalysis has a wide variety of methods, the two main groups are the interfacial and the non-interfacial methods. Interfacial methods are at the same time classified into two subgroups, the static and the dynamic ones. In the first case, the current is equal to zero while in the second case there is a flow of current (I≠0) due to redox reactions. When dynamic methods are employed, there is the possibility to control the potential, to control the current, or to measure the capacitance (impedance methods) [100,102]. A descriptive diagram is presented in Figure 1.13.

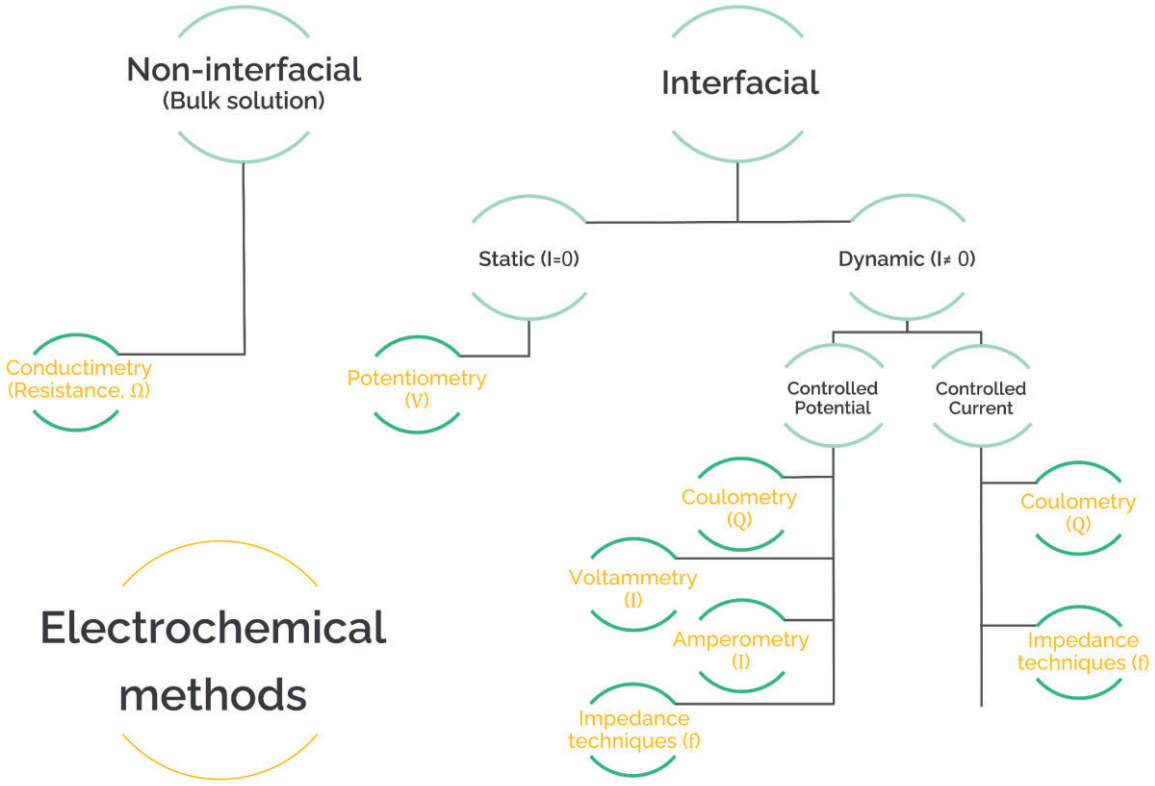

Figure 1.13. Overview of the most common electroanalytic methods.

In electrochemical cells may flow two kinds of currents, the faradaic and the non-faradaic. Faradaic currents, governed by Faraday's law, are defined in the IUPAC guideline as "*the currents produced by the electrooxidation or electroreduction of an electroactive substance*". While non-faradaic currents are produced with no charge-transfer reactions; for example, the ones produced by the diffusion of charged species, the adsorption, or the chemical changes of the solution [103].

According to some reference handbooks of electrochemistry, the most important electroanalytical methods are potentiometry, conductometry, coulometry, amperometry, voltammetry, and impedimetric techniques [100,102–104].

- *Potentiometry*

Potentiometric techniques are based on the measurement of the electrochemical cell potential across an ion-selective membrane when the current is equal to zero. One example is the pH meter, which is based on a glass membrane electrode.

- *Conductometry*

Conductometry techniques measure the electrolytic conductivity between two electrodes in a solution. Conductometric titrations are the most popular.

- *Coulometry*

Coulometric techniques measure the electrolytic reduction or oxidation of the analyte in a certain period of time. There are three different variants: coulometry at a constant potential, coulometry at a constant current, and electrogravimetry. In the first two, the amount of electricity consumed or produced due to the electrolytic reactions is measured, while in the last case, the mass increment of the electrode caused by the electrolytic deposition of the analyte is determined.

- *Amperometry*

Amperometric techniques measure the current associated with the redox reactions as a function of the time when a fixed potential is applied.

- *Voltammetry*

Voltammetric techniques measure the current as the potential is varied over time as a function of the applied potential. Since this is the chosen method to carry out the experimental part of the present dissertation, it will be discussed deeply in §1.3.1.

- *Impedimetric Techniques*

Impedimetric techniques measure impedance, in other words, they measure the frequency dependent resistance to the current flow. The most used technique in (bio)sensors is Electrochemical Impedance Spectroscopy (EIS), in §1.3.2 will be further discussed.

1.3.1 Voltammetry

In 1959 Jaroslav Heyrovsky won the Nobel Prize for discovering the polarographic methods. Who contributed to setting the basis for the modern voltammetric methods.

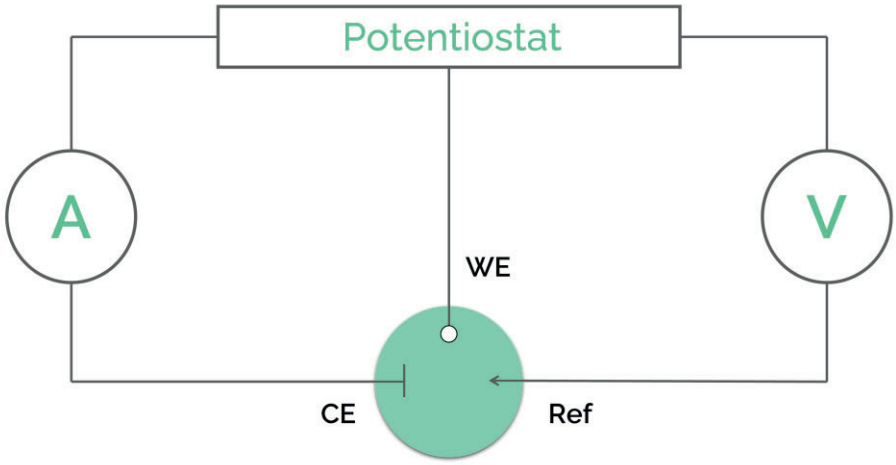

Figure 1.14. Schematic representation of the typical electrochemical cell based on a three-electrode configuration.

The electrochemical cell typically used for the voltammetric measurements is based on a three-electrode configuration. The electrodes are the working electrode (WE), where the redox reaction occurs, i.e., the sensor; the second electrode is the reference (Ref), as seen in Figure 1.14, Ref is used to control and ensure the applied potential; and the last electrode is the auxiliary or counter electrode (CE) which is used to close the circuit. With this configuration, both WE

and CE can work as anode or cathode depending on the potential applied to the system. As it can be deduced, the recorded signals will depend on the potential applied between the WE and the Ref electrode. The most common reference electrodes are the Saturated Calomel Electrode (SCE) and the one based on Ag/AgCl.

Since the electrochemical processes happen on the surface of the WE, some mechanisms move the species in solution. The most important ones are the movements from the place where the redox reaction takes place to the bulk solution and vice versa. There are three types of mechanisms, migration, caused by the influence of the electric field; convection, which is originated by a force in the solution such as agitation or bubbling; and diffusion, caused by the gradient of concentrations. In voltammetric experiments, migration is reduced to almost zero adding to the solution a supporting electrolyte. The supporting electrolyte also named inactive electrolyte, is a non-electroactive salt with high ionic strength and conductivity. When no external force is applied it can be considered that the unique mass transport effect is diffusion.

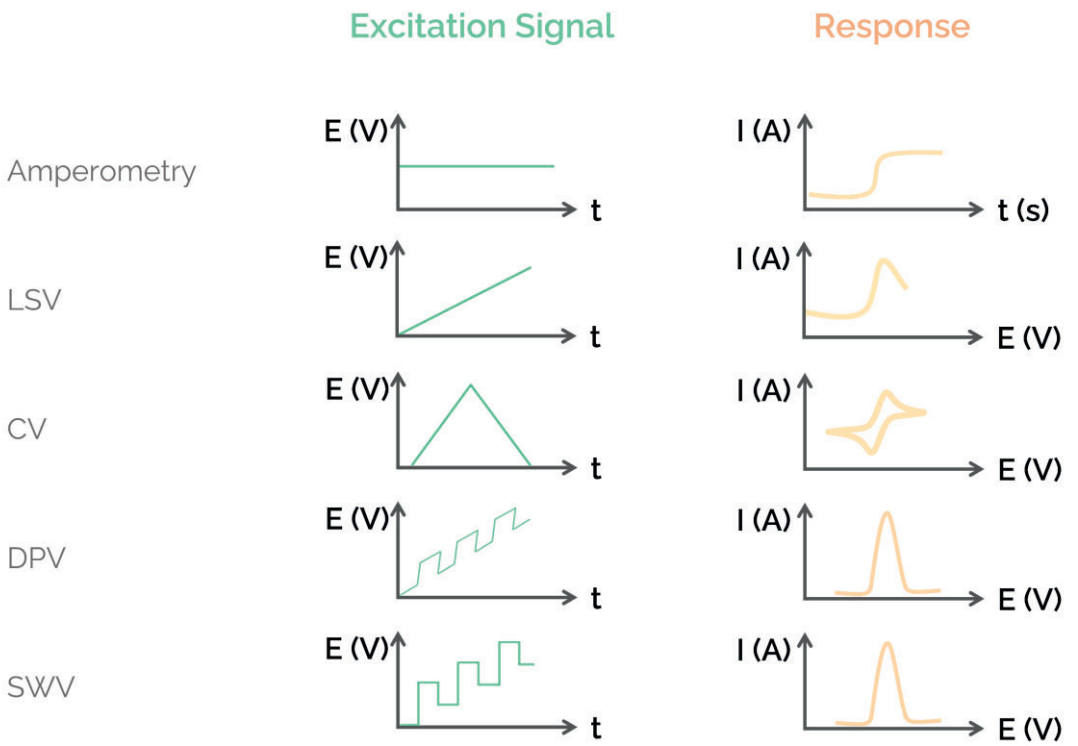

Figure 1.15. Summary of the main voltammetric techniques depending on the applied excitation signals.

As Figure 1.15 depicts, exist various types of excitation signals leading to the different techniques. Among them, the more appropriate one will be chosen according to the information to be extracted from the study. The most standard ones are the linear sweep voltammetry (LSV), the cyclic voltammetry (CV) (triangular function shape), the differential pulse voltammetry (DPV), and the square wave voltammetry (SWV). In LSV, the potential is increased linearly as a function of time; when this is reversed, thus forming a triangular potential scheme, it is known as CV, where the potential function describes a cyclic variation increasing and decreasing at the same scan rate. The cycle can be repeated as many times as desired. Another possibility is the application of pulsed potentials. When regular pulses are combined with a linear sweep function it results in a differential pulse signal, whereas when it is combined with a staircase shape it results in a square wave signal. In this scenario, the current is measured at the beginning and the end of the pulse in DPV or only at the end of the pulse in SWV.

In general, should be aware of the depiction of the voltammograms (plot of current (I) *vs.* potential (E) for a given system), because historically, European and American researchers have disagreed on their nomenclature IUPAC recommends the use of positive potentials for oxidation reactions (anodic currents), plotted at the right of the origin, and negative for the cathodic currents, at the left of the origin. Meanwhile, the American convention adopted the opposite style, to clarify the explanation Figure 1.16 depicts both notations [103,105]. Herein, unless oppositely indicated, the IUPAC guidelines will be followed.

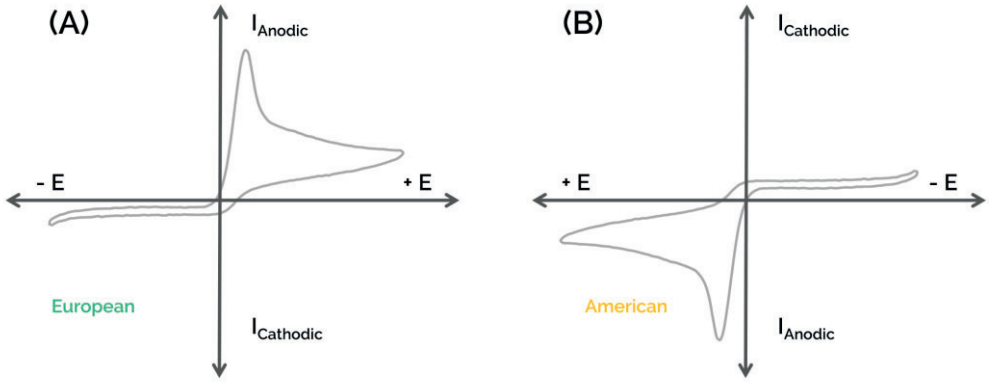

Figure 1.16. European (A) and American (B) nomenclature conventions for voltammograms.

The control of each technique is given by their individual characteristics and there is, therefore, a wide range of parameters to be optimized. As expected, tuning these parameters can vary the data extracted from the same sample. When the technique is being implemented it must be meticulous and optimize together all the parameters being conscious that some compromises have to be taken. It is then when the experience is of value.

From the mentioned techniques CV and DPV are the most usual in voltammetric investigations. CV is an interesting technique that is typically used at the starting points of the investigation because the anodic and cathodic response can be observed in a single measurement, making it an appealing technique to screen and get to know the redox system. On the other hand, since the DPV shows better performance than CV it is employed when the system is already characterized.

1.3.1.1 Cyclic Voltammetry

CV is a voltammetric technique that allows examining, over a wide range of potentials, numerous electroactive compounds, including intermediate products, in a sample. CV is not only employed to determine redox substances but also widely used to characterize the sensor behavior. Thanks to the information extracted from the I *vs.* E plots, it can be studied the surface in front of a standard electrochemical analyte, being possible to know some interesting parameters such as its charge transfer ability or its actual active area.

Figure 1.17A is shown an example of a CV voltammogram for an electrochemical standard, the pair redox $[Fe(CN)_6]^{-3/-4}$. In the same figure, the main information needed to understand the resulting CV plot is also depicted. In essence, the parameters involved in the peak analysis are the current and potential of the anodic and cathodic peaks, indicated as E_{pA}/I_{pA} and E_{pC}/I_{pC}, respectively. These values are obtained from the maximum of each peak. Taking into account the respective baseline it can be calculated the area and the height of each peak. Furthermore, the picture presents the limiting or switching potentials (indicated in the figure as E_i and E_e). Normally, the scanning window starts and ends in regions where no electrochemical reactions take place.

As mentioned above, voltammograms can give more information. For instance, it can be observed the reversibility of the chemical reaction. The example of Figure 1.17A shows a total reversible case, that is when under ideal circumstances I_A and I_C are equal in absolute value leading to a Nernst form relation. Moreover, the peak potential difference is *ca.* $0.0592/n$, where n is the number of electrons participating in the semi-reaction. If these requirements are not fulfilled, the CV voltammograms are shown as quasi-reversible (Figure 1.17B) meaning that the charge transference is sluggish, or irreversible (Figure 1.17C) when the return peak is absent.

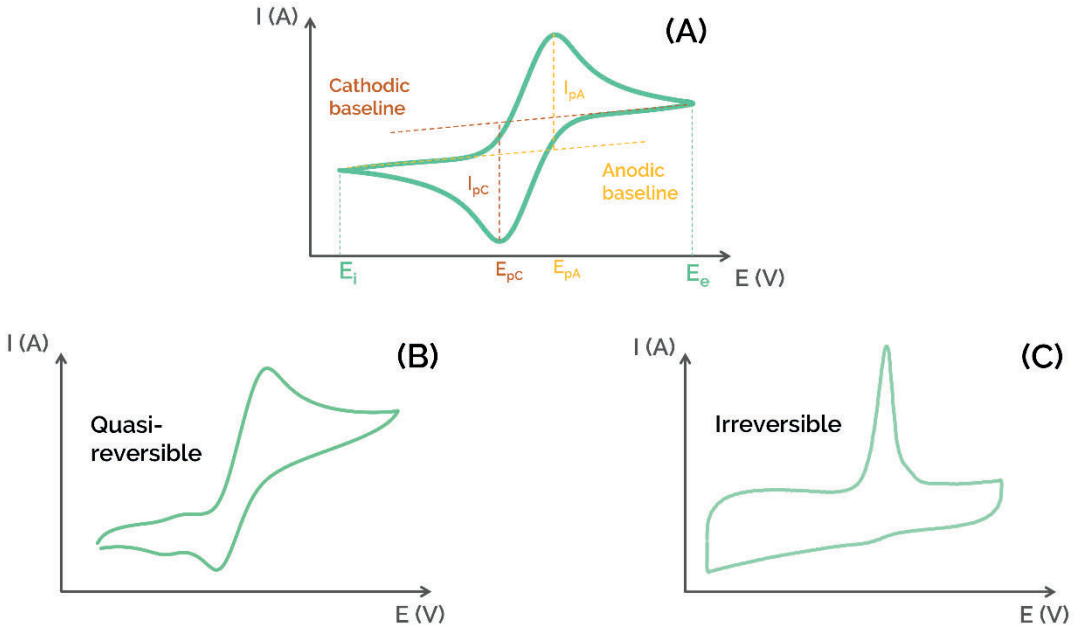

Figure 1.17. Example of CV voltammograms. It is observed (A) a reversible electron process and the most significant information (B) a quasi-reversible voltammogram and (C) an irreversible voltammogram.

The quantitative information of CV, also valid in LSV, is given by Randles-Ševčík equations, different for reversible (Equation (1)) and irreversible (Equation (2)) situations.

$$I_r = 0.446zFAc_0(zFDv / RT)^{1/2} \qquad \text{Equation (1)}$$

$$I_{irr} = 0.496(\alpha z')^{1/2}zFAc_0(FDv / RT)^{1/2} \qquad \text{Equation (2)}$$

Where I is the current in A, z is the number of electrons participating in the electrochemical reaction, z' the number of electrons before the determining step, F the Faraday's constant (96485 $s{\cdot}A{\cdot}mol^{-1}$), c the concentration in the bulk solution

($mol \cdot cm^{-3}$), R the gas constant (8.314 $kg \cdot m^2 \cdot s^{-2} \cdot K^{-1} \cdot mol^{-1}$), T the temperature (298.15 K), A the electrode active area in cm^2, D the diffusion coefficient for the measured compound ($cm^2 \cdot s^{-1}$), and v the applied scan rate ($cm^2 \cdot s^{-1}$).

1.3.1.2 Differential Pulse Voltammetry

In pulse methods, the current at the precise moment at which the difference between the faradaic curve and the capacitive current is maximum is measured. In DPV, as detailed in Figure 1.18, regular pulses with a sequential increase of the baseline voltage are applied. The pulses normally have amplitudes between 10 and 100 mV, and heights between 10 and 100 ms. The current sample is taken in S_1 and S_2, just before and after the pulse, the sample period goes from 10 to 20 ms [102,103]. The final current graph is generated by measuring the current increment for each pulse as a function of the potential, this is where the name of the technique comes from. The final display is a linear voltammogram where a peak appears, which height is directly proportional to the analyte concentration when a redox reaction takes place. The potential where the peak appears, for a reversible redox reaction, is defined by Equation (3), where $E_{1/2}$ is the half-peak potential, in other words, the potential corresponding to the current that is the one-half of the total peak current.

$$Ep = E_{1/2} - \frac{\Delta E}{2} \qquad \text{Equation (3)}$$

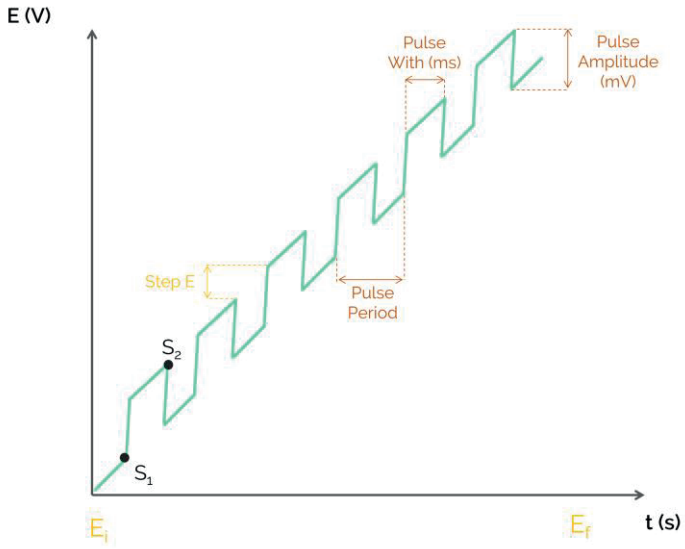

Figure 1.18. Excitation signal for DPV and corresponding parameters.

DPV presents some advantages given its inherent properties, such as excellent sensitivity, reduction of fouling onto the WE, and the ability to differentiate between compounds with similar redox potentials. The enhanced sensitivity of DPV can be attributed to different factors. The first one is the increase of faradaic current. Since the inter-sampling periods in DPV are shorter than in other voltammetric techniques, the precise moment when current increases before it arrives at the steady state can be monitored, that is, when the measure depends on the diffusion. The second point is the decrease of the non-faradaic current. The capacitive current is given by the charged double layer formed in the electrode surface. This charge decays even faster than the faradaic current. Thus, when the subtraction is made is obtained mainly faradaic currents, reducing the capacitative contribution and increasing in this way the signal to noise ratio.

1.3.2 Electrochemical impedance spectroscopy

Electrochemical Impedance Spectroscopy (EIS) is an electrochemical technique that measures the impedance as a function of alternating current (AC) frequency, the most common is carried out at constant potential. Impedance describes the electric resistance (R) of an AC electric circuit. When a simple electrical circuit is studied, R is defined by Ohm's law, Equation (4), but when AC perturbations are applied the equation change the R by the impedance (Z), see Equation (5). The total impedance of EIS data can be displayed as a vector, defined by the Z magnitude (Z_0) and the phase angle (φ), or by a complex number, $Z = Z_r + Z_i$, where Z_r is the real part of Z, and Z_i is the imaginary part. Both expressions are mathematically equivalent, as will be discussed over the next paragraphs.

$$E = IR \qquad \text{Equation (4)}$$

$$E = IZ \qquad \text{Equation (5)}$$

A sinusoidal potential can be defined by Equation (6), where $E(t)$ is the potential at time t, E_0 is the signal amplitude, and ω is the radial frequency ($\omega = 2\pi f$, where f is the frequency in Hz). The response to the AC potential is a sinusoidal current as a function of t, with the same ω, and a φ offset angle (Equation (7)). A schematic representation is shown in Figure 1.19.

$$E(t) = E_0\, sin(\omega t) \qquad \text{Equation (6)}$$

$$I(t) = I_0\, sin(\omega t + \varphi) \qquad \text{Equation (7)}$$

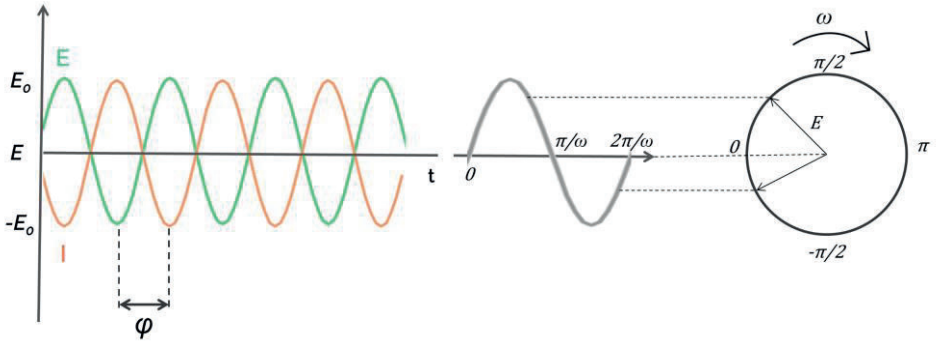

Figure 1.19. Schematic representation of the sinusoidal potential wave applied and the related current measured.

So then, taking into account Equation (5), Equation (6), and Equation (7) an alternative equation to Ohm's law for calculating the impedance of a circuit can be deduced (Equation (8)).

$$Z = \frac{E}{I} = \frac{E_0 \sin(\omega t)}{I_0 \sin(\omega t + \varphi)} = \mathbf{Z_0} \frac{\mathbf{sin}\,(\boldsymbol{\omega t})}{\mathbf{sin}\,(\boldsymbol{\omega t} + \boldsymbol{\varphi})} \qquad \text{Equation (8)}$$

Considering Euler's formula for general angles (Equation (9), where $j = \sqrt{-1}$), impedance can be represented as a vector that uses complex number notation (Equation (10), Equation (11), and Equation (12)).

$$e^{(j\varphi)} = \cos(\varphi) + jsin(\varphi) \qquad \text{Equation (9)}$$

$$E(t) = E_0\, e^{(j\omega t)} \qquad \text{Equation (10)}$$

$$I(t) = I_0\, e^{(j\omega t - j\varphi)} \qquad \text{Equation (11)}$$

$$Z = \frac{E}{I} = Z_0 e^{(j\varphi)} = Z_0\big(\cos(\varphi) + jsin(\varphi)\big) = \boldsymbol{Z_r} + \boldsymbol{jZ_i} \qquad \text{Equation (12)}$$

Figure 1.20 shows two typical plots used to represent EIS data, Nyquist and Bode plots. The Nyquist plot, shows the absolute value of the imaginary part (Z_i) *vs.* the real part (Z_r) of the impedance for different frequencies (ω), providing a visual representation of the electrochemical interface. Low ω are at the right part, while high frequencies are at the left part of the Nyquist plot. On the other side, the Bode diagram depicts $log|Z|$ and *φ (from -90º to 90º) vs.* $log(\omega)$. In this case, the graphic includes more detailed information. The advantage of Bode

representations is that it is more sensible than Nyquist ones, being easy to identify small changes. All components of an electrical circuit that cause an angle offset, i.e. capacitors or inductors, will contribute to Z_i whereas, the other ones will be included in the Z_r, (i.e. resistances).

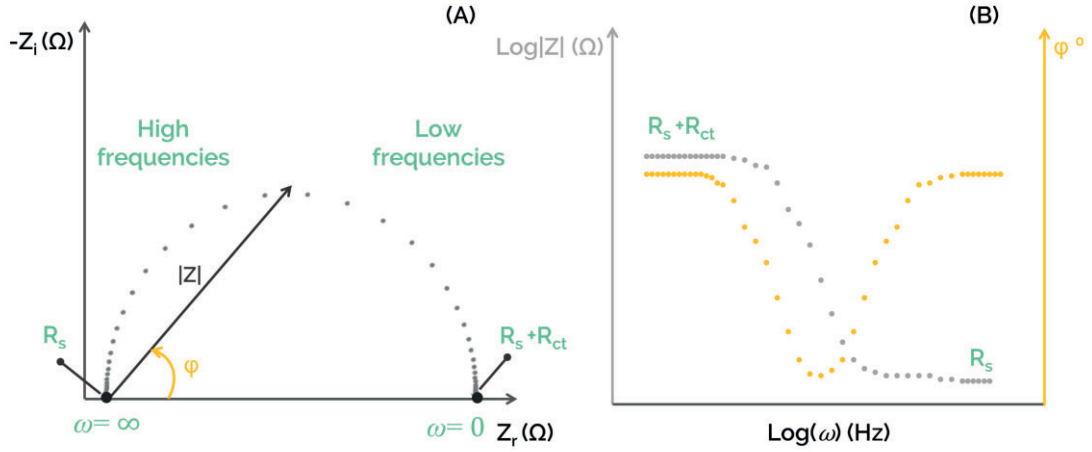

Figure 1.20. (A) Nyquist and (B) Bode plots.

As detailed with CV, recorded data can be analyzed to extract parameters that allow the characterization of the electrode or the quantification of analytes. To this aim, the electrochemical system can be modeled by a combination of electric components such as resistors, capacitors, constant phase elements, or inductors. The result is an equivalent circuit. Hence it is possible to fit the impedance data to the most common equivalent circuit to understand and calculate some parameters of the target case. Two common circuit and their corresponding Nyquist plots are schematized in Figure 1.21.

The simplest electrochemistry circuit includes an R_1 connected in series with a capacitor (C) and an R_2 connected in parallel. The first resistance, hereinafter referred to as R_s, is related to the resistance of the solution; R_2, from now on R_{ct}, is the charge transference resistance between the solution and the electrode surface; and C describes the effect of the double layer that appears onto the surface of the electrode. Figure 1.21A and Figure 1.21B show how each element is represented in an electrochemical system and their representation in a Nyquist and Bode plot.

In some cases, it is necessary to consider one more parameter, the Warburg element (W), associated with the mass transference between the

solution and the sensor surface, in other words, the diffusion process. Taking the previous circuit, W is added in series with R_{ct} (in parallel to C). This circuit is generally named Randles equivalent circuit and is by far the more commonly used in (bio)sensing. In the Nyquist plot, this element is observed as a straight line of *ca.* 45º in the low-frequency part of the actual semicircle.

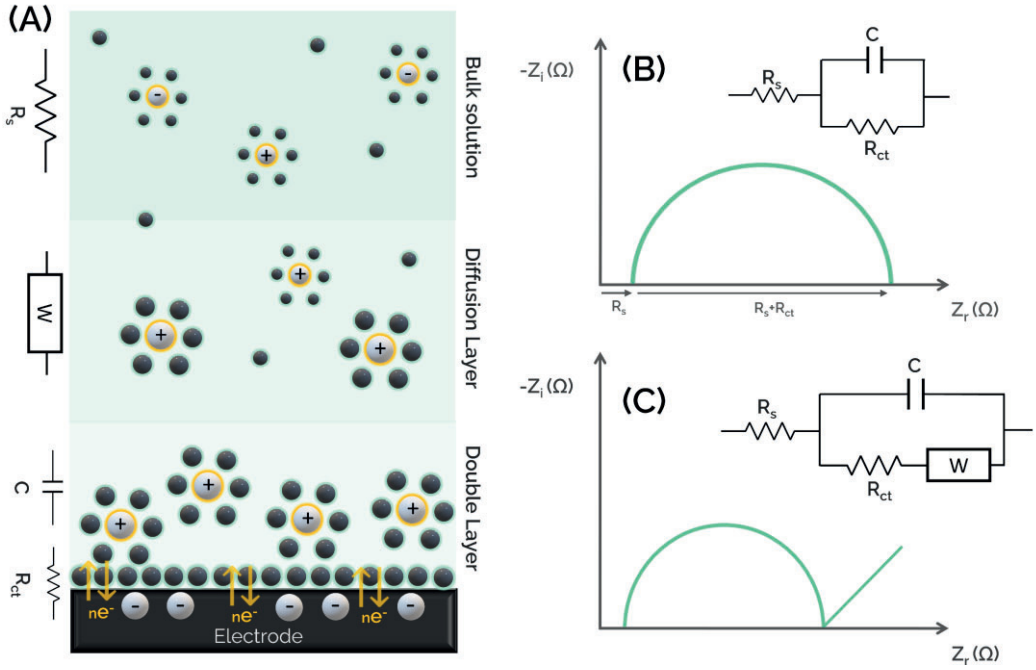

Figure 1.21. (A) schematic representation of EIS measurement and (B and C) the most common equivalent circuits used in EIS. In the left part, it is depicted the different layers produced in an open circuit potential. Where is found the movement of opposite charges, the target analyte solvated by the electrolyte traveling from the bulk solution to the charged surface electrode. Onto the surface, it is also observed the polarized solvent molecular layer.

To compensate for the non-ideal characteristics of most electrochemical cells, the C is replaced by a constant phase element (CPE). Its impedance is given by Equation (13) where α varies between 0 and 1. When it values 1, it is equivalent to a capacitor, while if it values 0 it is equivalent to a resistance.

$$Z_{CPE} = \frac{(j\omega)^{-\alpha}}{C} \qquad \text{Equation (13)}$$

Impedimetric techniques have despite being complex, have benefits that make them powerful. Some examples are the high precision, wide measurement ranges, or the ease to work with simplified and theoretical systems. For these reasons, EIS is used in a wide range of fields as studies and development of

corrosion [106], coatings [107], batteries [108,109], kinetic mechanisms [110,111], or biomedical and biological systems [112,113] among others.

1.4 Biomimetic systems

Investigators of a wide range of study areas are continuously discovering new and improved methods to overcome the actual arising issues. Since the Big Bang, the universe is continuously optimizing evolving towards the most optimal form. Thus, why not base our investigations on its experience? A popular example of nature-inspired gadgets is *Velcro*®, George de Mestral based his investigation on the burdock plant, whose seeds have a special kind of hooks that allow them to stick to the fur and fibers to reach a larger propagation area. Another example is the aerodynamics of the actual vehicles, inspired by animals such as birds or rapid mammals.

Although it is widely known that researchers and inventors have relied on nature many times, it was Otto Schmitt who coined the term "*biomimetics*". It was by 1957 when the physician used this word in his doctoral thesis, which was focused on the development of a device that mirrors the function of nerves propagation [114]. Nowadays, Collins dictionary defines biomimetic as "*a human-made product imitating nature or a natural process*" [115].

In particular, analytical chemistry is not different, and some biomimetic strategies can be found in the literature. Molecularly imprinted polymers (MIPs) are an exemplification of this concept. MIPs are polymers built specifically for one compound, acting in this way as an antibody or enzyme. Its combination with sensors leads to a powerful tool that is specific and sensible while avoiding the disadvantages that arise when working with biological elements [84,116]. A further instance are nanozymes, which, with similar aims to MIPs, attempting to address biological drawbacks by means of nanomaterials with enzyme-like behavior [117,118].

In the herein work, one objective is the use of (bio)electronic tongues ((bio)ETs), that as its name indicates, is a biomimetic system that mirrors the animal sense of taste. Although not only ET but also electronic noses (ENs), eyes (EEs), and even electronic skins (ESs), are also present in the bibliography.

As commented in §1.2.2, the development of a system presents some difficulties, the mimicking of animal senses was a response to the claims of the scientific community to obtain methods that determine the whole sample in the shortest time possible obtaining at the same time the maximum information.

1.4.1 Multisensor systems, the concept

Humans perceive the world through different senses, classically are enumerated as sight, smell, taste, touch, and hearing, but nowadays a couple more have been added to the list, balance, and movement. However, some researchers question the individuality of all the senses, believing it is more appropriate to describe them as a plural, given that to perceive an entity, the senses complement each other [119].

The sensing process starts with the specialized cells from each sensorial organ, which receive a stimulus and sent it to the brain as an electric signal via the nervous system. It is then when the brain forms a perception. Hence the system acts as a sensor where the receptor processes information to send a primary signal to the transducer which produces a secondary signal processed in a device to transform it to interpretable data.

As measurements, senses are affected by the environment. Life animals have a sensing threshold, similar to the chemical LOD, that is continuously evolving during our live by the acquisition of experiences. Moreover, the senses depend on the perception created by the brain, which is not always faithful to reality [119,120]. These facts difficult the artificial reproduction of the senses. When trying to mimic taste and smell, often classified as chemical senses, because they are related to the detection of changes in sample chemical composition, certain considerations must be taken into account. The main handicap is the lack of information about how works the natural perception function since similar chemical structures cause totally different perceptions. Furthermore, the perception of stimuli does not depend only on the chemical concentration, but also on synergism such as antagonism, and masking, among others.

In the herein project, the tongue will be the only studied system, hence Figure 1.22 is focused on the explanation of the analogy between natural *vs.*

artificial sensing processes. As shown in the first steps of Figure 1.22, the basis of the artificial process is the use of an array of non-specific electrodes equating to the biological receptor cells, which perceive the chemical changes of the sample. Afterward, the data is studied with effective mathematical tools to extract and process the recorded information, as the brain does, and finally, interpret the resulting data. As commented before, the biological sensing process changes with the experience, and this characteristic is also mimicked in the artificial case, where the ET must pass through a learning progress to identify the target fingerprints. Is for these reasons, that it is said that ET is a biomimetic system that mirrors the biological recognition system. But is important to note that what is mimicked is the sensing process, not the final application of the sensing organs. In other words, what is reproduced is the way how the information of the sample is extracted, and the analogies with the involved organs, but there are differences such as the number of sensors, or/and their operationality [121].

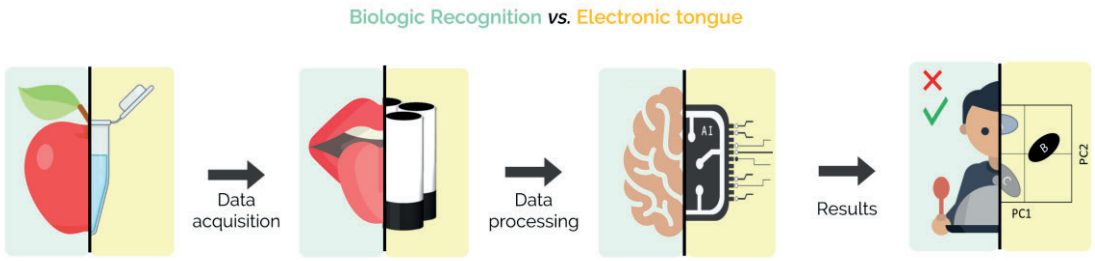

Figure 1.22. Comparison between the biological recognition system and the artificial system carried out by (bio)electronic tongues.

These kinds of arrangements are now applied in both qualitative and quantitative analysis. Qualitative analyses are used normally to classify the samples by their properties, while quantitative analyses are more difficult due to the complexity of the data treatment, but present a better acceptance among the analytical community because allow the simultaneous identification of the quantify the target analytes in complex samples.

Multisensor systems (MSS) present many advantages over the more classical analytical arrangements. One of the relevant points is that not only studied only one of the characteristics of the sample, but also a whole set of occurrences. As the brain does, chemometric tools create a model able to predict and recognize patterns in the sample. This quality permits the reduction of matrix

interference effects, thus facilitating the preparation of samples for their analysis avoiding physicochemical pre-treatments. Also is of significant interest in qualitative analyses owing to not being necessary to carry out a study to connect the analytes with a concrete feature as are considered the overall fingerprint.

As stated, the built model recognizes patterns in the responses and relates them with the content of the sample, this fact lets the user identify compounds that appear overlapped in the instrumental response. Hence using a set of non-equal sensors that apparently cannot achieve the resolution becomes feasible with this kind of approach.

Moreover, MSS might not require a specific optimization for each application as when using unspecific sensors, the layout can be applied to a wide range of cases only with tiny changes in the technique parameters.

Nevertheless, there are also some disadvantages which must be commented. As mentioned in §1.2.2, the ideal (bio)sensor must present some properties that not always are fulfilled. In MSS most of them can be overcome, but some of the others become even more relevant. More often than not, sensors present a drift during their lifetime, causing mandatory readjustments or renewal of the created models for a certain analyte. Some of these effects are caused by the fouling of sample compounds onto the surface of the WE, or by the inhibition/leakage of the (bio)recognition elements. Although this drawback can be solved with different proposals such as cleaning steps between samples measurements, regeneration of the surfaces of the sensor, or even replacing the WE every a certain number of measurements; the experimental procedure becomes more complex and tedious as more stages are added.

At the same time, one of its more attractive qualities is one of its most tedious handicaps. The learning stage involves the measurement of a large number of samples to enrich the model and represent as better as possible the experimental environment. Furthermore, it is not only necessary to feed the model but also to validate it, requiring an external set of samples to test the truthfulness of the results. At the same time, apart from dedicating effort and time to train MSS, it is also necessary to have a general understanding of the problem willing to figure out, since it has to be described as accurately as possible.

Besides that, while the performance of the experiments does not require highly trained staff, the statistical calculations do.

Overall, the above-exposed issues with MSS cause marginal application cases in industry and when used is as a screening procedure to apply a posteriori a classical method for the final determination.

1.4.1.1 Electronic tongue

The senses are designed to be aware of essential situations, depending on the species organoleptic system had evolved distinctly. In the case of mammals, it is well known how the olfactory system works, but the taste system is still underinvestigated.

As seen in Figure 1.23, the mammalian oral cavity has bulbs named papillae that contain the taste buds, the receptors of taste. Taste buds are shaped by cells with different functionalities (see the lower right part of Figure 1.23). Stimuli, originated by soluble compounds, travel from the oral cavity through facial and glossopharyngeal nerves until arriving at the brain. The orbitofrontal cortex is in charge of the connection between the raw signal (simple sensations of taste) and the final flavor [122].

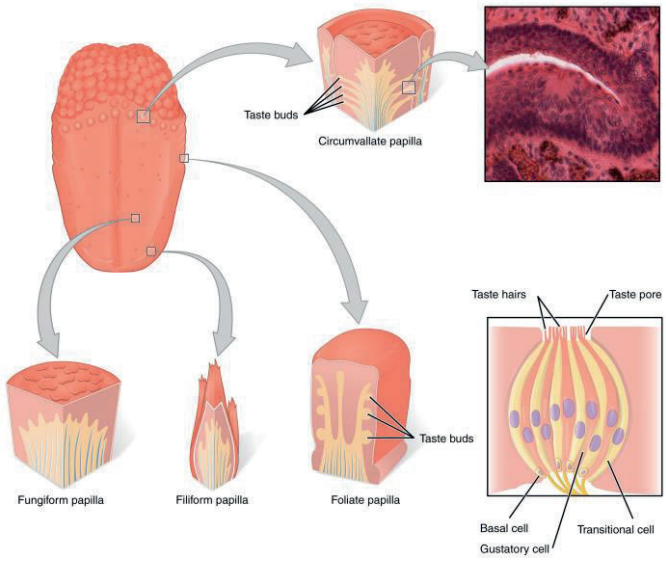

Figure 1.23. Description of the oral cavity and the disposition and structure of receptor taste cells on it. Image from the Textbook OpenStax Anatomy and Physiology.

The role of the receptors is broadly discussed in the bibliography. It is supposed that taste cells work as the olfactory receptors do. Meaning that every

cell detects multiple tastes, and a taste is detected at the same time by multiple distinct cells. In this way, the stimuli are processed by the combination of non-specific chemosensory transductors allowing to distinguish between a wide range of tastes [123,124]. For now, it seems that the widespread belief of the existence of a taste map is refuted, but on the other side, it is true that each zone of the tongue is indeed more sensible to one of the tastes [122,125].

IUPAC defines the ET as "*an analytical instrument comprising an array of nonspecific, low-selective, chemical sensors with high stability and cross-sensitivity to different species in solution, and an appropriate method of PARC and/or multivariate calibration for data processing*" [126]. Thus, an ET is an analytical system structured by an electrode array (commented in §1.2.4) that measures liquid samples and generates high dimensionality data, which is treated via chemometric tools to obtain a descriptive model of the aimed question.

In 1985, M. Otto and J. Thomas suggested the use of multisensor approaches for the analysis of free metal ions in liquid samples using non-specific ion-selective electrodes [58]. After some works focused on the topic in 1995 Y. Vlasov *et al.* put forward the first paper describing a sensor array as an ET [59]. In this work, the qualitative classification of some beverages was achieved. Almost simultaneously, the research group of Professor K. Toko opened a new trend on ET systems. They focused their work on the application of sensor arrays as an artificial taste sense by mimicking the taste buds and their affinity to the five typical tastes (sour, sweet, salat, acid, and umami); the reason why in some works these approaches are separately from ET and named taste sensors (TS) [127]. Was Toko's group the first to introduce the ET approach to the industry, as an alternative tool able to work in-line contrary to human professionals, and able to deal with dangerous samples as pharmaceutic compounds [69,128].

A few years later, the bioET appear at the scene. In 2005, E. Tønning *et al.* used the term for the first time in 1999 when the first publication of an ET employing biological receptors was published [129,130]. A BioET is defined generally as a sensor array that uses at least one biosensor. Following the definition, it can be found several arrangements of bioETs, the most common are the ones that use enzymes, but nowadays examples with aptamers, DNA, cells, or tissues can also be found in the bibliography [131–134]. In this direction, the

arrays can be formed by biosensors modified with recognition elements with cross-reactivity, with the same element but coming from different species, or with the same element but with a distinct chemical mediator. For example, C. Medina-Plaza *et al.* presented a paper working with glucose oxidase or tyrosinase (Tyr) arrays that present different responses against the analyte depending on the electrochemical mediator used for the modification of the electrode [135]. Another example of enzymatic bioET is the work of J. Lange *et al.*, who used an array of three kinds of amine oxidases for the detection of biological amines in food samples [136].

Until now, ETs have been mostly developed to improve food industry issues [72,74,137–139], but nowadays there are also proposals to apply it to security control areas [140,141], to environmental science [142], or the pharmaceutical industry [75,143–145].

1.4.1.2 Other examples of electronic senses

Although ETs are widely used, those are not the only biomimetic sense nor were the first to be proposed. In 1982 Professors K. Persaud and G. Dodd presented an array of non-specific but complementary gas sensors to mimic the animal olfactory system, which was referred to in this work as [146]. In other words, ETs and ENs have similar characteristics, being the state of the samples and the techniques of measurement the relevant differences. Nowadays, the use of ENs is mainly focused on two areas: the medical and security area, or the food industry [147,148]. Some attempts to use ENs systems in medical studies are the works of P. Mazzone *et al.,* N. Fens *et al.,* and S. Dragonieri *et al.*, who determined volatile organic compounds (VOCs), from patients with respiratory system diseases with ENs [149–151]. Another example is the paper presented by M. Mamat *et al.* who designed an EN for the classification of different beverages (kinds of milk and juices) [152].

Other MSSs are, the electronic eyes and the electronic skin [153–156]. T. Pallejà *et al.* illustrated the huge potential of the EE when they designed a device for the guidance of blind people. Concretely the array of the “electronic withe cane” was a combination of a laser imaging detection and ranging (LIDAR) and an accelerometer [157]. Meanwhile, one example of ES is the paper presented

by Zhang *et al.*, who developed an ES able to detect an arterial pulse, temperature, or breathing, among other physiological parameters, based on the use of piezoelectric sensors modified with micropattern films [158].

Finally, as already stated in §1.4.1 with the human senses, some researchers do not focus only on one system, but on their combination. An approach known as data fusion. Data fusion means the merging of responses from hybrid analysis systems, such as an ET and an EN, a combination of ET, EN, and EE, or even two equal systems with different arrays or measurement techniques. These methods are inspired in the plurality of the sense, commented in previous sections. One example is the analysis of wine; when humans evaluate a glass of wine, it is appraised the taste but also the appearance and the aroma. As could be expected, this is a challenging perspective because it must deal with data of high dimensionality, but also it must take into account the weight given to each sensor, with obviously non-comparable signals due to their different natures [159,160].

1.5 Multivariate analysis

The current picture in analytical chemistry is the obtention of valuable systems for the detection of as many as possible compounds in the shortest timeframe. One example is the at/in/on-line analyzers. In this case, a continuous flux of data is sent to the databases to analyze and follow the given procedures [161]. Owing to the large amount of data to be continuously analyzed and the latest computing improvements, the use of advanced mathematical tools has become increasingly prevalent over the last few decades. Concretely, in the late twentieth century in the chemistry study area appeared a new discipline named chemometrics. Chemometrics was coined by Svante Wold in 1972 as the word to define the field that deals with the extraction of information from the carried out assays. In 1997 Professor D. Massart *et al.* proposed a new definition, still in effect, "*Chemometrics is a chemical discipline that uses mathematics, statistics, and formal logic: (a) to design or to select optimal experimental procedures; (b) to provide maximum relevant chemical information by analyzing chemical data; and, (c) to obtain knowledge about chemical systems"* [162]. Since then, this discipline has become more popular, one example is the number of publications,

being more than 11200 works including "*chemometric*" as a keyword (data from Scopus, from 1979 to 2022). Another example is the new ICH guideline, which considers the multivariate statistical analysis (not yet published, but in preparation).

At these early stages, in the electrochemistry area, the chemometric tools used were of a basic level, but as the experiments have become more complicated, more advanced approaches, such as genetic algorithms, have been applied. Initially, techniques such as potentiometry were used in ET systems, but when CV experiments were performed the usual statistical tools were not enough. With CV measurements, richer data were obtained but requires in most cases of the data pre-treatment facilitating the later computing. Generally, these previous steps consist of the compressing of the data by screening the relevant information from the non-relevant features and the noise.

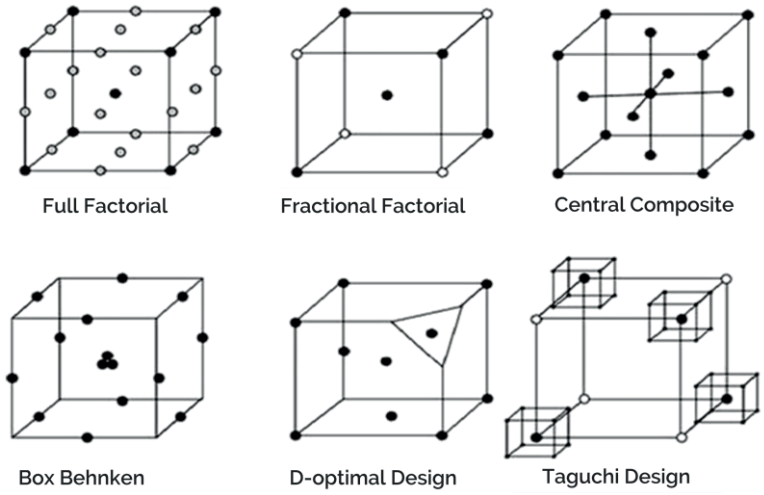

Figure 1.24. Schematic representation of most famous experimental designs

As abovementioned, chemometrics has three main uses, the first one is the design and optimization of experiments. Multivariate design of experiments (MDOE) is addressed to obtain the best experimental design by performing as few experiments as possible to obtain the maximum amount of information. The final results contemplate the most relevant interactions between the studied variables. One of the crucial steps in this approach is the distribution of the tested points in the whole experimental domain and carrying out it efficiently. Full factorial designs are the most common sample distributions when few variables are studied, hence it considers the full combinations of all levels of each variable.

These approaches give a lot of information because scan the entire experimental domain, but at expense of loss of time and effort. For this reason, when complex arrangements are studied, more optimal designs such as fractional factorial design, D-optimal, or Taguchi are taken into account. A schematic representation of different experimental designs is seen in Figure 1.24.

Regarding the description of chemometrics, the other two functions are related to the exploration and analysis of the recorded data. In this case, different mathematical tools can be employed. They can be classified by the final usage, as quantitative or qualitative, or by the data input, as supervised or unsupervised. Unsupervised tools are the ones that do not label the data, in these cases the algorithm finds hidden patterns in the introduced values. On the other side, in supervised tools, the model is fed with labeled data to train the algorithm to finally classify or predict the desired feature. Unsupervised tools are applied in exploratory analysis like in clustering, while supervised means are more focused on qualitative or quantitative systems.

1.5.1 Design of an electronic tongue

Generally, when the ET approach is applied, the system requires 5 steps (see Figure 1.25): selection of the sensors to be used, measurement of the set of samples, pre-processing (including weighting and compression of the obtained data) and building of the final model. Form these steps, only the measurement, and the modeling are mandatory, but they are recommended if it is wanted to exploit the approach to its full potential.

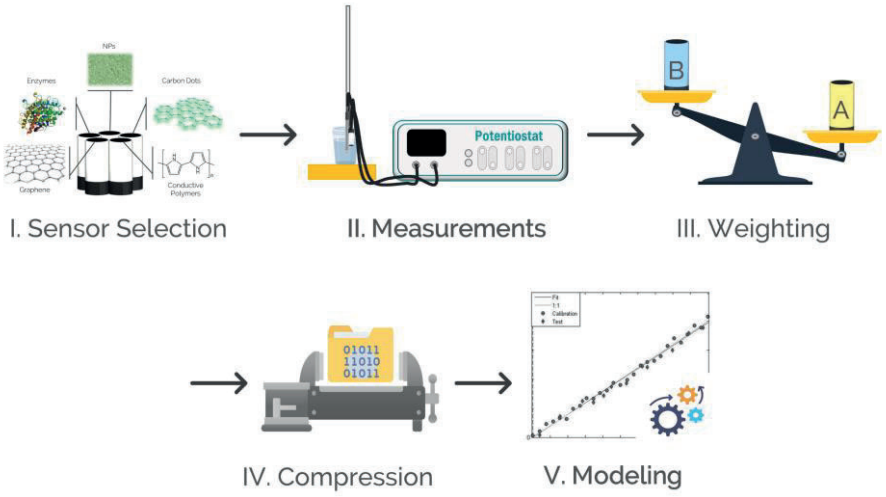

Figure 1.25. Recommended steps for data processing.

Sensor selection is not a field well explored in the bibliography. In the majority of works, it is used an array of sensors previously chosen by their ability to result in non-collinear responses. But new trends are appearing in the literature. One example is the work of D. Ortiz *et al.* or M. Sarma *et al.* who presented different index estimations for the selection of the best set of sensors for an ET system [163,164]. Concretely, in both papers, unsupervised clustering analysis was carried out to study the contribution of each sensor. In parallel to the selection of an optimal set of sensors, they must provide other essential characteristics in order to be able to proceed to the next step smoothly. Precision and operational stability are both required to proceed with an ET strategy, as it is highly necessary to avoid drifts in the sensors' responses.

The second step of the design of an ET is the measurement of the samples to feed the model. The samples must illustrate the whole experimental domain so as to it must be described as maximum information as possible, and consequently attribute to the model the generalization capability (ability to digest newly introduced data). This is a fundamental characteristic of a representative and consistent model. The number of samples and their distribution will be directly related to the final results. When the sample set is arranged, usually strategies similar to those of MDOE discipline are followed. As stated above, full factorial designs and variants as fractional factorial designs or tilted factorial designs are implemented (Figure 1.24). Once the design is established, and before measuring the samples, the order of those is usually randomized, so that, trends such as intrinsical errors, hysteresis, instrumental errors, or even handling errors, are prevented. Other easy tips are the periodical measurement of control samples or the remeasurement of some samples during the assay.

Once the data is recorded, a weighting step is highly recommended, but not mandatory. It must be considered that not always the individual responses can be compared directly because the variances and the scale between them are different. For this reason, is convenient to keep in mind the relative significance of each sensor. There are several tools for this purpose including centralization,

normalization, or autoscaling among others (see §1.5.2.1 for a more detailed description).

The next step is the dimensionality reduction of the recorded data, also named data compression. The reduction is achieved by only selecting the features with the most relevant data. Even though the response matrix is reduced, the computational work is reduced drastically. Also, the rule of thumb in all scientific investigations, the simpler the better. More information can be found in §1.5.2.2.

Finally, the last step is modeling. This is structured in two parts, the building of the model and its validation. The applied chemometric strategy will depend on the initial objective (for example the study of qualitative or quantitative systems). The validation of the model normally also determines which is the best architecture. These points will be further discussed in §1.5.3.1 and §1.5.3.2.

1.5.2 Data preprocessing

The preprocessing of the recorded data is made aiming to improve the signal/noise ratio, reduce and/or compress the inputs, and/or reduce the systematic errors or variations. Even though some modeling methods do not require this step it has been demonstrated that its use can improve the final results.

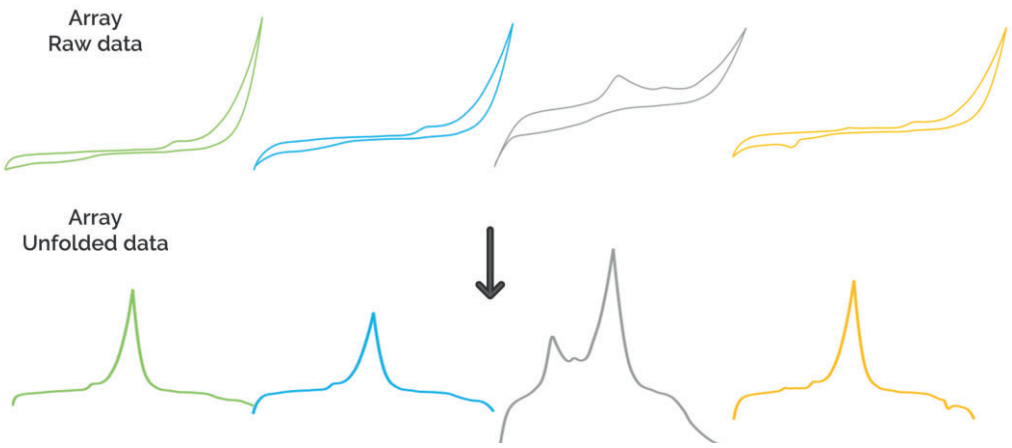

Figure 1.26. Schema of the unfolding of cyclic voltammetric data generated by a four-sensor array.

In some cases, the dimensionality of the voltammetric method hinders the use of some predictive methods which require monodimensional data. For this

reason, information must be adequate. Due to the ETs approach different electrodes have been used the final data set is a 3D tensor formed by n sensors, n variables (as currents associated with a voltammogram), and n samples. Consequently, intending to facilitate the computational work and adapt it to chemometric tools, it is recommendable to reduce the dimensionality of the matrix. One of the easiest ways to treat the raw data is making the unfolding the voltammograms. As Figure 1.26 shows, unfolding entails the direct elimination of the variable potential turning the measurement into a linear vector. This is a straightforward method, but it can sometimes constrain the building of the model. Owing to once the data is concatenated, each sensor brings a different variance. For example, the third voltammogram of Figure 1.26, in grey, can cause distorts in the optimization of the model [165]. For this reason, the softening of these effects can be achieved with a previous weighting of the data.

1.5.2.1 Weighting of data

Once the data is ready, the weighting step is highly recommended. In this stage, scales and variances are adjusted to guarantee that all the variables have a priori equal importance and therefore will not affect the statistical calculations. The most commonly reported methods are data centering, normalization, standardization, and autoscaling, also named standard normal variate transform (SNV). Moreover, other methods such as first and second derivates are also usually employed [166]. Note that these treatments can be used for rows or/and columns, depending on whether differences among signals or variables are corrected.

- Data centering

This approach refers all the data to the average value. Afterward, each group have an average equal to 0 ($\bar{x} = 0$).

$$x_i^* = x_i - \bar{x} = x_i - \frac{1}{n}\sum_{i=1}^{n} x_i \qquad \text{Equation (14)}$$

- Normalization

Consists of the scaling of the signal between two chosen values, typically -1 and 1 or 0 and 1.

$$x_i^* = \left(\frac{x_i - \min(x)}{\max(x) - \min(x)}\right)$$ Equation (15)

- Standardization

Corresponds to equate the dispersion from the array of sensors to obtain a standard deviation equal to 1 ($s = 1$).

$$x_i^* = \frac{x_i}{\sqrt{s_i}}$$ Equation (16)

- Autoscaling or SNV

This approach combines standardization and centering to acquire an $\bar{x}$ equal to 0 and a s equal to 1.

$$x_i^* = \frac{x_i - \bar{x}}{\sqrt{s_i}}$$ Equation (17)

1.5.2.2 Compression of data

As commented before data compression aims at minimizing the number of inputs (also named predictors), thus redundant information is discarded. There are multiple proposed compressing methods reported in the literature, being the most widely used principal component analysis (PCA) [167], sliced window integral method [168], kernel functions [169], fast Fourier transform (FFT), or discrete wavelet transform (DWT) [170]. Most compression methods can be classified under two groups, depending on how the original information is treated: feature selection or feature extraction. Briefly, the main difference between the two is that while feature selection selects data subsets maintaining the original data values, feature extraction “extract” the original data into a new feature space.

Feature selection

These methods aim at the selection of the most interesting variables from the raw data. It is a straightforward way to reduce the complexity of the data, while at the same time, it is obtained more robust and interpretable models rather than when all the voltammogram is analyzed.

- Manual selection

One of the easiest solutions to solve the high dimensionality issue is the manual selection of the variable. In electrochemistry being the redox peaks are

the most interesting features a priori. This method needs from a previous knowledge of the system. As expected, this subjective compression method is not one of the most used ones. On one side, is that it presupposed that all the relevant information is concentrated in the selected parts, and not always is feasible to select the whole and correct information subsets. On the other side, given the current computing power of today's computers and the new algorithms proposed in the literature, manual selection is falling into disuse. Nevertheless, still many works are using this method [171].

- Causal Index

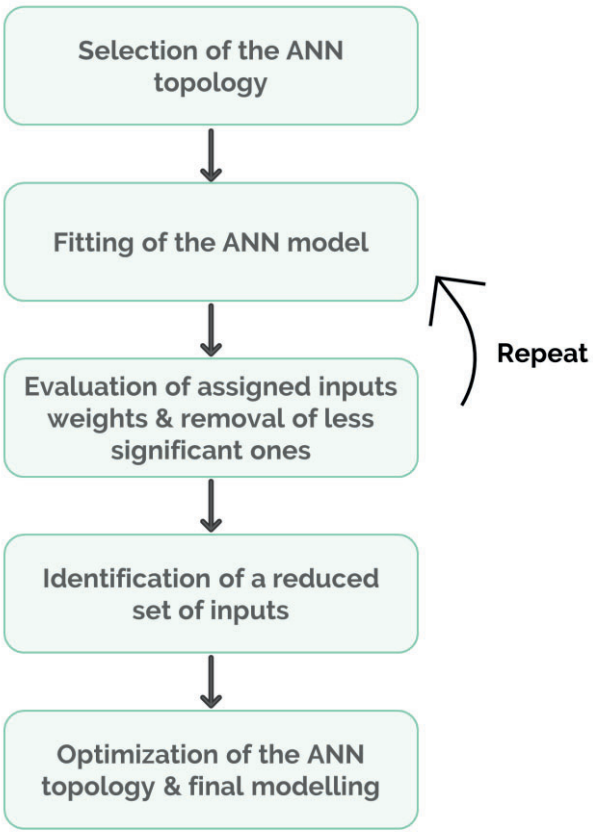

Figure 1.27. Flow chart of the necessary steps when the causal index method is used in combination with ANNs. At each iteration, the model is fitted in order to evaluate which inputs are the most relevant to the desired output.

Causal index (CI) is an iterative method that uses the modeling tool, normally artificial neural networks (ANNs), to select the most relevant inputs (discarding or pruning the lower ones) when the chemometric model is constructed. As seen in the flow chart of Figure 1.27, a first model is built with a certain initial setting and fed with the whole data. From it is selected the first set

of inputs studying not the final results but the weight given for the modeling tool to each one. The second stage is to repeat the modeling with the selected subsets to evaluate another time its relevance and prune the ones that do not contribute or almost make it. This step is repeated until achieving a near-optimal prediction subset of variables. Finally, when the data is selected, the model parameters are tuned as usual.

However, CI has also some drawbacks. Firstly, it must be taken into account that CI relies on the selected configuration of the model meaning that the initial point, in this case, the ANN configuration, will affect the final selected inputs. Secondly, the selected sets are not unique, and even more, can be overestimated if it is found a local change because the iterative calculation may run deadlocked. Lastly, it is a very time-consuming and computationally intensive tool.

Feature extraction

- Polynomial fitting

Polynomial fitting is a straightforward method to reduce data complexity. In this case, the voltammograms are fitted to typical polynomial distributions such as polynomial functions of n grade, sine and cosine functions, Legender polynomes, or gaussian among others. Figure 1.28 shows a graphical representation of the first four Legender polynomials and the formula that describes them, Rodrigues formula. The data entered to the model are the function coefficients obtained from the fitting [172–174].

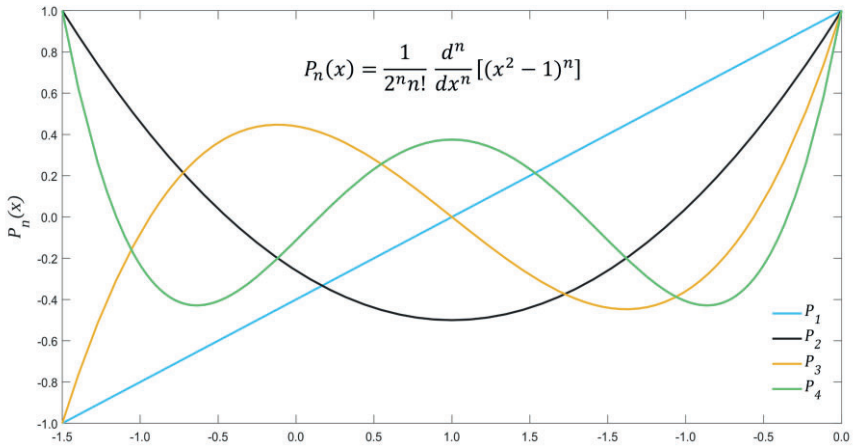

Figure 1.28. Graphical representation of the first four Legendre polynomials and the corresponding formula.

- Windowed slicing integral method

Windowed slicing integral method (Int) is an alternative method proposed in the ET field. This method is based on the division of the voltammogram in k sections and the calculation of the area under the curve, which are then used as the inputs for the model [175]. One example is depicted in Figure 1.29, where a voltammogram divided into eight sections (k=8) is presented.

The principle of the Int method is to suppose that each area is proportional to the average of the currents involved in each section. Thus, each area describes the voltammogram shape, related to chemical changes in the sample. This is a tool strongly connected with the classical electrochemical approaches, where the estimation of the area under the peak is proportional to the concentration of the target analytes in the sample.

Its major drawback is to decide in how many sections the signal will be divided because it is an arbitrary value. The optimal value will be a compromise between the compression ratio and the fidelity to the original data, so that, as occurs in other methods, this parameter can be added as a parameter to be optimized during the modeling step.

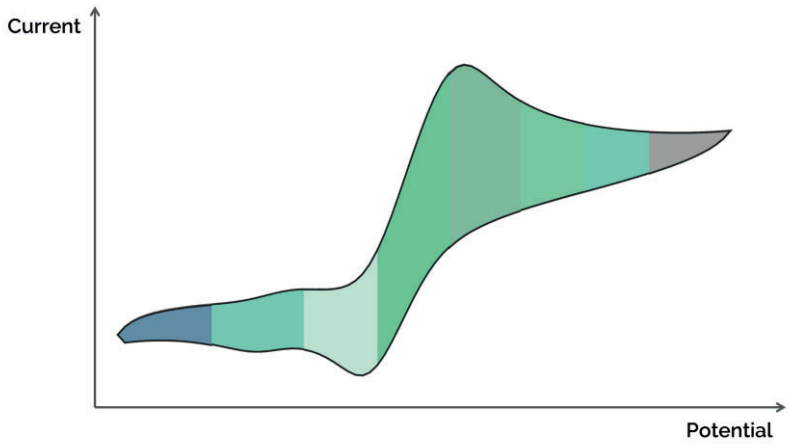

Figure 1.29. Representation of windowed slicing integral compression method when k=8.

- Principal component analysis

PCA is normally used as an unsupervised tool for exploratory analysis (§1.5.3.1), but it can also be employed as a compression method. The aim of using PCA as a compression tool lays in keeping the first obtained variables (the

principal components, shortened as PCs) as inputs for the model. PCs are obtained from the projection of the original variables to new coordinates. The first PC contains the maximum possible variance, the second PC the second maximum from the remaining, and so forth. Thus, the more PCs are used to feed the model, the more information will be obtained from the original voltammogram. But, as in other cases, a compromise must be taken into account between ratio and fidelity. For this reason, the accumulated variance can be used as a parameter to decide how many PCs will be selected.

- Fast Fourier Transform

Fourier transforms (FTs) are a mathematical algorithm based on the decomposition of complex signals from the time or space domain into a new subspace of time or space-depending frequencies (a descriptive schema is shown in Figure 1.30). In other words, FT allows the transformation of complex signals to sine/cosine functions of different amplitudes, phases, and frequencies. To each function is linked a coefficient, which depends on the contribution of the components into the original signal. The first functions, of lower frequencies, contain the most relevant and valuable information, while the higher frequencies are related to poor information (typically noise). This feature of the FT makes them a magnificent tool to compress and at the same time denoise high dimensionality data. While some FTs can be slow, there are alternative more efficient computational methods such as FFT, which make their implementation much more convenient.

As in the case of PCA, the data can be easily simplified keeping the first coefficients (related to the low frequencies) and excluding the others. Another advantage of these algorithms is that the transform can be reverted to obtain the data in the original domain. Thus, the inverse transform can be used to evaluate the number of coefficients to be input into the model and the reconstruction degree. The more coefficients selected the more similar to the original will be the reconstructed signal. This factor requires again the need of a compromise between the number of inputs and the information preserved.

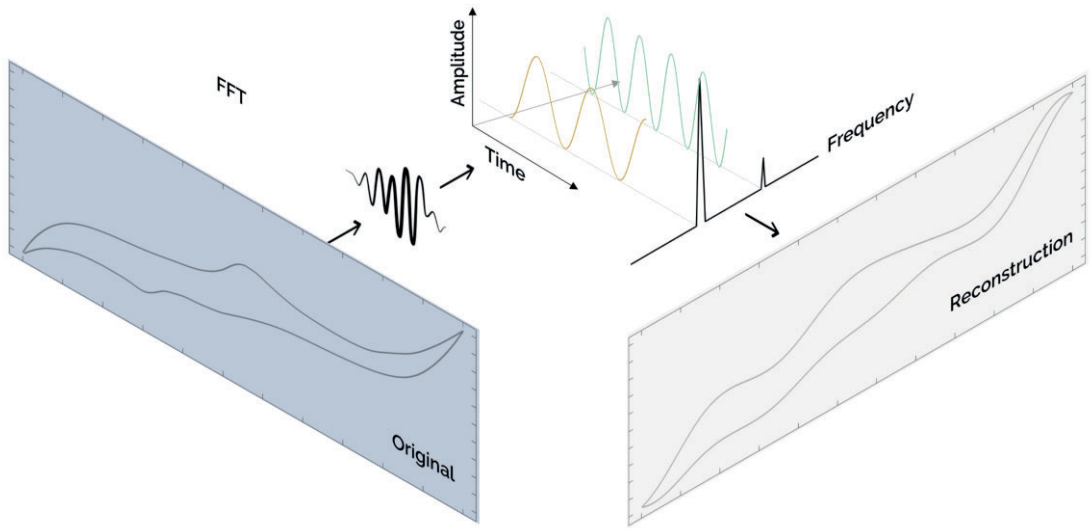

Figure 1.30. Fourier transform schema, where it can be seen how an entire voltammogram is transformed from the time to frequency domain, and later the inverse transformation is done to reconstruct it to the original space.

- Wavelet Transforms

Wavelet transforms, (WTs), like FTs, are mathematical tools that decompose a signal into a new subspace. In effect, WT is an evolution of FT which instead of using sine waves, is based on the scanning of a signal through a mother wavelet function, which is scaled every new cycle. Scaling or dilation of the mother wavelet retains information about the frequency domain while its translation is related to the position on the time. Hence WT is a more appreciated algorithm than FT because can identify not only the frequency, but also the location of the perturbation [176]. The information extracted from WT is in the time-scale domain. Wavelets are functions with maximum oscillations in the center, which decrease on the sides. Some examples are depicted in Figure 1.31. The choice of the best wavelet is conditional on the raw data. The most important mother-function family is the *Daubechies* wavelets.

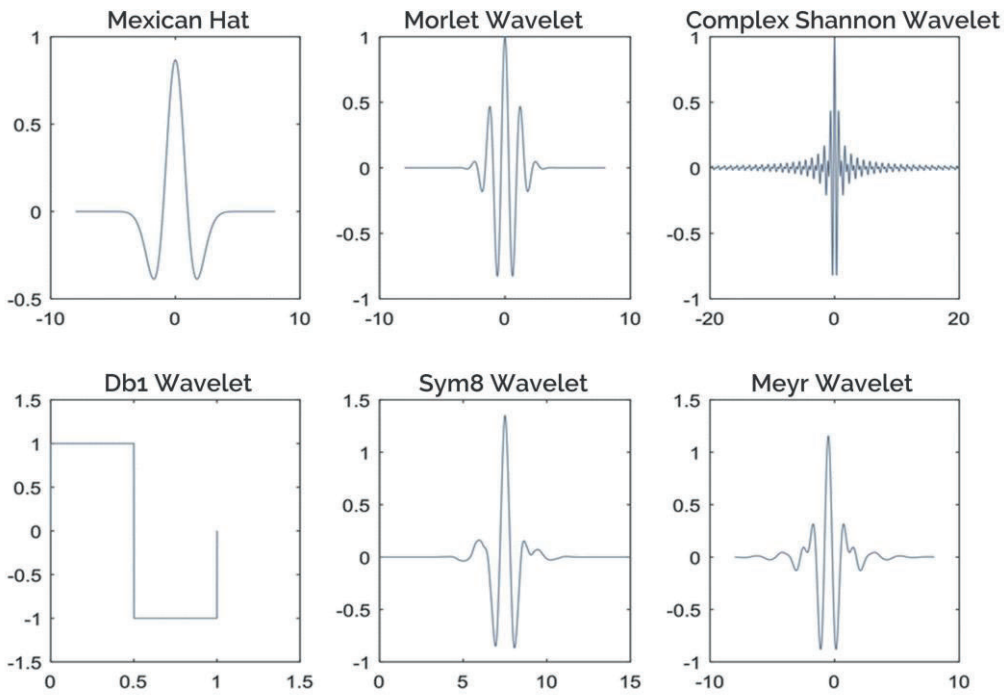

Figure 1.31. Representation of the most famous wavelets employed. In the analytical field.

WTs can be separated into two main groups, the continuous and the discrete. Continuous wavelet transform (CWT) is focused on continuous variables, therefore CWT will result in decomposing the signal in infinite functions. The application of WT in real cases is achieved with DWT using. Mallat's algorithm allows an efficient application of DWT [177]. Normally a multilevel decomposition (also named pyramidal or tree algorithms) is applied, see Figure 1.32A. DWT has two filters, the wavelet, (high pass filter), and the scaling function, (low pass filter). The process is schematized in Figure 1.32B. As it can be observed, the signal is scanned through two filters obtaining from an M length signal two orthogonal subspaces of ca. $M/2$ length each one. On the one side, low pass filters preserve low frequencies, the resulting coefficients are named *approximation coefficients* (cA), and retain the general trait of the original signal. On the other side, high pass filter is related to high frequencies, the obtained coefficients are named *detail coefficients* (cD), and as it can be expected retain the more concrete information. As Figure 1.32B depicts, between the filter and the coefficients there is an intermediate step, the *downsampling*, which halves the coefficient.

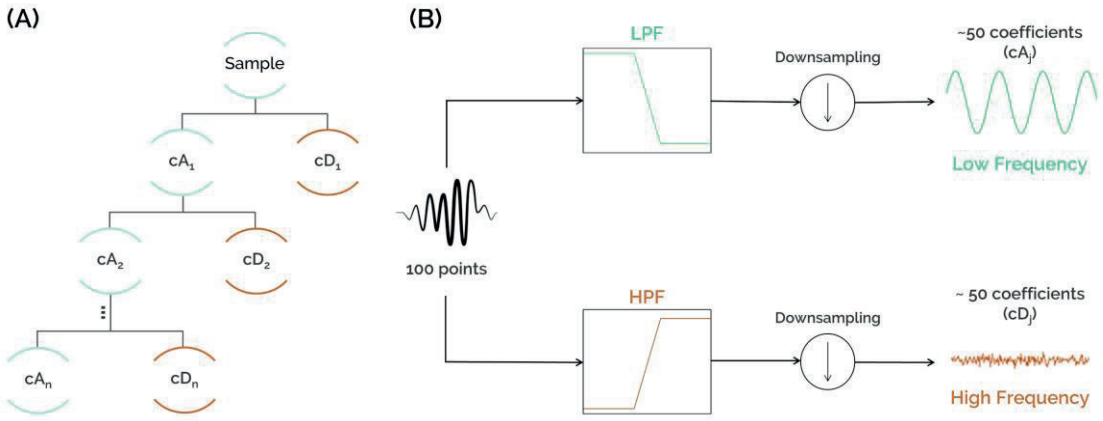

Figure 1.32. (A) Scheme of the pyramidal algorithm. (B) Representation of one level DWT decomposition including the low and high-pass filters (LPF and HPF, respectively), the downsampling process to obtain the high-frequency coefficients (containing the not valuable information), and the low-frequency coefficients (rich in information). (B)

In this direction, to compress the data, the filtering can be performed multiple times discarding the cD and reducing cA at each step. Keeping in this way the most significant information. The evaluation of the compression process can be done with the reconstruction of the signal by means of the maintained coefficients.

- Validation of the compression goodness

Thus, as mentioned before, the reconstruction of the signal by retransforming the coefficients to the original domain can be used to evaluate the number of coefficients to be input to the model. The goodness of the compression was defined in this work by two parameters, the determination coefficient (R^2) between the original and the compressed data, and a comparison factor named f_c, which considers the ratio between the intersection area of the original and reconstructed signal (A ∩ B) and the total area under both curves (A U B) (Equation (18)). Both values, R^2, and f_c, variate from 0 to 1, being 0 when the signals are completely different and 1 when the signals are equal.

$$f_c = \frac{A \cap B}{A \cup B} = \frac{\sum_{i=1}^{M}(max\langle a_i, b_i\rangle - |a_i - b_i|)}{\sum_{i=1}^{M}(min\langle a_i, b_i\rangle - |a_i - b_i|)} \qquad \text{Equation (18)}$$

1.5.3 Modeling

In chemometrics, a model is a mathematical structure that can predict the value of target variables considering the information extracted from the

responses. The performance of a complete approach depends on two stages, the model building and the validation of the model.

The first step during the modeling stage is the definition of the target variables and the character of the study to be performed. As abovementioned, normally those are classified in quantification and qualification models according to if the goal is to determine a certain variable or parameter, or to identify and/or classify the samples.

1.5.3.1 Chemometric strategies

- Principal Components Analysis

PCA is an unsupervised method that not only is used as feature extraction pre-treatment but also as a classification tool. PCA is based on the reduction of the dimensionality of a dataset, i.e. the original variables or predictors are reorganized in order to downsize it to the most important features, as already explained in §1.5.2.2. The obtained results are plotted in a visual graph where grouping/clustering of samples that present similar characteristics to each other may appear [162].

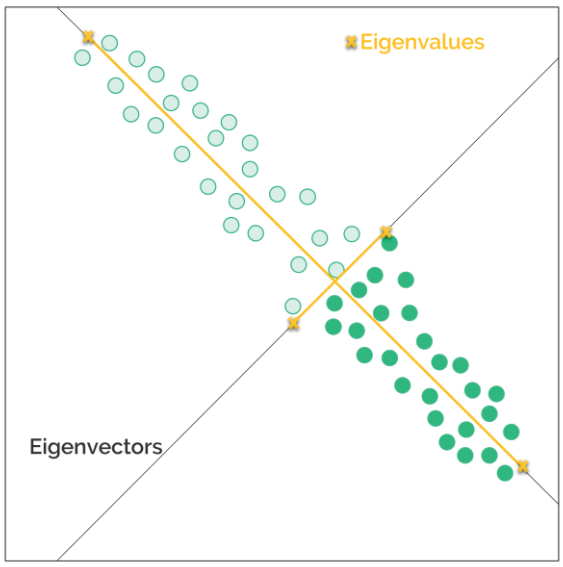

Figure 1.33. Plot of the original data containing the representation of eigenvectors (in black) and eigenvalues (in orange).

PCA algorithm transforms or projects the raw mean-centered dataset to new adjacent variables (“latent”), named principal components (PCs), via the linear combination of the original features into new coordinates (the scores) trying

to capture as much variance as possible. Each sample will have a score for each PC and as many PCs as variables will be obtained. Concretely, the transformation is carried out via eigenvectors and eigenvalues (schematized in Figure 1.33) obtained from the covariance matrix of the original data. As seen in Figure 1.33, eigenvectors are the axes of the PCs and define their direction, while eigenvalue defines the size (together forming the loadings). Thus, loadings are related by magnitude to the covariances between the variables. The first PC (PC1) will explain the maximum variance of the original data, the second PC (PC2) will contain the resting maximum variance, and so on. Each PC will be orthogonal to the previous one, ensuring then that the PCs are not correlated between them [178].

In Figure 1.34 the transformation of the original data to the new variables (the PCs) is schematized. As seen, firstly both variables contain non-separated data in which is difficult to find a pattern, but when transferred to the new coordinates, the PC score plot evidences perfectly two clusters, the blue, and the green. Moreover, as shown in the previous figure, the PCs are orthogonal among them.

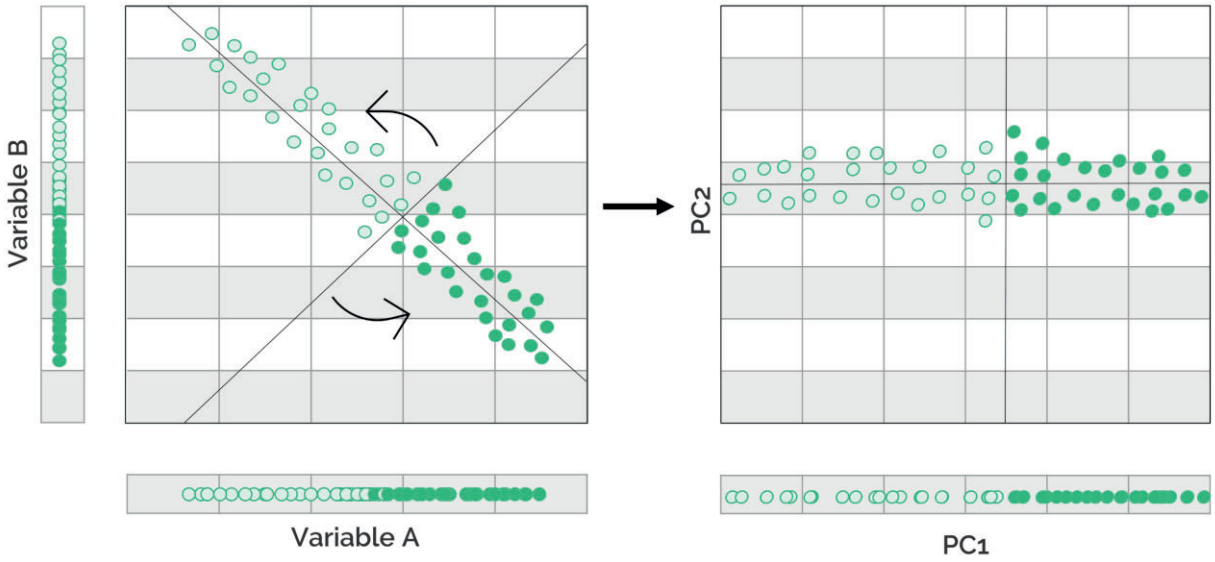

Figure 1.34. Schematization of the score plot representation. Concretely, is depicted how it is reduced one dimension to the original data (2D) and how its obtained the final plot.

PCA tool allows to analyze the experimental results from an alternative point of view, but it has to be remarked that as an individual tool cannot be

considered as a pattern recognition method per se. For this reason, it is recommended the use of complementary tools such as ANNs or PLS.

- Support Vector Machines

Support vector machines (SVMs) is a supervised algorithm used mainly for classification study cases.

The main objective of this tool is the creation of the best decision border (named hyperplane) that divides the set of samples into n new spaces in which the samples will be classified. The schema of this process is represented in Figure 1.35 where two different types of application are represented: when the data has a linear behavior (Figure 1.35A) and when the data is non-linear (Figure 1.35B). As seen in the image, the hyperplane is the border that maximizes the difference among the classes, then in the new spaces, the new points will be separated according to which side of the hyperplane they are placed on.

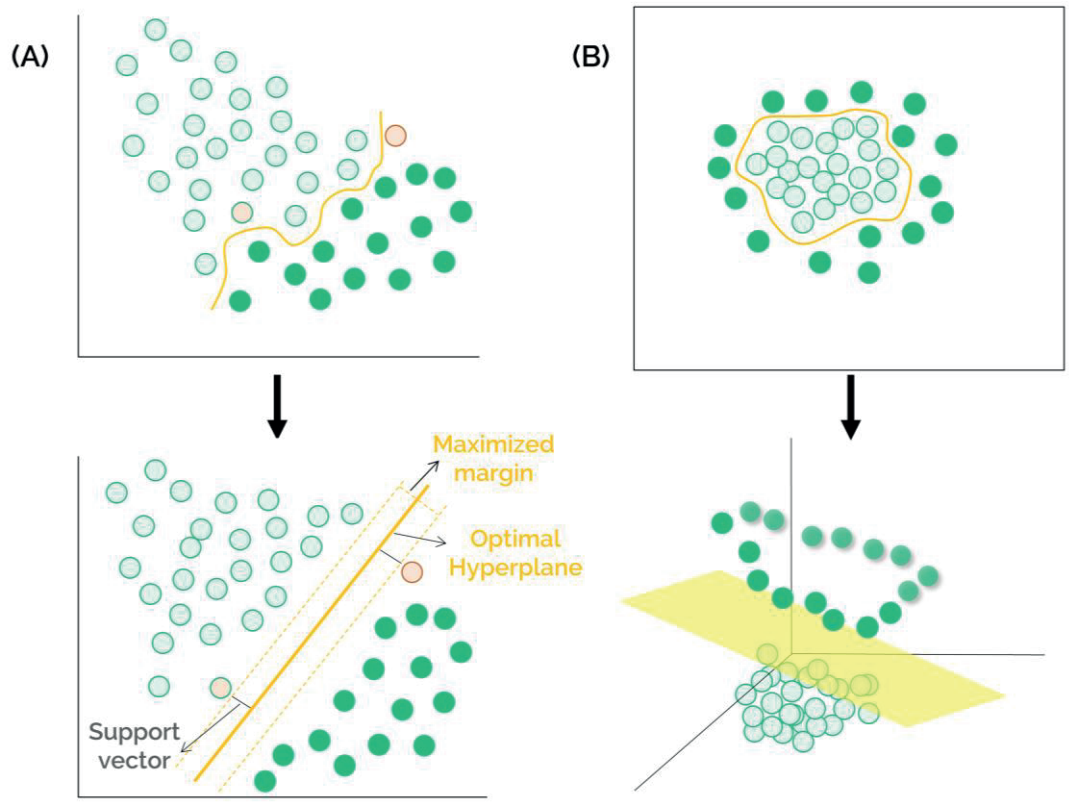

Figure 1.35. Schematization of the classification process followed by SVMs (A) for lineal data and (B) non-linear data.

The hyperplane is created considering the extreme cases of each class, i.e., the hyperplane nearest points. The vector created in this point is named

support vector. Then, to find the optimal border, the maximum margin between the support vectors and the hyperplane is sought (Figure 1.35A) [179,180].

Non-linear data refers to data that cannot be classified in a linear manner. For this reason, the data is transformed from the original space to a new space of higher dimensionality, in which it is possible to apply a linear separation plane (Figure 1.35B). The data transformation can be done by *kernel functions,* a process that is known as the "*kernel trick".*

The ability to work with every kind of data makes SVMs very powerful, which makes them a popular tool in classification problems.

- Partial least squares and multi-way partial least squares

Partial least squares (PLS) is a mathematical model that transforms the input data (both, the predictors (X) and the targets (Y) matrix) in order to find a combination that maximizes their covariance maintaining a maximum correlation with Y. The new space of X obtains a matrix formed by the components, also named latent variables or factors, which are the product of the linear combination of the original values. Thus, PLS gives information about the variance and the correlations. In Equation (19) and Equation (20) the parallel decomposition of X and Y are shown, where T and U are the scores matrices, P and Q are the values of the loading, and E and F the residual from the original values [162].

$$X = TP' + E \qquad \text{Equation (19)}$$

$$Y = UQ' + F \qquad \text{Equation (20)}$$

There are multiple algorithms for the data treatment in PLS, but the most common are the non-linear iterative partial least squares (NIPALS), and statistically inspired modification of the PLS (SIMPLS) [181,182].

PLS is limited to one variable, i.e. Y only depends on a unique predictor, while PLS-2, their alternative, is the extension to multidimensional predictors. In both cases, the number of latent variables is optimized to obtain the minimum error.

Recently, nPLS has been developed as a chemometric tool that is able to deal with high dimensionality data, concretely, can process data with more than

two dimensions. The nPLS opposed to PLS use tensors to describe the loading and score but follows the same logic, to maximize pairwise the covariance [183]. This method then is presented as an alternative to more common PLS or ANNs when having multidimensional data, avoiding in this way the discontinuities caused by the unfolding and later concatenation of the voltammograms. Although its advantages, nPLS methods have their own inconveniences being complex to implement and its linearity presumption the most relevant ones.

- Artificial Neural Networks

ANNs are a biomimetic mathematical model based on the mirror of the animal brain and nervous system. This is a widespread method in multivariate analysis, probably because is flexible and can deal with linear and non-linear data, or even with a combination of both. Oppositely, it is labor-intensive regarding its optimization and application.

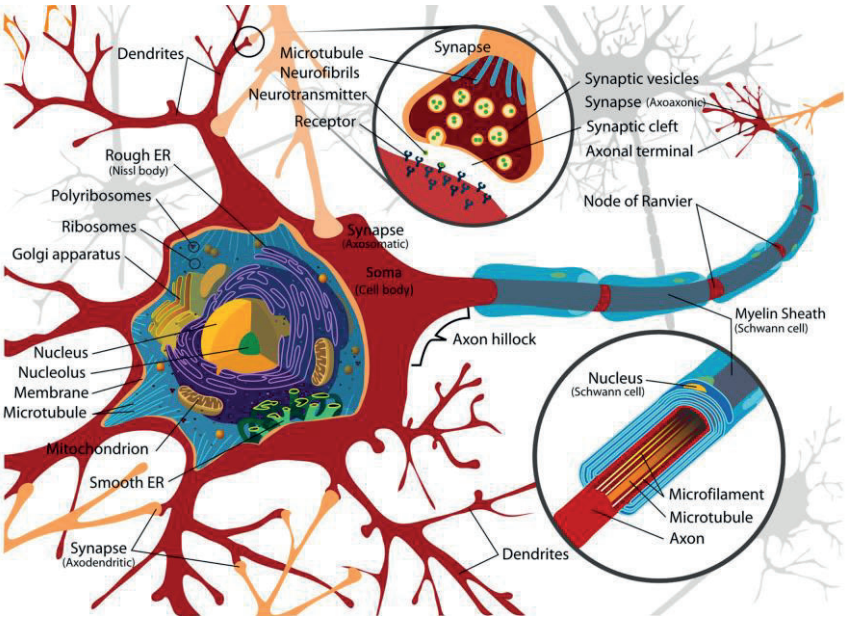

Figure 1.36. Biological neuronal parts. Image from Wikimedia Commons, Mariana Ruiz Villarreal.

As mentioned in §1.4, multisensory systems try to mimic the perception of the animal senses through the use of different sensors. In this case, ETs combined with ANNs approach not only percept the signals as animals but also process equally the data. This mathematical method is compared with the nervous system, which is in charge of receiving, processing, and transmitting the information acquired by the senses. One essential unit in this procedure is the neuron. Neurons depicted in Figure 1.36, are nerve cells composed of the soma,

the dendrites, the axon, and the terminal buttons. They communicate between them via the synapses, specialized connection structures that allow the interchange of chemical or electrical information. When dendrites receive a signal, it is propagated to the soma, where it is processed and sent through the axon to the other neurons. The stimuli are spread through the nervous system since arriving at the neurons, which combine and process all the incoming signals. These cause changes in the soma membrane potential, and if the impulse is able to reach the activation potential, the neuron will propagate the information. Depending on the potential received, the information is transmitted with greater or lesser intensity. The more times the pathway is repeated, the faster it occurs and therefore, the more rapid the response to the stimulus. In other words, the brain learns from its experiences [184].

In ANNs the equivalent to the neuron is an array of binary processors named nodes, neurons, or perceptron. The nodes act like neurons, combining the received information to transfer if relevant to the linked neurons. Concretely, nodes made the weighted sum of the signals taking into account the weight assigned to each connection (w_{ik}) and a scalar term related to the bias. If the result is enough to activate the node, as in the biological case, the processor gives an output signal. Since perceptrons obtain categoric information is used transference functions to turn them into continuous values.

The goal of the learning procedure of an ANN is to obtain the best pathway for the information transference. In other words, to train the inter-neuronal connections to find the best weights combination that minimize the error produced when predicting the variables. To become aware of the importance of the learning process and how it affects the generalization of the model, we can compare it to the human process of learning. Children are subjected to a learning process in which they learn to develop on their own, but in the event that they memorize an action, they will only be able to reproduce that particular one and no other similar acts. For example, the mathematical process of multiplying.

There are two ANNs learning modes, the incremental and the batch mode. The first one recalculates constantly the weights after estimating the error, while the batch mode analyses the errors for a certain batch of samples. Despite the

trashing problems (step-back calculations) that may appear when using incremental learning, it also avoids the halting of the computations in local minimums. For this reason, the present thesis uses this mode for the ANNs development [185].

For the training of the ANN, initially, a random value is allocated to each weight and in each complete learning cycle, named epoch in the machine learning language, it will be optimized until finding the nearest to the optimum possible. One of the most used groups of algorithms is the backpropagation [186], where an iterative calculation compares the outputs obtained using the actual setting with the theoretical values, after weights are balanced in order to approximate it to the expected. It must be mentioned that this process is done with the train subset of samples, validations subsets are not included. Cost, or loss function apports information about the goodness of the ANN model. Equation (21) shows one example of the loss function, the mean squared error (MSE), which expresses the weighted sum of the squares of the expected and predicted difference for each neuron.

$$Loss\ function = \frac{1}{n}\sum_{i=1}^{n}(y_{expected} - y_{predicted})^2 \qquad \text{Equation (21)}$$

From the backpropagation algorithms, the Bayesian regulation (BR) generalization method was the used to create the topology of the herein ANNs [187]. BR is based on the use of Bayes's theorem also named *inverse probability law* and it links the probability that occurs the act A when is occurring B with the probability that occurs B when A is occurring. Therefore, making possible to calculate predictions in the reverse direction. The final loss function is represented in Equation (22), where α and β are hyperparameters named learning index and momentum, respectively [188]. BR obtain the simplest ANN for each system. This regulation not only considers the minimum error but also the weight relevance in the system, concretely BR distributes the weights to avoid dependence on some of them.

$$Loss\ function = \beta\sum_{i=1}^{n}[y_{expected} - y_{predicted}]^2 + \alpha\sum_{j=1}^{n_w} w_j^2 \qquad \text{Equation (22)}$$

There are several types of ANNs applied in machine learning, the key difference lies in the mathematical approach. Some examples are the feedforward, the Modular, the Kohonen Self Organization, and the Convolutional Neural Networks. Due to the complexity of these mathematical treatments, this thesis work will be focused on the analysis and explanation of the herein employed ANNs, the feedforward Neural Network.

Feedforward Neural Networks represent the purest ANNs approach in which the information only travels unidirectionally from the input layer, layer by layer. The structure of feedforward neural networks is schematized in Figure 1.37, which is based on the distribution of logical processing units, the perceptrons, neurons, or nodes, in different layers. Normally there are three layers: the input, the hidden, and the output. It is possible to have more than one hidden layer, the one that really processes the data, but considering the premise that the simpler the system, the better it will be, in this work (and in most of the work in the ETs field) only one hidden layer is considered. In the structure, every unit is connected with all the neurons of the previous layer. The connections are not equal in each case, as commented before, they have different weights which are balanced in every epoch searching the optimal topology [189].

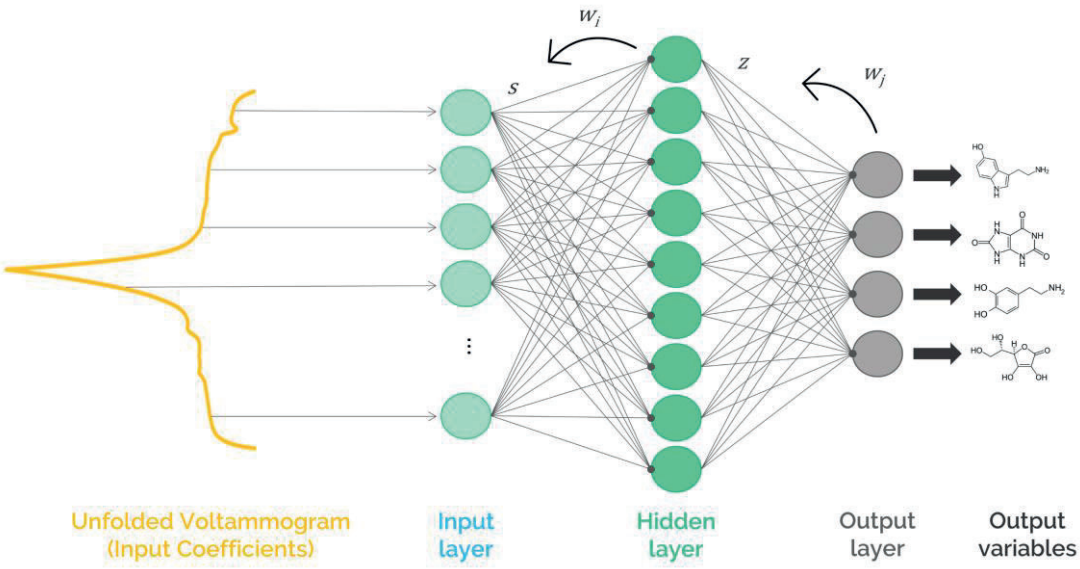

Figure 1.37. Schema of a feedforward neural network with a backpropagation learning algorithm. The ANN is composed of an input layer, one hidden layer with 9 neurons, and an output layer with 4 neurons.

By making an in-depth look at Figure 1.37, where it can be seen that from the unfolded voltammograms are obtained the coefficients to feed the ANNs (explained in detail in §1.5.2). These coefficients form the input layer, thus there will be as many nodes as input coefficients. The input layer is fully connected with the next layer nodes. Between both layers, the information is transferred through a transfer function (s), and another transfer function (z) transforms the information from the hidden layer to the output layer. Hence, the real computational effort is given in the hidden layer, where the raw data is transformed to the target information. Finally, it is obtained as many outputs as variables analyzed, in our case, molecules quantified.

To sum up, ANNs methods are much more versatile and consequently able to master other approaches. However, its usage requires previous experience and knowledge to carry out a reliable study of the ANN topology and avoid issues such as overfitting in the learning process. Nevertheless, it must be considered the limitations of ANN when an excessive number of input values are taken. In this direction, is highly recommended the pre-treatment of the original data to facilitate the computational calculous. Another drawback is the requirement of bidimensional data, which as commented before can be easily solved by the unfolding and concatenation of the data.

1.5.3.2 Validation of the model

Validation is mandatory to study the goodness of the model to external samples. Validation is carried out using an external set of samples, or what is the same, samples not involved in the model construction.

Validation samples are interpolated into the model to know about its predictive ability. If an acceptable agreement between correlation, slope, and intercept is achieved, the model suitable describes the studied case. Contrarily, when some problems occur, such as overfitting of the model, measurement of not representative samples, or errors in the correlation between the variables and the samples, the validation subset has poor results.

The overfitting of the model is one of the easiest mistakes to commit. It occurs when the model is overtrained to such an extent that it is no longer able to predict samples outside the calibration set. To avoid this handicap sometimes

another group of samples is added to proceed with an internal validation. Which used to make a preliminary validation to decide which is the most optimal configuration for the algorithm model.

There are multiple ways to split the data between the training and validation subsets, such as the Montecarlo, or the jack-knife, but the employed in this work, and the most common are:

- Split sample (Train/Test Subsets)

The most common approach in ETs uses an experimental design based on two subsets: the train or calibration and the test or validation. In this direction, the training subset is used to create the model, therefore to digest the data and fit the algorithm, and the test subset is employed for the validation, that is to evaluate the goodness of the obtained model. It has to be remarked that the test subset is not involved in the model building [190].

Additionally, it must be noticed the importance of the correct distribution of samples between groups because must be representative. In this sene, commonly training subset contains *ca.* 2/3 of the samples, these are strategically disposed inside the experimental concentrations range (experimental domain) using in the major of cases designs proposed by MDOE. The rest of the samples are included in the test subset. Those values are distributed randomized inside the experimental domain.

- Cross-validation

K-fold or leave-X-out is a cross-validation method based on the random division of the samples into K groups of X samples. The separation is made k times leaving one group of the K out (using it exclusively for the validation). The subsets can be organized by consecutive grouping or totally random, being especially popular leaving-one-out (Figure 1.38B and Figure 1.38C).

The results of the training subsets are averaged to obtain the matrix of predictors, while for the test subset those are simply combined. This method lets participate the samples equally in the training and the validation stage, ensuring the non-correlation provided for the sample distribution, being this an advantage when significative values for X are taken.

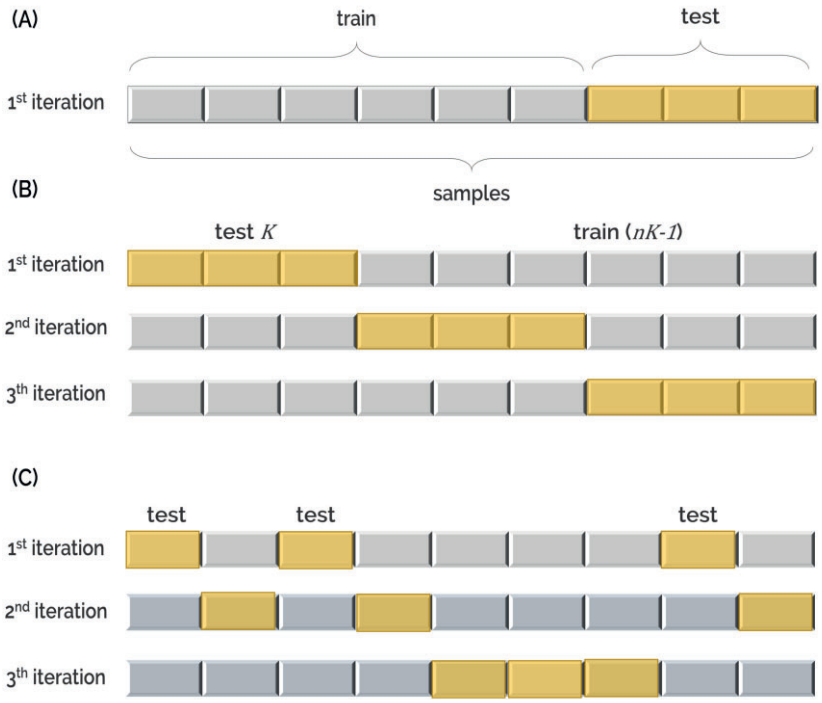

Figure 1.38. Schematic representation of train and test subsets, and the different approaches to divide the samples between the train subset and the test samples. (A) Split sample, (B) cross-validation using k-fold with K=3 or leave-3-out with the consecutive separation, and (C) the cross-validation with random choosing.

Once the model is validated, must be estimated its capabilities. The strategies followed for the quantitative and qualitative methods are different.

- Estimation of qualitative models

For qualitative methods, the samples that are correctly classified and the samples that are not well classified are summarized in a visual table (named confusion matrix, see Table 1.9), where only values should appear in the diagonal. Moreover, some numeric values such as the success ratio, the sensitivity, the specificity, and the Pearson test among others can be assessed.

Table 1.9. Example of a confusion matrix.

		Predicted	
		Positive	Negative
Expected	Positive	True Positive	False Negative
	Negative	False Positive	True Negative

The success ratio is the relation between the correctly classified samples and the number of samples for each class without considering other factors as the number of samples per class. The sensitivity, or true positive rate, is the estimation of the correctly classified samples taking into account the true total amount of samples that belong to the class. The specificity, or true negative, considers the correctly refused values. Thus, with the listed ratios, it is possible to describe the capacity of the model to separate correctly the samples in the corresponding classifiers. Lastly, with the Pearsons test, the goodness of the model can be described.

- Estimation of quantitative models

Regarding the quantitative models, the fitting errors, and separately, the expected *vs.* predicted graphs, are normally considered to evaluate the goodness of the model. Both methods are used to compare the obtained (predicted) points in front of the real values (expected).

RMSE and NRMSE give information about how far are the predicted values from the expected, in other words, RMSE is the residuals' standard deviation (Equation (23)). Similarly, NRMSE (Equation (24)) gives the same information but is normalized for the concentration range of each of the analyzed compounds (*j*). From these equations, are obtained the total error values, or what is the same, the error for the whole model, but the individual RMSE and NRMSE can be also calculated in the same way. The smaller the errors, the better the fitting, because it means that the predicted data is distributed near to the expected values. The advantage to using NRMSE in front of RMSE is that when measuring different concentration ranges for the different targets, the RMSE could lead to a bigger absolute error mostly affected by the analyte with higher concentration. Moreover, since the NRMSE value is normalized, it will provide a direct metric independent of the units or concentration ranges used in the measurements.

$$RMSE_{Total} = \sqrt{\frac{\sum_{ij}\left(Expected_{ij} - Predicted_{ij}\right)^2}{jn - j}} \qquad \text{Equation (23)}$$

$$NRMSE_{Total} = \frac{1}{j}\sum_{j}\frac{RMSE_j}{C_{j,max} - C_{\mathrm{j},min}} \qquad \text{Equation (24)}$$

Expected *vs.* predicted graphs are a visual tool that quickly allows the evaluation of the model This kind of fitting gives not only visual information of the points distribution and correlation but also numeric values to compare among models. The lineal fitting evaluates the slope, intercept point, and correlation of the data comparing it with the ideal values, which are 1, 0, and 1, respectively.

1.6 References

[1] E. Fitzer, K.H. Köchling, H.P. Boehm, H. Marsh, *Recommended terminology for the description of carbon as a solid*, Pure and Applied Chemistry. 67 (**1995**) 473–506. https://doi.org/10.1351/PAC199567030473.

[2] P. Avouris, C. Dimitrakopoulos, *Graphene: synthesis and applications*, Materials Today. 15 (**2012**) 86–97. https://doi.org/10.1016/S1369-7021(12)70044-5.

[3] K.S. Novoselov, D. Jiang, F. Schedin, T.J. Booth, V. v. Khotkevich, S. v. Morozov, A.K. Geim, *Two-dimensional atomic crystals*, Proceedings of the National Academy of Sciences. 102 (**2005**) 10451–10453. https://doi.org/10.1073/pnas.0502848102.

[4] P.R. Wallace, *The Band Theory of Graphite*, Physical Review. 71 (**1947**) 622. https://doi.org/10.1103/PhysRev.71.622.

[5] B.C. Brodie, *XIII. On the atomic weight of graphite*, Philosophical Transactions of the Royal Society of London. 149 (**1859**) 249–259. https://doi.org/10.1098/rstl.1859.0013.

[6] L. Staudenmaier, *Verfahren zur Darstellung der Graphitsäure*, Berichte Der Deutschen Chemischen Gesellschaft. 31 (**1898**) 1481–1487. https://doi.org/10.1002/cber.18980310237.

[7] W.S. Hummers, R.E. Offeman, *Preparation of Graphitic Oxide*, Journal of the American Chemical Society. 80 (**1958**) 1339–1339. https://doi.org/10.1021/ja01539a017.

[8] J.D. Bernal, *The structure of graphite*, Proceedings of the Royal Society of London. 106 (**1924**) 749–773. https://doi.org/10.1098/rspa.1924.0101.

[9] R. Garcia-Cortadella, G. Schwesig, C. Jeschke, X. Illa, A.L. Gray, S. Savage, E. Stamatidou, I. Schiessl, E. Masvidal-Codina, K. Kostarelos, A. Guimerà-Brunet, A. Sirota, J.A. Garrido, *Graphene active sensor arrays for long-term and wireless mapping of wide frequency band epicortical brain activity*, Nature Communications . 12 (**2021**) 211. https://doi.org/10.1038/s41467-020-20546-w.

[10] J.W. May, *Platinum surface LEED rings*, Surface Science. 17 (**1969**) 267–270. https://doi.org/10.1016/0039-6028(69)90227-1.

[11] M. Eizenberg, J.M. Blakely, *Carbon monolayer phase condensation on Ni(111)*, Surface Science. 82 (**1979**) 228–236. https://doi.org/10.1016/0039-6028(79)90330-3.

[12] H.P. Boehm, R. Setton, E. Stumpp, *Nomenclature and terminology of graphite intercalation compounds*, Carbon. 24 (**1986**) 241–245. https://doi.org/10.1016/0008-6223(86)90126-0.

[13] X. Lu, M. Yu, H. Huang, R.S. Ruoff, *Tailoring graphite with the goal of achieving single sheets*, Nanotechnology. 10 (**1999**) 269. https://doi.org/10.1088/0957-4484/10/3/308.

[14] K.S. Novoselov, A.K. Geim, S. v Morozov, D. Jiang, Y. Zhang, S. v Dubonos, I. v Grigorieva, A.A. Firsov, *Electric Field Effect in Atomically Thin Carbon Films*, Science. 306 (**2004**) 666–669. https://doi.org/10.1126/science.1102896.

[15] F. Schedin, A.K. Geim, S. V. Morozov, E.W. Hill, P. Blake, M.I. Katsnelson, K.S. Novoselov, *Detection of individual gas molecules adsorbed on graphene*, Nature Materials . 6 (**2007**) 652–655. https://doi.org/10.1038/nmat1967.

[16] H. Kim, K.Y. Park, J. Hong, K. Kang, *All-graphene-battery: bridging the gap between supercapacitors and lithium ion batteries*, Scientific Reports . 4 (**2014**) 5278. https://doi.org/10.1038/srep05278.

[17] T. Monetta, A. Acquesta, F. Bellucci, *Graphene/Epoxy Coating as Multifunctional Material for Aircraft Structures*, Aerospace. 2 (**2015**) 423–434. https://doi.org/10.3390/aerospace2030423.

[18] H.P. Boehm, A. Clauss, G. Fischer, U. Hofmann, *Surface properties of extremely thin graphite lamellae*, Proceedings of the Fifth Conference on Carbon. (**1962**) 73–80. https://doi.org/10.1016/B978-0-08-009707-7.50013-3.

[19] W.Y.H. Khoo, M. Pumera, A. Bonanni, *Graphene platforms for the detection of caffeine in real samples*, Analytica Chimica Acta. 804 (**2013**) 92–97. https://doi.org/10.1016/j.aca.2013.09.062.

[20] M. Bonet-San-Emeterio, N. Felipe Montiel, M. del Valle, *Graphene for the building of electroanalytical enzyme-based biosensors. Application to the inhibitory detection of emerging pollutants*, Nanomaterials. 11 (**2021**) 2094. https://doi.org/10.3390/nano11082094.

[21] A.K. Geim, K.S. Novoselov, *The rise of graphene*, Nature Materials. 6 (**2007**) 183–191. https://doi.org/10.1038/nmat1849.

[22] C.-L. Sun, C.-H. Su, J.-J. Wu, *Synthesis of short graphene oxide nanoribbons for improved biomarker detection of Parkinson's disease*, Biosensors and Bioelectronics. 67 (**2015**) 327–333. https://doi.org/https://doi.org/10.1016/j.bios.2014.08.046.

[23] T.A. Tabish, S. Zhang, *Graphene Quantum Dots: Syntheses, Properties, and Biological Applications*, Comprehensive Nanoscience and Nanotechnology. 3 (**2016**) 171–192. https://doi.org/10.1016/B978-0-12-803581-8.04133-3.

[24] P. Nemes-Incze, Z. Osváth, K. Kamarás, L.P. Biró, *Anomalies in thickness measurements of graphene and few layer graphite crystals by tapping mode atomic force microscopy*, Carbon. 46 (**2008**) 1435–1442. https://doi.org/10.1016/j.carbon.2008.06.022.

[25] L. Tang, X. Li, R. Ji, K.S. Teng, G. Tai, J. Ye, C. Wei, S.P. Lau, *Bottom-up synthesis of large-scale graphene oxide nanosheets*, Journal of Materials Chemistry. 22 (**2012**) 5676. https://doi.org/10.1039/c2jm15944a.

[26] Z. Wang, J.K. Nelson, H. Hillborg, S. Zhao, L.S. Schadler, *Graphene Oxide Filled Nanocomposite with Novel Electrical and Dielectric Properties*, Advanced Materials. 24 (**2012**) 3134–3137. https://doi.org/10.1002/adma.201200827.

[27] A.T. Smith, A.M. LaChance, S. Zeng, B. Liu, L. Sun, *Synthesis, properties, and applications of graphene oxide/reduced graphene oxide and their nanocomposites*, Nano Materials Science. 1 (**2019**) 31–47. https://doi.org/https://doi.org/10.1016/j.nanoms.2019.02.004.

[28] D.A.C. Brownson, C.E. Banks, The Handbook of Graphene Electrochemistry, Springer London, London, **2014**. https://doi.org/10.1007/978-1-4471-6428-9.

[29] C. Jacoboni, C. Canali, G. Ottaviani, A. Alberigi Quaranta, *A review of some charge transport properties of silicon*, Solid-State Electronics. 20 (**1977**) 77–89. https://doi.org/10.1016/0038-1101(77)90054-5.

[30] J.F. Wang, K.X. Wang, F.H. Du, X.X. Guo, Y.M. Jiang, J.S. Chen, *Amorphous silicon with high specific surface area prepared by a sodiothermic reduction method for supercapacitors*, Chemical Communications. 49 (**2013**) 5007–5009. https://doi.org/10.1039/c3cc41967c.

[31] M. Pumera, *Electrochemistry of graphene: new horizons for sensing and energy storage*, The Chemical Record. 9 (**2009**) 211–223. https://doi.org/10.1002/tcr.200900008.

[32] X.-Y. Wang, A. Narita, K. Müllen, *Precision synthesis versus bulk-scale fabrication of graphenes*, Nature Reviews Chemistry . 2 (**2018**) 0100. https://doi.org/10.1038/s41570-017-0100.

[33] P.G. Karagiannidis, S.A. Hodge, L. Lombardi, F. Tomarchio, N. Decorde, S. Milana, I. Goykhman, Y. Su, S. v. Mesite, D.N. Johnstone, R.K. Leary, P.A. Midgley, N.M. Pugno, F. Torrisi, A.C. Ferrari, *Microfluidization of Graphite and Formulation of Graphene-Based Conductive Inks*, ACS Nano. 11 (**2017**) 2742–2755. https://doi.org/10.1021/acsnano.6b07735.

[34] M. Bonet-San-Emeterio, A. González-Calabuig, M. del Valle, *Artificial Neural Networks for the Resolution of Dopamine and Serotonin Complex Mixtures Using a*

Graphene-Modified Carbon Electrode, Electroanalysis. 31 (**2019**) 390–397. https://doi.org/10.1002/elan.201800525.

[35] A. Ambrosi, A. Bonanni, Z. Sofer, M. Pumera, *Large-scale quantification of CVD graphene surface coverage*, Nanoscale. 5 (**2013**) 2379–2387. https://doi.org/10.1039/c3nr33824j.

[36] H. Gürsu, M. Gençten, Y. Şahin, *One-step electrochemical preparation of graphene-coated pencil graphite electrodes by cyclic voltammetry and their application in vanadium redox batteries*, Electrochimica Acta. 243 (**2017**) 239–249. https://doi.org/10.1016/j.electacta.2017.05.065.

[37] N.L. Rangel, J.C. Sotelo, J.M. Seminario, *Mechanism of carbon nanotubes unzipping into graphene ribbons*, The Journal of Chemical Physics. 131 (**2009**) 031105. https://doi.org/10.1063/1.3170926.

[38] M.T.H. Aunkor, I.M. Mahbubul, R. Saidur, H.S.C. Metselaar, *The green reduction of graphene oxide*, RSC Advances. 6 (**2016**) 27807–27828. https://doi.org/10.1039/c6ra03189g.

[39] X. Xu, R. Ray, Y. Gu, H.J. Ploehn, L. Gearheart, K. Raker, W.A. Scrivens, *Electrophoretic Analysis and Purification of Fluorescent Single-Walled Carbon Nanotube Fragments*, Journal of the American Chemical Society. 126 (**2004**) 12736–12737. https://doi.org/10.1021/ja040082h.

[40] L.E. Brus, *Electron–electron and electron-hole interactions in small semiconductor crystallites: The size dependence of the lowest excited electronic state*, The Journal of Chemical Physics. 80 (**1984**) 4403. https://doi.org/10.1063/1.447218.

[41] Y.P. Sun, B. Zhou, Y. Lin, W. Wang, K.A.S. Fernando, P. Pathak, M.J. Meziani, B.A. Harruff, X. Wang, H. Wang, P.G. Luo, H. Yang, M.E. Kose, B. Chen, L.M. Veca, S.Y. Xie, *Quantum-sized carbon dots for bright and colorful photoluminescence*, Journal of the American Chemical Society. 128 (**2006**) 7756–7757. https://doi.org/doi.org/10.1021/ja062677d.

[42] H. Li, X. He, Z. Kang, H. Huang, Y. Liu, J. Liu, S. Lian, C.H.A. Tsang, X. Yang, S.T. Lee, *Water-Soluble Fluorescent Carbon Quantum Dots and Photocatalyst Design*, Angewandte Chemie International Edition. 49 (**2010**) 4430–4434. https://doi.org/10.1002/ANIE.200906154.

[43] X. Wang, Y. Feng, P. Dong, J. Huang, *A Mini Review on Carbon Quantum Dots: Preparation, Properties, and Electrocatalytic Application*, Frontiers in Chemistry. 7 (**2019**) 671. https://doi.org/10.3389/fchem.2019.00671.

[44] C. Doñate-Buendia, R. Torres-Mendieta, A. Pyatenko, E. Falomir, M. Fernández-Alonso, G. Mínguez-Vega, *Fabrication by Laser Irradiation in a Continuous Flow Jet of Carbon Quantum Dots for Fluorescence Imaging*, ACS Omega. 3 (**2018**) 2735–2742. https://doi.org/10.1021/acsomega.7b02082.

[45] Y. Jiang, B. Wang, F. Meng, Y. Cheng, C. Zhu, *Microwave-assisted preparation of N-doped carbon dots as a biosensor for electrochemical dopamine detection*, Journal of Colloid and Interface Science. 452 (**2015**) 199–202. https://doi.org/10.1016/j.jcis.2015.04.016.

[46] P. Shen, Y. Xia, *Synthesis-modification integration: One-step fabrication of boronic acid functionalized carbon dots for fluorescent blood sugar sensing*, Analytical Chemistry. 86 (**2014**) 5323–5329. https://doi.org/10.1021/AC5001338.

[47] J.J. Liu, D. Li, K. Zhang, M. Yang, H. Sun, B. Yang, *One-Step Hydrothermal Synthesis of Nitrogen-Doped Conjugated Carbonized Polymer Dots with 31% Efficient Red Emission for In Vivo Imaging*, Small. 14 (**2018**) 1703919. https://doi.org/10.1002/SMLL.201703919.

[48] Y. Hou, Q. Lu, J. Deng, H. Li, Y. Zhang, *One-pot electrochemical synthesis of functionalized fluorescent carbon dots and their selective sensing for mercury ion*, Analytica Chimica Acta. 866 (**2015**) 69–74. https://doi.org/10.1016/j.aca.2015.01.039.

[49] A. Hulanicki, S. Glab, F. Ingman, *Chemical sensors: definitions and classification*, Pure and Applied Chemistry. 63 (**1991**) 1247–1250. https://doi.org/10.1351/pac199163091247.

[50] L.C. Clark, Electrochemical device for chemical analysis, 2913386, **1956**.

[51] L. Nei, *Some Milestones in the 50-year History of Electrochemical Oxygen Sensor Development*, ECS Transactions. 2 (**2007**) 33. https://doi.org/10.1149/1.2409016.

[52] F.R. Simões, M.G. Xavier, Electrochemical Sensors, in: A.L. da Róz, M. Ferreira, F. de Lima Leite, O. Oliveira (Eds.), Nanoscience and Its Applications, Elsevier, London, **2017**: pp. 155–178. https://doi.org/10.1016/B978-0-323-49780-0.00006-5.

[53] L.C. Clark, C. Lyons, *Electrode systems for continuous monitoring in cardiovascular surgery*, Annals of the New York Academy of Sciences. 102 (**2006**) 29–45. https://doi.org/10.1111/j.1749-6632.1962.tb13623.x.

[54] A.D. McNaught, A. Wilkinson, The IUPAC Compendium of Chemical Terminology, 2nd ed., Blackwell Scientific Publications, Oxford, **1997**. https://doi.org/10.1351/goldbook.

[55] C. Dincer, R. Bruch, E. Costa-Rama, M.T. Fernández-Abedul, A. Merkoçi, A. Manz, G.A. Urban, F. Güder, *Disposable Sensors in Diagnostics, Food, and Environmental Monitoring*, Advanced Materials. 31 (**2019**) 1806739. https://doi.org/10.1002/adma.201806739.

[56] Y. Vlasov, A. Legin, *Non-selective chemical sensors in analytical chemistry: from electronic nose to electronic tongue*, Fresenius' Journal of Analytical Chemistry. 361 (**1998**) 255–260. https://doi.org/10.1007/s002160050875.

[57] G.G. Guilbault, J.G. Montalvo, *Urea-specific enzyme electrode*, Journal of the American Chemical Society. 91 (**1969**) 2164–2165. https://doi.org/10.1021/ja01036a083.

[58] Matthias. Otto, J.D.R. Thomas, *Model studies on multiple channel analysis of free magnesium, calcium, sodium, and potassium at physiological concentration levels with ion-selective electrodes*, Analytical Chemistry. 57 (**1985**) 2647–2651. https://doi.org/10.1021/ac00290a049.

[59] A. Legin, A. Rudnitskaya, Y. Vlasov, C. di Natale, F. Davide, A. D'Amico, *Tasting of beverages using an electronic tongue*, Sensors and Actuators B: Chemical. 44 (**1997**) 291–296. https://doi.org/https://doi.org/10.1016/S0925-4005(97)00167-6.

[60] S.A. Piletsky, Yu.P. Parhometz, N. V Lavryk, T.L. Panasyuk, A. V El'skaya, *Sensors for low-weight organic molecules based on molecular imprinting technique*, Sensors and Actuators B: Chemical. 19 (**1994**) 629–631. https://doi.org/https://doi.org/10.1016/0925-4005(93)01216-Q.

[61] P. Borman, D. Elder, Q2(R1) Validation of Analytical Procedures, in: ICH Quality Guidelines, John Wiley & Sons, Ltd, **2017**: pp. 127–166. https://doi.org/10.1002/9781118971147.ch5.

[62] A. Menditto, M. Patriarca, B. Magnusson, *Understanding the meaning of accuracy, trueness and precision*, Accreditation and Quality Assurance. 12 (**2007**) 45–47. https://doi.org/10.1007/s00769-006-0191-z.

[63] P. De Bièvre, *The 2012 International Vocabulary of Metrology: "VIM,"* Accreditation and Quality Assurance. 17 (**2012**) 231–232. https://doi.org/10.1007/s00769-012-0885-3.

[64] ISO (2006) 3534-1, Statistics - Vocabulary and symbols - Part 1: General statistical terms and terms used in probability, Geneva, **2006**.

[65] M. Thompson, S.L.R. Ellison, R. Wood, *Harmonized guidelines for single-laboratory validation of methods of analysis (IUPAC Technical Report)*, Pure and Applied Chemistry. 74 (**2002**) 835–855. https://doi.org/10.1351/pac200274050835.

[66] P. Gründler, Chemical sensors: An introduction for scientists and engineers, Springer , Berlin, **2007**. https://doi.org/10.1007/978-3-540-45743-5.

[67] R.W. Cattrall, Chemical Sensors, Oxford: University Press, Oxford, **1997**. https://doi.org/10.1023/A:1016741111333.

[68] M. del Valle, *Electronic Tongues Employing Electrochemical Sensors*, Electroanalysis. 22 (**2010**) 1539–1555. https://doi.org/10.1002/ELAN.201000013.

[69] K. Toko, *A taste sensor*, Measurement Science and Technology. 9 (**1998**) 1919. https://doi.org/10.1088/0957-0233/9/12/001.

[70] M. del Valle, *Bioinspired Sensor Systems*, Sensors. 11 (**2011**) 10180–10186. https://doi.org/10.3390/s111110180.

[71] J. Seiter, M. Degrandpre, *Redundant chemical sensors for calibration-impossible applications*, Talanta. 54 (**2001**) 99–106. https://doi.org/10.1016/S0039-9140(00)00635-4.

[72] A. Herrera-Chacon, A. González-Calabuig, I. Campos, M. del Valle, *Bioelectronic tongue using MIP sensors for the resolution of volatile phenolic compounds*, Sensors and Actuators B: Chemical. 258 (**2018**) 665–671. https://doi.org/10.1016/j.snb.2017.11.136.

[73] X. Cetó, F. Céspedes, M. del Valle, *BioElectronic Tongue for the quantification of total polyphenol content in wine*, Talanta. 99 (**2012**) 544–551. https://doi.org/10.1016/j.talanta.2012.06.031.

[74] A. González-Calabuig, M. del Valle, *Voltammetric electronic tongue to identify Brett character in wines. On-site quantification of its ethylphenol metabolites*, Talanta. 179 (**2018**) 70–74. https://doi.org/10.1016/j.talanta.2017.10.041.

[75] D. Ortiz-Aguayo, M. Bonet-San-Emeterio, M. del Valle, *Simultaneous voltammetric determination of acetaminophen, ascorbic acid and uric acid by use of integrated array of screen-printed electrodes and chemometric tools*, Sensors (Switzerland). 19 (**2019**) 3286. https://doi.org/10.3390/s19153286.

[76] C. Kalinke, P.R. de Oliveira, M. Bonet San Emeterio, A. González-Calabuig, M. del Valle, A. Salvio Mangrich, L. Humberto Marcolino Junior, M.F. Bergamini, *Voltammetric Electronic Tongue Based on Carbon Paste Electrodes Modified with Biochar for Phenolic Compounds Stripping Detection*, Electroanalysis. 31 (**2019**) 2238–2245. https://doi.org/10.1002/elan.201900072.

[77] J.S. Schultz, R.F. Taylor, eds., Handbook of Chemical and Biological Sensors, CRC Press, Boca Ratón, **1996**. https://doi.org/10.1201/9780367802516.

[78] M. Bonet-San-Emeterio, X. Cetó, M. del Valle, Chapter 4-Voltammetric electronic tongues, in: F.M. Shimizu, M.L. Braunger, A. Riul Jr (Eds.), Electronic Tongues, IOP Publishing, **2021**: pp. 1–25. https://doi.org/10.1088/978-0-7503-3687-1CH4.

[79] N. Serrano, A. González-Calabuig, M. del Valle, *Crown ether-modified electrodes for the simultaneous stripping voltammetric determination of Cd(II), Pb(II) and Cu(II)*, Talanta. 138 (**2015**) 130–137. https://doi.org/10.1016/J.TALANTA.2015.01.044.

[80] N.U. Nazir, S.R. Abbas, H. Nasir, I. Hussain, *Electrochemical sensing of limonene using thiol capped gold nanoparticles and its detection in the real breath sample of a cirrhotic patient*, Journal of Electroanalytical Chemistry. 905 (**2022**) 115977. https://doi.org/10.1016/J.JELECHEM.2021.115977.

[81] C. Pérez-Ràfols, N. Serrano, J.M. Díaz-Cruz, C. Ariño, M. Esteban, *A screen-printed voltammetric electronic tongue for the analysis of complex mixtures of metal ions*, Sensors and Actuators, B: Chemical. 250 (**2017**) 393–401. https://doi.org/10.1016/j.snb.2017.04.165.

[82] M. Algarra, A. González-Calabuig, K. Radotić, D. Mutavdzic, C.O. Ania, J.M. Lázaro-Martínez, J. Jiménez-Jiménez, E. Rodríguez-Castellón, M. del Valle, *Enhanced electrochemical response of carbon quantum dot modified electrodes*, Talanta. 178 (**2018**) 679–685. https://doi.org/10.1016/J.TALANTA.2017.09.082.

[83] M. Bonet-San-Emeterio, M. Algarra, M. Petković, M. del Valle, *Modification of electrodes with N- and S-doped carbon dots. Evaluation of the electrochemical response*, Talanta. 212 (**2020**) 120806. https://doi.org/10.1016/j.talanta.2020.120806.

[84] A. Herrera-Chacón, Ş. Dinç-Zor, M. del Valle, *Integrating molecularly imprinted polymer beads in graphite-epoxy electrodes for the voltammetric biosensing of*

histamine in wines, Talanta. 208 (**2020**) 120348. https://doi.org/10.1016/j.talanta.2019.120348.

[85] M. Wang, X. Cetó, M. del Valle, *A novel electronic tongue using electropolymerized molecularly imprinted polymers for the simultaneous determination of active pharmaceutical ingredients*, Biosensors and Bioelectronics. 198 (**2022**) 113807. https://doi.org/10.1016/J.BIOS.2021.113807.

[86] A. Ambrosi, M. Pumera, *3D-printing technologies for electrochemical applications*, Chemical Society Reviews. 45 (**2016**) 2740–2755. https://doi.org/10.1039/C5CS00714C.

[87] C. Kalinke, N.V. Neumsteir, P. Roberto de Oliveira, B.C. Janegitz, J.A. Bonacin, *Sensing of L-methionine in biological samples through fully 3D-printed electrodes*, Analytica Chimica Acta. 1142 (**2021**) 135–142. https://doi.org/10.1016/J.ACA.2020.10.034.

[88] A. Kaliyaraj Selva Kumar, Y. Zhang, D. Li, R.G. Compton, *A mini-review: How reliable is the drop casting technique?*, Electrochemistry Communications. 121 (**2020**) 106867. https://doi.org/10.1016/J.ELECOM.2020.106867.

[89] Q. Huang, S. Hu, H. Zhang, J. Chen, Y. He, F. Li, W. Weng, J. Ni, X. Bao, Y. Lin, *Carbon dots and chitosan composite film based biosensor for the sensitive and selective determination of dopamine*, Analyst. 138 (**2013**) 5417–5423. https://doi.org/10.1039/c3an00510k.

[90] A. Cipri, M. del Valle, *Pd nanoparticles/multiwalled carbon nanotubes electrode system for voltammetric sensing of tyrosine.*, Journal of Nanoscience and Nanotechnology. 14 (**2014**) 6692–8. https://doi.org/10.1166/jnn.2014.9370.

[91] A. Merkoçi, M. Vasjari, E. Fàbregas, S. Alegret, *Determination of Pb and Cu by anodic stripping voltammetry using glassy carbon electrodes modified with mercury or mercury-nafion films*, Mikrochimica Acta. 135 (**2000**) 29–33. https://doi.org/10.1007/s006040070015.

[92] J.H.T. Luong, T. Narayan, S. Solanki, B.D. Malhotra, *Recent Advances of Conducting Polymers and Their Composites for Electrochemical Biosensing Applications*, Journal of Functional Biomaterials. 11 (**2020**) 71. https://doi.org/10.3390/jfb11040071.

[93] M.I. Pividori, S. Alegret, Electrochemical genosensing of food pathogens based on graphite–epoxy composite, in: S. Alegret, A. Merkoçi (Eds.), Comprehensive Analytical Chemistry, Elsevier, Amsterdam, **2007**: pp. 439–466. https://doi.org/10.1016/S0166-526X(06)49021-8.

[94] S.L. Moura, A. Pallarès-Rusiñol, L. Sappia, M. Martí, M.I. Pividori, *The activity of alkaline phosphatase in breast cancer exosomes simplifies the biosensing design*, Biosensors and Bioelectronics. 198 (**2022**) 113826. https://doi.org/10.1016/j.bios.2021.113826.

[95] J.F. Kennedy, J.M.S. Cabral, Immobilisation of biocatalysts by metal-link/chelation processes, Artif Cells Blood Substit Immobil Biotechnol, **1995**. https://doi.org/10.3109/10731199509117940.

[96] M. Pellissier, F. Barrière, A.J. Downard, D. Leech, *Improved stability of redox enzyme layers on glassy carbon electrodes via covalent grafting*, Electrochemistry Communications. 10 (**2008**) 835–838. https://doi.org/10.1016/j.elecom.2008.03.010.

[97] C. Ocaña, A. Hayat, R. Mishra, A. Vasilescu, M. del Valle, J.-L. Marty, *A novel electrochemical aptamer–antibody sandwich assay for lysozyme detection*, The Analyst. 140 (**2015**) 4148–4153. https://doi.org/10.1039/C5AN00243E.

[98] F. Šulek, D.P. Fernández, Ž. Knez, M. Habulin, R.A. Sheldon, *Immobilization of horseradish peroxidase as crosslinked enzyme aggregates (CLEAs)*, Process Biochemistry. 46 (**2011**) 765–769. https://doi.org/10.1016/j.procbio.2010.12.001.

[99] D.N. Tran, K.J. Balkus, *Perspective of Recent Progress in Immobilization of Enzymes*, ACS Catalysis. 1 (**2011**) 956–968. https://doi.org/10.1021/cs200124a.

[100] A.J. Bard, L.R. Faulkner, Electrochemical Methods: Fundamentals and Applications, 2nd ed., Wiley, New York, **2000**.

[101] C.M.A. Brett, A.M.O. Brett, Electroanalysis, Oxford, **2005**.

[102] D.A. Skoog, D.J. Holler, S.R. Crouch, Principios de análisis instrumental, 6ª ed., McGraw-Hill, Madrid, **2008**.

[103] J.M. Pingarrón, J. Labuda, J. Barek, C.M.A. Brett, M.F. Camões, M. Fojta, D.B. Hibbert, *Terminology of electrochemical methods of analysis (IUPAC Recommendations 2019)*, Pure and Applied Chemistry. 92 (**2020**) 641–694. https://doi.org/10.1515/PAC-2018-0109.

[104] D.C. Harris, Quantitative Chemical Analysis, 6th ed., Freeman and Co, New York, **2006**.

[105] C.G. Zoski, Handbook of Electrochemistry, Elsevier, Las Cruces, **2007**.

[106] M.A. Rodríguez, R.M. Carranza, R.B. Rebak, *Influence of halide ions and alloy microstructure on the passive and localized corrosion behavior of alloy 22*, Metallurgical and Materials Transactions A. 36 (**2005**) 1179–1185. https://doi.org/10.1007/s11661-005-0210-4.

[107] J. Pouladi, S.M. Mirabedini, H. Eivaz Mohammadloo, N.G. Rad, *Synthesis of novel plant oil-based isocyanate-free urethane coatings and study of their anti-corrosion properties*, European Polymer Journal. 153 (**2021**) 110502. https://doi.org/10.1016/j.eurpolymj.2021.110502.

[108] C. Liu, C. Li, K. Ahmed, Z. Mutlu, C.S. Ozkan, M. Ozkan, *Template Free and Binderless NiO Nanowire Foam for Li-ion Battery Anodes with Long Cycle Life and Ultrahigh Rate Capability*, Scientific Reports . 6 (**2016**) 1–8. https://doi.org/10.1038/srep29183.

[109] L.A. Middlemiss, A.J.R. Rennie, R. Sayers, A.R. West, *Characterisation of batteries by electrochemical impedance spectroscopy*, Energy Reports. 6 (**2020**) 232–241. https://doi.org/10.1016/j.egyr.2020.03.029.

[110] I. Gallardo, J. Pinson, N. Vilà, *Spontaneous Attachment of Amines to Carbon and Metallic Surfaces*, The Journal of Physical Chemistry B. 110 (**2006**) 19521–19529. https://doi.org/10.1021/jp063368c.

[111] D.A. García-Osorio, R. Jaimes, J. Vazquez-Arenas, R.H. Lara, J. Alvarez-Ramirez, *The Kinetic Parameters of the Oxygen Evolution Reaction (OER) Calculated on Inactive Anodes via EIS Transfer Functions:•OH Formation*, Journal of The Electrochemical Society. 164 (**2017**) E3321–E3328. https://doi.org/10.1149/2.0321711jes.

[112] D. Ortiz-Aguayo, *Label-Free Aptasensor for Lysozyme Detection Using Electrochemical Impedance Spectroscopy*, Sensors. 18 (**2018**) 354. https://doi.org/10.3390/s18020354.

[113] C. Ocaña, S. Lukic, M. del Valle, *Aptamer-antibody sandwich assay for cytochrome c employing an MWCNT platform and electrochemical impedance*, Microchimica Acta 2015 182:11. 182 (**2015**) 2045–2053. https://doi.org/10.1007/S00604-015-1540-6.

[114] J.M. Harkness, *In Appreciation A Lifetime of Connections: Otto Herbert Schmitt, 1913 - 1998*, Physics in Perspective . 4 (**2002**) 456–490. https://doi.org/10.1007/S000160200005.

[115] J.F.V. Vincent, O.A. Bogatyreva, N.R. Bogatyrev, A. Bowyer, A.-K. Pahl, *Biomimetics: its practice and theory*, Journal of The Royal Society Interface. 3 (**2006**) 471–482. https://doi.org/10.1098/rsif.2006.0127.

[116] A. Herrera-Chacón, X. Cetó, M. del Valle, *Molecularly imprinted polymers - towards electrochemical sensors and electronic tongues*, Analytical and Bioanalytical Chemistry. 413 (**2021**) 6117–6140. https://doi.org/10.1007/S00216-021-03313-8.

[117] M. Liang, X. Yan, *Nanozymes: From New Concepts, Mechanisms, and Standards to Applications*, Accounts of Chemical Research. 52 (**2019**) 2190–2200. https://doi.org/10.1021/acs.accounts.9b00140.

[118] B. Das, J. Lou Franco, N. Logan, P. Balasubramanian, M. Il Kim, C. Cao, *Nanozymes in Point-of-Care Diagnosis: An Emerging Futuristic Approach for Biosensing*, Nano-Micro Letters . 13 (**2021**) 193. https://doi.org/10.1007/S40820-021-00717-0.

[119] A. Mroczko-Wąsowicz, ed., Perception-Cognition Interface & Cross-Modal Experiences: Insights into Unified Consciousness, Frontiers Media, **2017**.

[120] A.J. Privitera, Sensation and Perception, in: R. Biswas-Diener, E. Diener (Eds.), Noba Textbook Series: Psychology, DEF publishers, Champaign, **2021**.

[121] P. Mielle, B. Hivert, G. Mauvais, *Are gas sensors suitable for on-line monitoring and quantification of volatile compounds?*, Proceedings of Bioflavour . 95 (**1995**) 81–84.

[122] S.D. Roper, *Taste: Mammalian Taste Bud Physiology*, The Curated Reference Collection in Neuroscience and Biobehavioral Psychology. (**2017**) 887–893. https://doi.org/10.1016/B978-0-12-809324-5.02908-4.

[123] B. Lindemann, *Receptors and transduction in taste*, Nature . 413 (**2001**) 219–225. https://doi.org/10.1038/35093032.

[124] E. Adler, M.A. Hoon, K.L. Mueller, J. Chandrashekar, N.J.P. Ryba, C.S. Zuker, *A Novel Family of Mammalian Taste Receptors*, Cell. 100 (**2000**) 693–702. https://doi.org/10.1016/S0092-8674(00)80705-9.

[125] J. Chandrashekar, M.A. Hoon, N.J.P. Ryba, C.S. Zuker, *The receptors and cells for mammalian taste*, Nature . 444 (**2006**) 288–294. https://doi.org/10.1038/nature05401.

[126] Yu. Vlasov, A. Legin, A. Rudnitskaya, C. Di Natale, A. D'Amico, *Nonspecific sensor arrays ("electronic tongue") for chemical analysis of liquids (IUPAC Technical Report)*, Pure and Applied Chemistry. 77 (**2005**) 1965–1983. https://doi.org/10.1351/pac200577111965.

[127] A. Legin, D. Kirsanov, M. del Valle, *Avoiding nonsense in electronic taste sensing*, TrAC - Trends in Analytical Chemistry. 121 (**2019**) 115675. https://doi.org/10.1016/j.trac.2019.115675.

[128] Y. Kobayashi, M. Habara, H. Ikezazki, R. Chen, Y. Naito, K. Toko, *Advanced Taste Sensors Based on Artificial Lipids with Global Selectivity to Basic Taste Qualities and High Correlation to Sensory Scores*, Sensors . 10 (**2010**) 3411–3443. https://doi.org/10.3390/S100403411.

[129] T.T. Bachmann, R.D. Schmid, *A disposable multielectrode biosensor for rapid simultaneous detection of the insecticides paraoxon and carbofuran at high resolution*, Analytica Chimica Acta. 401 (**1999**) 95–103. https://doi.org/10.1016/S0003-2670(99)00513-9.

[130] E. Tønning, S. Sapelnikova, J. Christensen, C. Carlsson, M. Winther-Nielsen, E. Dock, R. Solna, P. Skladal, L. Nørgaard, T. Ruzgas, J. Emnéus, *Chemometric exploration of an amperometric biosensor array for fast determination of wastewater quality*, Biosensors and Bioelectronics. 21 (**2005**) 608–617. https://doi.org/10.1016/J.BIOS.2004.12.023.

[131] J. Wang, S. Kong, F. Chen, W. Chen, L. Du, W. Cai, L. Huang, C. Wu, D.W. Zhang, *A bioelectronic taste sensor based on bioengineered Escherichia coli cells combined with ITO-constructed electrochemical sensors*, Analytica Chimica Acta. 1079 (**2019**) 73–78. https://doi.org/10.1016/j.aca.2019.06.023.

[132] C. Qin, Z. Qin, D. Zhao, Y. Pan, L. Zhuang, H. Wan, A. di Pizio, E. Malach, M.Y. Niv, L. Huang, N. Hu, P. Wang, *A bioinspired in vitro bioelectronic tongue with human T2R38 receptor for high-specificity detection of N-C=S-containing compounds*, Talanta. 199 (**2019**) 131–139. https://doi.org/10.1016/j.talanta.2019.02.021.

[133] G. Hui, S. Mi, Q. Chen, X. Chen, *Sweet and bitter tastant discrimination from complex chemical mixtures using taste cell-based sensor*, Sensors and Actuators, B: Chemical. 192 (**2014**) 361–368. https://doi.org/10.1016/j.snb.2013.10.119.

[134] D. Ebrahimi, E. Chow, J.J. Gooding, D.B. Hibbert, *Multi-analyte sensing: A chemometrics approach to understanding the merits of electrode arrays versus*

single electrodes, Analyst. 133 (**2008**) 1090–1096. https://doi.org/10.1039/b804811h.

[135] C. Medina-Plaza, C. García-Hernández, J.A. de Saja, J.A. Fernández-Escudero, E. Barajas, G. Medrano, C. García-Cabezón, F. Martin-Pedrosa, M.L. Rodriguez-Mendez, *The advantages of disposable screen-printed biosensors in a bioelectronic tongue for the analysis of grapes*, LWT - Food Science and Technology. 62 (**2015**) 940–947. https://doi.org/10.1016/j.lwt.2015.02.027.

[136] J. Lange, C. Wittmann, *Enzyme sensor array for the determination of biogenic amines in food samples*, Analytical and Bioanalytical Chemistry. 372 (**2002**) 276–283. https://doi.org/10.1007/s00216-001-1130-9.

[137] Á.A. Arrieta, M.L. Rodríguez-Méndez, J.A. de Saja, C.A. Blanco, D. Nimubona, *Prediction of bitterness and alcoholic strength in beer using an electronic tongue*, Food Chemistry. 123 (**2010**) 642–646. https://doi.org/10.1016/j.foodchem.2010.05.006.

[138] N. Serrano, X. Cetó, O. Núñez, M. Aragó, A. Gámez, C. Ariño, J.M. Díaz-Cruz, *Characterization and classification of Spanish paprika (Capsicum annuum L.) by liquid chromatography coupled to electrochemical detection with screen-printed carbon-based nanomaterials electrodes*, Talanta. 189 (**2018**) 296–301. https://doi.org/10.1016/j.talanta.2018.06.085.

[139] X. Cetó, J.M. Gutiérrez, M. Gutiérrez, F. Céspedes, J. Capdevila, S. Mínguez, C. Jiménez-Jorquera, M. del Valle, *Determination of total polyphenol index in wines employing a voltammetric electronic tongue*, Analytica Chimica Acta. 732 (**2012**) 172–179. https://doi.org/10.1016/j.aca.2012.02.026.

[140] A. González-Calabuig, X. Cetó, M. del Valle, *Electronic tongue for nitro and peroxide explosive sensing*, Talanta. 153 (**2016**) 340–346. https://doi.org/10.1016/j.talanta.2016.03.009.

[141] E.G. Breijo, C.O. Pinatti, R.M. Peris, M.A. Fillol, R. Martínez-Máñez, J.S. Camino, *TNT detection using a voltammetric electronic tongue based on neural networks*, Sensors and Actuators A: Physical. 192 (**2013**) 1–8. https://doi.org/10.1016/j.sna.2012.11.038.

[142] A. Gutés, F. Céspedes, S. Alegret, M. del Valle, *Determination of phenolic compounds by a polyphenol oxidase amperometric biosensor and artificial neural network analysis*, Biosensors and Bioelectronics. 20 (**2005**) 1668–1673. https://doi.org/10.1016/j.bios.2004.07.026.

[143] A. Legin, A. Rudnitskaya, D. Clapham, B. Seleznev, K. Lord, Y. Vlasov, *Electronic tongue for pharmaceutical analytics: quantification of tastes and masking effects*, Analytical and Bioanalytical Chemistry 2004 380:1. 380 (**2004**) 36–45. https://doi.org/10.1007/S00216-004-2738-3.

[144] T. v. Shishkanova, G. Broncová, A. Skálová, V. Prokopec, M. Člupek, V. Král, *Potentiometric Electronic Tongue for Taste Assessment of Ibuprofen Based Pharmaceuticals*, Electroanalysis. 31 (**2019**) 2024–2031. https://doi.org/10.1002/ELAN.201900334.

[145] G.A. Campbell, J.A. Charles, K. Roberts-Skilton, M. Tsundupalli, C.K. Oh, A. Weinecke, R. Wagner, D. Franz, *Evaluating the taste masking effectiveness of various flavors in a stable formulated pediatric suspension and solution using the Astree™ electronic tongue*, Powder Technology. 224 (**2012**) 109–123. https://doi.org/10.1016/j.powtec.2012.02.038.

[146] K. Persaud, G. Dodd, *Analysis of discrimination mechanisms in the mammalian olfactory system using a model nose*, Nature . 299 (**1982**) 352–355. https://doi.org/10.1038/299352a0.

[147] F. Röck, N. Barsan, U. Weimar, *Electronic Nose: Current Status and Future Trends*, Chemical Reviews. 108 (**2008**) 705–725. https://doi.org/10.1021/cr068121q.

[148] E.A. Baldwin, J. Bai, A. Plotto, S. Dea, *Electronic Noses and Tongues: Applications for the Food and Pharmaceutical Industries*, Sensors . 11 (**2011**) 4744. https://doi.org/10.3390/S110504744.

[149] P.J. Mazzone, *Analysis of Volatile Organic Compounds in the Exhaled Breath for the Diagnosis of Lung Cancer*, Journal of Thoracic Oncology. 3 (**2008**) 774–780. https://doi.org/10.1097/JTO.0b013e31817c7439.

[150] N. Fens, A.H. Zwinderman, M.P. van der Schee, S.B. de Nijs, E. Dijkers, A.C. Roldaan, D. Cheung, E.H. Bel, P.J. Sterk, *Exhaled Breath Profiling Enables Discrimination of Chronic Obstructive Pulmonary Disease and Asthma*, American Journal of Respiratory and Critical Care Medicine. 180 (**2012**) 1076–1082. https://doi.org/10.1164/RCCM.200906-0939OC.

[151] S. Dragonieri, R. Schot, B.J.A. Mertens, S. le Cessie, S.A. Gauw, A. Spanevello, O. Resta, N.P. Willard, T.J. Vink, K.F. Rabe, E.H. Bel, P.J. Sterk, *An electronic nose in the discrimination of patients with asthma and controls*, Journal of Allergy and Clinical Immunology. 120 (**2007**) 856–862. https://doi.org/10.1016/J.JACI.2007.05.043.

[152] M. Mamat, S.A. Samad, M. Hannan, *An Electronic Nose for Reliable Measurement and Correct Classification of Beverages*, Sensors. 11 (**2011**) 6435–6453. https://doi.org/10.3390/s110606435.

[153] J.C. Yang, J. Mun, S.Y. Kwon, S. Park, Z. Bao, S. Park, *Electronic Skin: Recent Progress and Future Prospects for Skin‐Attachable Devices for Health Monitoring, Robotics, and Prosthetics*, Advanced Materials. 31 (**2019**) 1904765. https://doi.org/10.1002/adma.201904765.

[154] S.J. Xie, S. Yoon, J. Shin, D.S. Park, *Effective Fingerprint Quality Estimation for Diverse Capture Sensors*, Sensors. 10 (**2010**) 7896–7912. https://doi.org/10.3390/S100907896.

[155] G. Botella, J.A.M. H., M. Santos, U. Meyer-Baese, *FPGA-Based Multimodal Embedded Sensor System Integrating Low- and Mid-Level Vision*, Sensors . 11 (**2011**) 8164–8179. https://doi.org/10.3390/S110808164.

[156] F. Vidal-Verdú, Ó. Oballe-Peinado, J. Sánchez-Durán, J. Castellanos-Ramos, R. Navas-González, *Three realizations and comparison of hardware for piezoresistive tactile sensors*, Sensors. 11 (**2011**) 3249–3266. https://doi.org/10.3390/S110303249.

[157] T. Pallejà, M. Tresanchez, M. Teixidó, J. Palacin, *Bioinspired electronic white cane implementation based on a LIDAR, a tri-axial accelerometer and a tactile belt*, Sensors. 10 (**2010**) 11322–11339. https://doi.org/10.3390/S101211322.

[158] Y. Zhang, Y. Zhao, W. Zhai, G. Zheng, Y. Ji, K. Dai, L. Mi, D. Zhang, C. Liu, C. Shen, *Multifunctional interlocked e-skin based on elastic micropattern array facilely prepared by hot-air-gun*, Chemical Engineering Journal. 407 (**2021**) 127960. https://doi.org/10.1016/J.CEJ.2020.127960.

[159] M.L. Rodriguez-Mendez, C. Apetrei, I. Apetrei, S. Villanueva, I.J.A. de Saja, I. Nevares, M. del Alamo, Combination of an electronic nose, an electronic tongue and an electronic eye for the Analysis of Red Wines aged with alternative methods, in: 2007 IEEE International Symposium on Industrial Electronics, IEEE, **2007**: pp. 2782–2787. https://doi.org/10.1109/ISIE.2007.4375050.

[160] L. Vera, L. Aceña, J. Guasch, R. Boqué, M. Mestres, O. Busto, *Discrimination and sensory description of beers through data fusion*, Talanta. 87 (**2011**) 136–142. https://doi.org/10.1016/j.talanta.2011.09.052.

[161] L. Dagge, K. Harr, M. Paul, G. Schnedl, *Classification of process analysis: offline, atline, online, inline* , Cement International. 7 (**2009**) 72–81.

[162] D.L. Massart, B.G.M. Vandeginste, L.M.C. Buydens, S. de Jong, P.J. Lewi, J. Smeyers-Verbeke, eds., Handbook of Chemometrics and Qualimetrics: Part A and B, Elsevier, Amsterdam, **1998**.

[163] D. Ortiz-Aguayo, K. de Wael, M. del Valle, *Voltammetric sensing using an array of modified SPCE coupled with machine learning strategies for the improved identification of opioids in presence of cutting agents*, Journal of Electroanalytical Chemistry. 902 (**2021**) 115770. https://doi.org/10.1016/j.jelechem.2021.115770.

[164] M. Sarma, N. Romero, X. Cetó, M. del Valle, *Optimization of Sensors to be Used in a Voltammetric Electronic Tongue Based on Clustering Metrics*, Sensors. 20 (**2020**) 4798. https://doi.org/10.3390/s20174798.

[165] X. Cetó, F. Céspedes, M. del Valle, *Comparison of methods for the processing of voltammetric electronic tongues data*, Microchimica Acta. 180 (**2013**) 319–330. https://doi.org/10.1007/S00604-012-0938-7/FIGURES/5.

[166] P. Oliveri, M.C. Casolino, M. Forina, *Chemometric Brains for Artificial Tongues*, Advances in Food and Nutrition Research. 61 (**2010**) 57–117. https://doi.org/10.1016/B978-0-12-374468-5.00002-7.

[167] X. Cetó, C. Saint, C.W.K. Chow, N.H. Voelcker, B. Prieto-Simón, *Electrochemical fingerprints of brominated trihaloacetic acids (HAA3) mixtures in water*, Sensors and Actuators B: Chemical. 247 (**2017**) 70–77. https://doi.org/10.1016/J.SNB.2017.02.179.

[168] C. Medina-Plaza, J.A. de Saja, M.L. Rodriguez-Mendez, *Bioelectronic tongue based on lipidic nanostructured layers containing phenol oxidases and lutetium bisphthalocyanine for the analysis of grapes*, Biosensors and Bioelectronics. 57 (**2014**) 276–283. https://doi.org/10.1016/j.bios.2014.02.023.

[169] C. Garcia-Hernandez, C. Garcia-Cabezon, F. Martin-Pedrosa, M.L. Rodriguez-Mendez, *Analysis of musts and wines by means of a bio-electronic tongue based on tyrosinase and glucose oxidase using polypyrrole/gold nanoparticles as the electron mediator*, Food Chemistry. 289 (**2019**) 751–756. https://doi.org/10.1016/j.foodchem.2019.03.107.

[170] A. Cipri, C. Schulz, R. Ludwig, L. Gorton, M. del Valle, *A novel bio-electronic tongue using different cellobiose dehydrogenases to resolve mixtures of various sugars and interfering analytes*, Biosensors and Bioelectronics. 79 (**2016**) 515–521. https://doi.org/10.1016/j.bios.2015.12.069.

[171] E. Richards, C. Bessant, S. Saini, *Multivariate Data Analysis in Electroanalytical Chemistry*, Electroanalysis. 14 (**2002**) 1533–1542. https://doi.org/10.1002/1521-4109.

[172] M. Cortina, A. Duran, S. Alegret, M. del Valle, *A sequential injection electronic tongue employing the transient response from potentiometric sensors for anion multidetermination*, Analytical and Bioanalytical Chemistry. 385 (**2006**) 1186–1194. https://doi.org/10.1007/S00216-006-0530-2.

[173] V. Pravdová, M. Pravda, G.G. Guilbault, *Role of chemometrics for electrochemical sensors*, Analytical Letters. 35 (**2002**) 2389–2419. https://doi.org/10.1081/AL-120016533.

[174] J. Simons, M. Bos, W.E. van der Linden, *Data processing for amperometric signals*, Analyst. 120 (**1995**) 1009–1012. https://doi.org/10.1039/AN9952001009.

[175] X. Cetó, F. Céspedes, M. del Valle, *Assessment of Individual Polyphenol Content in Beer by Means of a Voltammetric BioElectronic Tongue*, Electroanalysis. 25 (**2013**) 68–76. https://doi.org/10.1002/elan.201200299.

[176] L. Moreno-Barón, R. Cartas, A. Merkoçi, S. Alegret, M. del Valle, L. Leija, P.R. Hernandez, R. Muñoz, *Application of the wavelet transform coupled with artificial neural networks for quantification purposes in a voltammetric electronic tongue*, Sensors and Actuators, B: Chemical. 113 (**2006**) 487–499. https://doi.org/10.1016/j.snb.2005.03.063.

[177] S.G. Mallat, *A Theory for Multiresolution Signal Decomposition: The Wavelet Representation*, IEEE Transactions on Pattern Analysis and Machine Intelligence. 11 (**1989**) 674–693. https://doi.org/10.1109/34.192463.

[178] I.T. Jolliffe, Principal Component Analysis, 2nd ed., Springer New York Inc., New York, **2002**. https://doi.org/10.1007/B98835.

[179] D. Meyer, F. Leisch, K. Hornik, *The support vector machine under test*, Neurocomputing. 55 (**2003**) 169–186. https://doi.org/10.1016/S0925-2312(03)00431-4.

[180] C. Cortes, V. Vapnik, L. Saitta, *Support-vector networks*, Machine Learning . 20 (**1995**) 273–297. https://doi.org/10.1007/BF00994018.

[181] S. de Jong, *SIMPLS: An alternative approach to partial least squares regression*, Chemometrics and Intelligent Laboratory Systems. 18 (**1993**) 251–263. https://doi.org/10.1016/0169-7439(93)85002-X.

[182] M. Blanco, V. Cerdá Martín, Temas avanzados de quimiometría, Universitat de les Illes Balears Servei de Publicacions i Intercanvi Científic, Palma, **2007**.

[183] R. Bro, Multi-way Analysis in the Food Industry Models, Algorithms, and Applications, **1998**.

[184] A. Hoffmann, Artificial and Natural Computation, in: N.J. Smelser, P.B. Baltes (Eds.), International Encyclopedia of the Social & Behavioral Sciences, Pergamon, Oxford, **2001**: pp. 777–783.

[185] F. Despagne, D.L. Massart, D. Luc Massart, *Neural networks in multivariate calibration*, The Analyst. 123 (**1998**) 157–178. https://doi.org/10.1039/a805562i.

[186] M.T. Hagan, H.B. Demuth, M.H. Beale, O. de Jesús, Neural network design, PWS Publishing Co., Boston, **1996**.

[187] D.J.C. MacKay, *Bayesian Interpolation*, Neural Computation. 4 (**1992**) 415–447. https://doi.org/10.1162/NECO.1992.4.3.415.

[188] F. Burden, D. Winkler, *Bayesian Regularization of Neural Networks*, Methods in Molecular Biology. 458 (**2008**) 23–42. https://doi.org/10.1007/978-1-60327-101-1_3.

[189] M.T. Hagan, M.B. Menhaj, *Training Feedforward Networks with the Marquardt Algorithm*, IEEE Transactions on Neural Networks. 5 (**1994**) 989–993. https://doi.org/10.1109/72.329697.

[190] A.M. Molinaro, R. Simon, R.M. Pfeiffer, *Prediction error estimation: a comparison of resampling methods*, Bioinformatics. 21 (**2005**) 3301–3307. https://doi.org/10.1093/bioinformatics/bti499.

Chapter II. Objectives

2 OBJECTIVES

(Bio)sensors field sought the ideal device, for this reason, novel materials and methodologies are being developed in the current scope of science. One of the fundamental parts in the actual state of the art is the inclusion of advanced materials in the sensors in order to achieve the desired target. Additionally, nowadays the improvements are reached not only with the direct chemical improving but also focusing the topic from a more mathematical point of view. It consists of the process and study of the recorded data in order to discriminate the value and aimed information. Thereby, the main goal of the present thesis work is the inclusion of advanced carbon nanomaterials, graphene and carbon dots, on voltammetric sensors for their application in electronic tongues approaches, thus combining two of the most striking fields in analytical chemistry.

The specific objectives in this work were separated into two blocks:

1. To develop a stable graphene sensory platform.

I. To study and characterize graphene from different sources and choose the best nanomaterial for their integration in voltammetric electrodes.

II. To develop a suitable protocol for the modification of the sensor surface.

III. To study and characterize the modified sensor to prove the goodness of the nanomaterial integration.

IV. To apply the graphene sensor in real problematics.

- To exploit the characteristics of graphene to resolve and quantify complex mixtures of dopamine, serotonin, and their principal interferents, ascorbic acid and uric acid.
- To modify the graphene platform with biorecognition elements, enzymes, in order to create improved electrodes for the quantification of phenolic compounds in wine.
- To use chemometric tools together with the abovementioned cases to achieve the proposed goals.

2. To develop sensors with different modified carbon dots.

I. To develop a stable and reproducible electrode modification protocol.

II. To corroborate the proper electrode modification.

III. To search the applicability of the developed electrodes in real cases.

Chapter III. Experimental

3 EXPERIMENTAL

The experimental part of this thesis work considers the publications mentioned on the initial page of this manuscript.

The main goal of this section is to describe the specific designs and characteristics of the experiments.

3.1 Chemicals and buffers

The buffers used in each paper are summed up in Table 3.1. As it can be seen, most of the works were carried out in phosphate-buffered saline solution (PBS). The pHs were optimized in each case considering the solubilities of the target molecules, and the responses of the working electrodes against them. Moreover, in the case of biosensors were taken into account the isoelectronic point of the enzymes in order to work at the most suitable point.

On the other side, ferrocyanide redox salt (Merck KGaA, DEU) was used as an electrochemical standard to study the behavior of the developed sensors.

Impedimetric measurements were carried out in $[Fe(CN)_6]^{3-/4-}$ 10 mM (1:1) solution, which was diluted with the corresponding measurement buffer

Table 3.1. Summary table of herein employed buffers. It is specified the salt, the concentrations, the pH, and the papers in which each is used.

Buffer	Concentration	pH	Article
PBS 1	50 mM PBS 100 mM KCl	7.4	[1–3]
PBS 2	100 mM PBS 100 mM KCl	7.0	[4]

The target molecules in this thesis work can be divided into two different groups: volatile phenolic compound from wine [2,3], and neurotransmitters, (dopamine (DA), serotonin (5-HT), and its interferent molecules ascorbic acid (AA) and uric acid (UA)) [1]. Moreover, the first attempt of carbon dot modified electrode was tested with AA, salicylic acid (SA), and cysteine (CYS) [4]. Table 3.2 resumes the analytes used in each paper and where were purchased.

GO materials used in the modification of the electrode were from two different origins. The first was synthesized in the laboratory collaboratively with two coworkers. The second sample was obtained from Nanoinnova Tech (ESP). In the same way, CDs and modified CDs were synthesized in a partnership with Professor Manuel Algarra from the Public University of Navarra, Pamplona.

The biorecognition elements incorporated in the biosensors were laccase (Lac) and tyrosinase (Tyr) enzymes, both catalysts for the oxidation of phenolic compounds. Lac was obtained from *Agaricus Bisporus* (EC 420-150-4, 7.2 $U \cdot mg^{-1}$) and *Trametes Versicolor* (EC 1.10.3.2, 21 $U \cdot mg^{-1}$) organisms, and Tyr from mushroom (EC 1.14.18.1, 4276 U mg^{-1}).

Graphite epoxy composite (GEC) electrodes were prepared using two different epoxy resins, the specifications and building procedures are defined in §3.4.1.1.

Table 3.2. Summary table of analytes employed in the experimental part of this thesis work.

Analyte	Company	Article
Dopamine	Merck KGaA	
Ascorbic Acid	Panreac Química (ESP)	[1]
Uric Acid	Merck KGaA	
Catechol		
EDTA[1]	Merck KGaA	[2]
Benzoic Acid		
Catechol		
4-Ethylphenol	Merck KGaA	[3]
4-Ethylcatechol		
4-Ethylguaiachol		
Ascorbic Acid	Panreac Química	
Salicylic Acid	Merck KGaA	[4]
Cysteine	Acros Organics (BEL)	

[1]Ethylenediaminetetraacetic acid

As specified in §3.5.2.2, polystyrene inks must be activated before its use, for this purpose, a dissolution of H_2O_2 50 mM in PBS 50 mM + KCl 100 mM was used.

In order to improve the features of the sensors, some treatments were developed. For example, in the measurement of DA, which produces a fouling effect on the surface of the electrode. When it was measured was implemented a further stage, an electrochemical cleaning. This step involved the application of +1.20 V during 40 s in a solution of HCl 100 mM between measurements.

All the solutions were prepared in deionized water (Millipore, USA) with a conductivity of 18.2 MΩ·cm. Moreover, it must be pointed out that all the raw chemicals are of an analytical grade.

3.2 Instruments

This work was carried out using voltammetric techniques such as DPV, CV, and EIS. Voltammetric measurements were performed in an Autolab PGStat20 with 6 channels (Metrohm Autolab BV, NLD) and in a PalmSens

MultiEmStat multichannel potentiostat (PalmSens BV, NLD). While EIS measurements were carried out in an IM6e Impedance Measurement Unit (BAS-Zahner, DEU) or in an Autolab PGStat20 in the single-channel modus.

Regarding the imaging of the electrode surface, a scanning electron microscope EVO®MA10 (Zeiss, DEU) was used for the scanning electron microscopy (SEM). Transmission electron microscopy (TEM); was recorded in a JEM-2011 microscope (JEOL Ltd., JPN). AFM images were obtained in a Veeco Dimension 3100 Microscope (Bruker, USA).

Elemental analysis, matrix-assisted laser desorption/Ionization time of flight mass spectrometry (MALDI TOF MS), and X-ray photoelectron spectroscopy (XPS) were charged to external services. The elemental analysis in a FLASH 2000 (Thermo Fisher Scientific, USA), the XPS was done in a PHOIBOS (SPECs Group, DEU), and the MALDI TOF MS in an Autoflex Max Device (Bruker, USA).

3.3 Software

The software to control potentiostats were GPES 4.7 and GPES Multichanle 4.7 for voltammetric measurements, and FRA for impedimetric experiments (Metrohm Autolab BV, NLD), when used Autolab potentiostats, Thales when used BAS-Zhaner potentiostat (BAS-Zahner, DEU), and Multitrace 4.2 when used PalmSens potentiostat (PalmSens BV, NLD).

Mathematical and data treatments were performed in MATLAB versions 2017b, and 2020a (The MathWorks Inc., USA), and Excel (Microsoft, USA). The representation tool was OriginPro 8 (OriginLab Corporation, USA)

Topographic studies were performed in CasaXPS (Casa Software Ltd, USA) software for the XPS data, and with ImageJ (National Institute of Health, USA) was analyzed the SEM and TEM recorded images [5].

3.4 Graphene synthesis

The synthesis of graphene was carried out twice together with laboratory partners and following a modified Hummers's method [5].

The top-down synthesis of GO is performed starting from ultra-pure graphite (Merck). The oxidation of graphite is achieved using strong chemical oxidation agents: H_2SO_4 (98%), $NaNO_3$ (99%), and $KMnO_4$ (99%), all reagents purchased in Merck.

Firstly, 1.5 g of graphite and 0.75 g of $NaNO_3$ are mixed with 35 mL of H_2SO_4 previously cooled at 0 ^{0}C. After 4.5 g of $KMnO_4$ are added to the previous flask, it must be taken into account that in order to avoid temperatures beyond 70 ^{0}C, the solid should be carefully added in small portions during *ca.* 2 hours. Once the reagents are together, the mixture is stirred for 4 hours at room temperature, and finally 30 minutes at 35 ^{0}C. The oxidation time was previously optimized in the laboratory and discussed in Y. Aceta work [6]. Th end of the graphite oxidation process is made under controlled temperature (<70 ^{0}C) by adding 75 mL of deionized water into the reaction. The resulting solution is kept at 70 ^{0}C for 15 minutes. In this stage the graphite oxide is obtained, which must be separated and purified.

The purification method starts with the neutralization of the remaining oxidation agents. At first, the resulting product is diluted in 300 mL of deionized water to be treated with a certain volume of H_2O_2 (30%, Riedel-de Haën, DEU) until no effervescence appears. Then the mixture is filtered, being the slush part the interesting one. This brown paste is washed three times with 500 mL of deionized water (until fulfil a pH *ca.* 7) and centrifugated at 6000 rpm for 10 minutes. The resulting material is treated with cationic and anionic resins (cationic resin C100E, and anionic resin A520E, both from Purolite brand purchased in Merck) to separate the remaining ions, each resin stays in contact for 30 minutes with the GO, the process takes part under stirring. Finally, to check if there are sulphate ions in the sample, a test with $Ba(NO_3)_3$ (Acros Organics) is carried out, being negative if a white solid is not formed and indicating GO is successfully synthetized. Finally, the obtained slurry is dried in a vacuum oven at 60 ^{0}C for 48h. A schematic summary is depicted in Figure 3.39.

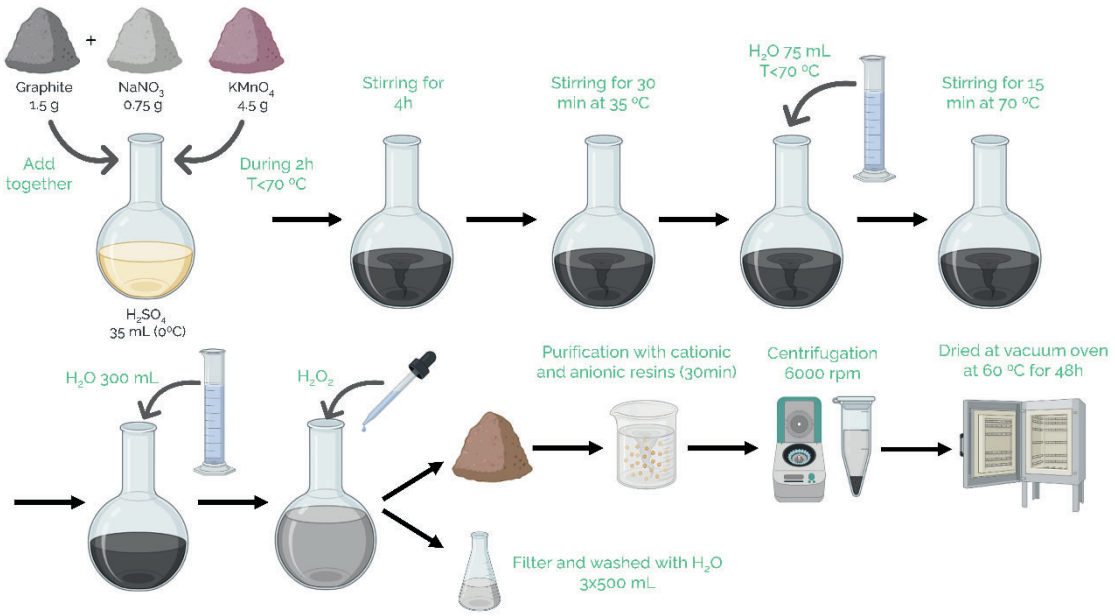

Figure 3.39. Flow chart of the top-down GO synthesis.

3.5 Protocols for (Bio)sensors

3.5.1 Electrode construction

In this project, the working electrode platforms were GECs and glassy carbon (GC), of a commercial domain, when used carbon dots as modifiers. In the next sections, special descriptions will be indicated.

3.5.1.1 Graphite Epoxy Composite electrodes

GECs as the name indicates, are devices based on a composite of an epoxy resin and graphite. Epoxy resins are characterized by their high mechanical resistance, low shrinkage, low cost, low toxicity, and chemical resistance, but on the other hand, have poor conductivity. For this reason, the adhesion of graphite at the composite is mandatory to obtain a feasible transducer. Epoxy resin is divided into two parts, the hardener, and the liquid resin. To obtain the desired composite, both parts are mixed following the manufacturer's recommendations together with the graphite. Regarding the proportion of graphite, the percolation curves performed with Resineco Epoxy resin (Resineco green composites, Spain) indicate that the optimum ratio of resin:graphite is 48:52 w/w.

As Figure 3.2 shows, to build the electrode, firstly a 5 mm ø cupper disk is welded on a gold connector. Notice that previously the cupper plate is immersed

in chlorohydric acid to eliminate the oxidated upper layer. Afterward, is wedged the structure in a PVC tube of *ca.* 25 mm of length and 6 mm of inner ø, thus obtaining the body of the electrode. Once the frame is ready, the remaining hole is filled with the previously prepared composite. As abovementioned the composite was prepared with graphite (50 µm particle size, from Merck KGaA), part A of the resin kit (the liquid epoxy resin), and part B (the hardener), all in the proper proportions. Then the mixture is homogenized for 40 minutes and infilled into the structure. Hereafter, it is put in the oven until the composite is hardened. The hardening parameters depend also on the brand, in this case, Resineco needs 3 days at 40 ^{o}C. Finally, the composite is polished with different sizes of abrasive paper until obtaining a homogeneous, fine, and mirror surface. The final geometric area is nearby 28 mm^2.

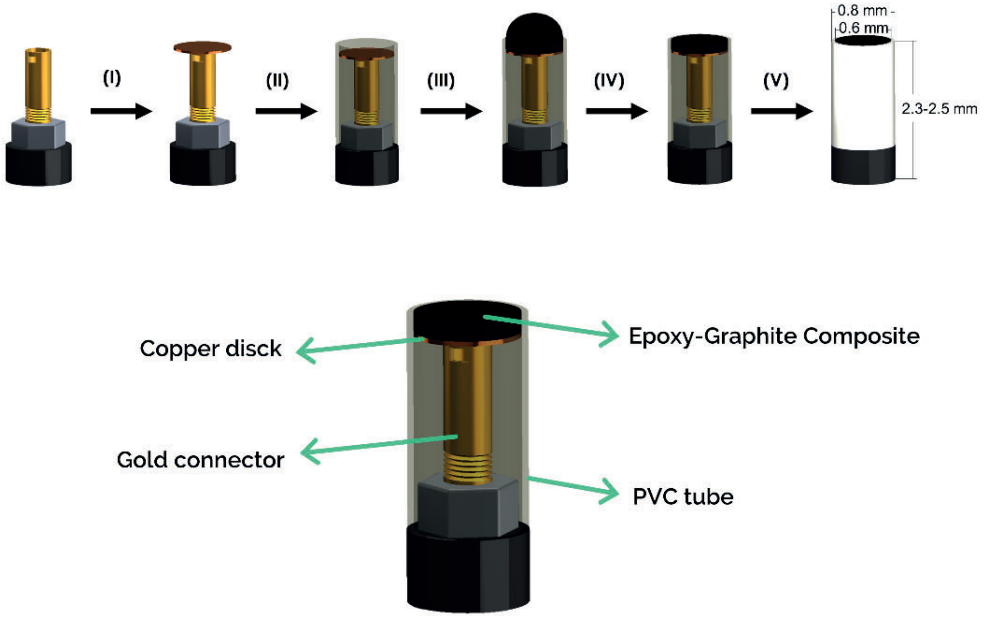

Figure 3.2 Schematic image of the Graphite Epoxy Composite electrodes construction, once finished the inner diameter is 0.6 mm. It includes the transversal cut with the parts identified.

3.5.1.2 Glassy Carbon electrodes

GC or vitreous carbon electrodes are a widespread component in analytical laboratories, they are stable, have a well-known response, and are commercially available. The working electrode material is a random combination of basal and edge graphitic planes with sp^2 electron configuration [7].

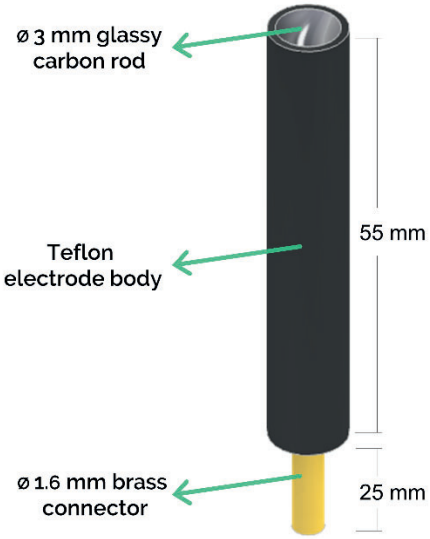

Figure 3.3. Schematic representation of a GC electrode.

3.5.2 (Bio)sensors modification

The electrodes can be modified basically in two ways, in bulk or only onto the surface. Obviously, when using GC electrodes only the surface can be modified, being in this sense, the own production of GEC electrodes, a clear advantage (detailed in §3.5.1.1). In the next sections will be addressed the strategies employed for the modification of the surface of the electrode.

3.5.2.1 Simple drop-casting for GO modified electrodes

Drop casting as explained in the introduction (§1.2.5.1), is a modification technique based on the coating of surfaces by depositing suspensions, i.e. non-soluble materials, on top of a platform. When the liquid in which the modifier is dispersed evaporates, the modified platform with a randomly ordered and non-homogeneous layer is obtained.

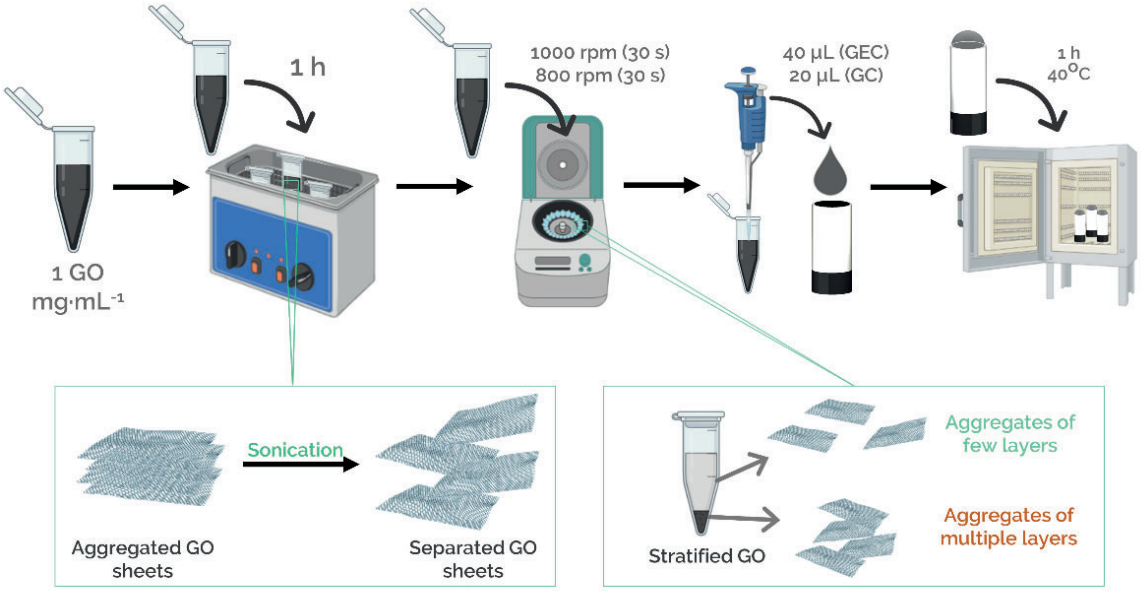

Figure 3.4. Schematic description of the drop-casting modification procedure applied in a GEC electrode modified with GO.

In this work, drop-casting has been used for the integration of GO and CDs onto the surface of GEC and GC, respectively. Figure 3.4 depicts the integration of GO onto the GEC electrodes. The first step is to prepare a dispersion of GO 1 $mg \cdot mL^{-1}$ in deionized water, which is let 1 hour in an ultrasound bath in order to separate the layers of the different GO aggregates. After the dispersion is put in the centrifuge 30 seconds at 1000 rpm and 30 seconds more at 800 rpm. Once de GO is ready, the GEC electrode is placed onto the electrode surface and then in the oven for 1 hour until all the water is evaporated. As commented in the introduction GO is an insulator, for this reason, the recovery of graphene features is mandatory if used as a catalyzer in voltammetric practical cases. In this direction, since we work in an electrochemical laboratory it was chosen the electrochemical reduction of GO as the best option. ERGO was obtained via voltammetry by the application of a potential window from +1.9 V to -2.3 V for 10 cycles and after 5 cycles concreting from +0.1 V to -0.7 V, all at 100 $mV \cdot s^{-1}$.

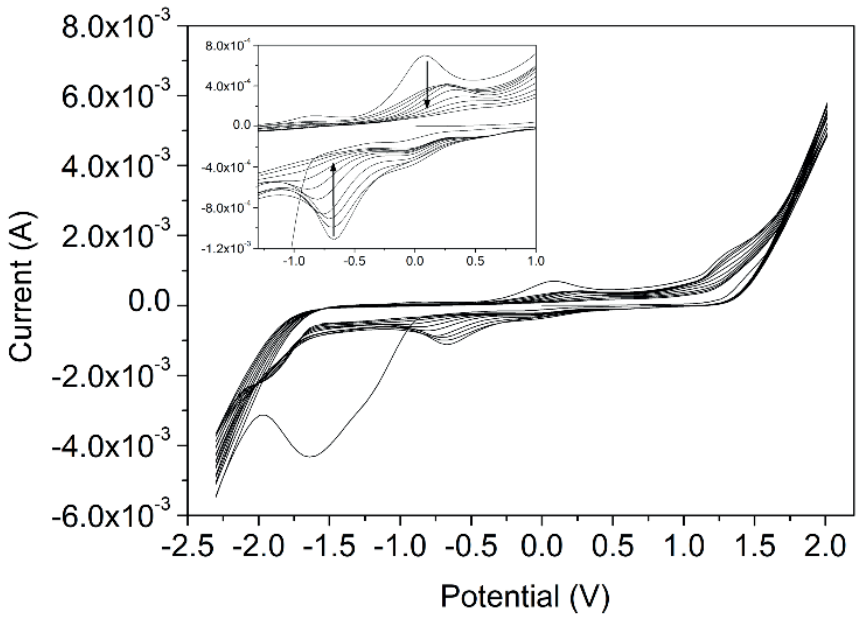

Figure 3.5. Voltammogram resulting from the GO reduction in PBS 50 mM + 100 mM KCl solution at pH 7.4.

This window was firstly studied with aiming to eliminating the peaks that appear from −1.0 V to −0.5 V (vs. Ag/AgCl). These peaks belong to the reduction of the oxygenated groups from GO to hydroxyls (at medium pH and aqueous solutions) [8,9]. The reduction of GO to ERGO has been performed in PBS solution 50 mM + 100 mM KCl at pH 7.4. Figure 3.5 is an example of the reduction process voltammogram.

3.5.2.2 Polystyrene Inks drop-casting

Polystyrene inks were presented in this work as a solution to one of the essential points of the direct drop-casting technique, the insolubility of the modifier in the measurement medium. When the CD project starts, it was found that N and S-CDs were soluble in water. For this reason, after evaluating different options, the inclusion of CDs in a matrix of polystyrene inks was chosen as one viable option.

In the next lines, it will be described the followed procedure to prepare the modified GC electrodes (see Figure 3.6). The first step is to prepare the ink. In this sense, graphite, polystyrene, and the modifier (the different CDs), are mixed in a 58:32:10 ratio (w/w), then 250 µL of mesitylene for each 100 g is added. Once the inks are ready, they are stirred for 2 hours and sonicated for 2 more minutes. With these steps, a homogeneous dispersion is obtained. Finally, 5 µL

of the ink is cast onto the clean and mirror surface of the GC. As in the case of simple drop-casting, the electrodes are put in the oven until the complete evaporation of the solvent.

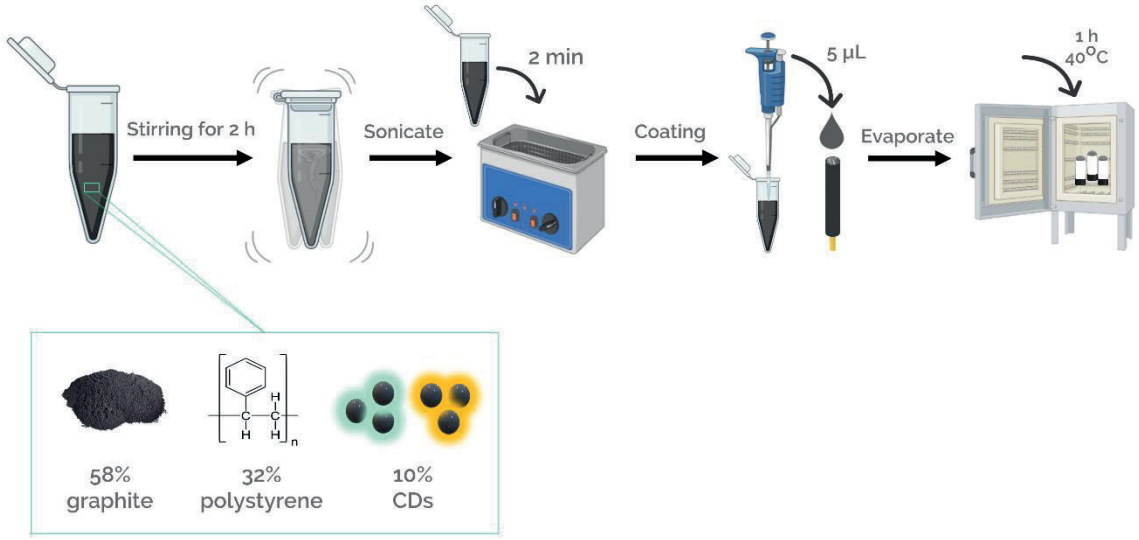

Figure 3.6. Schematic description of the modification procedure for the preparation and drop-casting of polystyrene inks onto GC electrodes.

Since polystyrene is not a conductive polymer, the electroactivation of the surface was highly recommended. In the bibliography, the authors use a wide range of products, from sulphuric acid to hydrogen peroxide. Additionally, most of them are also applying extreme potentials. In the case of the herein paper, was carried out an electric activation of the surface in hydrogen peroxide 50 mM (diluted in PBS solution at pH 7.0) by applying 10 cycles from -1.5 V to +1.5 V at 50 $mV \cdot s^{-1}$. Figure 3.7 shows the activation process, which was followed via CV (Figure 3.7A) and EIS techniques (Figure 3.7B and Figure 3.7C). In the voltammogram, it is shown how as the cycles progress, the response against the H_2O_2 is increased. Regarding the Nyquist plots the response of the before (Figure 3.7B) and after (Figure 3.7C) activation process is shown. These figures demonstrate a general improvement of the electrode conductivity. In conclusion, the results indicate the correct activation of the surface electrode. This effect could be caused by two main reasons. The first option would be the creation of oxygenated groups that would increase the electroactive are. Besides, the second option, which is the most plausible and shared by the experts in the field,

would be the creation of channels or pores that would exposes the conductive materials to the medium.

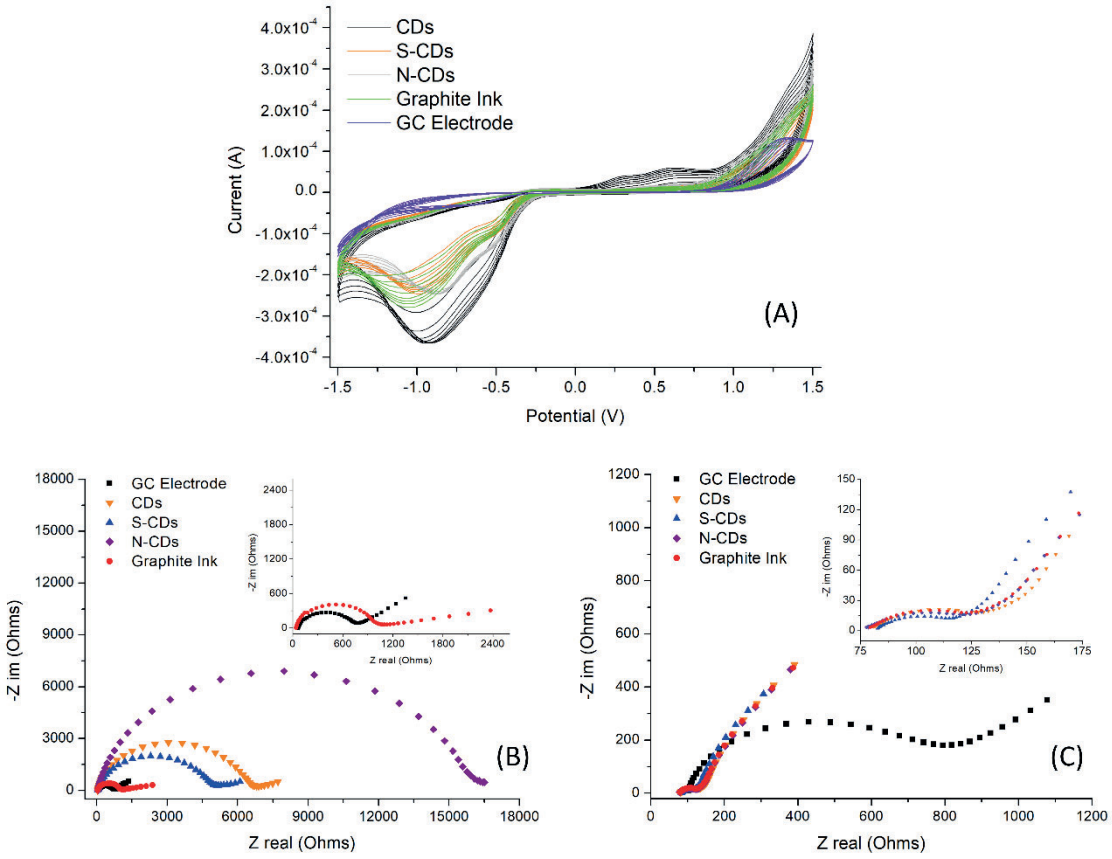

Figure 3.7. (A) Voltammograms and Nyquist plots for the (B) before and (C) after the activation of polystyrene inks in a 50 mM H_2O_2 solution in PBS pH 7.0.

3.5.2.3 Covalent bonding

Given the well stablished protocols, the advantages of the method and the characteristics of our sensor, it was decided to immobilize covalently the enzymes onto the already prepared ERGO-GEC sensors. As mentioned before, carboxylic groups remain on the surface of the ERGO modified electrode, which can be used as anchor points for the biological elements. For this purpose, 1-(3-dimethylaminopropyl)-3-ethylcarbodiimide hydrochloride (EDAC), was sued as crosslinker to facilitate the reaction between the carboxylic groups form the sensor surface and the nitrogenated groups of the enzymes. Figure 3.8 describes the procedure followed for the development of the different biosensors.

Firstly, deposited GO is electroreduced to obtain the ERGO-GEC modified electrode. Once the starting platform is ready, the sensor is immersed overnight

at 8 ^{0}C in an aqueous solution that contains 500 ppm of NHS, 1000 ppm of EDAC, and 10000 ppm of the target enzyme. Finally, in order to eliminate the non-bonded materials the sensor is rinsed for 1 hour in PBS.

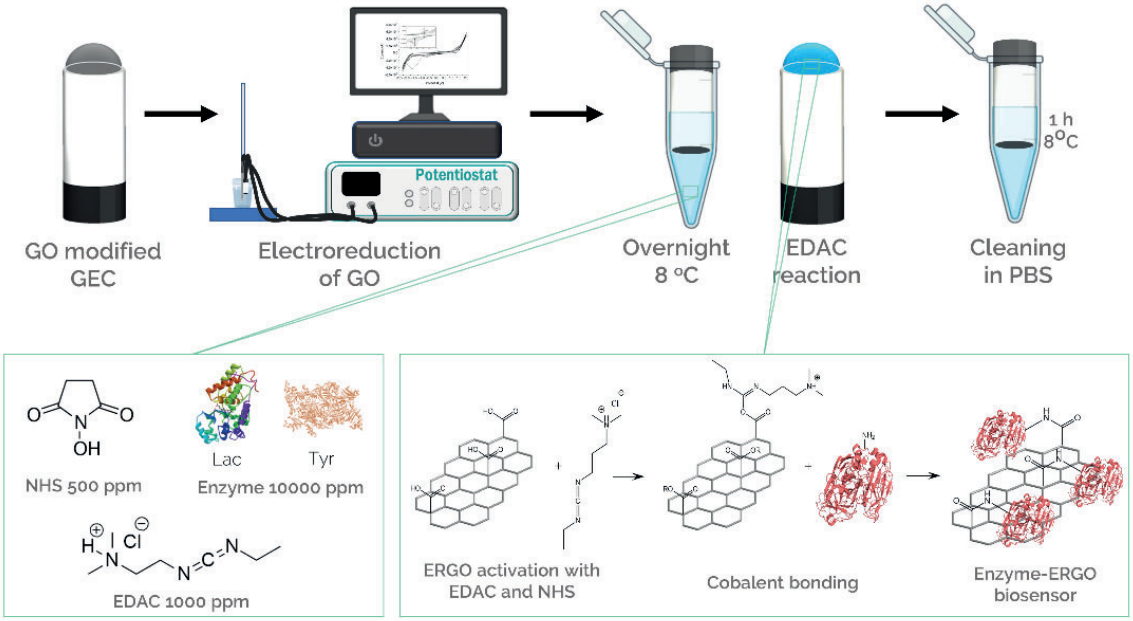

Figure 3.8. Schematic description of the enzymatic immobilization.

3.6 Multivariate experiments

3.6.1 Experimental design

The experimental design methods (§1.5) were made trying to obtain the maximum information as quickly and efficiently as possible. Figure 3.9 depicts the distribution of the calibration points used for the herein-developed measurements. In Figure 3.9A, an L36 full factorial design is depicted, this was used for the analysis of DA, 5-HT, AA, and UA. On the other side, Figure 3.9B, represents the tilted fractional factorial design used for the analysis of volatile phenols in wine. It is of the utmost importance to note that the samples are measured randomly in order to avoid undesired bias and trends.

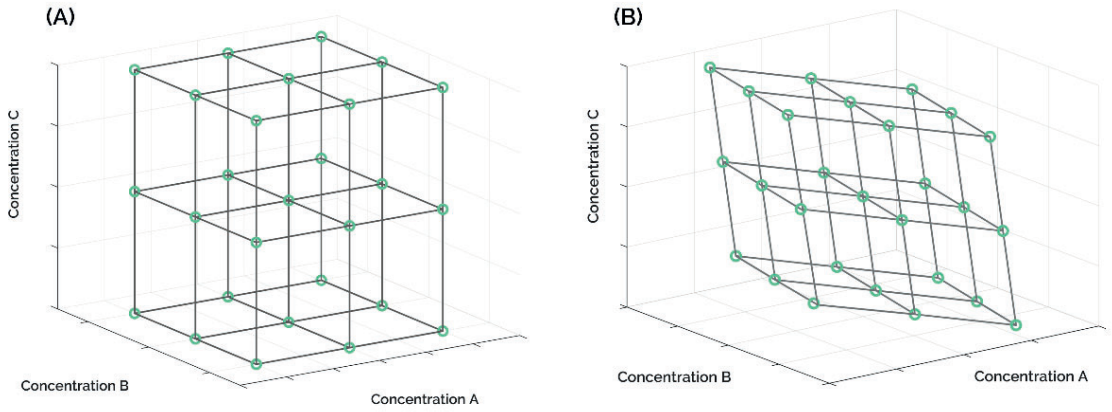

Figure 3.9. Experimental designs used in the articles that compose this thesis work. (A) L36 Full Factorial Design (B) Tilted Fractional Factorial Design.

3.6.2 Data processing

Once the data is recorded, it must be organized to be pre-processed and fed the model with the obtained coefficients.

It must be noted that when it is used supervised chemometric tools, it must be introduced also a matrix with the true values for the variables to predict. Then the model is validated with the test samples, which are distributed arbitrarily among the experimental domain, one example is plotted in Figure 3.10. Finally, is estimated the generalization ability of the model (extensive explanation in §1.5).

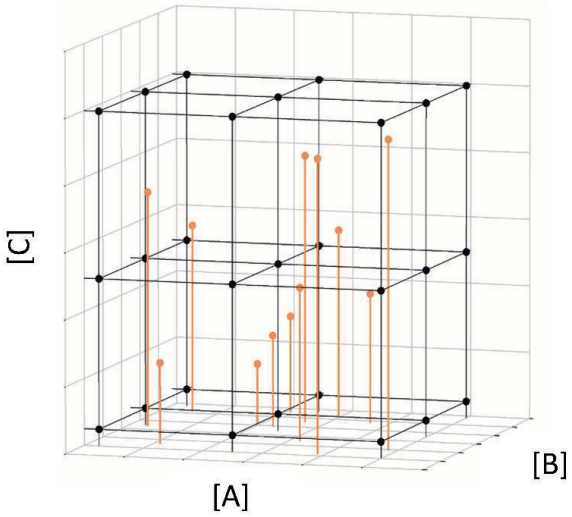

Figure 3.10. Sample distribution for a 3^3 full factorial design experiment. In this figure black dots correspond to the train samples, and orange dots with the test [4].

3.6.2.1 Artificial Neural Networks parameters

To obtain the best structure for the neural network the algorithm is tested through trial and error with all possible combinations of parameters. The examined and/or fixed values are:

- The number of neurons in the hidden layer

One of the testes parameters is the best number of nodes, normally the number is among 1 and 10. The input and the output layers, as explained in §1.5.3.1, are determined by the number of entry coefficients and studied variables, respectively. Nevertheless, if CI pre-treatment is used, the input neurons will be a parameter to optimize.

- Learning algorithm

As mentioned in the introduction (§1.5.3.1), there are multiple choices regarding the learning algorithm. In this case, was chosen in all performed ANN models the backpropagation-BR. With this mathematical function the use of an internal validation set of samples is avoided, being easier the measurement and training procedure. For the BR cost function, an α of 0.01 and a β of 0.4 (these values were extracted from previous works related to the field and experiences in the lab) were fixed.

- Transfer function

The transfer function is the mathematical equation that translates the binary information from the nodes to continuous values. There is a wide range of functions, in fact, it can be any mathematical function that meets the requirements: monotone increasing, and have a continuous derivate, all in the application range. The most common, and the ones employed in this thesis project, are the derivates from sinusoidal functions. Figure 3.10 depicts all the functions tested in this work.

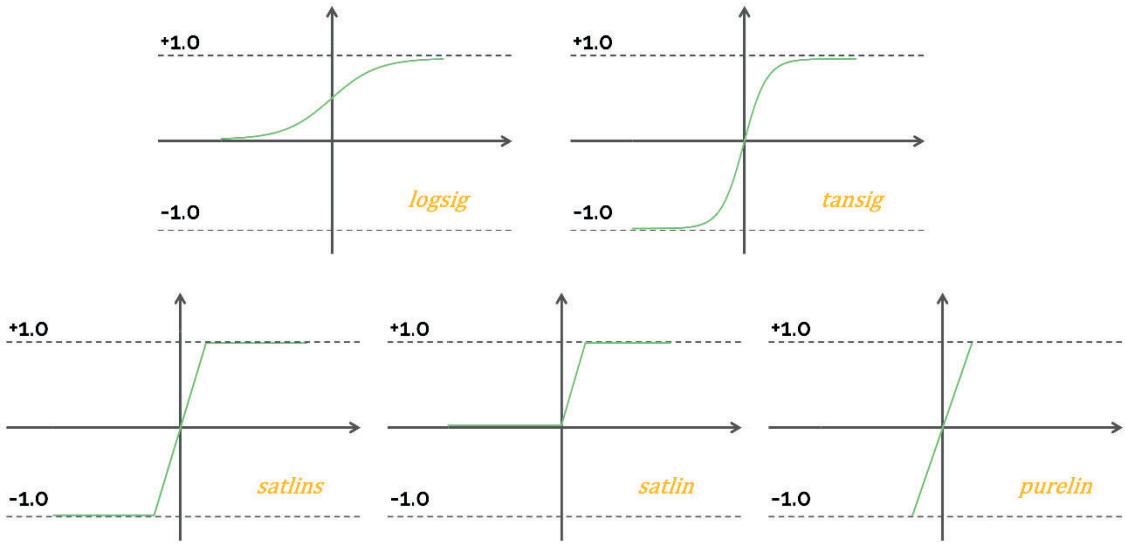

Figure 3.11. Most common transfer functions used in ANNs work. Being "purelin", "satlin", and "satlins" for lineal functions; and "logsig", and "tansig" for non-linear functions.

3.7 Measurement process

In the voltammetric measurement, a typical three electrodes cell was employed. Concretely, was used the pseudoreference device 52 61 from Crison (Hach, USA) composed of a Pt plate, the CE, and an Ag wire coated with AgCl (in KCl 3M) as the Ref electrode. The third one, the WE, is the sensor developed in each work. The whole system is depicted in Figure 3.12, where Figure 3.12A shows the setting for the PalmSens device, and Figure 3.12B the arrangement prepared when measuring in the 6 multi-channel Autolab Potentiostat.

Figure 3.12. (A) PalmSens and (B) Autolab assemblies for voltammetric measurements.

Since the technique settings must be adjusted in each work, Table 3.4 shows a summary of the most relevant parameters. In all the cases, the measurements were carried out without stirring and at room temperature. In the

case of GO-GEC, and the Tyr and Lac biosensors, they were regenerated after every set of measurements. Regarding the determination of DA and 5-HT, since these compounds generates fouling, an extra step was added to the measurement procedure. Concretely, the drift handicap was overcome with an electrochemical cleaning step, performed in hydrochloric acid 0.1M.

Table 3.4. Summary table of the measurement parameter for each paper.

WE	Technique	Parameters	Article
GO-GEC	CV	Range: -0.20 to +0.7 V Scan rate: 10 mV/s Step potential: 4.5 mV	[1]
Lac-GO-GEC	CV	Range: depends on the compound Scan rate: 10 mV/s Step potential: 1 mV	[2]
Lac/Tyr-GO-GEC	CV	Range: -0.20 to +0.8 V Scan rate: 10 mV/s Step potential: 10 mV	[3]
N/S-CDs-GC	CV	Range: depends on the compound Scan rate: 50 mV/s Step potential: 10 mV	[4]
Various	EIS	Range: 0.5 MHz to 0.05 Hz AC Amplitude: 10 mV Potential: OCP[1]	[1–4]

[1] Open Circuit Potential (OCP), normally near to 0.17 V, the equilibrium potential for the redox pair $[Fe(CN)_6]^{3-/4-}$ *vs.* Ag/AgCl reference electrode.

3.8 References

[1] M. Bonet-San-Emeterio, A. González-Calabuig, M. del Valle, Artificial Neural Networks for the Resolution of Dopamine and Serotonin Complex Mixtures Using a Graphene-Modified Carbon Electrode, Electroanalysis. 31 (**2019**) 390–397. https://doi.org/10.1002/elan.201800525.

[2] M. Bonet-San-Emeterio, N. Felipe Montiel, M. del Valle, Graphene for the building of electroanalytical enzyme-based biosensors. Application to the inhibitory detection of emerging pollutants, Nanomaterials. 11 (**2021**) 2094. https://doi.org/10.3390/nano11082094.

[3] M. Bonet-San-Emeterio, A. González-Calabuig, M. del Valle, Bioelectronic tongue based on alcohol oxidases modified graphene electrodes for the detection of Brettanomyces defect in wine (not published), (**2022**).

[4] M. Bonet-San-Emeterio, M. Algarra, M. Petković, M. del Valle, Modification of electrodes with N- and S-doped carbon dots. Evaluation of the electrochemical response, Talanta. 212 (**2020**) 120806. https://doi.org/10.1016/j.talanta.2020.120806.

[5] W.S. Hummers, R.E. Offeman, Preparation of Graphitic Oxide, Journal of the American Chemical Society. 80 (**1958**) 1339–1339. https://doi.org/10.1021/ja01539a017.

[6] Y. Aceta, M. del Valle, Graphene electrode platform for impedimetric aptasensing, Electrochimica Acta. 229 (**2017**) 458–466. https://doi.org/10.1016/j.electacta.2017.01.113.

[7] V. Uskoković, A historical review of glassy carbon: Synthesis, structure, properties and applications, Carbon Trends. 5 (**2021**) 100116. https://doi.org/10.1016/J.CARTRE.2021.100116.

Chapter IV. Results and Discussions

4 RESULTS AND DISCUSSIONS

Following the research line of the group, it was decided to focus this thesis work on the development of new voltammetric sensors to work as items in (bio)ETs sensors arrays. In this direction, the first idea was to work with carbon nanomaterials, leading-edge products in the electrochemical sensors and biosensors field. The discovery of new electrochemical platforms in the scientific community regarding (bio)ETs is of the utmost priority, not only because the electrodes are the basis of the arrangement, but also to overcome and improve the current methods. As explained in §1.4.1, sensors from an array must be globally selective and give non-redundant signals. For this reason, it is sought electrodes that discriminate the target analytes from the matrix, but not extremely selective, because as much information obtained as better the model. In this section will be shown the results obtained from testing the bare and the modified materials in order to obtain a proper electrode array to be applied in an ET arrangement. The final applications are related to the pharmaceutical and medical field, beverage and food industry, and environmental science.

As mentioned during this memory, the global industry demands rapid, direct, and easy protocols for the analysis of multiple samples, this fact in unison with the almost complete automation of the ongoing sector, are the sources of the changes in the classical research tendencies. Nowadays, it is not only appreciated the results of the proposed method but also its cost, the effects that can cause to the environment, and the option to be included directly in the production line.

For the stated reasons, in the present thesis work, it was selected carbon derivate nanomaterials, which besides their physical and chemical stunning properties, also present low toxicity, low production prices, and the ability to be easily modified.

This chapter will be organized by articles, where it will be found 4 individual summaries (complete publications in Annex I). The list of the articles and their nomenclatures are defined below:

- Works with graphene

Article 1: M. Bonet-San-Emeterio, A. González-Calabuig, M. del Valle, Artificial Neural Networks for the Resolution of Dopamine and Serotonin Complex Mixtures Using a Graphene-Modified Carbon Electrode, *Electroanalysis*. 31 (**2019**) 390-397. doi:10.1002/elan.201800525

Article 2: M. Bonet-San-Emeterio, N.F. Montiel, M. Del Valle, Graphene for the building of electroanalytical enzyme-based biosensors. Application to the inhibitory detection of emerging pollutants, *Nanomaterials*. 11 (**2021**) 2094. doi:10.3390/nano11082094

Article 3: Bioelectronic tongue based on alcohol oxidases modified graphene electrodes for the detection of Brettanomyces defect in wine (not published).

- Works with carbon dots and related

Article 4: M. Bonet-San-Emeterio, M. Algarra, M. Petković, M. del Valle, Modification of electrodes with N-and S-doped carbon dots. Evaluation of the electrochemical response, *Talanta*. 212 (**2020**) 120806. doi: 10.1016/j.talanta.2020.120806

Article 1

Artificial Neural Networks for the Resolution of Dopamine and Serotonin Complex Mixtures Using a Graphene-Modified Carbon Electrode

M. Bonet-San-Emeterio, A. González-Calabuig, M. del Valle

Electroanalysis, 31 (2019) 390-397

4.1 Artificial neural networks for the resolution of dopamine and serotonin complex mixtures using a graphene-modified carbon electrode

The article target was the detection of DA and 5-HT in presence of their electrochemical interference AA and UA. DA and 5HT are important monoamine neurotransmitters that act in the nervous system. The abnormal concentrations of these compounds lead to neurological disorders such as Parkinson's, Alzheimer's, and anxiety. Given their electroactivity, they are considered a good target to be analyzed by voltammetry techniques. The proposed strategy to solve the quaternary mixture was the use of graphene modified GEC electrode coupled with ANNs.

4.1.1 Characterization of the electrode

In this direction, the electrode was firstly optimized and characterized in order to ensure its proper function. As stated in §3.4.2.1, the bare GEC electrode was modified with GO suspended in deionized water (1 mg·mL^{-1}) using the drop-casting technique, in this case, it was used commercial GO (specifications in §3.4.2.1). The finally optimized volume was 40 µL, which was added onto the GEC surface, obtaining a GO-GEC.

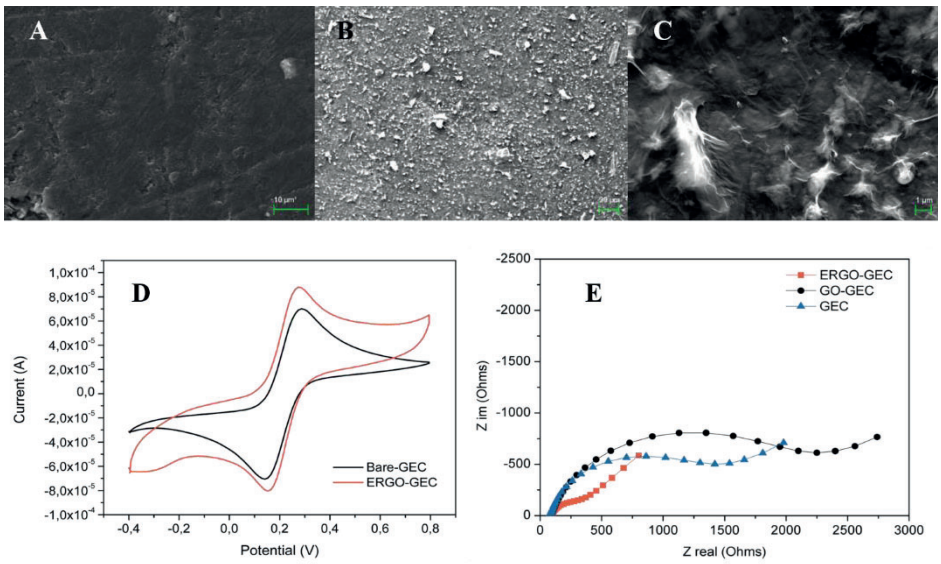

Figure 4.1. Characterization of the graphene modified electrode. (A) bare GEC electrode, (B and C) ERGO-GEC, images obtained by SEM. (D) CV measurements were it is compared the GEC and ERGO-GEC. (E) Nyquist plot comparing the response for all the electrodes.

The previous resulting platform was not conductive, hence it was mandatory to recover the graphene conductivity. Thus, GO was reduced, given this step was carried out electrochemically so, the final material was named electrochemically reduced graphene oxide (ERGO). This procedure was followed by EIS and CV techniques, and by surface imaging, using an SEM microscope. With these results, it was confirmed the good design of the modification protocol.

4.1.2 Individual electrochemical detection

Once the electrode was ready, it was proceeded to analyze the target molecules in phosphate buffer with KCl at pH 7.4. Individually, the calibration curves carried out considering the human body concentration range, present an improvement when measured with the ERGO-GEC electrode. The effect of graphene was observed also in the enhancement of sensitivities, and then in the LOD.

Finally, it was studied the DA, 5-HT, AA, and UA mixture behavior. When measured together, 20 µM of DA, 5 µM of 5-HT, 75 µM of AA, and 50 µM of UA, as shown in Figure 4.2, 5-HT and UA were completely overlapped, being impossible to identify them individually. In addition, the peak of AA was faded by the increase of the baseline produced by the high electrochemical response of UA.

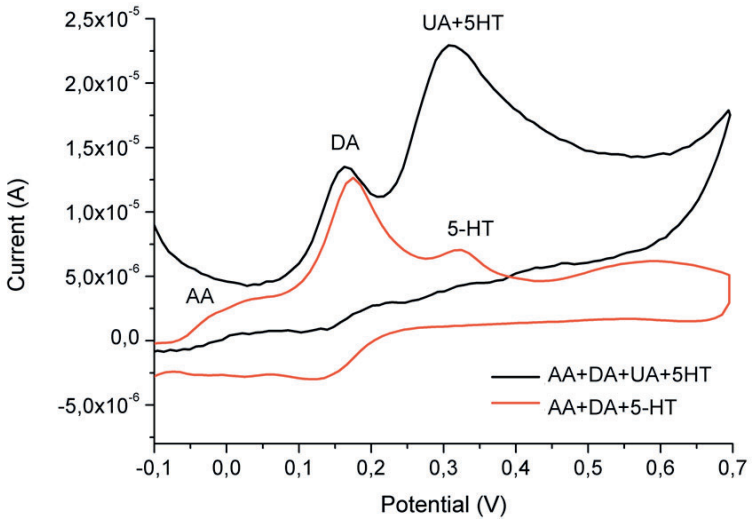

Figure 4.2. ERGO-GEC CV measurement for the target molecules mixture.

4.1.3 Simultaneous electrochemical detection

When it is performed a multivariate regression analysis is needed an experimental design model, as explained in §1.5 it is made to obtain the maximum information performing as less experiments as possible. The selected model was an L36 fractional design composed of 3 concentration levels and 4 factors, i.e. the 4 analytes. Then the model has 36 training samples and 9 more from the test, created randomly in the experimental domain.

Since 45 samples had to be measured one after the other, it was necessary to ensure operational stability so as not to provide variability in the data. Therefore, it was studied how many samples could be measured without significant changes in the electrode response. The first performance showed that DA has a fouling effect, being a handicap for the whole experimental design. After attempting different cleaning procedures, the final proposed solution used to overcome this issue was the electrochemical cleaning in HCl 0.1 M during 40 s at 1.2 V, it was applied after each measurement.

Finally, it was tested the precision of the measurement method obtaining acceptable values for 15 measures, in other words, indicating that the electrode can measure without disruptions at least 15 consecutive samples. Moreover, it was studied the difference between electrodes, which indicates that all the electrodes lead to comparable results, being possible to interchange the electrode during the multivariate regression experiment.

Once it was optimized and validated the experimental design, it was proceeded to create the quantification model for the target molecules, which surprisingly, was able to quantify not only DA and 5-HT but also AA and UA. The concrete parameters of the model and the numeric results can be found in §6, article 1. Herein Figure 4.3 depicts the model performance for the train subset, in black, and the generalization ability obtained with the test subset, in white.

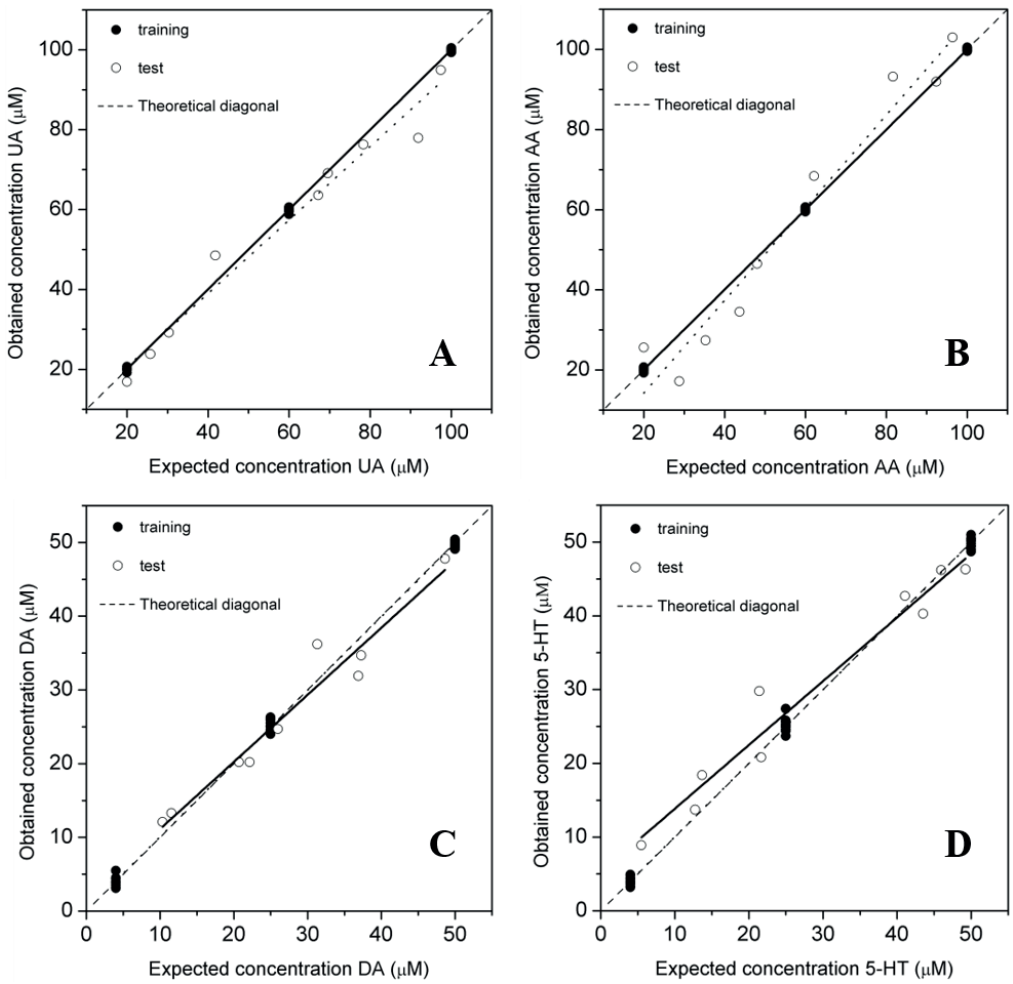

Figure 4.3. Predicted vs. Expected curves obtained with DWT-ANN.

Therefore, it was set out a strategy that combined advanced chemometric tools and a leading nanomaterial to overcome the overlapping in electrochemical signals. Concretely, it was developed a quantification model for DA, 5-HT, AA, and UA, based on the use of an ERGO-GEC electrode and DWT-ANNs data treatment.

Article 2

Graphene for the building of electroanalytical enzyme-based biosensors. Application to the inhibitory detection of emerging pollutants

M. Bonet-San-Emeterio, N.F. Montiel, M. Del Valle

Nanomaterials, 11 (2021) 2094

4.2 Graphene for the building of electroanalytical enzyme-based biosensors. Application to the inhibitory detection of emerging pollutants

This article is focused on the development of a laccase-graphene biosensor for the detection via inhibition of contaminants of emerging concern (CECs), concretely, EDTA and benzoic acid. CECs are compounds that are considered as new pollutants that are not already legislated and can be harmful to human health.

The strategy for the detection of these contaminants was based on the study of the inhibition of the laccase biosensor, which is meanly affected when the target molecules are present. From the standard analytes catalyzed by phenolic oxidized, we chose catechol to carry out the biosensor characterization and the inhibition studies.

4.2.1 Graphene synthesis, integration, and characterization.

The graphene used in this work was obtained from the synthesis of GO via a top-down modified Hummers protocol. The oxidation of graphite was made using $NaNO_3$, H_2SO_4, and $KMnO_4$. Finally, the resulting multilayered GO, also considered graphite oxide depending on the number of layers, has been led to neutral pH and purified with anionic exchange resins.

The presence of the GO in the obtained brown paste was proven by imaging techniques. One on hand the sample was analyzed at TEM. As observed in Figure 4.4A, Figure 4.4B, and Figure 4.4C, was found a wrinkled and thin material, both features directly related to the presence of few-layered graphene flakes, which can be clearly identified in Figure 4.4B. Moreover, in Figure 4.4C, a darker island was captured, which probably belongs to the unreacted graphite. On the other hand, was also performed an XPS analysis in order to study the carbon-oxygen ratio and the structure of the material. As expected, the most abundant bond is the sp^2 carbon, followed by the simple carbon-carbon. The calculated carbon-oxygen ratio for our sample was 2.14, being accepted in the Hummers work values from 2.1 to 2.9 for graphitic oxide samples [1].

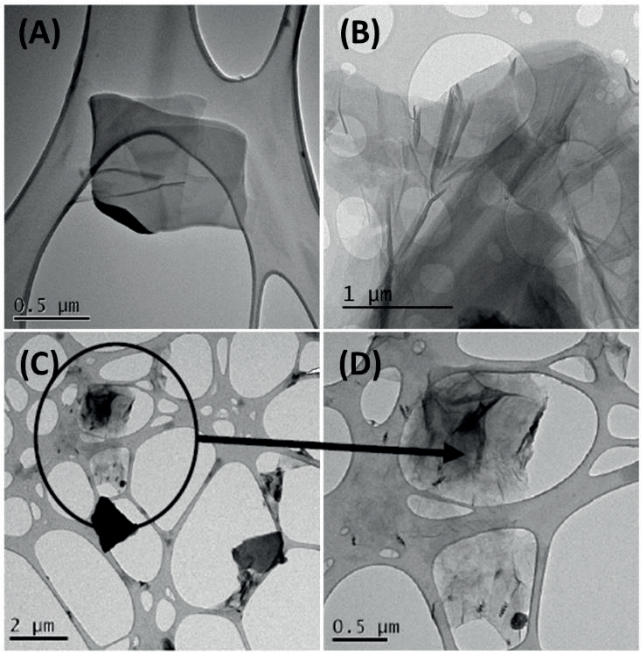

Figure 4.4. TEM imaging of synthesized GO (in ethanol absolute).

Once the GO was ready, it was integrated onto the electrode following the already established protocol, described in §4.1.1 [2], to sum up, it was dispersed in deionized water and deposited onto the surface of the electrode via drop-casting. The volume to be added was firstly optimized, obtaining that 40 µL is the most adequate quantity. The reduction of GO was followed by CV and EIS. As seen in Figure 4.5B, the redox peaks, typical of the redox character of oxygenated groups, became smaller, indicating the decrease of their concentration in the sample. The correct reduction is also proven in Figure 4.5C, where the Nyquist plot shows how the GO-GEC electrode presents much bigger Rct values (Rct_{GO}= 2256 Ω, Rct_{ERGO}= 206 Ω, Rct_{bare}= 1638 Ω), in other words, it is proven the conductivity improvement in the graphene recovery step.

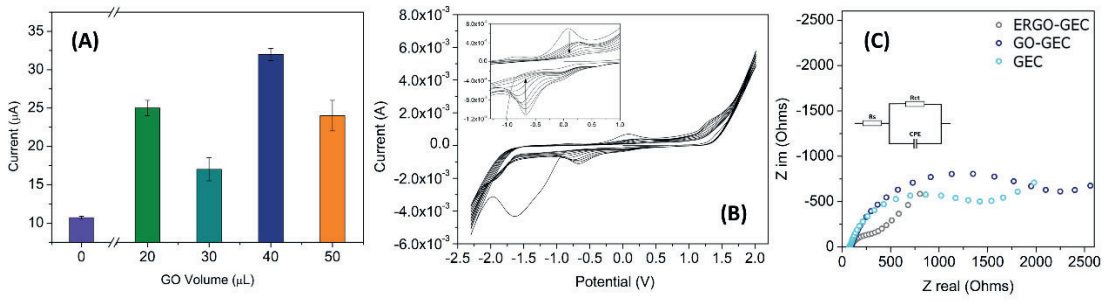

Figure 4.5. Study of ERGO modified electrode.

Finally, the topography of the modified electrode surface was studied via AFM. As observed in Figure 4.6, the surface is rougher for the modified electrode than for the bare GEC. These images are also comparable to TEM ones, which present parts with few-layered graphene, recognized by the tissue-like wrinkles (indicated with an arrow in Figure 4.6C), together with graphene flakes, more voluminous.

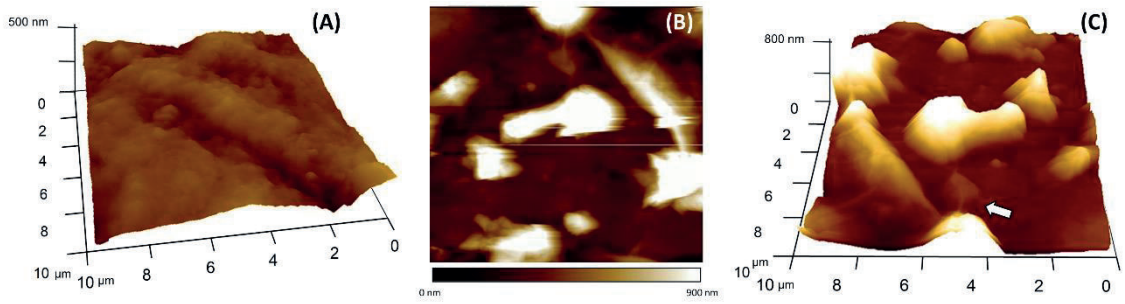

Figure 4.6. AFM images obtained from (A) GEC electrode, (B, C) GO-GEC electrode.

4.2.2 Study and construction of the laccase biosensor

The biosensor was achieved by taking advantage of the remaining oxidized groups after the electrochemical reduction of the GO. Via 1-ethyl-3-(3-dimethylaminopropyl)carbodiimide (EDAC) and N-hydroxysuccinimide (NHS) molecules, it was formed a covalent binding among the carboxylic groups of the ERGO and the amino groups of the enzyme (see Figure 4.7).

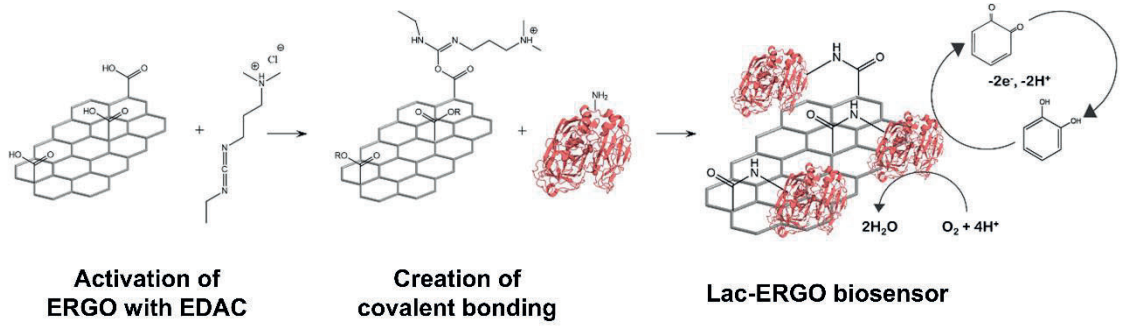

Figure 4.7. Integration of laccase enzyme to the modified ERGO-GEC electrode via EDAC coupling agent.

Once the electrode was ready, we proceeded to validate its functionality. First of all was studied the surface of the biosensor via the EIS technique, which indicates, as expected little difference in Rct results for ERGO and Lac-ERGO electrodes and a higher value for the bare one.

The response of the biosensor was tested, as mentioned before, with catechol. The resulting calibration curves showed a linear range, in the insert of Figure 4.8A, from 2 to 100 µM, for the biosensor electrode and from 2 to 800 µM and 2 to 1500 µM, for ERGO and GEC respectively. In the same image, it can be also observed a sensitivity enhancement for the biosensor.

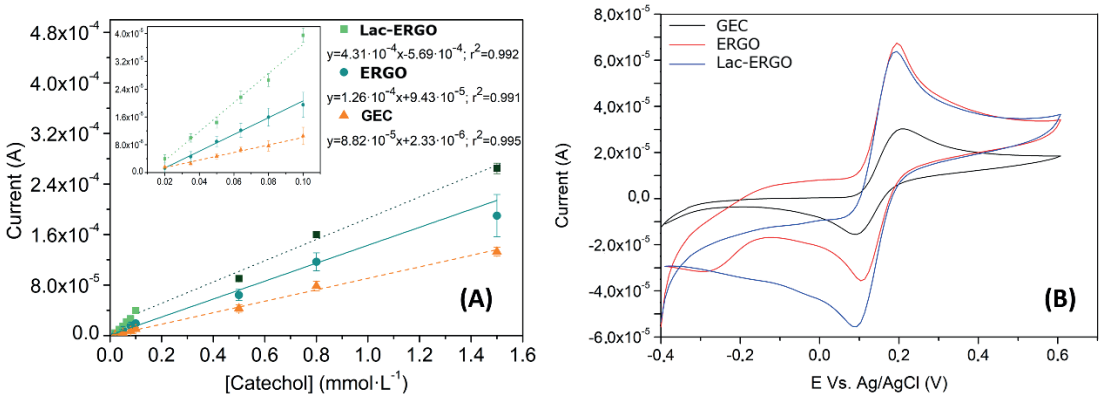

Figure 4.8. Biosensor response against catechol.

Figure 4.8B, depicts the responses for each electrode, where changed in the oxidation baseline and consequently in the reduction peak contrast the good function of the Lac onto the electrode.

Some of the most relevant analytical properties of the biosensor were tested. Among them, it was carried out studies of the LOD and LOQ, repeatability, biosensor reliability during the day, intermediate precision, lifetime, and selectivity. All of them were considered acceptable. The concrete discussion can be found in §6.

4.2.3 Kinetic inhibition study

The goal of the article was to detect CECs by the inhibition of the Lac enzyme. After studying some characteristic enzymatic parameters, such as K_M, V_{max}, and h, was concluded that the presented biosensor follows Michaelis-Menten kinetics.

After studying the behavior of complex enzyme-catechol, was proceeded to study the behavior of the inhibitor-enzyme-substrate complex. In this case, there are three possible scenarios: competitive, non-competitive, and uncompetitive inhibition. Their difference lies in how interacts the inhibitor with the enzyme and substrate.

In order to identify the concrete situation, it must be studied the effects that cause different concentrations of the inhibitor to the substrate-enzyme response. Figure 4.9 and Figure 4.10, for benzoic acid and EDTA respectively, elucidate that the studied case is referred to as competitive inhibition, where $K_M < K'_M$ and $V_{max} = V'_{max}$. Both cases it is demonstrated the maintenance of the V_{max} values and the increase of the K_M for the inhibited enzyme.

The reached inhibition rate (Figure 4.11) obtained for benzoic acid was *ca.* 60% and *ca.* of 25% for the EDTA. Moreover, there are plotted the CV response for catechol when there is or not the inhibitor.

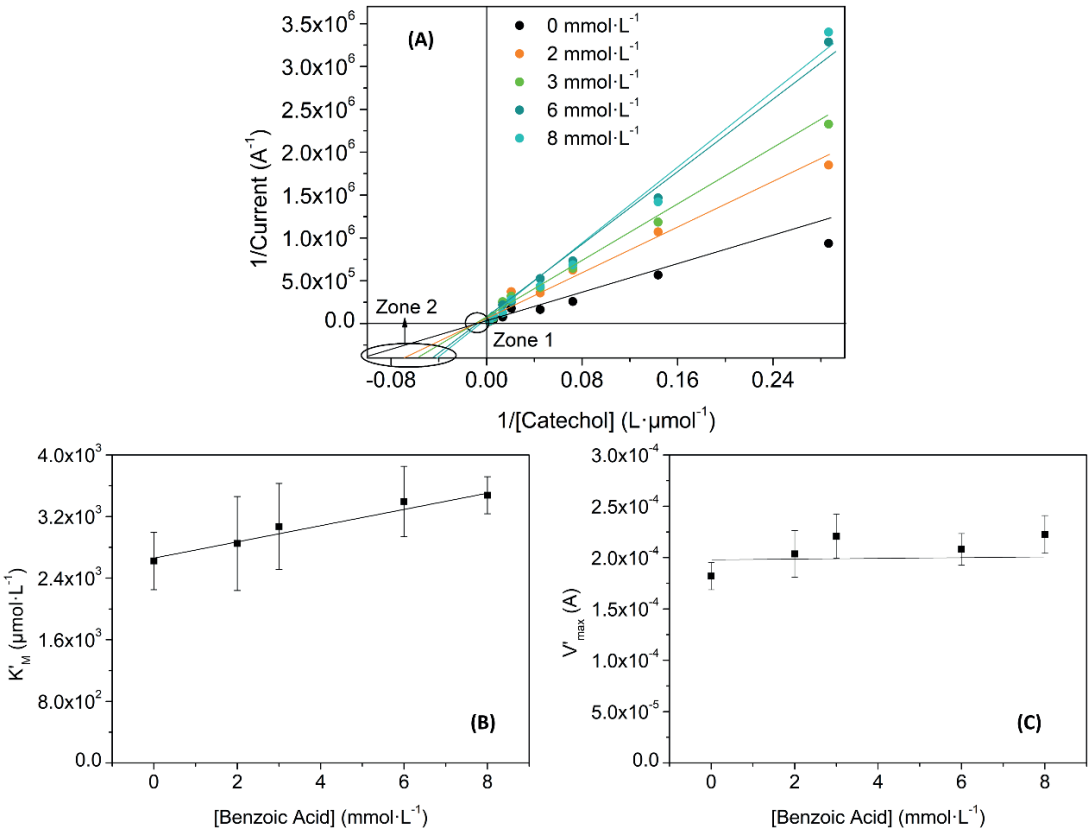

Figure 4.9. (A) Lineweaver-Burk linearization for benzoic acid regression curves. (B and C) depicts differences produced by the inhibitor for K'_M and V'_{max}.

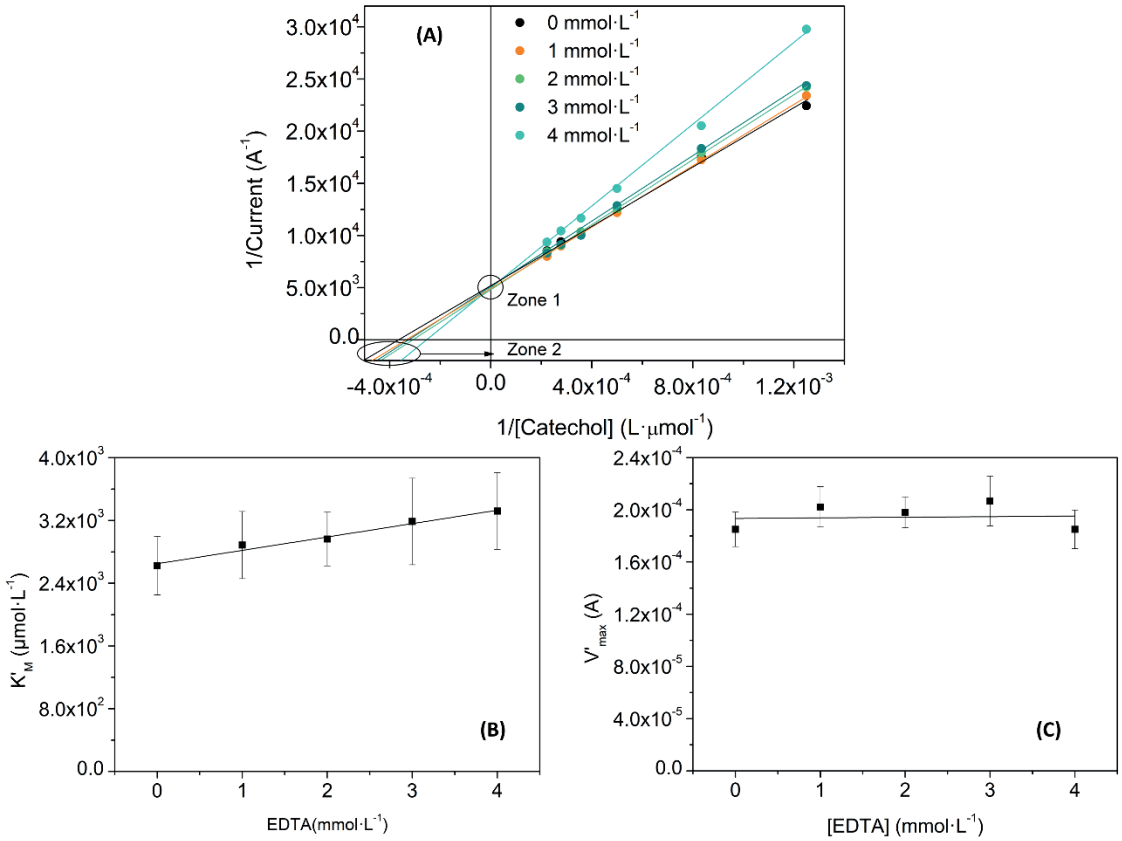

Figure 4.10. (A) Lineweaver-Burk linearization for EDTA regression curves. (B and C) depicts differences produced by the inhibitor for K'M and V'max.

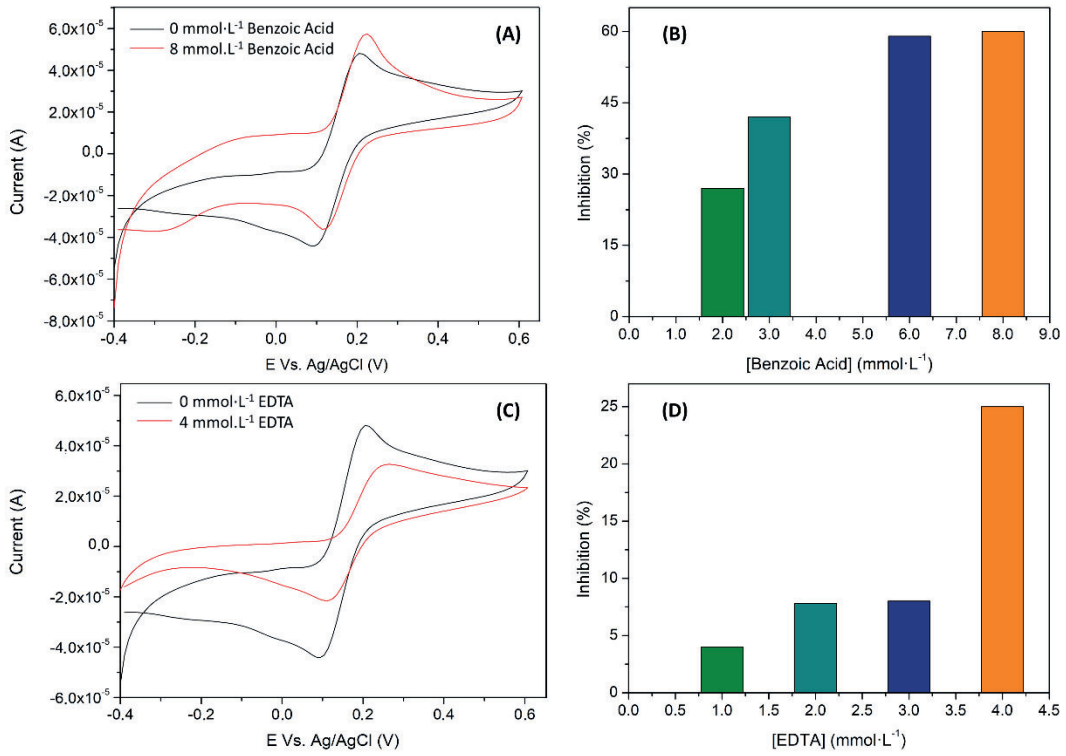

Figure 4.11. Effects of (A and B) benzoic acid, and (C and D) EDTA.

In conclusion, this work presents a proof of concept for the detection of CECs via an inhibitory enzymatic method. Moreover, it was developed and validated the Lac-ERGO electrode and carried out and comprehensive kinetic study for the Lac and catechol complex.

Article 3

Bioelectronic tongue based on alcohol oxidases modified graphene electrodes for the detection of Brettanomyces defect in wine

M. Bonet-San-Emeterio, A. González-Calabuig, M. del Valle

4.3 Bioelectronic tongue based on phenol oxidases modified graphene electrodes for the detection of Brettanomyces defect in wine

Brettanomyces is a type of yeast present in wine products that is related to the formation of ethylphenols. These compounds can produce spoilage in rosé and red wines causing tastes that may remind to horse sweat, wet animals, and urine. For this reason, the detection of Brett character is a key point for the wine industry. In this paper is proposed the use of a bioelectronic tongue in order to not only detect their presence but also quantify three representative family products, 4-ethylphenol (EP), 4-ethylcatechol (EC), and 4-ethylguaiacol (EG). The followed strategy is the use of already established electroreduced graphene oxide (ERGO) platforms as the starting point for the building of two enzymatic biosensors, laccase (Lac) and tyrosinase (Tyr), both classified as phenolic oxidases.

4.3.1 Biosensors characterization

In previous works [3], it was developed a Lac-ERGO voltammetric biosensor for the indirect detection of CECs. In this case, the experience allows us to perform a similar scheme for the building of a new Tyr-ERGO platform. In this paper was used commercial GO. This assessment was made taking into account that there are non-significant differences between the commercial GO and GO synthesized electrochemical responses, and also the available amount of each product.

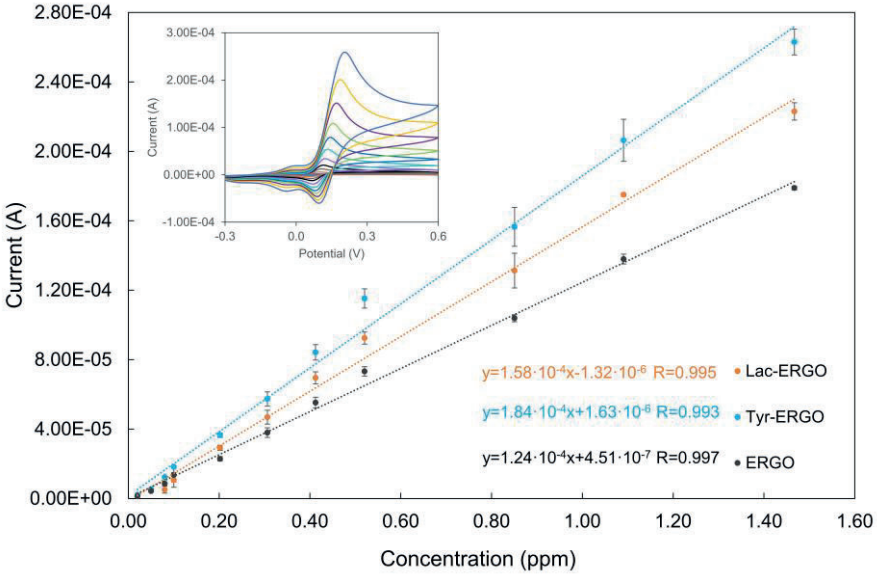

Figure 4.12. Calibration curve of Tyr-ERGO electrode for different concentrations of catechol.

In order to understand the biosensors' behavior, they were first tested with a standard for phenolic oxidases enzymes, the catechol. These experiments, as seen in Figure 4.12, present better sensitivities for Lac and Tyr modified biosensors than for the ERGO electrode. At this point was also determined the intermediate precision of the biosensor construction which resulted in less than 9% in both cases.

Additionally, it was carried out a selectivity test for not only the target molecules (EP, EC, and EG), but also other products with comparable structures, such as acetaminophen, catechin, and catechol. Figure 4.13 depicts the score plot obtained from the first three principal components considering the Lac-ERGO, Tyr-ERGO, and ERGO electrodes. As it can be seen, the score plot shows the discrimination of the target phenols, clearly separated in three separated clusters, EC in purple, EP in light blue, and EP in green. Also, the same plot demonstrates the selectivity of the (bio)sensors, which can differentiate among *para*-hydroxybenzenes (4-EP and acetaminophen) and *ortho*-dihydroxybenzenes (4-EC, catechol, and catechin).

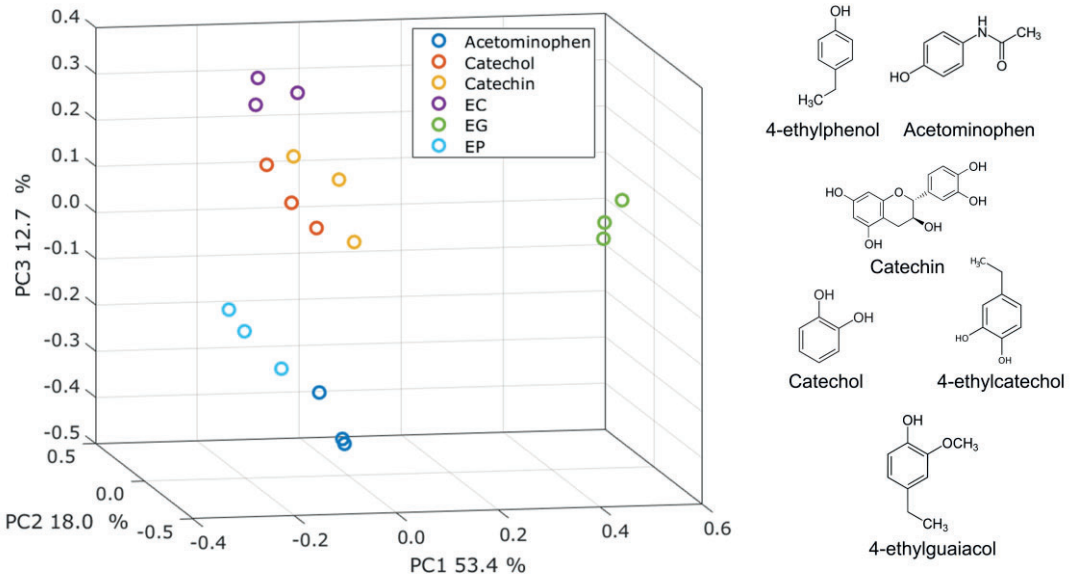

Figure 4.13. Score plot of the first three principal components of ERGO, Lac-ERGO, and Tyr-ERGO electrodes.

4.3.2 Multivariable analysis

Once the electrodes were individually developed, was proceeded to study how they work as part of the bioelectronic tongue array. Firstly, was tested the operational time. This parameter is of high interest because the electrodes have to have non-variable responses in time. In Figure 4.14 is plotted the responses for 15 alternative measurements of blanck and catechol. As seen in Figure 4.14A, the Lac-ERGO biosensor presents and stable response, making feasible its use in the whole bioET learning process.

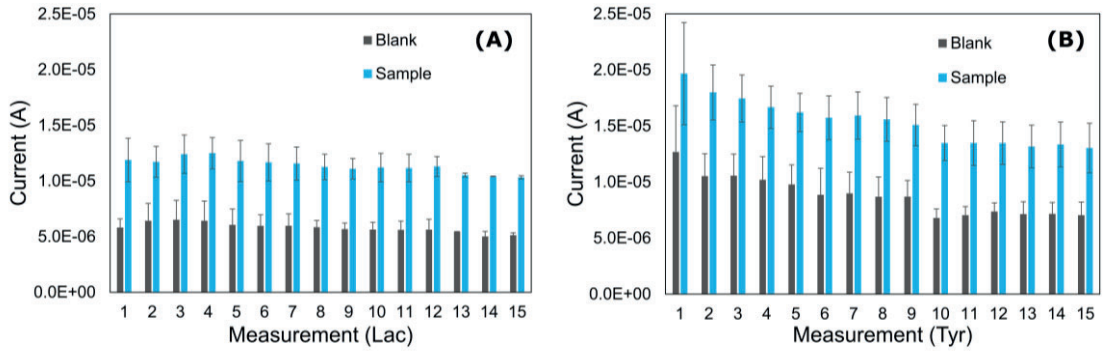

Figure 4.14. Operational stability of (A, B) Lac-ERGO and (C) Tyr-ERGO electrodes. Measurements were carried out in a solution of 5 ppm of catechol.

Contrary, the Tyr-ERGO biosensor shows a drop in the response. Thus, these results together with the good precision obtained for the immobilization

process of the biosensors lead to decide to use three identical groups of electrodes to measure the entire set of samples.

Another important feature when developing an electronic tongue approach is the non-correlation of the electrodes, i.e., each electrode must contribute with non-redundant information. There are multiple ways to study their response, one is the comparison of the responses given by each electrode for each compound. Figure 4.15 shows the responses given by the electrode array in front of the target ethylphenols.

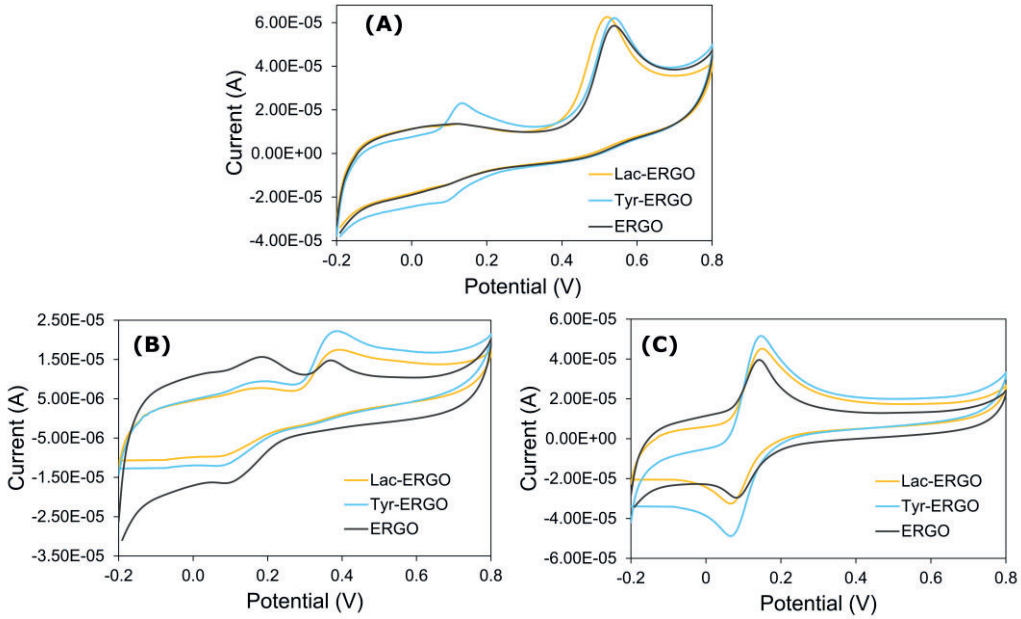

Figure 4.15. Comparison of the responses of each electrode for (A) EP, (B) EC, and (C) EG.

Lastly, was carried out the development of the quantification models. In this paper were presented two models, the first performed in buffer solution (Figure 4.16A) and the second one in wine real sample (Figure 4.16B). Both models present slopes and determination coefficients near to 1, and interceptions *ca.* 0. Moreover, once the final model was obtained, it was demonstrated its fitting goodness capability predicting the real concentration of 4 spiked wine samples, the results are present in Table 4.1.

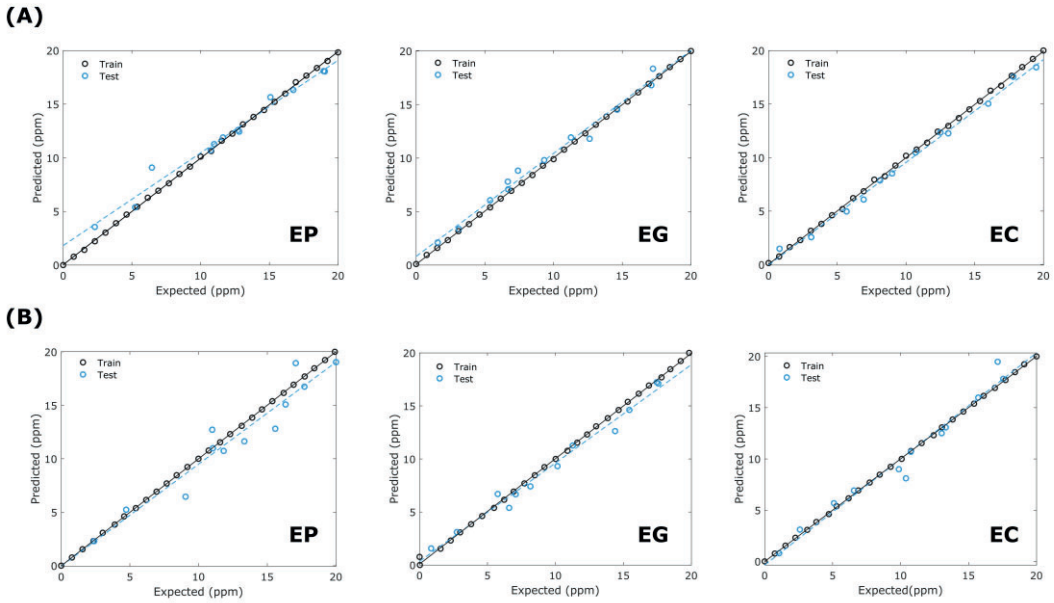

Figure 4.16. ANN models carried out in (A) buffer, and (B) real sample.

Table 4.1. Detailed results for the spiked real samples obtained from the ANN and PLS models.

	EP				
	Spiked concentration (ppm)	ANN Results (ppm)	PLS Results (ppm)	Recovery yield ANN (%)	Recovery yield PLS (%)
Sample 1	11.82	10.73	9.77	90.8	91.0
Sample 2	4.73	5.23	5.78	110.6	110.4
Sample 3	13.33	11.63	12.10	87.2	104.0
Sample 4	10.99	12.71	10.64	115.7	83.7
	EG				
	Spiked concentration (ppm)	ANN Results (ppm)	PLS Results (ppm)	Recovery yield ANN (%)	Recovery yield PLS (%)
Sample 1	17.45	17.23	19.13	98.7	111.0
Sample 2	15.44	14.62	15.92	94.7	108.9
Sample 3	10.15	9.32	10.25	91.8	110.0
Sample 4	8.15	7.41	8.06	90.9	108.8
	EC				
	Spiked concentration (ppm)	ANN Results (ppm)	PLS Results (ppm)	Recovery yield ANN (%)	Recovery yield PLS (%)
Sample 1	13.02	12.50	15.28	96.0	122.3
Sample 2	6.57	6.91	7.89	105.3	114.1
Sample 3	5.10	5.68	6.31	111.4	111.2
Sample 4	17.55	17.81	17.37	101.5	97.6

Article 4

Modification of electrodes with N-and S-doped carbon dots. Evaluation of the electrochemical response

M. Bonet-San-Emeterio, M. Algarra, M. Petković, M. del Valle

Talanta, 212 (2020) 120806

4.4 Modification of electrodes with N-and S-doped carbon dots. Evaluation of the electrochemical response

CDs are wide employed in analytical chemistry due to one of their most popular features, fluorescence. The light color depends on their specific physical and chemical properties. Thus, together with the biocompatibility, stability, and solubility, makes this novel nanomaterial is a hot topic. Alternatively, their carbonaceous structure and their inherent properties make them good candidates for electrochemical catalysts. For this reason, this paper tries to integrate and test different CDs as a modifier in a voltammetric sensor.

4.4.1 Synthesis of the nanomaterials

Adapted synthetic pathways were employed for the obtention of CDs, N-CDs, and S-CDs. The reactions took place on a Teflon-lined steel reactor which was filled with the corresponding starting material. Polyvinylpyrrolidone and poly(4-styrenesulphonic acid) sodium salt were the reagents for N-CDs and S-CDs, respectively, meanwhile, for the raw CDs, it was used graphite. All of them were centrifuged and purified in overnight dialysis. Finally, the resulting solutions were lyophilized.

4.4.2 Chemical and morphological characterization

All the obtained materials were intensively characterized by different techniques. All of them corroborate the presence of N or S in the modified CDs and the small size of each one.

On one hand, it was carried out an elementary analysis (CHNS) which indicates *ca.* 10% of the modification element, S and N. These results were supported by XPS, in where was found functional groups that contain N and S. On the other side, it was also studied the morphological features, in this direction, SEM images (Figure 4.17) were taken for each sample, the pertinent histograms show distributed sizes of as much as 17.7 nm, which are near to the theoretical size value. Complementary to the SEM imaging was performed also MALDI-TOF mass spectra (Figure 4.18), which indicates the formation of small portions of carbon that contain S or N, depending on the analyzed sample.

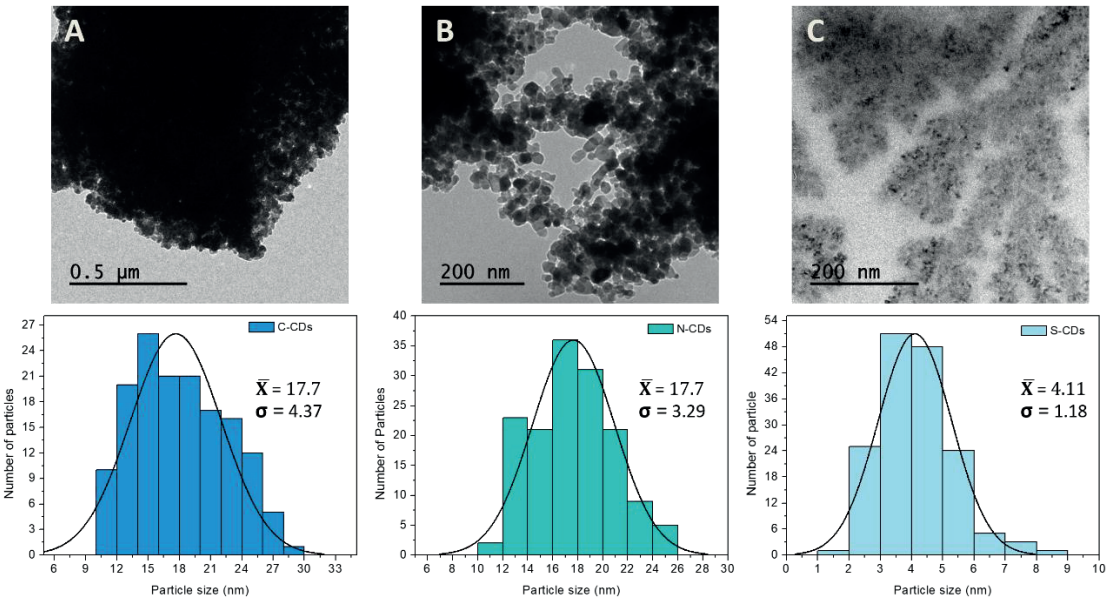

Figure 4.17. Histograms obtained from TEM images for CDs, N-CDs, and S-CDs.

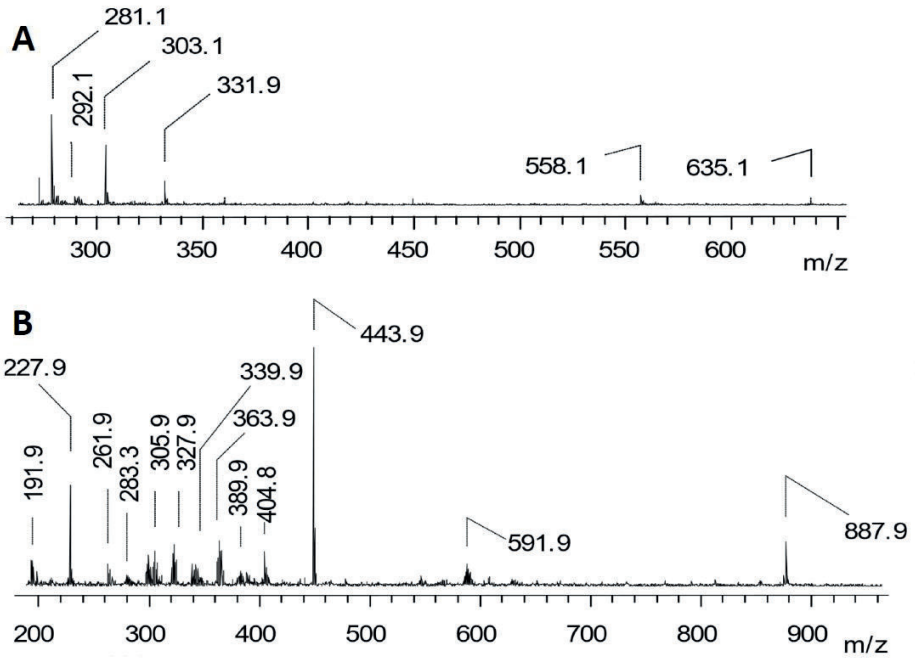

Figure 4.18. MALDI-TOF mass spectra for (A) N-CDs and (B) S-CDs.

4.4.3 Electrochemical characterization

For the electrochemical characterization, the different CDs were integrated onto the GC electrodes. Thus, as detailed in §3.4.2.2, the target nanomaterials were cast onto the electrode using polystyrene-based inks. From the tested methods, the creation of modified inks, was which seemed more efficient and convenient in our case because both modified CDs, present water solubility, which hinders their use as dispersions. Once the method has been decided the

electrode modification method, was studied the effect of the ink activation. As Figure 4.19 shows, the pretreatment of the electrodes enhances their response. The results are not only appreciated in the activation voltammograms but also in the EIS results, where the Rct value is clearly reduced for all ink cases. Moreover, it was tested the precision of the modification method leading to assume that the method is precise, thus the electrodes generated using this protocol will be equal.

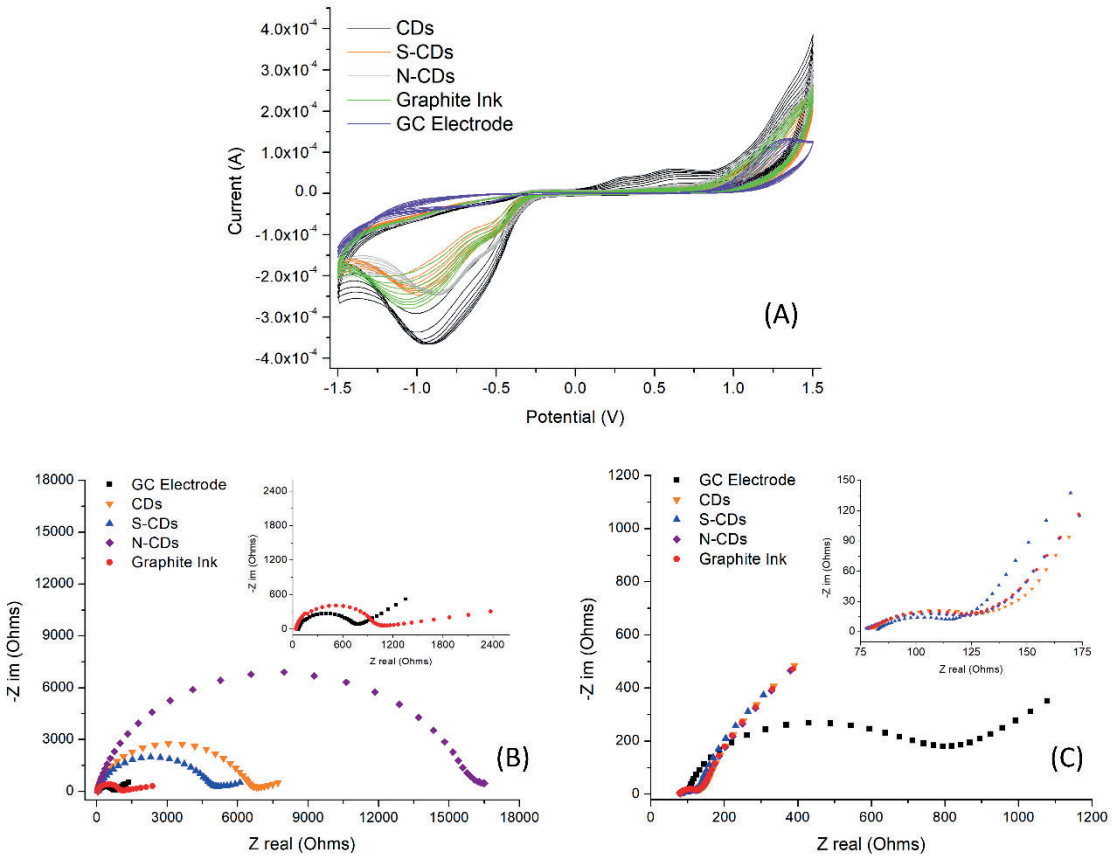

Figure 4.19. Electrochemical characterization of the modified GC electrodes (A) activation in H_2O_2 50 mM. Nyquist plots of (B) before and (C) after the activation step.

The electrodes were applied measuring compounds from different chemical families, AA, cysteine (CYS), and salicylic acid (SA). These compounds are interesting due to their poor electroactivity and extreme redox potentials. The results, depicted in Figure 4.20 demonstrate the difference among electrodes and the improvement in the potential and current, one of the most remarkable facts is the catalysis of the SA redox potential, which in the case of the bare GC it is not detected. The calibration curves for each sample, show better sensitivities for inks than for the bare electrode. But one of the most characteristic things in these

electrodes are the differentiated signals, which makes them a suitable candidate to be applied as modifiers in an electronic tongue array.

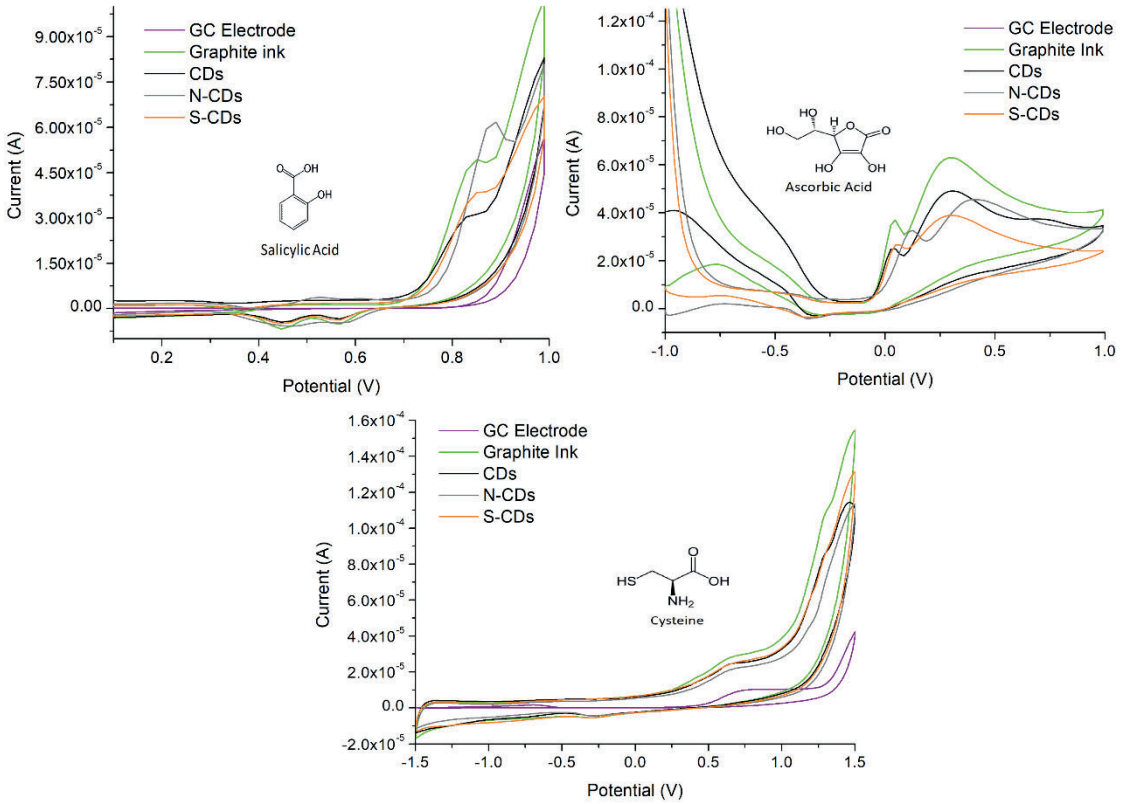

Figure 4.20. Responses of the modified electrodes against salicylic acid, ascorbic acid, and cysteine.

This paper demonstrates the successful synthesis of N and S modified CDs by its characterization using multiple techniques. Moreover, it is found its potential in the electrochemical field, both for the current and potential improvements they provide. Finally, as a future perspective, it is found that modified carbon dots apports different information from the same sample, being one of the key points in the electronic tongue arrangements.

4.5 References

[1] W.S. Hummers, R.E. Offeman, *Preparation of Graphitic Oxide*, Journal of the American Chemical Society. 80 (**1958**) 1339–1339. https://doi.org/10.1021/ja01539a017.

[2] M. Bonet-San-Emeterio, A. González-Calabuig, M. del Valle, *Artificial Neural Networks for the Resolution of Dopamine and Serotonin Complex Mixtures Using a Graphene-Modified Carbon Electrode*, Electroanalysis. 31 (**2019**) 390–397. https://doi.org/10.1002/elan.201800525.

[3] M. Bonet-San-Emeterio, N. Felipe Montiel, M. del Valle, *Graphene for the building of electroanalytical enzyme-based biosensors. Application to the inhibitory detection of emerging pollutants*, Nanomaterials. 11 (**2021**) 2094. https://doi.org/10.3390/nano11082094.

Chapter V. Conclusions

5 CONCLUSIONS

5.1 Conclusions

In the present doctoral thesis, an assortment of carbon platforms was developed to address them as part of an array for (bio)ET. Compiling all the data presented in this work, it is demonstrated the synergy of graphene and CDs combined with electrochemical sensors. For this reason, they are considered a powerful tool not only as an electrochemical catalyst but also as a starting point for new sensing platforms, for example as an anchoring site for different biorecognition elements. From ETs point of view, the greater the number of electrodes with non-redundant responses, the better when it is the moment to form a suitable array. This is why the possibility to create on-demand or to have available a broad library is critically important. Finally, with the achieved devices, were developed different quantification models for relevant fields of the industry, such as the pharmaceutical and medical area, the beverage and food industry, and environmental science. Hence, making evident the possibility of applying the different elements of this project in different areas of concern.

In the following points are specified the conclusions drawn from this thesis project. The previously established scheme will be followed in this section, where each item will be discussed according to the order of the articles in chapter 4, *results and discussion*.

1. Graphene sensory platforms.

    I. The two different graphene sources, handmade and commercial GO, do not present significant differences when applied onto an electrochemical sensor.

    II. The proposed protocol for the modification of the electrodes, based on the drop casting of the dispersed nanomaterial, presents appropriate characteristics, such as good operational stability, precision, and electrochemical properties.

    III. It is established that the protocol developed to reduce the GO of the electrode surface is reliable and reproducible.

    IV. The characterization of both, the raw graphene, and the already modified electrodes, lead to stunning results. Concretely, on one side, the imaging, and spectroscopic evaluations demonstrate the presence of GO, at the same time how it is deposited onto the surface. On the other side, the electrochemical measurements carried out show simultaneously the presence of graphene on the surface of the electrodes and how it is affected when the protocol developed to reduce it is applied.

    V. The GO is fully adapted to voltammetric sensors, being possible to apply them for the quantification of dopamine, serotonin, ascorbic acid, and uric acid. Having the developed sensors better features than the reference devices, in this case, the bare GEC electrode. In conclusion, it is proved the potential of enhanced transducers with chemometric tools for the resolution of complex samples.

    VI. The ERGO-GEC electrode is successfully used as a platform for two enzymatic biosensors (Lac-ERGO and Tyr-ERGO). Once

there were tested, both biosensors show better properties, such as selectivity and sensitivity.

VII. Lac-ERGO GEC is used as a proof of concept for the indirect detection of EDTA and benzoic acid. The kinetics study provides enough information to understand how the inhibitors (EDTA and benzoic acid) interact with Lac. The results indicate a competitive interaction.

VIII. It is successfully applied the developed (bio)sensors as part of an array for a bioET arrangement. Lac-ERGO and Tyr-ERGO biosensors are used for the detection of *Brett* spoilage in wines via the quantification of three volatile phenols, 4-ethylphenol, 4-ethylguaiacol, and 4-ethylcatechol.

2. Sensors with different modified carbon dots

I. The characterization of all CDs, N, S, and pristine CDs, demonstrate that each material has the expected elemental characteristics. Moreover, it was studied the morphological and chemical properties, which indicate that all the different nanomaterials were appropriate for their use as sensor modifiers.

II. It was developed a successful protocol for the integration of the nanomaterials onto the bare electrodes, being precise, and robust. Moreover, it was also developed a protocol to activate the modified electrodes, which is also validated, and then reliable.

III. The CDs and the modified CDs have favorable results in the electrochemical measurements.

IV. It is sought real applications for the developed electrodes, finding that they have a powerful potential taking part in ET approaches.

5.2 Ongoing works and future perspectives

After the experience gained throughout this journey, you cannot help looking back and reflecting on how the results obtained could be improved, or how the research could be continued. In the following lines, it is explained the ongoing works and the future perspectives.

Nowadays, we are working in the development of a new ET approach having as electrode array a set of electrodes modified with N-CDs, S-CDs, CDs, and ERGO. The goal of this work is to solve and quantify complex mixtures of biogenic amines in real samples, in this case in animals food. The first attempts show reliable and promising results.

As future perspectives, there is a wide range of challenges to confront. One example is the study of new carbon forms and modifiers to expand the alternatives when is selected an array for an electronic tongue experiment. For instance, the integration of new biorecognition elements, such as amine oxidases or alcohol oxidases. As abovementioned, the know-how gained would now help me to choose better and to visualize the problem from a completely new perspective. Precisely in the case of the choosing of the biorecognition elements, the final characteristics of the biosensors could have been improved by applying changes such as the measurement medium, the purification of the enzymes, or testing different enzyme sources, among others.

The building of electrodes is also a key point to be considered, new methods such as the printed electrodes, either in ink forms or 3D format, certainly is an interesting option as not all the employed electrodes in the herein proposals have the option to be miniaturized. Moreover, it could be studied to use eco-friendly materials and design the complete arrangement taking into account to reach a cost-effective and scalable device.

For the purpose of applying the achieved models in the industry for which they are designed, firstly more and a wider range of real samples must be measured in order to improve the quality and generalization ability of the models. Furthermore, it is interesting to find a self-evaluation protocol and a way to re-train them when some changes occur in the system (changes of electrodes,

changes of batch sample, or small changes in the measurement procedure among others). To sum up, these are some of the issues that must be addressed before totally implementing the models and demonstrating their real value.

ANNEX I. Publications included in the thesis

Article 1

Artificial Neural Networks for the Resolution of Dopamine and Serotonin Complex Mixtures Using a Graphene-Modified Carbon Electrode

M. Bonet-San-Emeterio, A. González-Calabuig, M. del Valle

Electroanalysis, 31 (2019) 390-397

DOI: 10.1002/elan.2018005

Article 2

Graphene for the building of electroanalytical enzyme-based biosensors. Application to the inhibitory detection of emerging pollutants

M. Bonet-San-Emeterio, N.F. Montiel, M. Del Valle

Nanomaterials, 11 (2021) 2094

nanomaterials

MDPI

Article

Graphene for the Building of Electroanalytical Enzyme-Based Biosensors. Application to the Inhibitory Detection of Emerging Pollutants

Marta Bonet-San-Emeterio, Noelia Felipe Montiel and Manel del Valle *

Sensors and Biosensors Group, Department of Chemistry, Universitat Autònoma de Barcelona, Edifici CN, 08193 Bellaterra, Spain; marta.bonet@uab.cat (M.B.-S.-E.); Noelia.FelipeMontiel@uantwerpen.be (N.F.M.)
* Correspondence: manel.delvalle@uab.es; Tel.: +34-93-5813235

Abstract: Graphene and its derivates offer a wide range of possibilities in the electroanalysis field, mainly owing to their biocompatibility, low-cost, and easy tuning. This work reports the development of an enzymatic biosensor using reduced graphene oxide (RGO) as a key nanomaterial for the detection of contaminants of emerging concern (CECs). RGO was obtained from the electrochemical reduction of graphene oxide (GO), an intermediate previously synthesized in the laboratory by a wet chemistry top-down approach. The extensive characterization of this material was carried out to evaluate its proper inclusion in the biosensor arrangement. The results demonstrated the presence of GO or RGO and their correct integration on the sensor surface. The detection of CECs was carried out by modifying the graphene platform with a laccase enzyme, turning the sensor into a more selective and sensitive device. Laccase was linked covalently to RGO using the remaining carboxylic groups of the reduction step and the carbodiimide reaction. After the calibration and characterization of the biosensor versus catechol, a standard laccase substrate, EDTA and benzoic acid were detected satisfactorily as inhibiting agents of the enzyme catalysis obtaining inhibition constants for EDTA and benzoic acid of 25 and 17 mmol·L^{-1}, respectively, and a maximum inhibition percentage of the 25% for the EDTA and 60% for the benzoic acid.

Keywords: graphene; biosensing; inhibition; phenols; laccase enzyme

Citation: Bonet-San-Emeterio, M.; Felipe Montiel, N.; del Valle, M. Graphene for the Building of Electroanalytical Enzyme-Based Biosensors. Application to the Inhibitory Detection of Emerging Pollutants. *Nanomaterials* **2021**, *11*, 2094. https://doi.org/10.3390/nano11082094

Academic Editors: Daniela Iannazzo and Run Zhang

Received: 18 June 2021
Accepted: 13 August 2021
Published: 18 August 2021

1. Introduction

A chemical sensor is defined by IUPAC as a device that transforms chemical information into an useful analytical signal [1]. The use of sensors has progressed over the years with the constant development of new technologies and devices. Researchers try to improve the selectivity of these designs with a wide range of techniques, such as the modification of the transducer material, the use of chemometric data processing, or the inclusion of sample pretreatment. An example of the former is the concept of biosensors. A biosensor may be described as a sensor combined with a recognition element from the biological world, which is the one responsible for conferring paramount selectivity. Actually, this is what makes the difference from common sensors and grants their success. Since the discovery of graphene and its derived products, they have been gaining importance in the sensors and biosensors field [2]; one of the reasons for this is due to their synergistic effect when they are implemented as transducing materials [3,4]. It can be proven that the usage of graphene is becoming widespread when you search how many publications exist with "graphene" as a keyword, since 2004, when graphene was strictly discovered. Almost 150,000 publications can be listed in total; from these, 14,117 can be found using the "graphene + sensor" keyword combination (data according to Scopus database).

Among others, graphene and its derivates have gained popularity in electroanalysis due to their interesting inherent properties, such as biocompatibility, low-cost raw materials, and their easy tuning [3,4]. In this work, graphene is used not only as a key material to

enhance the response of a bare electrochemical sensor, but also to show its properties as a linkage platform for enzyme immobilization [5–7]. Graphene allows to avoid sensor pretreatment or modifications that can be costly, time-consuming, and complex. One example is electrochemical grafting, where the carboxylic groups of an organic layer are attached to a conductive surface [8–10].

Graphene synthesis can be classified into two groups: top-down, and bottom-up synthesis. Furthermore, new strategies may be mentioned in the state of the art of the topic; for example, the cracking of multiwalled carbon nanotubes to create graphene oxide (GO)ribbons [11,12]. Bottom-up syntheses are the ones that start from simple carbon structures to create a pristine single-atom graphene layer with minimum defects and a *sp2* configuration. Some examples of bottom-up approaches are the chemical vapor deposition (CVD) or the epitaxial growth [13,14]. Nevertheless, these synthetic pathways have important drawbacks, such as the complex adaptation to large scale production and the expensive and complex arrangements [15]. For this reason, top-down syntheses are popular when large amounts of materials are required. Hummers' synthesis is the most frequently used method for the top-down production of graphene [16,17]. This wet synthesis uses strong oxidizing agents for exfoliating graphite to GO. As it is known, GO is a hydrophilic non-conductive material, which needs further synthetic steps to recover the pristine graphene properties, one of them the conductivity, an essential feature in electrochemistry [15,17]. Thus, a further step is needed, the GO conversion to the reduced graphene oxide (RGO). This step can be done electrochemically, chemically, mechanically, or even thermally. Even though, in the sensors study area, the most used reduction techniques are the electrochemical and the chemical [18–20]. Both methods are interesting due to their reproducibility and easy applicability; however, the electrochemical approach presents several clear advantages over the chemical approach, e.g., low-cost, speed, environmentally friendliness and simplicity [20]. Therefore, in this work, RGO has been produced electrochemically. This method is based on the reduction of oxidized moieties present on the GO surface. As an additional advantage, the electrochemical reduction allows to easily and effectively control the oxidation degree of the RGO by simply adjusting the applied potential, which may be interesting for different final applications [21,22].

Graphene is not the unique strategic nanomaterial used to enhance the sensors response. For example, carbon dots and nanotubes have been also widely used as electrode modifiers. Carbon dots, also named graphene quantum dots or carbon nanodots, are a new trend in electroanalysis applications. Up to recent times, this material has been used mainly in photoluminescence-based determinations; but in current years it is growing strongly also in the electrochemical field [23–26]. On the other side, carbon nanotubes, considered as a rolled layer of graphene [27], have been extensively studied as a sensor modifier as well. Like other materials from the carbon family, carbon nanotubes ascribe catalytic effects and sensing improvements to the electrode behavior [28–30].

Enzymes such as laccase, tyrosinase, and glucose oxidase have been employed for a long time in bioanalytical chemistry, especially in biosensing. Their relevance is related to their ability to interact only with their matching substrates, conferring to the device one of the most desired characteristics: the specificity and the ability to distinguish the analyte in complex matrices. One of the most famous case is the glucose biosensor, already commercialized as a device for diabetic patients [31,32]. On the other side, laccase, a protein with a copper nucleus, has been extensively studied as a biorecognition element in various areas owing to its ability to oxidize a wide range of phenolic compounds, being catechol one of the standards for its activity analysis [33,34]. But not only there have been studies on the direct interaction with the substrates, but also on the interaction of the enzymes with their inhibitors. An interesting example is its use in detecting pollutants in products for human consumption, especially in drinking water. UNESCO reports as a pollutant any synthetic or naturally occurring chemical or microorganism that is not commonly monitored or regulated in the environment. This group includes pharmaceuticals, personal care products, pesticides, industrial additives, and industrial and household products [35].

New pollutants, also named emerging pollutants or contaminants of emerging concern (CECs), are appearing continuously. These chemicals have become an increasing problem over the years. Fortunately, at the same time, technology has been developed which has introduced new and improved methods to isolate and/or detect CECs in human consumption products. However, the existing commercial techniques are time-consuming and expensive, which encourages researchers to find new alternatives. Moreover, it must be considered that at this moment there are no reference methods in the European legislation to control the presence of these compounds in water. Nevertheless, different factors will force their consideration in the near future. The first reason is the conclusions from recently published articles, which determine that certain CECs, in special endocrine disruptors, interfere in the human and animal endocrine system [36–38]. The second reason is that these pollutants are not only found in water but also in soil and marine species such as shellfish and oily fish, increasing the contact of humans with these compounds with still unknown long-term effects. This work reports the preparation and characterization of a laccase-graphene biosensor for the detection of CECs (EDTA and benzoic acid) by the inhibition of the laccase enzyme.

2. Materials and Methods

2.1. Chemical and Reagents

All reagents were of an analytical grade and all solutions were prepared using deionized water from Milli-Q system (Millipore, Billerica, MA, USA). Samples for electrochemical measurements were prepared on phosphate buffer in the presence of KCl as a background electrolyte, reagents purchased from Merck KGaA (Darmstadt, Germany).

For the graphene synthesis, it was used as a graphite powder (50 μm, sulfuric acid (98%), sodium nitrate (99%), and potassium permanganate (99%), purchased from Merck KGaA (Darmstadt, Germany); hydrogen peroxide (30%) was purchased from Riedel-de Haën (Germany). Used ionic resins were strong cationic resin C100E and weak anionic resin A520E (Purolite) purchased from Merck KGaA. $Ba(NO_3)_2$ was purchased at Acros Organics (Geel, Belgium).

The material needed for the building of the electrode were: Resineco Epoxy Kit 125 resin supplied from Resineco green composites (Barcelona, Spain) and graphite powder (particle size < 50 μm) was received from BDH (BDH Laboratory Supplies, Poole, UK). For the biosensor, Laccase from *Agaricus Bisporus*, 7.2 $U \cdot mg^{-1}$ (EC number: 420-150-4), 1-ethyl-3-(3-dimethylaminopropyl carbodiimide (EDAC), and N-hydroxysulfosuccinimide (sulfo-NHS) (purchased from Merck KGaA) were used.

Finally, catechol, acid benzoic, and EDTA were purchased from Merck KGaA.

2.2. Electrochemical Measurements

Voltammetric measurements were performed on a AUTOLAB PGSTAT30 (Ecochemie, Netherlands) controlled by GPES software. Electrochemical Impedance Spectroscopy (EIS) experiments were performed on a Bas-Zahner IM6e (Kronach, Germany) potentiostat controlled by Thales software. For both electrochemical techniques a typical three electrode circuit was used. In the used assembly it can be found: the working electrode based on a graphite epoxy composite (electrode already optimized in our laboratory [39–41]), an Ag/AgCl (0.1 $mol \cdot L^{-1}$ KCl) electrode as a reference and a Pt electrode as a counter. All measurements were carried out at room temperature without stirring using as an electrolyte solution phosphate buffer 50 $mmol \cdot L^{-1}$ + KCl 100 $mmol \cdot L^{-1}$ at pH 7.4.

Parameters for the cyclic voltammetry (CV) measurement were optimized for its use; at the end, a scan rate of 10 $mV \cdot s^{-1}$ and a step potential of 0.001 V was applied. The analysis of CV was performed with the GPES software, in particular using the inset tool to calculate the base line and the corresponding peak height of the recorded data.

2.3. Sensor Characterization

Morphological characterization of the raw materials was carried essentially by Transmission Electron Microscopy (TEM); TEM images were obtained using a JEOL JEM-2011 microscope. Moreover, X-ray photoelectron spectroscopy (XPS) analysis was carried out to describe the structure of the synthetized GO; a SPECS PHOIBOS 150 hemispherical energy analyzer with monochromatic Cu–Kα radiation was used. CasaXPS software was used to acquire the fitted values.

Surface roughness assessment was done by processing of topographic atomic force microscopy (AFM) images obtained using a Veeco Dimension 3100 AFM Microscope (Bruker, Billerica, MA, USA).

2.4. Graphene Synthesis and Characterization

A top-down synthesis based on a modified Hummers' method was used for the synthesis of GO [16,18,42]. In short, the protocol consists of the addition of 1.5 g of graphite and 4.5 g of $NaNO_3$ to 35 mL of sulfuric acid (98%) cooled at 0 °C. Afterwards, 4.5 g of $KMnO_4$ in fine powder form was added in small portions over a period of 2 h, avoiding temperature from rising and the mixture was stirred for an additional 4 h. The resulting mixture was heated at 35 °C for 30 min and the oxidation process was completed by slowly adding 75 mL of deionized water. In this highly exothermic step, it is important to avoid boiling. The reaction finishes 15 min after being kept at 70 °C. In order to eliminate unreacted oxidizing compounds, the solution was treated with 300 mL of 10% hydrogen peroxide. The resulting brown paste (the densest GO) was washed multiple times with deionized water, recovering the solid by centrifugation at 6000 rpm. This process was repeated several times, till the pH approached neutrality. With a pH close to 7, the sample of GO was treated with cation and anion exchange resins to eliminate the remaining salt impurities. This was done just by placing in contact, under vigorous stirring, the sample and resin for 30 min. The separation was achieved by using a 50 µm sieve. Sulfate ions were eliminated with $Ba(NO_3)_2$. Finally, the obtained slurry was dried in a vacuum oven at 60 °C for 48 h.

2.5. Graphene Oxide Modification and Immobilization of the Enzyme for the Biosensor Building

The graphite epoxy composite (GEC) electrode, used as base transducer, had an average geometric area of 28 mm^2 (Ø = 6 mm), as it is specified in the reference bibliography [39,40,43]; the composite conductive paste was added in an assembly formed by an electrical connector and a PVC tube. Afterwards, the conductive material was hardened in an oven at 40 °C. Finally, the electrode was polished with different grain sandpapers until a homogeneous and pristine surface was obtained. The polishing step can be applied when needed to regenerate the surface and obtain again the bare platform. Figure 1 sketches the construction process.

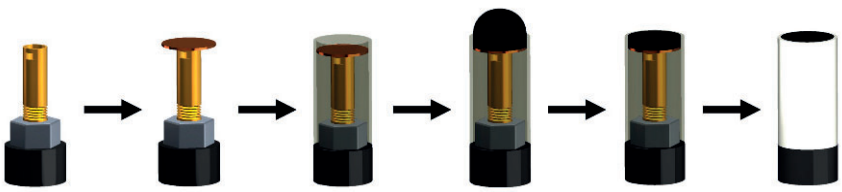

Figure 1. Scheme of the mechanic assembly for the construction of the base graphite-epoxy voltammetric transducer.

Once the conductive element of the proposed biosensor was ready, it was modified with GO. The selected technique to modify the electrode surface was drop casting, based on the physical adsorption of the GO to the base carbon material. Firstly, 40 µL of the GO dispersion (1 $mg \cdot mL^{-1}$ in deionized water) was deposited on the GEC electrode. It may be noted that the GO suspension must be sonicated previously for 1 h and centrifugated for

1 min at 800 rpm to use only the part of the dispersion that content the flakes with fewer layers. After this, the electrode was dried at 40 °C to promote physisorption. The RGO was obtained by the electrochemical reduction of the previous electrode. As it was first optimized [43], the reduction was carried out via CV; in particular, 10 cycles were applied in a potential range going from +1.90 V to −2.30 V at 0.1 $V \cdot s^{-1}$.

The laccase enzyme was covalently bonded to the RGO via carbodiimide (EDAC, N-(3-dimethylaminopropyl)-N′-ethylcarbodiimide hydrochloride) chemistry. The EDAC reaction proved to be the most suitable strategy to immobilize the enzyme since it is able to react (through a free amino group) with the remaining carboxylic groups from RGO (that were not reduced in the reduction step) to obtain the amide bond. Concretely, after the reduction, a solution of 10 $mg \cdot mL^{-1}$ of laccase in water was prepared, where 100 µL of EDAC solution (1000 ppm) and 50 µL of sulfo-NHS solution (1000 ppm) were added. Once the solution was homogenized, the RGO electrode was incubated overnight in an Eppendorf tube [44–47]. The last step was to clean the non-bonded compounds from the surface of the electrode by rinsing it for 1 h in the working phosphate buffer.

As Figure 2 depicts, the EDAC coupling agent is used to activate the carboxylic groups from the RGO surface and form an intermediate complex that can react with the primary amine group from the laccase chain. In this article, sulfo-NHS was additionally used to obtain a more stable and efficient intermediate complex.

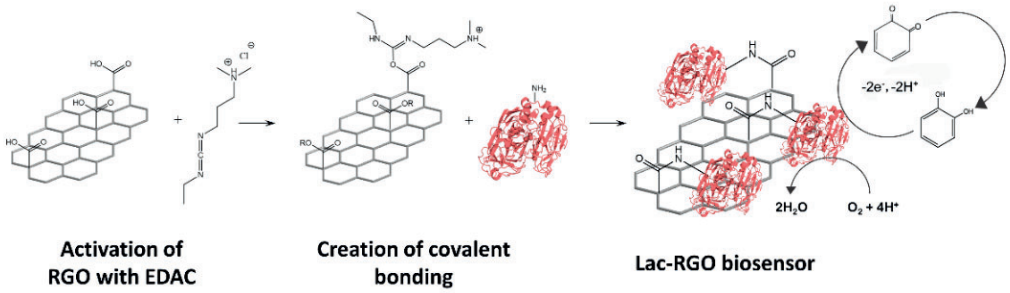

Figure 2. Scheme of the laccase immobilization. Step 1: activation of the RGO using EDAC (and NHS to increase the efficiency), Step 2: bonding creation between the primary amine from the enzyme and the intermediate complex of the RGO surface. Finally, the catalytic reaction is described.

3. Results

3.1. Study of the Synthesized Graphene Oxide

The obtained GO was characterized by TEM. Figure 3 shows some representative images resulting from this technique. Herein, the main part of graphene flakes was thin and transparent enough to see the CuTEM grid through them. The presence of GO was corroborated when its characteristic wrinkles were identified, present, for example, in Figure 3A,B,D [48,49]. The main presence of few layers of aggregates, which is supported because not only the transparency is achieved but also clear borders, is also noticed. Particularly, in Figure 3A,D can be seen clear and sharp edges, whereas in Figure 3B the presence of a large number of layers can be deduced from the multiple grey shades at the edge of the flake. These hypotheses were compared with the literature, where other researchers have similar TEM images [22,50,51]. The opaque materials in Figure 3C may be associated with the graphite residues coming from the starting synthesis reagents.

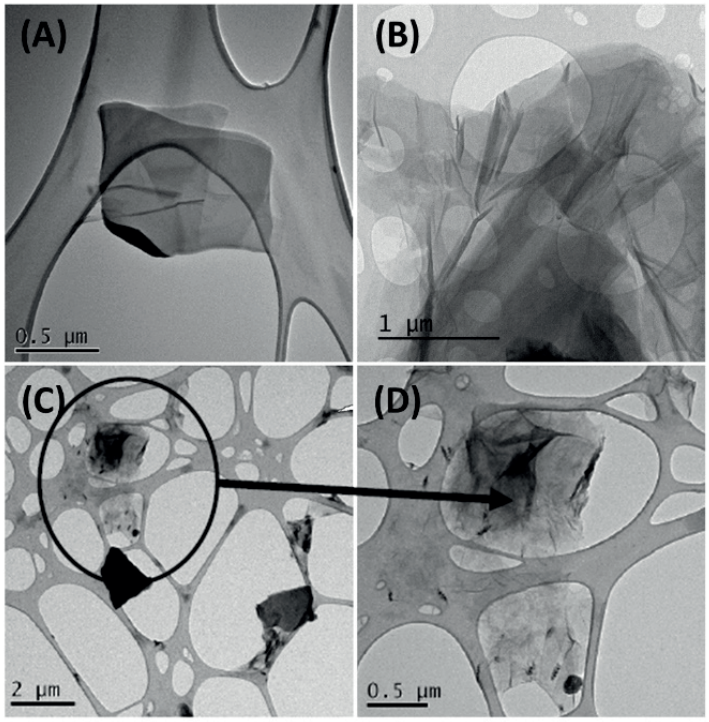

Figure 3. TEM images of synthesized GO. The samples were suspended in ethanol absolute (≥99%) and casted on a CuTEM grid. (**A**,**C**) show entire flakes of graphene oxide meanwhile in figures (**B**,**D**) it is presented a specific part where graphene characteristics can be spotted.

In addition to TEM, XPS analysis was carried out to study the obtained GO (Figure 4). Table 1 presents the dominating groups assigned to C 1s core level after its deconvolution. Different groups could be found in the material, corresponding to the wide range of oxygen functional groups from the synthetic pathway. To confirm this hypothesis, the oxygen and carbon ratio was calculated, being equal to 2.14. Normally, the approved ratio values range between 2.1 and 2.9 for GPO samples [16].

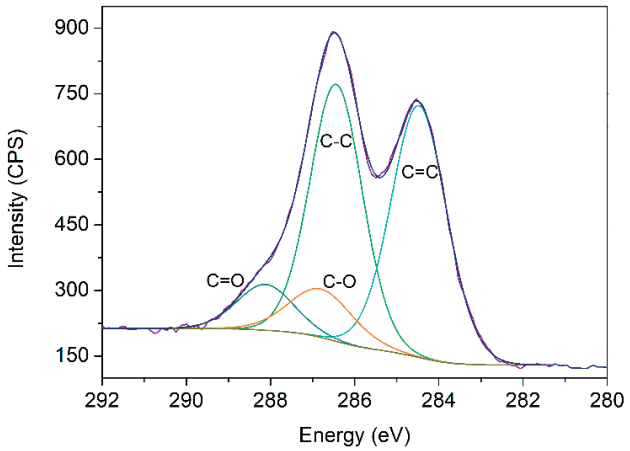

Figure 4. GO-Fitted XPS spectra of C 1s and its deconvolution. Blue line corresponds to the fitted curve.

Table 1. XPS-obtained distributions for the synthetized GO for the C 1s spectra.

Bond	Energy (eV)	% Area (RSD) *
C=C	284.5	42.81 (1.30%)
C-C	286.4	40.39 (2.1%)
C-O	286.9	10.24 (8.3%)
C=O	288.2	6.56 (9.5%)

* Relative standard deviation.

Briefly, the resulting material of the modified Hummers' method has similar properties and characteristics to comparable works in the literature [17,20,22,52], reflecting then the good performance.

3.2. Modification and Characterization of the Graphene Sensor

The optimization of the sensor assembly was carefully addressed. First, the optimal amount of GO solution to be deposited onto the electrode was studied. In this case, drop-casting was chosen as the modification method, due to its rapid and easy application. The effect of four different volumes (20, 30, 40, and 50 µL) of a 1 mg·mL^{-1} GO dispersion (in deionized water) was studied. As mentioned above, GO is not conductive. For this reason, after the deposition, it was reduced to RGO to analyze its response using electrochemical techniques. The analytical performance was studied by using a CV technique, by measuring the height of the oxidative peak at a potential of 0.18 V (vs. Ag/AgCl reference electrode) in the electrochemical standard $[Fe(CN)_6]^{3-/4-}$ 5 mmol·L^{-1} (diluted in phosphate buffer 50 mmol·L^{-1} at pH 7.4) as analyte. The goal was to find a volume that covers all the electrode surface and did not saturate the response. As can be observed in Figure 5A, the obtained results, together with visual checking, demonstrate that smaller volumes did not cover the whole area of the electrode, but at the same time volumes higher than 40 µL formed aggregates too large to be stacked in the surface for long periods of time, deteriorating any graphene benefits in the electrochemical responses. At the sight of these results, 40 µL was the selected volume for preparing the graphene-modified electrode.

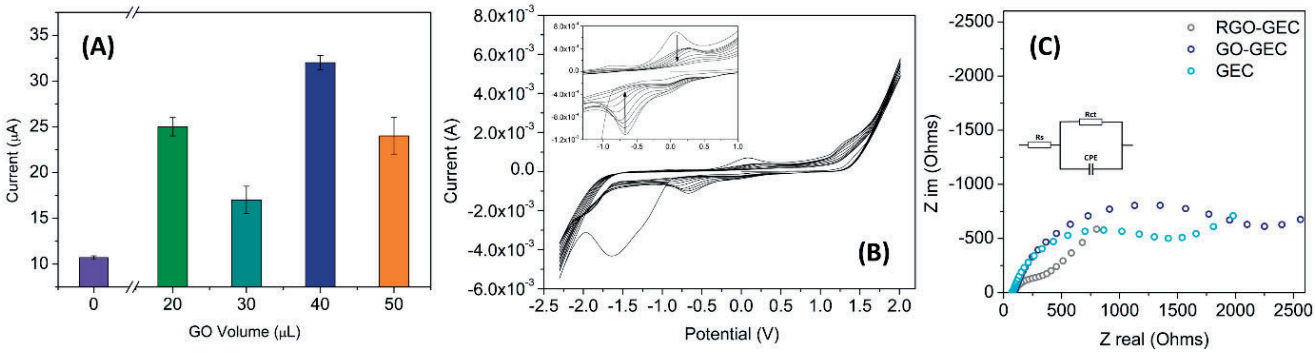

Figure 5. Optimization of the critical parameters for the use of the sensor. In (**A**) the deposited volume of GO via drop casting (n = 3) (**B**,**C**) activation step of GO to RGO. (**B**) depiction of the 10 cycles reduction step; (**C**) shows the Nyquist plot after the reduction of GO.

The electrode surface was characterized also topographically via AFM, in order to visualize how the graphene was distributed onto the electrochemical platform. Figure 6A shows the surface of a bare GEC electrode, and Figure 6B,C is a representative region of a GO modified GEC electrode, all images have a scanned surface of 10 × 10 µm. As it can be seen in Figure 6A, the GEC electrode presents a crumpled surface with a root mean square roughness (R_{RMS}) of 73.5 nm; meanwhile, the surface modified with GO has a R_{RMS} of 123.3 nm. Those values, along with the AFM images, verify the presence of graphene flakes. Moreover, the 3D AFM image (Figure 6C) indicates the presence of multiple and separated GO flakes, some of them clearly with less height than the others.

Even in image 6C (marked with an arrow), it is possible to notice the GO wrinkles, also observed in TEM images (Figure 3). To sum up, AFM images demonstrated the correct stacking of GO, which lays in the surface increasing the rugosity, and consequently, the active sites of the electrode surface.

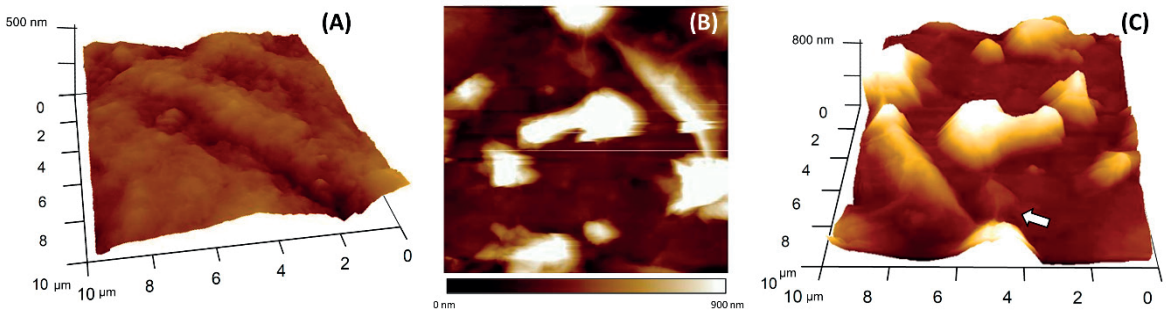

Figure 6. AFM images comparing (**A**) bare GEC electrode and (**B**) a GEC electrode modified with GO. (**C**) 3D AFM representation of the GO-GEC electrode.

One essential step for the building of the biosensor is the correct reduction of GO to RGO; in this work, the electrochemical reduction step was followed via CV, and verified with EIS by the comparison of the different surfaces. In Figure 5B, the CV plot corresponding to the electrochemical reduction of the GO to RGO is shown. Specifically, the good performance of the process was assessed through the oxidation and reduction peaks that appear in the range of −1.0 V to −0.5 V (vs. Ag/AgCl) (see insert on Figure 5B). According to the literature, these peaks are related to the reduction of oxygen groups present in the deposited GO in aqueous medium and neutral pH [20,53]. An EIS technique was also used to confirm the efficiency of the electrochemical reduction. The differences in the electrode surface of the sensors can give information on the electron transfer and thus demonstrates the increment in conductivity of the RGO. In this case, the impedance characterization experiments were carried out in $[Fe(CN)_6]^{3-/4-}$ 5 mmol·L^{-1} between 0.5 MHz and 0.1 Hz at a sinusoidal voltage perturbation of 10 mV amplitude. Figure 5C shows the Nyquist plot for each modification phase; the bare GEC electrode, the electrode when the GO material was deposited and finally when the last material, RGO, was obtained. In the same figure is inserted the Randles' equivalent circuit, which includes: (i) Rs, the ohmic resistance of the bulk solution; (ii) Rct, the charge transfer resistance, which describes the difficulty of the electrochemical reaction; and (iii) CPE, a constant phase element, the component that gives information on the double layer capacitance. Figure 5C shows a smaller Rct for RGO-GEC electrode (206 Ω) than for GEC (1638 Ω) and GO-GEC (2256 Ω), indicating that the conductivity of graphene is regenerated with the electrochemical method applied in this work. Additionally, the data demonstrate the better conductivity of the RGO-modified electrode than the non-modified one.

These observations allowed us to confirm that GO is deposited correctly onto the GEC surface using 40 µL; moreover, it could be assumed that the reduction method is good enough to recover the conductive properties of graphene and proceed to covalently immobilize the enzyme via the EDAC reaction.

3.3. Characterization and Application of the Biosensor

3.3.1. Electrochemical Response of the Laccase Biosensor

Once the enzyme was immobilized, EIS was used to compare and contrast the biosensor against the already-evaluated platform.

The results of Table 2 compare Rs, Rct and CPE values for the most significant steps of the electrode modification. The most characteristic value in impedance results is the Rct; in this case, it is easy to see the little difference between the electrodes, RGO (206 Ω) and the laccase-RGO (231 Ω) electrodes, which expose less resistance to the current flow than the bare one (1638 Ω). The effects seen in Rct of the laccase-RGO electrode could be explained

with the negative charge formed in the carboxylic groups of the amino acids, which are deprotonated at pH 7.4, generating a minimal increase in the electronic transference between the electrode surface and the negative complex used as analyte. Moreover, CPE, a complex value with empirical significance, was adjusted. The results indicate changes that may be related to the double layer capacitance thickens the decrease. Rs, as mentioned above, describes the bulk features of the solution and the diffusion characteristics; therefore, it may not be affected by the modifications on the electrode surface as can be observed in the table, indicating the ideal situation.

Table 2. Fitted values of circuit elements in the equivalent electric circuit for the different studied surfaces.

Electrode	Rs (Ω)	Rct (Ω)	CPE (F)
GEC	240.7 ± 4	1638 ± 62	$7.9 \times 10^{-5} \pm 0.7 \times 10^{-5}$
RGO	252.0 ± 3	206 ± 142	$4.2 \times 10^{-5} \pm 0.5 \times 10^{-5}$
Laccase-RGO	252.0 ± 2	231 ± 138	$4.3 \times 10^{-5} \pm 0.4 \times 10^{-5}$

Finally, the resulting biosensor was tested versus a phenolic compound, catechol, which is a standard substrate of the laccase enzyme. In Figure 7A is shown the excellent performance of the enzyme by the comparison of the responses of each sensor against different concentrations of catechol. Note that the anodic peak was used as the analytical signal in the following experiments since, contrary to what was expected, it is the part where the synergistic effect of all the system elements was best [54–56]. In the calibration curves, observed a linear trend from 2 to 100 μmol·L^{-1} for the biosensor and a wider range for the bare and the RGO electrodes was observed, which goes from 2 to 1500 μmol·L^{-1} and from 2 to 800 μmol·L^{-1} respectively. In the same image is also noted a clear enhancement in the sensitivity of the system, increasing by more than threefold the initial slope value.

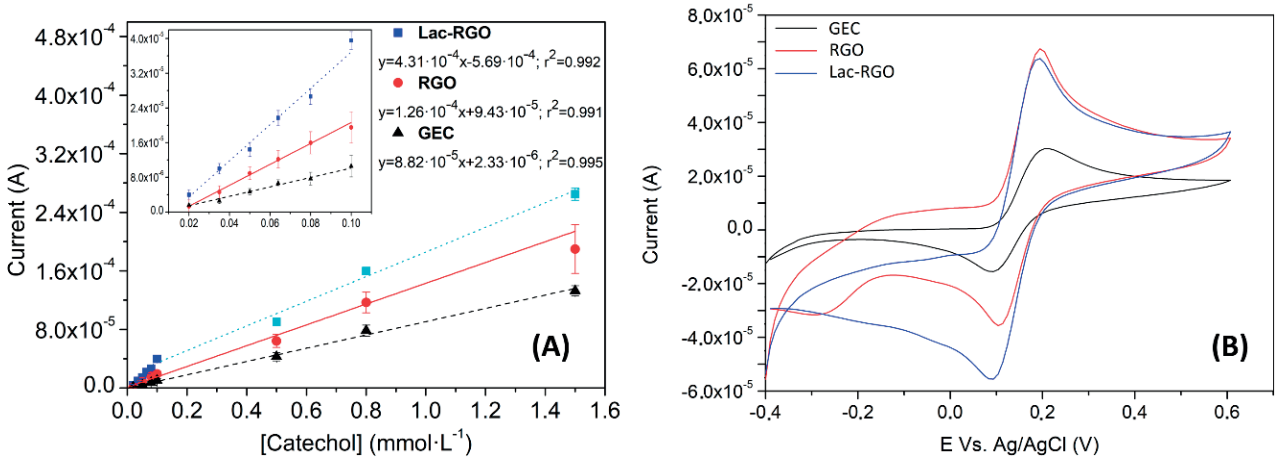

Figure 7. (**A**) Calibration curves for Lac-RGO electrode (■), RGO electrode (●) and GEC electrode (▲) for the same concentrations of catechol. Currents for the oxidative peak (**B**) CV voltammograms response of the three electrodes in the same concentration of catechol. Measures in phosphate buffer + KCl solution, pH 7.4.

Figure 7B compares GEC, RGO, and Lac-RGO responses against the same concentration of catechol. In the figure, as expected from the previous characterization, a current enhancement can be observed when the GEC electrode is modified with graphene. On the other side, some differences are appreciated when RGO and Lac-RGO responses are compared, which leads us to assume the laccase activity. Two of the most characteristic changes are observed in the oxidation baseline and the reduction peak. These facts are caused by the catalysis of the anodic reaction, and consequently there is a significant enlargement of the cathodic pathway.

3.3.2. Analytical Characterization of the Biosensor

Once the biosensor operation was confirmed, their analytical properties were studied in detail. The properties studied were the linear range, limit of detection (LOD), limit of quantification (LOQ), repeatability, intermediate precision, selectivity, and lifetime.

The linear range is generally defined as the area in the calibration curve where the signals are directly proportional to the concentration. This parameter is typically evaluated using the correlation coefficient. As can be observed in the inset of Figure 7A, the linear range found spanned from 2 to 100 μmol·L^{-1}. The correlation coefficient for this range was 0.992, indicating a satisfactory linearity.

Regarding the LOD and LOQ, there are multiple ways to calculate them, such as the use of the calibration curve for the target analyte (see Equation (1), where m is the slope of the calibration curve and σ the standard deviation of the response at a 95% confidence level), the measure of signal/noise ratio or by the use of the blank standard deviation [57,58]. In this work, we used the first option, obtaining an LOD of 2.1 μmol·L^{-1} and a LOQ of 7.7 μmol·L^{-1}.

$$\text{LOD} = \frac{3.3\ \sigma}{m}\ \text{LOQ} = \frac{10.0\ \sigma}{m} \quad (1)$$

The repeatability is defined for the European Medicines Agency (EMEA) as the "term that expresses the precision under the same operating conditions over a short interval of time" [59]. In this case, 10 consecutive measurements of a 50 μmol·L^{-1} catechol solution were performed, obtaining a relative standard deviation (RSD) value equal to 8%. Moreover, a second repeatability test was done to check the reliability of the biosensor during the day. For this purpose, 3 calibration experiments were repeated in 3 different time instants of the day (9 a.m., 1 p.m. and 4 p.m., see Figure 8A). The results showed an RSD for each point of the curve not larger than 8%. All repeatability tests were taken as positive, considering that a group of data is significantly equal when the RSD value is lower than 10%. In the EMEA guideline, is also defined the intermediate precision [59]. This term expresses "the within-laboratories variations, for example, when considering different days of analysis, different analyst or analysis in different equipment". This test measured, across three different days, three different calibration curves, from three regenerated biosensors, checking at the same time two parameters, the difference between days and the difference of the electrode surface regeneration procedure (see Figure 8B). The findings indicated that there were no differences between the regenerated electrodes or the measurements on different days (RSD = 6%). The last studied parameter was the lifetime of the biosensor (or the intermediate precision of different days). To perform this test, an electrode was stored in the fridge at 4 °C in a closed Eppendorf and a measurement was done every day (without regeneration of the surface) using a 50 μmol·L^{-1} catechol solution. The RSD results were 3% (n = 3).

To visualize the selectivity of the biosensor, a Principal Component Analysis (PCA) (executed in Matlab R2020a) was carried out to show the ability of the biosensor to distinguish between the different substances considered. In particular, six substances from different families were analyzed with a Lac-RGO-modified electrode. As can be seen in Figure 9, the score plot shows that substances without phenols in their molecular structure as ibuprofen and cadaverine have similar behaviors to the buffer response. This fact demonstrates then the correct performance against the specific substrates.

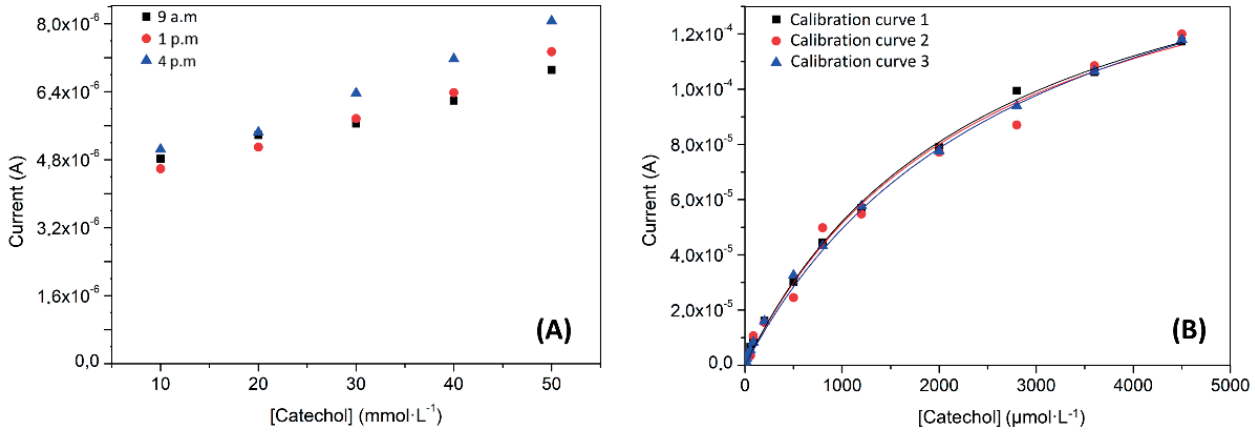

Figure 8. Study of the Lac-RGO analytical biosensor properties, (**A**) calibration curves repeatability test; measurements carried out in three-time instants and without regeneration of the electrode, (**B**) intermediate precision test made with 3 calibration curves on 3 different days with renewed electrode surface.

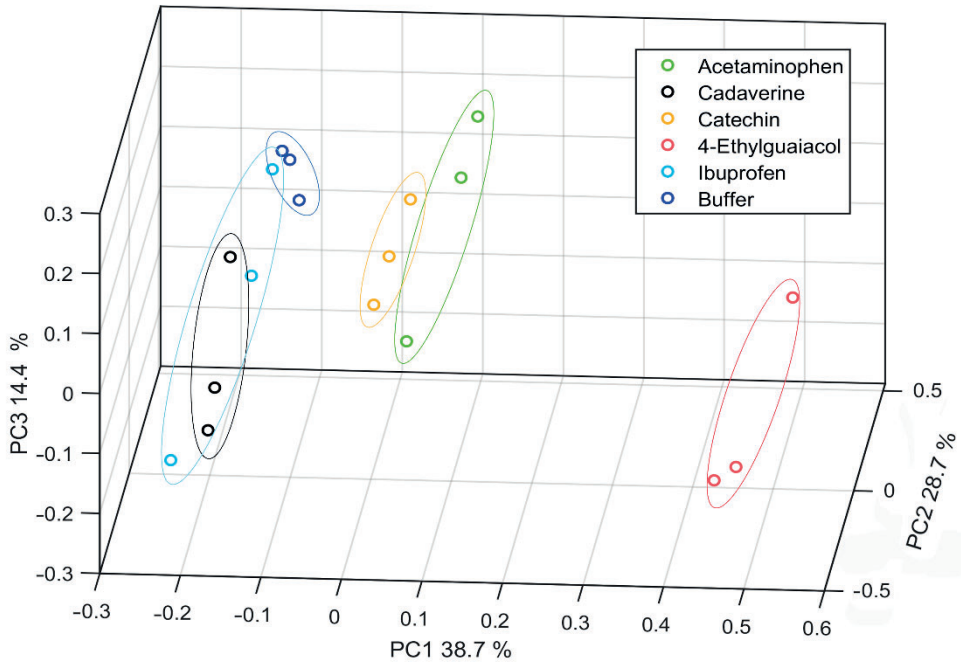

Figure 9. PCA Score plot for the three principal components of 6 different molecules, acetaminophen, cadaverine, catechin, 4-Ethylguaiacol, and ibuprofen.

Table 3 was built to compare the results in the presented work with the others in the literature. From here, it can be concluded that our biosensor has a similar behavior to devices with similar properties, even if it is compared with electrodes that include more than one catalytic material.

Table 3. Reported values for the analytical study of sensors and biosensors for the quantification of catechol.

Method	Electrode	LOD (μM)	Sensitivity ($\mu A \cdot \mu M^{-1}$)	Linear Range (μM)	Ref
CV	Lac/rGO/GEC	2.1	0.431 (15.39 $\mu A\ \mu M^{-1}\ cm^{-2}$)	2–100	-
CV	Tyrosinase-polysaccharide	6	0.001	60–800	[60]
CV	Lac/PANI/GCE [1]	2.07	0.23	3.2–19.6	[55]
CV	Lac/AP-rGOs/GCE [2]	7	15.79	15–700	[61]
CV	Lac/AA/LuPc2 [3]	0.58	0.36	4–150	[62]
CV	AuNPs/ZnO/Al2O3/GO/chitosan/GCE	3.1	-	0.5–40	[63]
CV	FePP/MWCNT/Nafion/GCE [4]	3.75	0.1867	65–1600	[64]
Amp. [11]	N-OMC/PVA/Lac/AuE [5]	0.31	0.29	0.39–8.98	[65]
Amp.	Lac/CNTs–CS/GCE [6]	0.66	-	1.2–30	[66]
Amp	Lac/PAP/MWCNTs/SPE [7]	0.20	5.8×10^4	0.63–20.7	[47]
Amp	Lac/Nafion/MWCNTs/SPE	0.45	1.6×10^4	1.4–65.4	[47]
Amp	Lac/MWCNTs/SPE	0.73	1.5×10^4	2.4–134.4	[47]
DPV	Lac/MWCNT-COOH/AuNPs/SDBS/PEDOT/GCE [8]	12.26	0.012	12.0–94.1	[67]
DPV	RGO-MWCNT/GCE	1.8	0.07	5.5–540	[68]
DPV	MWCNT-PMG/GCE [9]	5.8	1.3 $\mu A\ \mu M^{-1}\ cm^{-2}$	30–1190	[69]
DPV	MWCNT/PMT/GCE [10]	0.05	1.895	0.5–150	[70]

[1] Laccase/Polyaniline/Glassy carbon electrode. [2] Lac/aminopyrene-reduced graphene oxide/GCE [3] Lac/arachidic acid/Lutetium bisphthalocyanine [4] Iron porphyrins/multi-walled carbon nanotubes/Nafion/GCE [5] Nitrogen-doped ordered mesoporous carbon/Polyvinyl alcohol/Lac/Au electrode [6] Lac/Carbon nanotubes-chitosan/GCE [7] Lac/Polyazetidine prepolymer/MWCNTs/Screen printed electrode [8] Lac/MWCNT-COOH/AuNPs/sodium dodecyl benzene sulfonate/Poly(3,4-ethylenedioxythiophene)/GCE [9] MWCNT- poly(malachite green)/GCE [10] MWCNT/ poly (3-methylthiophene)/GCE [11] Amperometry.

3.3.3. Kinetic and Inhibition Study

The kinetics in enzymatic studies is one of the most interesting features as it is unique for each enzyme and substrate. For this reason, this issue is normally studied in detail; Leonor Michaelis and Maud Menten developed one of the most common models. This relates the enzyme substrate concentration ([S]) with the reaction rate (V). In this model, the enzyme rate depicts a saturation curve arriving to a steady state situation. At this point, the reaction rate achieves its maximum (V_{max}). This typical behavior is clearly observable in Figures 7A and 8B. From here, Michaelis and Menten deduced their equation (Equation (2)), where K_M is the Michaelis–Menten's constant, defined as the concentration of substrate needed to reach half of the maximum rate [71]. It is important to take into account that the K_M and V_{max} values will be unique for each pair of enzyme and substrate.

To determine experimentally these parameters, the Lineweaver-Burk linearization is normally used (see its tailored version in Equation (3)) [72]. However, to assure that the Michaelis–Menten kinetics are valid for the studied system, first, the Hills coefficient (h, see Equation (4)) is commonly calculated. In this way, when h results are being close to 1, a Michaelis–Menten model can be assumed.

In this work, the h estimated value from the catechol calibration curve was 0.99 ± 0.09, demonstrating that the Lac-RGO biosensor followed the already explained kinetics. The rate parameters K_M and V_{max}, obtained from Equation (4), were 2.62 ± 0.50 μmol·L^{-1} and $1.90 \times 10^{-4} \pm 0.13 \times 10^{-4}$ A, respectively.

$$V_0 = V_{max} \frac{[S]}{[S] + K_M} \quad (2)$$

$$\frac{1}{V} = \frac{K_M}{V_{max}} \cdot \frac{1}{[S]} + \frac{1}{V_{max}} \quad (3)$$

$$V = \frac{V_{max} \cdot ([S]/K_M)^h}{1 + ([S]/K_M)^h} \quad (4)$$

As commented in the introduction section, there are common household products that have been used for a long period of time, that are now under scrutiny due to their possible effects on the environment and health. Examples are the emerging pollutants found in cosmetics, processed food, or pharmaceutical compounds. The inhibition study of the Lac-RGO biosensor was carried out using benzoic acid and EDTA, two examples of CECs. Benzoic acid is a colorless crystalline compound that is widely used in pharmaceutical products either as an active product ingredient (for its antifungal properties) or as an excipient (as a lubricant in tablets). Both in the food and cosmetics industry, it is used as a preservative [73,74]. On the other hand, EDTA is a colorless and soluble product used in various and distinct applications; for example, in the paper industry as a metal chelate agent or in the food and cleaning industries as a preservative [75,76]. Regarding the legislated limits for the herein target compounds, there is not an individual value. Nevertheless, the WHO made preliminary studies that recommend as maximum values 5 mg·kg^{-1} for the benzoic acid and 600 μg·L^{-1} for the EDTA (values for drinking-water) [77,78].

Any substance that in a particular context can decrease the kinetics of an enzyme will be considered as an enzymatic inhibitor. As mentioned before, the Michaelis–Menten constants (Equation (2)) are unique for a specific enzyme-substrate system, so the presence of inhibitors will lead to renaming the K_M and V_{max} to K'_M and V'_{max}.

There are three modelled scenarios [23]. The first situation is competitive inhibition, where the inhibitor and the substrate compete for the same active site; thus, $K_M < K'_M$ and $V_{max} = V'_{max}$. The second situation is named non-competitive inhibition; in this case, the inhibitor is not a direct competitor but is bound in an allosteric site that deactivates the enzyme. The changes in the constants are noted as $K_M = K'_M$ and $V_{max} > V'_{max}$. Finally, the last scenario is the uncompetitive inhibition, where the inhibitor is bound, producing a

bigger affinity between the substrate and the enzyme, leading to fewer active sites in the system, in that case $K_M > K'_M$ and $V_{max} = V'_{max}$ [72].

Experimentally, the changes can be elucidated comparing the Lineweaver-Burk linearization for different concentrations of inhibitor. In this sense, Figures 10 and 11 show the inhibition effects of different concentrations of benzoic acid and EDTA in a Lac-RGO electrode. Both figures show a typical behavior of the first scenario: a competitive inhibition. Figures 10A and 11A depict the calibration curves of catechol using a Lac-RGO electrode in the presence of different concentrations of benzoic acid and EDTA, respectively. Zone 1 highlighted the steady V_{max} and zone 2 in the increase in K_M with the inhibitor concentration. In Table 4 there are complementary data used to corroborate the conclusions from Figures 10A and 11A; concretely, it includes the slopes from the K'_M and V'_{max} (calculated from the linear regressions on Figures 10A and 11A), when inhibitor concentrations are varied. In this table, positive slopes confirm the Michaelis constant increase (significant variation of K'_M with slope values above uncertainties), and the constant trend for the maximum velocity (the uncertainties include the zero-slope value). This state is supported by Figure 10B,C and Figure 11B,C, where the calculated K_M' and V_{max}' values, and their trends, are plotted.

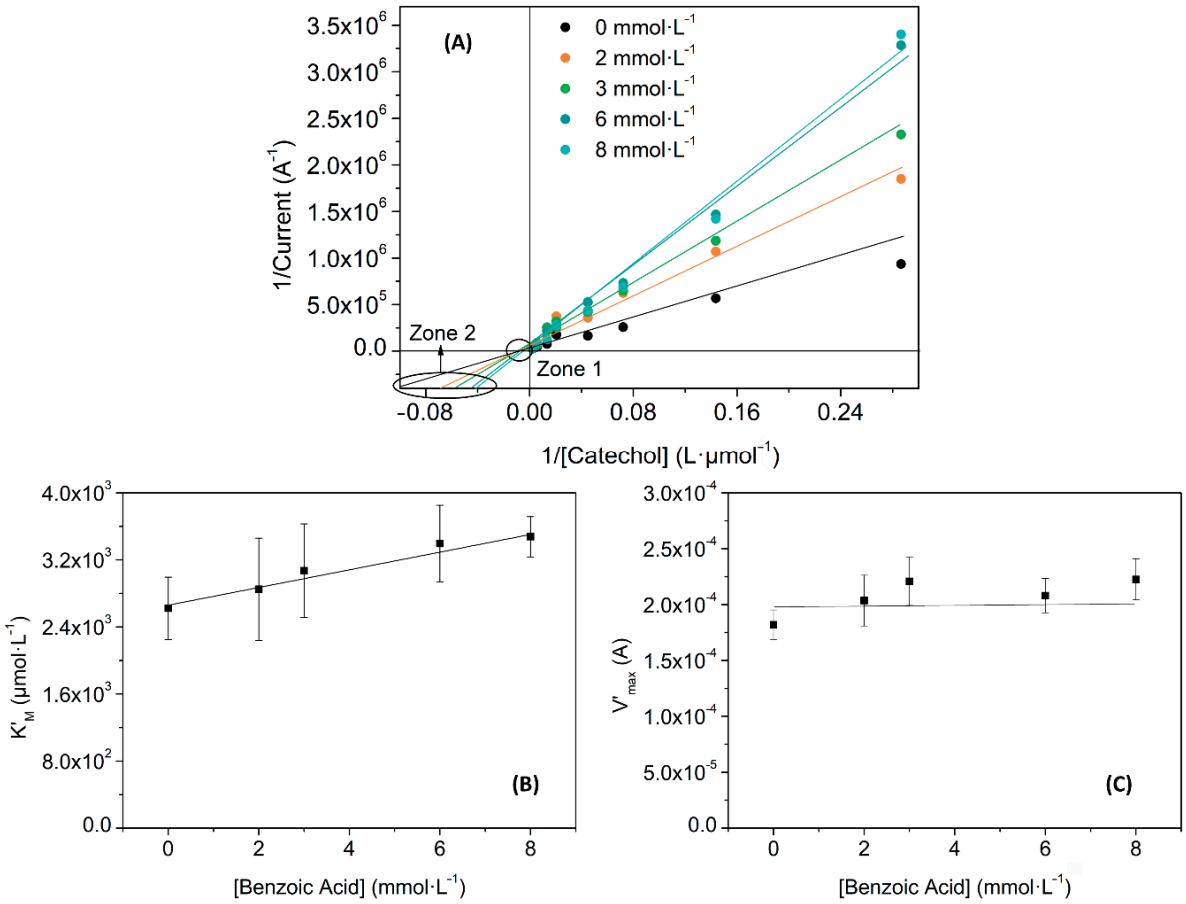

Figure 10. Biosensors kinetic study, (**A**) Lineweaver–Burk linearization for four benzoic acid concentrations; (**B**) representation of the obtained K'_M values for each inhibitor concentration; and (**C**) V'_{max} obtained values for each inhibitor concentration.

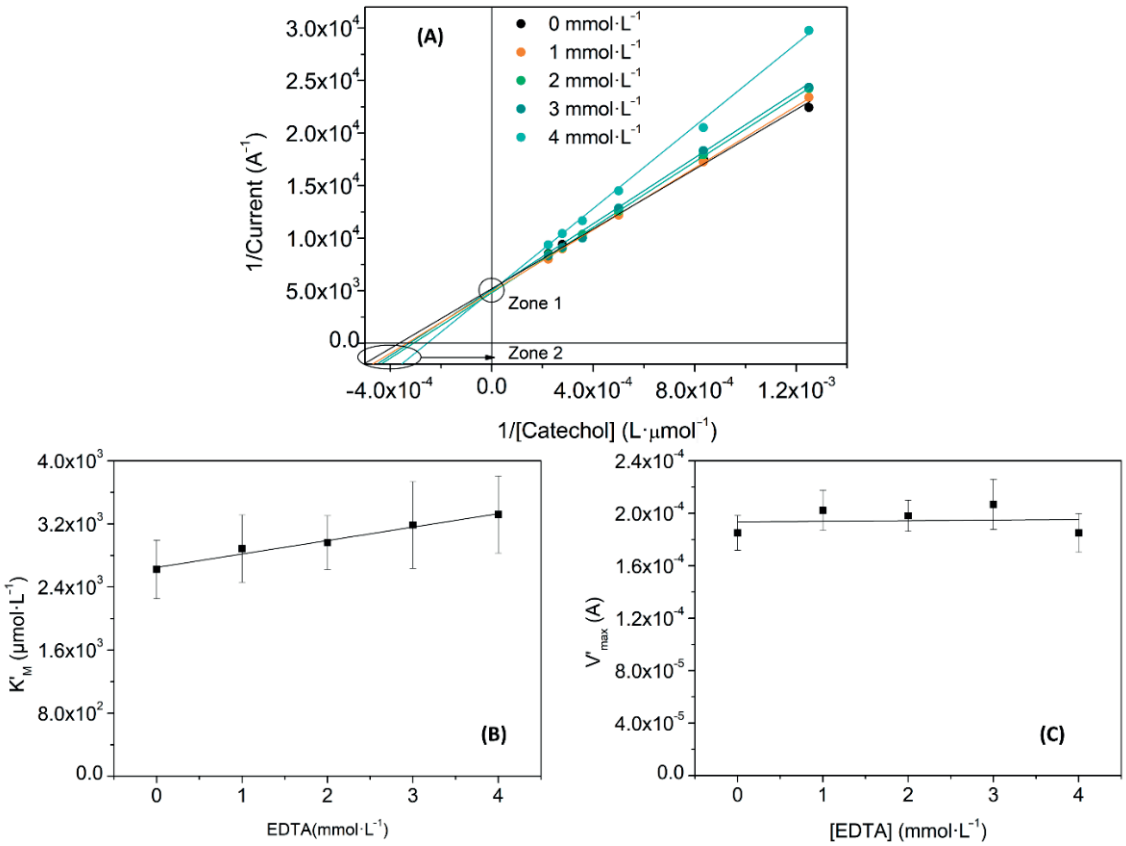

Figure 11. Biosensors kinetic study, (**A**) Lineweaver–Burk linearization for four EDTA concentrations; (**B**) representation of the obtained K'_M values for each inhibitor concentration; and (**C**) V'_{max} obtained values for each inhibitor concentration.

Table 4. Variation of kinetic parameters vs. inhibitor concentration. Values of the linear trend K'_M and V'_{max} vs. Inhibitor concentration when kinetics of the laccase enzyme is evaluated. Inhibition values from calibration curves of catechol in different concentrations of acid benzoic and EDTA inhibitors.

Substance	Slope of K'_M ($\mu mol \cdot L^{-1}$) vs. [I]	Slope of V'_{max} ($A \cdot L \cdot mmol^{-1}$) vs. [I]	K_I ($mmol \cdot L^{-1}$)
Benzoic acid	0.11 ± 0.04	$3 \cdot 10^{-6} \pm 6 \cdot 10^{-6}$	25 ± 19
EDTA	0.2 ± 0.1	$0 \pm 1 \cdot 10^{-5}$	17 ± 9

Moreover, the inhibition constant (K_I) for each inhibitor. Table 4 shows the higher affinity of benzoic acid (25 $mmol \cdot L^{-1}$) to Laccase than EDTA (17 $mmol \cdot L^{-1}$). To calculate K_I values, expression (5), corresponding to competitive inhibition, was used.

$$K'_M = K_M \cdot \left(1 + \frac{[I]}{K_I}\right) \quad (5)$$

On a further visualization of the inhibition effect, Figure 12B,D shows the percentage of the inhibition achieved for each pollutant in 800 $\mu mol \cdot L^{-1}$ of catechol. A bigger effect for benzoic acid, as expected from the previous comments, was fulfilled. In detail, a maximum $\approx$ 60% of inhibition was reached for the benzoic acid system in front of the $\approx$25% for EDTA. Voltammograms presented in Figure 12A,C shows the biosensor response in front of the catechol in the presence or absence of the inhibitor. In each case, the shape of the RGO voltammogram profile is recovered (Figure 7B) when benzoic acid and EDTA are in solution, indicating that laccase has lost its activity when they are present. To sum

up, the expected inhibition effect was verified, permitting the quantification of EDTA and benzoic acid in controlled samples.

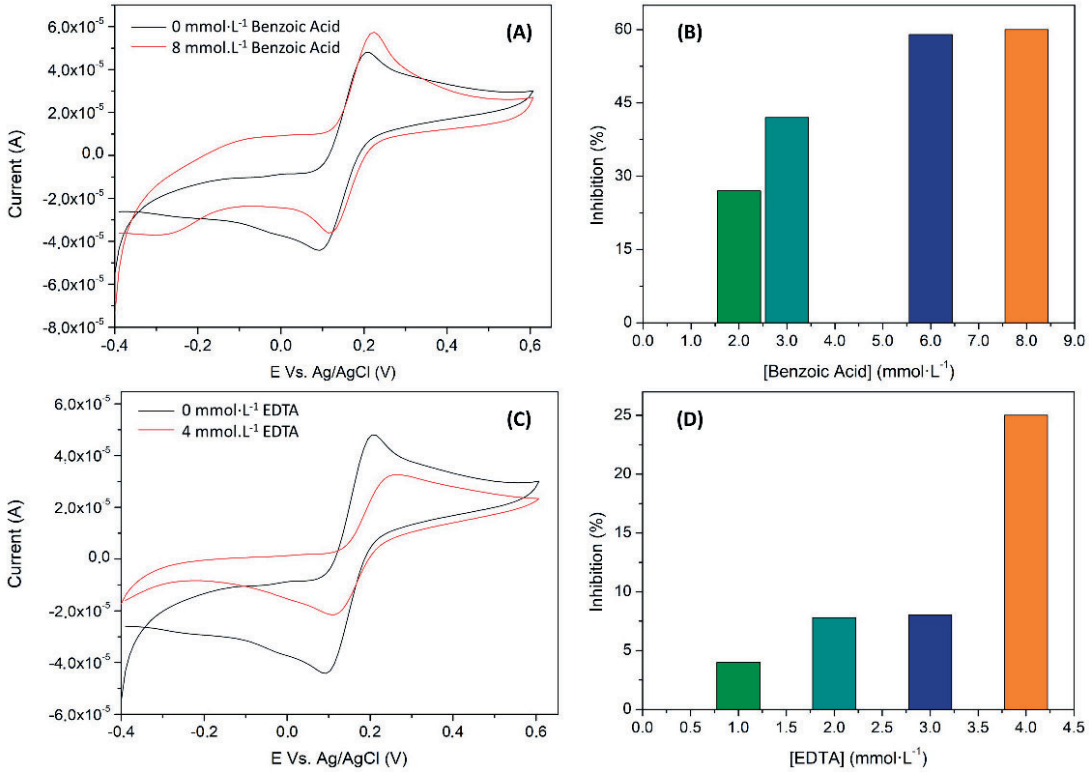

Figure 12. Biosensor inhibition study in a constant concentration of catechol (800 μmol·L^{-1}) when different concentrations of (**A**,**B**) benzoic acid and (**C**,**D**) EDTA inhibitors are present in the sample. (**A**,**C**) depicts the CV obtained for the maximum inhibition percentage and (**B**,**D**) the inhibition percentage profile when varying the inhibitor concentration. Percentage of inhibition calculated according to the relative maximum rate velocities, 100·(1 − V′/V).

4. Conclusions

The reported work has shown the capabilities of graphene as a nanomaterial to improve and facilitate the development of electrochemical biosensors, specifically those employing redox enzymes. The advantages observed can be attributed to two factors: the first one is the amelioration of the electrochemical transduction properties, thanks to inherent electrical characteristics of graphene. The second, the conjunction with the chemical properties of the material, as it serves as a linkage platform for immobilization of biomolecules such as enzymes.

All this makes this combination an unbeatable choice for electrochemical biosensing. The case specified in here, the biosensing of catechol, has demonstrated an improvement of sensitivity of ca. 30%, which in turn improves the direct determination of phenolic compounds or opens the door to consider inhibition. In this inhibitory biosensing application, two different chemicals, EDTA and benzoate, have been verified as inhibitors of the enzyme reaction, which may constitute the basis for a future analytical device or system to monitor CECs in water.

Author Contributions: Conceptualization, M.d.V.; methodology, M.d.V.; Investigation, M.B.-S.-E. and N.F.M.; writing—original draft preparation, M.B.-S.-E.; writing—review and editing, M.d.V.; supervision, M.d.V.; funding acquisition, M.d.V. All authors have read and agreed to the published version of the manuscript.

Funding: This research was funded by the Spanish Government (Ministerio de Economía y Competitividad) grant number PID2019-107102RB-C21. M.B.S. was funded by Secretaria d'Universitats i Recerca del Departament d'Empreses i Coneixement de la Generalitat de Catalunya and by European Social Fund, European Union through a FI fellowship. M.d.V. thanks the support from program ICREA Academia.

Institutional Review Board Statement: Not applicable.

Informed Consent Statement: Not applicable.

Data Availability Statement: Not applicable.

Acknowledgments: The authors thanks to Anna Herrera Chacón from the Universitat Autònoma de Barcelona for her collaboration with TEM images and to M.J Esplandiu from ICN2, for the AFM study.

Conflicts of Interest: The authors declare no conflict of interest.

References

1. Hulanicki, A.; Glab, S.; Ingman, F. Chemical sensors: Definitions and classification. *Pure Appl. Chem.* **1991**, *63*, 1247–1250. [CrossRef]
2. Novoselov, K.S.; Geim, A.K.; Morozov, S.V.; Jiang, D.; Zhang, Y.; Dubonos, S.V.; Grigorieva, I.V.; Firsov, A.A. Electric field effect in atomically thin carbon films. *Science* **2004**, *306*, 666–669. [CrossRef]
3. Tung, T.T.; Nine, M.J.; Krebsz, M.; Pasinszki, T.; Coghlan, C.J.; Tran, D.N.H.; Losic, D. Recent advances in sensing applications of graphene assemblies and their composites. *Adv. Funct. Mater.* **2017**, *27*, 1702891. [CrossRef]
4. Pasinszki, T.; Krebsz, M.; Tung, T.T.; Losic, D. Carbon nanomaterial based biosensors for non-invasive detection of cancer and disease biomarkers for clinical diagnosis. *Sensors* **2017**, *17*, 1919. [CrossRef]
5. Medina-Plaza, C.; García-Hernández, C.; de Saja, J.A.; Fernández-Escudero, J.A.; Barajas, E.; Medrano, G.; García-Cabezón, C.; Martin-Pedrosa, F.; Rodriguez-Mendez, M.L. The advantages of disposable screen-printed biosensors in a bioelectronic tongue for the analysis of grapes. *LWT Food Sci. Technol.* **2015**, *62*, 940–947. [CrossRef]
6. Zhou, M.; Zhai, Y.; Dong, S. Electrochemical sensing and biosensing platform based on chemically reduced graphene oxide. *Anal. Chem.* **2009**, *81*, 5603–5613. [CrossRef] [PubMed]
7. Suhito, I.R.; Koo, K.M.; Kim, T.H. Recent advances in electrochemical sensors for the detection of biomolecules and whole cells. *Biomedicines* **2021**, *9*, 15. [CrossRef]
8. Ocaña, C.; Lukic, S.; del Valle, M. Aptamer-antibody sandwich assay for cytochrome c employing an MWCNT platform and electrochemical impedance. *Microchim. Acta* **2015**, *182*, 2045–2053. [CrossRef]
9. Serrano, N.; Prieto-Simón, B.; Cetó, X.; Del Valle, M. Array of peptide-modified electrodes for the simultaneous determination of Pb(II), Cd(II) and Zn(II). *Talanta* **2014**, *125*, 159–166. [CrossRef]
10. Bélanger, D.; Pinson, J. Electrografting: A powerful method for surface modification. *Chem. Soc. Rev.* **2011**, *40*, 3995–4048. [CrossRef]
11. Sun, C.-L.; Su, C.-H.; Wu, J.-J. Synthesis of short graphene oxide nanoribbons for improved biomarker detection of Parkinson's disease. *Biosens. Bioelectron.* **2015**, *67*, 327–333. [CrossRef]
12. Martín, A.; Batalla, P.; Hernández-Ferrer, J.; Martínez, M.T.; Escarpa, A. Graphene oxide nanoribbon-based sensors for the simultaneous bio-electrochemical enantiomeric resolution and analysis of amino acid biomarkers. *Biosens. Bioelectron.* **2015**, *68*, 163–167. [CrossRef]
13. Barua, S.; Geng, X.; Chen, B. Graphene-based nanomaterials for healthcare applications. In *Photonanotechnology for Therapeutics and Imaging*; Choi, S.-K., Ed.; Micro and Nano Technologies; Elsevier: Amsterdam, The Netherlands, 2020; pp. 45–81. ISBN 978-0-12-817840-9.
14. Pottathara, Y.B.; Grohens, Y.; Kokol, V.; Kalarikkal, N.; Thomas, S. Synthesis and processing of emerging two-dimensional nanomaterials. In *Nanomaterials Synthesis*; Pottathara, B.Y., Thomas, S., Kalarikkal, N., Grohens, Y., Kokol, V., Eds.; Micro and Nano Technologies; Elsevier: Amsterdam, The Netherlands, 2019; pp. 1–25. ISBN 978-0-12-815751-0.
15. Smith, A.T.; La Chance, A.M.; Zeng, S.; Liu, B.; Sun, L. Synthesis, properties, and applications of graphene oxide/reduced graphene oxide and their nanocomposites. *Nano Mater. Sci.* **2019**, *1*, 31–47. [CrossRef]
16. Hummers, W.S.; Offeman, R.E. Preparation of graphitic oxide. *J. Am. Chem. Soc.* **1958**, *80*, 1339. [CrossRef]
17. Marcano, D.C.; Kosynkin, D.V.; Berlin, J.M.; Sinitskii, A.; Sun, Z.; Slesarev, A.; Alemany, L.B.; Lu, W.; Tour, J.M. Improved synthesis of graphene oxide. *ACS Nano* **2010**, *4*, 4806–4814. [CrossRef] [PubMed]
18. Aceta, Y.; del Valle, M. Graphene electrode platform for impedimetric aptasensing. *Electrochim. Acta* **2017**, *229*, 458–466. [CrossRef]
19. Xu, J.; Wang, Y.; Hu, S. Nanocomposites of graphene and graphene oxides: Synthesis, molecular functionalization and application in electrochemical sensors and biosensors. A review. *Microchim. Acta* **2017**, *184*, 1–44. [CrossRef]
20. Toh, S.Y.; Loh, K.S.; Kartom Kamarudin, S.; Ramli, W.; Daud, W. Graphene production via electrochemical reduction of graphene oxide: Synthesis and characterisation. *Chem. Eng. J.* **2014**, *251*, 422–434. [CrossRef]

21. Dreyer, D.R.; Park, S.; Bielawski, C.W.; Ruoff, R.S. The chemistry of graphene oxide. *Chem. Soc. Rev.* **2010**, *39*, 228–240. [CrossRef]
22. Pumera, M. Graphene-based nanomaterials and their electrochemistry. *Chem. Soc. Rev.* **2010**, *39*, 4146–4157. [CrossRef]
23. Jian, X.; Liu, X.; Yang, H.M.; Guo, M.M.; Song, X.L.; Dai, H.Y.; Liang, Z.H. Graphene quantum dots modified glassy carbon electrode via electrostatic self-assembly strategy and its application. *Electrochim. Acta* **2016**, *190*, 455–462. [CrossRef]
24. Bonet-San-Emeterio, M.; Algarra, M.; Petković, M.; del Valle, M. Modification of electrodes with N-and S-doped carbon dots. Evaluation of the electrochemical response. *Talanta* **2020**, *212*, 120806. [CrossRef]
25. Algarra, M.; González-Calabuig, A.; Radotić, K.; Mutavdzic, D.; Ania, C.O.; Lázaro-Martínez, J.M.; Jiménez-Jiménez, J.; Rodríguez-Castellón, E.; del Valle, M. Enhanced electrochemical response of carbon quantum dot modified electrodes. *Talanta* **2018**, *178*, 679–685. [CrossRef] [PubMed]
26. Shereema, R.M.; Rao, T.P.; Sameer Kumar, V.B.; Sruthi, T.V.; Vishnu, R.; Prabhu, G.R.D.; Sharath Shankar, S. Individual and simultaneous electrochemical determination of metanil yellow and curcumin on carbon quantum dots based glassy carbon electrode. *Mater. Sci. Eng. C* **2018**, *93*, 21–27. [CrossRef] [PubMed]
27. Merkoçi, A.; Pumera, M.; Llopis, X.; Pérez, B.; Del Valle, M.; Alegret, S. New materials for electrochemical sensing VI: Carbon nanotubes. *TrAC Trends Anal. Chem.* **2005**, *24*, 826–838. [CrossRef]
28. Cipri, A.; Del Valle, M. Pd nanoparticles/multiwalled carbon nanotubes electrode system for voltammetric sensing of tyrosine. *J. Nanosci. Nanotechnol.* **2014**, *14*, 6692–6698. [CrossRef]
29. Moore, R.R.; Banks, C.E.; Compton, R.G. Basal plane pyrolytic graphite modified electrodes: Comparison of carbon nanotubes and graphite powder as electrocatalysts. *Anal. Chem.* **2004**, *76*, 2677–2682. [CrossRef]
30. Fusco, G.; Bollella, P.; Mazzei, F.; Favero, G.; Antiochia, R.; Tortolini, C. Catalase-based modified graphite electrode for hydrogen peroxide detection in different beverages. *J. Anal. Methods Chem.* **2016**, *2016*, 1–12. [CrossRef] [PubMed]
31. Montañez, J.L.; Ramos, E.G.; Alegret, S.; Delgado, R.J. Biosensor de glucosa basado en un biocompósito disperso de grafito-epoxi-platino-glucosa oxidasa. *Inf. Technol.* **2011**, *22*, 29–40. [CrossRef]
32. Zacco, E.; Pividori, M.I.; Alegret, S.; Galve, R.; Marco, M.P. Electrochemical magnetoimmunosensing strategy for the detection of pesticides residues. *Anal. Chem.* **2006**, *78*, 1780–1788. [CrossRef]
33. Tuomela, M.; Hatakka, A. Oxidative fungal enzymes for bioremediation. In *Comprehensive Biotechnology*; Moo-Young, M., Ed.; Pergamon: Oxford, UK, 2019; pp. 224–239. ISBN 978-0-444-64047-5.
34. Rodríguez-Couto, S. Solid-state fermentation for laccases production and their applications. In *Current Developments in Biotechnology and Bioengineering*; Pandey, A., Larroche, C., Soccol, C.R., Eds.; Elsevier: Amsterdam, The Netherlands, 2018; pp. 211–234. ISBN 978-0-444-63990-5.
35. Zandaryaa, S. Chemical contaminants: Those invisible additives in our drink. *A World Sci.* **2011**, *9*, 18–21.
36. Frye, C.; Bo, E.; Calamandrei, G.; Calzà, L.; Dessì-Fulgheri, F.; Fernández, M.; Fusani, L.; Kah, O.; Kajta, M.; Le Page, Y.; et al. Endocrine disrupters: A review of some sources, effects, and mechanisms of actions on behaviour and neuroendocrine systems. *J. Neuroendocrinol.* **2012**, *24*, 144–159. [CrossRef]
37. Monneret, C. What is an endocrine disruptor? *C. R. Biol.* **2017**, *340*, 403–405. [CrossRef] [PubMed]
38. Diamanti-Kandarakis, E.; Bourguignon, J.P.; Giudice, L.C.; Hauser, R.; Prins, G.S.; Soto, A.M.; Zoeller, R.T.; Gore, A.C. Endocrine-disrupting chemicals: An endocrine society scientific statement. *Endocr. Rev.* **2009**, *30*, 293–342. [CrossRef] [PubMed]
39. Céspedes, F.; Martínez-Fàbregas, E.; Alegret, S. New materials for electrochemical sensing I. Rigid conducting composites. *TrAC Trends Anal. Chem.* **1996**, *15*, 296–304. [CrossRef]
40. Alegret, S.; Alonso, J.; Bartrolí, J.; Céspedes, F.; Martínez-Fàbregas, E.; del Valle, M. Amperometric biosensors based on bulk-modified epoxy graphite biocomposites. *Sens. Mater.* **1996**, *8*, 147–153.
41. Kalinke, C.; de Oliveira, P.R.; Bonet-San-Emeterio, M.; González-Calabuig, A.; del Valle, M.; Salvio Mangrich, A.; Humberto Marcolino Junior, L.; Bergamini, M.F. Voltammetric electronic tongue based on carbon paste electrodes modified with biochar for phenolic compounds stripping detection. *Electroanalysis* **2019**, *31*, 2238–2245. [CrossRef]
42. Eng, A.Y.S.; Ambrosi, A.; Chua, C.K.; Šaněk, F.; Sofer, Z.; Pumera, M. Unusual inherent electrochemistry of graphene oxides prepared using permanganate oxidants. *Chem. A Eur. J.* **2013**, *19*, 12673–12683. [CrossRef]
43. Bonet-San-Emeterio, M.; González-Calabuig, A.; del Valle, M. Artificial neural networks for the resolution of dopamine and serotonin complex mixtures using a graphene-modified carbon electrode. *Electroanalysis* **2019**, *31*, 1–9. [CrossRef]
44. Ortiz-Aguayo, D.; del Valle, M. Label-free aptasensor for lysozyme detection using electrochemical impedance spectroscopy. *Sensors* **2018**, *18*, 354. [CrossRef]
45. Ocaña, C.; Hayat, A.; Mishra, R.; Vasilescu, A.; Del Valle, M.; Marty, J.-L. A novel electrochemical aptamer-antibody sandwich assay for lysozyme detection. *Analyst* **2015**, *140*, 4153. [CrossRef]
46. Cattaruzza, F.; Cricenti, A.; Flamini, A.; Girasole, M.; Longo, G.; Prosperi, T.; Andreano, G.; Cellai, L.; Chirivino, E. Controlled loading of oligodeoxyribonucleotide monolayers onto unoxidized crystalline silicon; fluorescence-based determination of the surface coverage and of the hybridization efficiency; parallel imaging of the process by atomic force microscopy. *Nucleic Acids Res.* **2006**, *34*, 2–13. [CrossRef]
47. Tortolini, C.; Rea, S.; Carota, E.; Cannistraro, S.; Mazzei, F. Influence of the immobilization procedures on the electroanalytical performances of trametes versicolor laccase based bioelectrode. *Microchem. J.* **2011**, *100*, 8–13. [CrossRef]

48. Khoo, W.Y.H.; Pumera, M.; Bonanni, A. Graphene platforms for the detection of caffeine in real samples. *Anal. Chim. Acta* **2013**, *804*, 92–97. [CrossRef]
49. Hui, K.H.; Ambrosi, A.; Pumera, M.; Bonanni, A. Improving the analytical performance of graphene oxide towards the assessment of polyphenols. *Chem. Eur. J.* **2016**, *22*, 3830–3834. [CrossRef]
50. Shang, N.G.; Papakonstantinou, P.; McMullan, M.; Chu, M.; Stamboulis, A.; Potenza, A.; Dhesi, S.S.; Marchetto, H. Catalyst-free efficient growth, orientation and biosensing properties of multilayer graphene nanoflake films with sharp edge planes. *Adv. Funct. Mater.* **2008**, *18*, 3506–3514. [CrossRef]
51. Haditale, M.; Dariani, R.S.; Ghasemian Lemraski, E. Electrical behavior of graphene under temperature effect and survey of I–T curve. *J. Theor. Appl. Phys.* **2019**, *13*, 351–356. [CrossRef]
52. Ambrosi, A.; Bonanni, A.; Sofer, Z.; Cross, J.S.; Pumera, M. Electrochemistry at chemically modified graphenes. *Chem. A Eur. J. A Eur. J.* **2011**, *17*, 10763–10770. [CrossRef] [PubMed]
53. Anonymous. *Organic Electrochemistry: Revised and Expanded*, 5th ed.; Hammerich, O., Speiser, B., Eds.; CRC Press: Boca Raton, FL, USA, 2015.
54. Palanisamy, S.; Ramaraj, S.K.; Chen, S.M.; Yang, T.C.K.; Pan, Y.F.; Chen, T.W.; Velusamy, V.; Selvam, S. A novel laccase biosensor based on laccase immobilized graphene-cellulose microfiber composite modified screen-printed carbon electrode for sensitive determination of catechol. *Sci. Rep.* **2017**, *7*, 41214. [CrossRef] [PubMed]
55. Nazari, M.; Kashanian, S.; Rafipour, R. Laccase immobilization on the electrode surface to design a biosensor for the detection of phenolic compound such as catechol. *Spectrochim. Acta Part A Mol. Biomol. Spectrosc.* **2015**, *145*, 130–138. [CrossRef] [PubMed]
56. Fernández-Sánchez, C.; Tzanov, T.; Gübitz, G.M.; Cavaco-Paulo, A. Voltammetric monitoring of laccase-catalysed mediated reactions. *Bioelectrochemistry* **2002**, *58*, 149–156. [CrossRef]
57. Harris, D.C. *Quantitative Chemical Analysis*, 7th ed.; Freeman and Co.: New York, NY, USA, 1948.
58. McNaught, A.D.; Wilkinson, A. *The IUPAC Compendium of Chemical Terminology*, 2nd ed.; Blackwell Scientific Publications: Oxford, UK, 1997; ISBN 0-9678550-9-8.
59. Borman, P.; Elder, D. Q2(R1) Validation of analytical procedures. In *ICH Quality Guidelines*; John Wiley & Sons: Hoboken, NJ, USA, 2017; pp. 127–166. ISBN 9781118971147.
60. Tembe, S.; Inamdar, S.; Haram, S.; Karve, M.; D'Souza, S.F. Electrochemical biosensor for catechol using agarose–guar gum entrapped tyrosinase. *J. Biotechnol.* **2007**, *128*, 80–85. [CrossRef] [PubMed]
61. Zhou, X.H.; Liu, L.H.; Bai, X.; Shi, H.C. A reduced graphene oxide based biosensor for high-sensitive detection of phenols in water samples. *Sens. Actuators B Chem.* **2013**, *181*, 661–667. [CrossRef]
62. Medina-Plaza, C.; de Saja, J.A.; Rodriguez-Mendez, M.L. Bioelectronic tongue based on lipidic nanostructured layers containing phenol oxidases and lutetium bisphthalocyanine for the analysis of grapes. *Biosens. Bioelectron.* **2014**, *57*, 276–283. [CrossRef]
63. Nazari, M.; Kashanian, S.; Moradipour, P.; Maleki, N. A novel fabrication of sensor using ZnO-Al_2O_3 ceramic nanofibers to simultaneously detect catechol and hydroquinone. *J. Electroanal. Chem.* **2018**, *812*, 122–131. [CrossRef]
64. Bin, Z.; Yanhong, C.; Jiaojiao, X. Biomimetic oxidase sensor based on functionalized surface of carbon nanotubes and iron prophyrins for catechol detection. *Bioprocess Biosyst. Eng.* **2018**, *42*, 279–290. [CrossRef]
65. Guo, M.; Wang, H.; Huang, D.; Han, Z.; Li, Q.; Wang, X.; Chen, J. Amperometric catechol biosensor based on laccase immobilized on nitrogen-doped ordered mesoporous carbon (N-OMC)/PVA matrix. *Sci. Technol. Adv. Mater.* **2014**, *15*, 1–9. [CrossRef]
66. Zhao, Q.-L.; Zhang, Z.-L.; Huang, B.-H.; Peng, J.; Zhang, M.; Pang, D.-W. Facile preparation of low cytotoxicity fluorescent carbon nanocrystals by electrooxidation of graphite. *Chem. Commun.* **2008**, 5116. [CrossRef]
67. Albayati, S.A.R.; Kashanian, S.; Nazari, M.; Rezaei, S. Novel fabrication of a laccase biosensor to detect phenolic compounds using a carboxylated multiwalled carbon nanotube on the electropolymerized support. *Bull. Mater. Sci.* **2019**, *42*, 1–8. [CrossRef]
68. Hu, F.; Chen, S.; Wang, C.; Yuan, R.; Yuan, D.; Wang, C. Study on the application of reduced graphene oxide and multiwall carbon nanotubes hybrid materials for simultaneous determination of catechol, hydroquinone, p-cresol and nitrite. *Anal. Chim. Acta* **2012**, *724*, 40–46. [CrossRef] [PubMed]
69. Umasankar, Y.; Periasamy, A.P.; Chen, S.M. Electrocatalysis and simultaneous determination of catechol and quinol by poly(malachite green) coated multiwalled carbon nanotube film. *Anal. Biochem.* **2011**, *411*, 71–79. [CrossRef] [PubMed]
70. Zhang, H.; Zhao, J.; Liu, H.; Liu, R.; Wang, H.; Liu, J. Electrochemical determination of diphenols and their mixtures at the multiwall carbon nanotubes/poly (3-methylthiophene) modified glassy carbon electrode. *Microchim. Acta* **2010**, *169*, 277–282. [CrossRef]
71. Berg, J.M.; Tymoczko, J.L.; Stryer, L. The Michaelis-Menten model accounts for the kinetic properties of many enzymes. In *Biochemistry*; W H Freeman: New York, NY, USA, 2002.
72. Roskoski, R. *Michaelis-Menten Kinetics*; Elsevier: Amsterdam, The Netherlands, 2015.
73. Hazan, R.; Levine, A.; Abeliovich, H. Benzoic acid, a weak organic acid food preservative, exerts specific effects on intracellular membrane trafficking pathways in saccharomyces cerevisiae. *Appl. Environ. Microbiol.* **2004**, *70*, 4449–4457. [CrossRef] [PubMed]
74. Nair, B. Final report on the safety assessment of benzyl alcohol, benzoic acid, and sodium benzoate. *Int. J. Toxicol.* **2001**, *20*, 23–50. [CrossRef] [PubMed]
75. Wolf, K.; Gilbert, P.A. EDTA—Ethylenediaminetetraacetic acid. In *Detergents. Anthropogenic Compounds*; de Oude, N.T., Ed.; Springer: Berlin/Heidelberg, Germany, 1992; Volume 3, pp. 243–259.
76. Oviedo, C.; Rodríguez, J. EDTA: The chelating agent under environmental scrutiny. *Quim. Nova* **2003**, *26*, 901–905. [CrossRef]

77. World Health Organization & International Programme on Chemical Safety. *Benzoic Acid and Sodium Benzoate*; Concise International Chemical Assessment Document, 26; World Health Organization: Geneva, Switzerland, 2000.
78. World Health Organization & International Programme on Chemical Safety. Health criteria and other supporting information. In *Guidelines for Drinking-Water Quality*; World Health Organization: Geneva, Switzerland, 1996; ISBN 9241544805.

Article 3

Bioelectronic tongue based on alcohol oxidases modified graphene electrodes for the detection of Brettanomyces defect in wine

M. Bonet-San-Emeterio, A. González-Calabuig, M. del Valle

Bioelectronic tongue based on phenol oxidases modified graphene electrodes for the detection of Brettanomyces defect in wine

Marta Bonet-San-Emeterio, Andreu González-Calabuig and Manel del Valle *

Sensors and Biosensors Group, Department of Chemistry, Universitat Autònoma de Barcelona, Edifici CN, 08193 Bellaterra, Barcelona, Spain.

*e-mail: manel.delvalle@uab.es

Highlights

1. *Microscopic techniques have been used for the (bio)sensors characterization.*
2. Tyrosinase and laccase biosensors were developed onto graphene platforms.
3. Obtained (bio)sensors were arranged in an electronic tongue approach.
4. Application of machine learning, DWT combined with ANN or PLS, to obtain quantification response models.
5. Successful resolution of 4-ethylphenol, 4-ethylguaiacol, and 4-ethylcatechol in wine matrix.

Keywords: Bioelectronic tongue, phenol oxidases, graphene, artificial neural networks, partial least squares

Graphical abstract

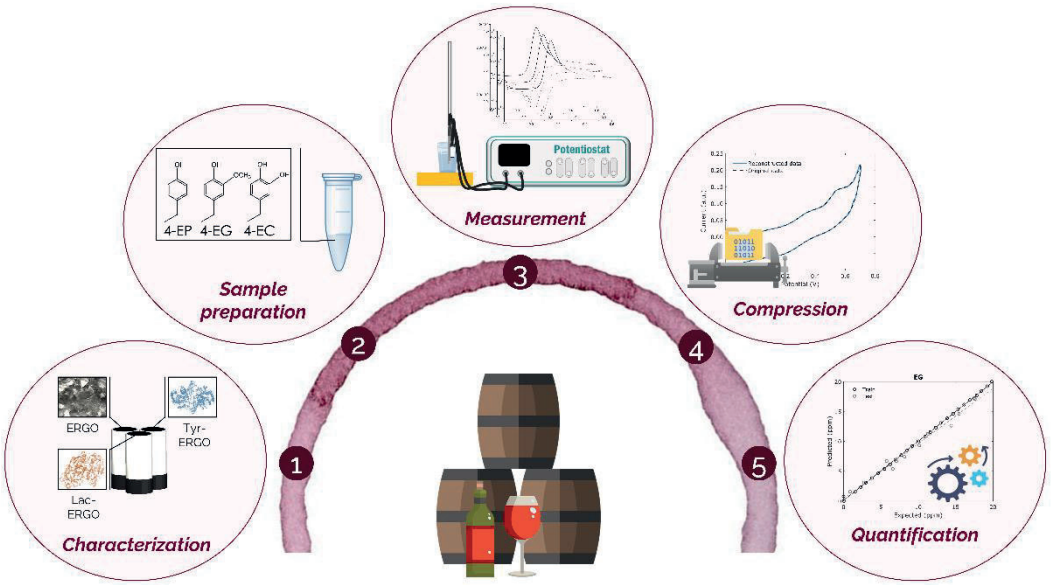

Abstract: This work presents an enzymatic bioelectronic tongue (bioET) for the quantification analysis of volatile phenols related to *Brettanomyces* spoilage in red wines. *Brettanomyces* yeast defect causes presence of 4-ethylphenols, which taints the organoleptic properties of wines. To avoid this defect, new and better detection strategies are sought. This article proposes the use of a three (bio)sensors array in an ET arrangement for the detection of 4-ethylphenol, 4-ethylguaiacol, and 4-ethylcatechol. With the proposed approach it is clearly seen the synergy between nanomaterials and the biorecognition elements, which together with advanced chemometric tools allows the obtention of a successful quantification response model. The obtained prediction errors (normalized root mean square error) for developed model, carried out in real samples, are 0.005 and 0.060 for the train and test subset, respectively; correlation coefficients of the predicted *vs.* predicted 4-ethylphenol concentrations are better than 0.98 when a discrete wavelet transform pretreatment is coupled with an artificial neural network response model.

1. Introduction

Nowadays, the food industry together with the pharmaceutical and security factories, are three of the most demanding fields regarding the quantity and the quality of the chemical analysis needed. This fact is probably given by extensive linked regulations; made to assure the consumer's safety [1]. In this direction, the present work is focused on viniculture products. Wine is a beverage that depends strictly on the analytical field because it needs further tests and controls during the fruit ripening, being a key point the sugar content, and after when the wine is produced and stored. However, despite the interests and producer’s needs, wine quality control is still highly dependent on wine tasters. The main reasons are the complexity of samples and the difficulty to reproduce human perceptions using classical analytical techniques [2]. Some important parameters to control when doing wine elaboration is the presence of spoilages, for example, the content of volatile phenolic compounds in red wines. These products can be related to organoleptic and sensorial properties. Among them there are the 4-ethylphenols which have a significant influence on wine aroma due to their characteristic flavor and low detection threshold (0.5 ppm for human taste), concretely their taints are normally identified as tastes that may remind to horse sweat, wet animals, and urine. The presents of these non-desired phenols are usually attributed to *Brettanomyces* spoilage. *Brettanomyces* is a non-spore counterpart of the genus *Dekkera*, a yeast present on the surface of grapes. These species of yeast produce vinylphenols and ethylphenols (typically associated with white wines and red wines, respectively) from hydroxyl cinnamic acids. The wine ethylphenol content tends to

increase with time, especially when the aging takes place in used barrels. This fact is linked to the highly porous nature of oak wood, which is favorable for yeast growth[2,3].

Given *Brettanomyces* spoilage is naturally present in the fruits it is not straightforward to control their proliferation. Nowadays, there are two ways to detect the presence of this circumstances, known as *Brett* character or *Brett* defect, in an early stage. The first one is the microorganism detection, used to identify the yeast proliferation a goal that can be met through cell culture, specific gene detection or immunesensing [4–6]. The second option is the detection of 4-ethylphenols by normally chromatographic method, concretely via gas or liquid chromatography [7,8]. The latter options involve complex and time-consuming pretreatments protocols that can be avoided using electrochemical biosensors as those proposed in this communication. Herein is suggested the use of laccase (Lac) and tyrosinase (Tyr) enzymatic biosensors to form together with a graphene-modified electrode an array for a bioelectronic tongue (bioET) approach.

Graphene and its derivatives are one-atom-layer nanomaterials that show awsome properties in the electrochemical field due to their electric and structural features. Concretely, in the biosensing field their advantageous utilizations leads to significant improvements since they increase the specific surface area, catalyze the electrochemical reaction, and provide the chance of attaching biomolecules directly to their surface avoiding the use of harsh-biocompatible protocols [9–11].

In this publication is proposed the use of a bioET as a strategy to resolve complex mixtures of volatile 4-ethylphenols in wine matrix. Commonly, electronic tongues (ETs) are defined as “an analytical instrument comprising an array of non-specific, poorly selective chemical sensors with partial specificity (cross-sensitivity) to different compounds in a solution, coupled to an appropriate chemometric tool for data processing”, alternatively, the IUPAC defines ETs as “ a multisensor system, which consists of a number of low-selective sensors and uses advanced mathematical procedures for signal processing based on Pattern Recognition and/or Multivariate data analysis—Artificial Neural Networks (ANNs), Principal Component Analysis (PCA), and so forth].” [12] The form reminds the taste sensorial ability in animals, where a few receptors respond to a wide range of compounds using combinatorial principles [13]. Brief, this work aims to demonstrate the synergy and capabilities of bioET combined with advanced nanomaterials, which together permits to resolve and quantify complex mixtures even in real complex sample matrices.

2. Experimental

2.1. Reagents and chemicals

All reagents were used analytical reagents grade. All solutions were prepared using deionized water from Mili-Q system (Millipore, Billerica, MA, USA). All samples were prepared on saline phosphate buffer (50 mM K_2HPO_4, 50 mM KH_2PO_4 plus 0.1 M KCl at pH 7.4). The different salts used were purchased from Sigma-Aldrich (St. Louis, USA). Resineco Epoxy Kit 125 resin was supplied from Resineco green composites (Barcelona, ESP), and graphite powder (particle size < 50 µm) was received from BDH (BDH Laboratory Supplies, Poole, GBR). Graphene oxide was supplied for Nanoinnova Tech. (Madrid, ESP). Tyrosinase from mushrooms (EC number 1.14.18.1, 2687 $U \cdot mg^{-1}$), Laccase from *Trametes Versicolor* (EC number 1.10.3.2, 21.0 $U \cdot mg^{-1}$), 1-ethyl-3-(3-dimethylaminopropyl carbodiimide (EDAC), N-hydroxysulfosuccinimide (NHS). and finally, catechol, 4-ethylcatechol, 4-ethylphenol, and 4-ethylguaiacol were purchased from Sigma Aldrich.

2.2. Biosensor construction

The biosensor platform was a graphite-epoxy resin composite (GEC) electrode [14]. These devices were built manually in the laboratory using as starting point a gold connector. Onto the connector is welded a copper disk and all this assembly is put into a longer PVC tube, forming in this way the body of the electrode. Finally, the cavity formed onto the copper disk was filled with the conductive composite abovementioned. Concretely, the composite contains a graphite resin ratio of 58:42. After the composite hardening, it was polished with different grit sizes of abrasive paper resulting in a mirror-like and homogeneous surface.

The obtained electrode was then modified with 40 µL of a dispersion of 1 $mg \cdot mL^{-1}$ of graphene oxide (GO). Due to the low conductivity properties of GO, it was necessary a further step, its reduction. Reduced GO, in this case, electroreduced GO (ERGO), was achieved using cyclic voltammetry. For this, 10 cycles of a potential window from +1.9 V to -2.3 V, in cathodic direction, at 100 $mV \cdot s^{-1}$ were performed. The modification and reduction protocols were established and validated in previous works, where it was demonstrated the successful performance of a graphene electrode modified with this strategy [15].

Covalent immobilization of the enzyme in order to obtain the biosensor was conducted via the EDAC chemistry. This reaction is based on the formation of covalent bonds between the outer amino groupsof the enzyme, and the intact acid carboxylic groups of the ERGO using the

EDAC molecule as the activator a momentaneous crosslinker. In order to stabilize the intermediate complex in the immobilization protocol, it was used also NHS [16]. As in the case of the ERGO electrode, the enzymatic immobilization onto graphene platforms procedure was firstly studied and evaluated in previous works, where a Lac-ERGO biosensor was designed for the indirect detection of emerging pollutants [17].

2.3. Topographical characterization

Topographical characterization of the surface of the electrode was carried out by scanning electron microscopy (SEM), specifically with an EVO®MA10 (Zeiss, DEU) microscope operated at 20.00 kV. Surface roughness study was done by atomic force microscopy (AFM), the images were obtained using a Veeco Dimension 3100 AFM microscope (Bruker, USA).

2.4. Electrochemical measurements

All the electrochemical measurements were carried out in an 6-channel AUTOLAB PGSTAT30 via the GPES Multichannel 4.7 software package. Voltammetric measurements were performed without stirring and at room temperature using a classical three-electrode cell, using a pseudo combination electrode, where the reference was an Ag/AgCl, and the auxiliar a wire of metallic platinum (Crison 52 61). The bare working electrodes were laboratory made laccase or tyrosinase enzyme sensors, prepared departing from graphite epoxy composite (GEC) [14]. These devices were modified as specified in the above sections. Cyclic voltammetric (CV) measurements were recorded by scanning a suitable potential window in an anodic direction with a step potential of 5 mV and a scan rate of 10 $mV \cdot s^{-1}$. All the measurements were performed in phosphate buffer, or in real sample diluted in phosphate buffer. No special cleaning or pre-treatment was necessary between sample analysis.

2.5. Data processing

Chemometric calculations were performed by specific routines written by the authors in MATLAB 2021b (MathWorks, USA); for this purpose it was used the Wavelet (version 6.0), and the Statistics and Machine Learning (version 12.2) toolboxes [18,19]. The same program was also used to carry out the graphical representation of the results.

The measurement of the bioET generates a large volume of high-dimensional data corresponding to set measurements. This information is organized in one tensor of proper dimensions [current *x* sample *x* electrode]. First step is to reduce the initial dimensionality is to make an unfolding of each voltammogram and the following concatenation per sensor. This

process leads to the direct reduction of the 3D tensor to a matrix (current x sample). It must be noted that the unfolded data were firstly individually normalized. Once the data is ready for the computational calculus, it was applied a preprocessing step to discard the redundant and not significant information. For this, the discrete wavelet transformation (DWT) was applied as a feature extraction tool [20,21]. This process is based on the multilevel decomposition of the input signal into low and high frequencies, wherein each level is maintained and downsampling the low-frequency domain, the one which contains the most relevant information. This process is followed and validated through the reconstruction of the signals. The resulting information must be representative of the initial data, for this purpose, the reconstruction ratio (f) and the determination coefficient (R^2) of the new curves are calculated [22].

For the response model, a feedforward ANN arrangement was carried out with the Bayesian regularization backpropagation algorithm, which avoids the use of an internal validation subset [23]. Partial least squares (PLS) regressions [24] were performed with the same data prepared for the ANN arrangement. For these calculations was used the statistically inspired modification of the PLS (SIMPLS) algorithm [25]. The validation of the models was carried out with the previous split of the samples into two subsets, the train, and the test [26]. Train, as its name indicates, was used for the proper training of the model, its design is based on the use of MDOE discipline tools [27], normally this subset contains ca. 2/3 of the total amount of samples, while the other 1/3 correspond to the test samples, which are used for the validation of the built model. The last subset is formed by the random distribution of the points into the experimental domain.

3. Results and discussion

3.1. Biosensors characterization

The GO material was deposited using the drop casting technique, to sum up, it was deposited a certain volume onto the pristine GEC surface. This procedure was inspected by AFM and SEM microscopy, see figure 1 and figure 2 respectively (comparative images from the bare GEC electrode in the supplementary). Figure 1 and figure s1 show the topographical characterization of GO onto the bare composite. Concretely, in figure s1, it is observed the pristine composite, which as seen, does not present a totally uniform surface. When the lower roughness zones are observed, it can be seen as in figure 1(A), and figure 1(B), the effects of GO deposited onto the composite surface are evident. In both cases, the GO material forms, as expected for its intrinsic features, wrinkles making cloth-like shapes (marked with arrows). Figure 1(C) the height profile

obtained from figure 1(B), a maximum height of 21.7 nm is measured, indicating the presence of graphene flakes with a low number of layers. These results are comparable to the obtained by the SEM technique. In this case, figure 2 also demonstrate the cloth-like forms onto islands that can be caused by the composite. In conclusion, the images obtained in both techniques lead to assume that the GO, and then the ERGO, are well deposited onto the electrode surface.

3.2. Voltammetric response of the array

Aiming to understand the target (bio)sensors electrochemistry they were first characterized with its standard substrate, the catechol. This molecule is a regular substrate when studying the phenol oxidases enzymes, making possible the immediate comparison of the behavior of the electrodes. In this sense, multiple calibration curves were performed in a concentration range equal for all the electrodes which goes from 0.02 ppm to 1.5 ppm. As seen in figure 3, different sensitivities were obtained being the best one for the Tyr-ERGO electrode, followed by the Lac-ERGO, and finally the one obtained for the ERGO electrode. From the calibration curves the limits of detection (LOD) were estimated considering the formula $3.3 \cdot s_{y/x} \cdot slople^{-1}$ [28]. The obtained values were 0.02 ppm for Tyr, 0.03 ppm for Lac, and 0.06 ppm for ERGO. It must be noted, that as in the previous works, the calibration curves were carried out with the anodic peak, contrary to what can be expected from this kind of enzyme, which normally present their catalysis in the cathodic zone. Comparison plots of both calibration curves are shown in figure s2 (supplementary info), added with the purpose of demonstrating visually the higher response obtained with the anodic peak than with the cathodic one. The explanation might reside in the catalytic properties of the ERGO itself.

In order to evaluate the intermediate precision of the electrodes, three calibrations in three different days were carried out. The relative standard deviation (RSD) obtained for each electrode was 9%, 8%, and 1%, for Tyr-ERGO, Lac-ERGO, and ERGO respectively. Given in all the cases the value is less than 10 % it was considered that the electrodes had a good intermediate precision for the herein proposed arrangement.

The successive steps were focused on the specific study of the electrodes as a target for the bioET arrangement for the determination of the volatile phenols related to the *Brett* defect. In this case, it is not as interesting the individual features as the comparison of the entire responses. One of the features to study is the co-linearity of the sensors array. This is an important issue to avoid when working in (bio)ET systems. The motivations is that generating different signals for the different electrodes when measuring the same compound, is the ideal

departure point for any (bio)ET application [29]. Thus, individual measurements of 1.5 ppm in phosphate buffer of 4-EP, 4-EG, and 4-EC were compared. The experiment was carried out under the conditions described in the experimental section 2.4 and considering the potential range used a posteriori for the bioET assay (from -0.2 V to 0.8 V). As seen in figure 4, the three electrodes differ in the responses for the analyzed compounds, in other words, the responses of the array are not co-linear or redundant. Moreover, in the same figure, it can be observed the quasi-reversible shape of some voltammograms, linked to the oxidation of the phenol to the quinone form and vice versa. Additionally, it can also be seen the catalytic effect of tyrosinase, and laccase modified biosensors, especially in the case of 4-EC (figure 4(C)).

Figure 4 not only depicts the variability provided by the (bio)sensors to each compound but also the ability of the array to distinguish among them. As suggested by the set of voltammograms, each compound contributes with a different signal shape, and therefore, the sensor array is able to identify them individually. The responses can be recognized mainly by the number of peaks, (two in the case of 4-EG and for the Tyr-ERGO electrode measuring 4-EP, and one for the others), and for the peak potentials, *ca.* of 0.52 V (prevailing peak) for 4-EP, 0.16 V for EC, and 0.20 V and 0.40 V for 4-EG.

Furthermore, in order to prove the ability of distinguishing the compounds with the selected electrodes, a principal component analysis (PCA) was performed which included the 4-ethylphenols plus three phenolic compounds with related structures. The measurements were carried out with the abovementioned conditions, in triplicate, and with equivalent concentration for all the analytes, 1.5 ppm (in phosphate buffer). The PCA treatment employed as departure information the three voltammograms generated by the three sensors in the array (Lac-ERGO, Tyr-ERGO, and ERGO) employed as a single vector of currents. Figure 5 depicts the resulting score plot for the first three principal components, which represents an 84.1 % of the accumulated explained variance. There can be clearly identified three clusters, where each of them contains one of the target molecules (4-EP in light blue, 4-EG in green, and 4-EC in purple). Moreover, it can be appreciated that each cluster is correlated with the structural composition of the molecules, where it is differentiated among *para*-hydroxybenzenes (4-EP and acetaminophen) and *ortho*-dihydroxybenzenes (4-EC, catechol, and catechin).

Besides, a further test was done, the study of the operational stability. Electrochemical sensors undergo natural drift when measured complex samples due to the chemical or physical poisoning of the electrode surface. This stability may still be more critical issue when dealing with biosensors, that may present higher variability or more reduced lifetime than ordinary

sensors. But here, changes in the electrode response may become a handicap for the generalization of the response models. In figure 6 it is plotted the currents obtained in 15 alternative measurements of a constant concentration of catechol and blank. This test was performed with the same conditions as the above and with renewing every time both solutions, the blank and the sample. Moreover, it has to be taken into account that the biosensors were priorly activated with 5 consecutive cycles in the same concentration of catechol in order to reach a stable measurement. As observed in figure 6(A), and figure 6(B), even though for Lac-ERGO biosensor the current response remains constant for at least 15 samples (RSD=6%), for the Tyr-ERGO device is observed a tendency, which was corroborated with the RSD value of 12%. In other words, in the case of tyrosinase modified electrode, it cannot be neglected the intrinsic drift of the sensor, hence, it was decided to use more of one set of electrodes for the operation in the bioET experiment. Concretely, during its carrying out, there were used 3 equal sets of sensors, each one measuring 13 samples. It must be remarked that the ERGO operational stability was tested in previous works, establishing that it can be used for measuring around 20 samples without any perturbation [15].

Once proved the different responses of the electrodes array toward the 4-ethylphenols, the capability to generate non-redundant information, and the operational stability, the next step was obtaining the bioET response model against the mixture.

3.3. Bioelectronic tongue design and results of the response models

In this section it will be commented the preparation and the modeling of two different response models, the first one carried out in phosphate buffer, and the second one made in a wine (table red wine from the brand *Don Simon,* ESP) which was diluted in phosphate buffer (50:50) for carrying out the experiment. The objective is to check and demonstrate the functionality of the (bio)sensor array in real samples. Moreover, the modeling was not only performed with the most common multivariate tool, the PLS, but also was done with ANN, as a more advanced chemometric strategy.

The experimental design of the herein proposed models was based on the splitting of the samples using two separate sets for the learning and checking of the built response models [29]. As commented in section 2.5 train and test samples were used for the learning process of the model, and the external validation of the resulting model, respectively. In this case, the train samples were distributed into the experimental domain following a modified or tilted 3^3 factorial design [30], composed of 27 samples, while the test set was obtained from 12 points randomly

distributed in the same concentration domain. The range of concentrations considered was from 0 to 20 ppm for each compound, these values are in accordance with the thresholds find in real spoiled samples and with limits detected by professional wine tasters.

The measurements of the bioET tongue were carried out randomly as precaution to avoid tendencies during the process. Once the data was acquired, it was first pre-processed. The first step was its compression. Given the huge number of variables and their dimensionality, it was mandatory to deal with their reduction. The compression of the obtained information not only reduces the number of points to feed the model, but it also discards the information with lower significance. After applying different feature extraction methods, the best reconstruction degrees with the DWT were achieved [22,31]. From all the tested mother wavelets, the option that fits better with the herein treated data was the *Daubechies* wavelet (DB). When measuring the samples in phosphate buffer, DB4 and a 3rd level of decomposition was the optimum compression, while for the data provided from the analysis in wine was applied a DB 3 and a 2nd level of decomposition. By means of this compression, it was achieved a reduction of *ca.* 84% for the experiment in phosphate buffer, and *ca.* of 73% for wine performance. In order to illustrate the effect of the compression step, it can be seen the figure s3, which shows the reconstruction signals for the different DWT applied. As it is elucidated, at the end, to choose the final configuration it must be accepted a compromise between the number of points and the held information.

Once the data was ready to fit the model it was proceeded to create the quantification response models. On one hand, it was tested the PLS; in this case, the models were carried out using 6 latent variables for the phosphate buffer experiment, while the model created for the wine samples had 7. On the other hand, was obtained the models also with ANN treatment. These models, contrary to PLS, had to be optimized using a trial-error strategy, in order to find the best topology and configuration for each model. The checked parameters were the number of neurons in the hidden layer, and the transfer function in the hidden and the output layers. The final ANNs architectures had for the buffer experiment 78 neurons in the input layer, 10 neurons in the hidden layer, and 3 neurons in the output layer, which corresponds to the 3 analyzed compounds. The transfer functions used in hidden and for the output layer were *purelins* and *satlins,* respectively. Regarding the ANN architecture for the wine sample quantification, the input layer had 129 neurons, the hidden layer had 9 neurons, and the output layer had 3 neurons. The corresponding transfer functions were *tansig* and *satlins*, in the hidden and output layers, respectively.

The prediction ability of the obtained models was evaluated through the comparison graphs for train and test sets, which represent the predicted vs expected concentrations. As seen in figure 7 and figure 8, in general traits, it can be observed that ANN models present better trends than PLS, which presents a larger dispersion for both train and test sets. Moreover, as expected, train samples present better correlation values because it is the subset used to optimize the ANN topology; nevertheless, the results obtained for the test subset, also near to ideality, support a good prediction ability for the generated models.

To facilitate the elucidation of the comparison graphs results, table 1 and table 2 present a summary of the model characteristics. To indicate the goodness of fit of the generated models was calculated the normalized root mean square error (NRMSE) in each case. This value can be used to compare models. As detailed in the tables, the fittings proof satisfactory results for correlation, slope, and intercept (considering ideal values of 1 for slope and correlation, and 0 for the intercept), and also low values for the NRMSE.

Furthermore, it must be noted that the results obtained in the real sample matrix, are totally comparable to the ones in controlled buffer conditions, being the values in the same magnitude. Even more, comparative behavior for the test subset is clearly improved with the ANN modeling. Hence, it can be supported the idea to apply this method directly to real samples. Thus, four spiked wine samples were interpolated to the PLS and ANN model in order to predict their volatile phenols concentration. The results are summarized in table 3, where the recovery percentage indicated promising results.

Comparing the prediction models, and as the numeric values lead to presume, it can be concluded that PLS and ANN are similar. However, details such as the dispersion of the data in the regression lines, which cause confidence intervals bigger than expected, or the NRMSE, indicate that ANN is a better strategy for developing quantification prediction models.

4. Conclusions

This work presents a bioET strategy for the successful quantification of 4-ethylphenol, 4-ethylguaiacol, and 4-ethylcatechol, indicators of the *Brett* spoilage of wine. The used sensor array includes three voltammetric (bio)sensors modified with ERGO, Lac-ERGO, and Tyr-ERGO. The developed electrodes not only are validated for their use in ET arrangement but also it is demonstrated their synergy with the chemometric advanced tools in order to extract the three compounds considered. Regarding the obtained models, both PLS and ANN demonstrate promising future applications in the food industry given their stunning results in the recoveries

and the powerful features such as simplicity when applied in real samples, the short time of measurement, and the low price. In summary, the work presented here shows a bioET methodology with performance close to heavy instrumentation like HPLC or hyphenated methods.

Acknowledgments

This research was funded by the Spanish Government (Ministerio de Economía y Competitividad) grant number PID2019-107102RB-C21. Marta Bonet-San-Emeterio thanks to Secretaria d'Universitats i Recerca del Departament d'Empreses i Coneixement de la Generalitat de Catalunya and to European Social Fund, European Union for the FI fellowship.

References

[1] Publications Office of the European Union, Council Regulation 1493/1999/EC on the common organisation of the market in wine, (1999).

[2] M.V. Moreno-Arribas, M.C. Polo, Wine chemistry and biochemistry, Springer, Madrid, 2009. https://doi.org/10.1007/978-0-387-74118-5.

[3] R.B. Gilliland, Brettanomyces. Occurrence, characteristics, and effects on beer flavour, Journal of the Institute of Brewing. 67 (1961) 257–261. https://doi.org/10.1002/j.2050-0416.1961.tb01791.x.

[4] B. Borisova, M.L. Villalonga, M. Arévalo-Villena, A. Boujakhrout, A. Sánchez, C. Parrado, J.M. Pingarrón, A. Briones-Pérez, R. Villalonga, Disposable electrochemical immunosensor for Brettanomyces bruxellensis based on nanogold-reduced graphene oxide hybrid nanomaterial, Analytical and Bioanalytical Chemistry. 409 (2017) 5667–5674. https://doi.org/https://doi.org/10.1007/s00216-017-0505-5.

[5] L. Cocolin, K. Rantsiou, L. Iacumin, R. Zironi, G. Comi, Molecular Detection and Identification of Brettanomyces Dekkera bruxellensis and Brettanomyces Dekkera anomalus in Spoiled Wines, Applied and Environmental Microbiology. 70 (2004) 1347–1355. https://doi.org/10.1128/AEM.70.3.1347-1355.2004.

[6] I. Lopez, F. Ruiz-Larrea, L. Cocolin, E. Orr, T. Phister, M. Marshall, J. VanderGheynst, D.A. Mills, Design and Evaluation of PCR Primers for Analysis of Bacterial Populations in Wine by Denaturing Gradient Gel Electrophoresis, Applied and Environmental Microbiology. 69 (2003) 6801–6807. https://doi.org/10.1128/AEM.69.11.6801-6807.2003.

[7] P. Viñas, C. López-Erroz, J.J. Marín-Hernández, M. Hernández-Córdoba, Determination of phenols in wines by liquid chromatography with photodiode array and fluorescence detection, Journal of Chromatography A. 871 (2000) 85–93. https://doi.org/10.1016/S0021-9673(99)01087-0.

[8] J.D. Carrillo, M.T. Tena, Determination of ethylphenols in wine by in situ derivatisation and headspace solid-phase microextraction–gas chromatography–mass spectrometry, Analytical and Bioanalytical Chemistry. 387 (2007) 2547–2558. https://doi.org/10.1007/s00216-006-1086-x.

[9] A. Ambrosi, A. Bonanni, Z. Sofer, J.S. Cross, M. Pumera, Electrochemistry at Chemically Modified Graphenes, Chemistry - A European Journal . 17 (2011) 10763–10770. https://doi.org/10.1002/chem.201101117.

[10] S. Barua, X. Geng, B. Chen, Graphene-based nanomaterials for healthcare applications, in: S. ki Choi (Ed.), Photonanotechnology for Therapeutics and Imaging, Elsevier, 2020: pp. 45–81. https://doi.org/10.1016/B978-0-12-817840-9.00003-5.

[11] A.M. Pinto, I.C. Gonçalves, F.D. Magalhães, Graphene-based materials biocompatibility: A review, Colloids and Surfaces B: Biointerfaces. 111 (2013) 188–202. https://doi.org/10.1016/J.COLSURFB.2013.05.022.

[12] Yu. Vlasov, A. Legin, A. Rudnitskaya, C. Di Natale, A. D'Amico, Nonspecific sensor arrays (electronic tongue) for chemical analysis of liquids (IUPAC Technical Report), Pure and Applied Chemistry. 77 (2005) 1965–1983. https://doi.org/10.1351/pac200577111965.

[13] Yu.G. Vlasov, A. v Legin, A.M. Rudnitskaya, A. D'Amico, C. di Natale, «Electronic tongue» — new analytical tool for liquid analysis on the basis of non-specific sensors and methods of pattern recognition, Sensors and Actuators B: Chemical. 65 (2000) 235–236. https://doi.org/https://doi.org/10.1016/S0925-4005(99)00323-8.

[14] S. Alegret, J. Alonso, J. Bartrolí, F. Céspedes, E. Martínez-Fàbregas, M. del Valle, Amperometric biosensors based on bulk-modified epoxy graphite biocomposites, Sensors and Materials. 8 (1996) 147–153.

[15] M. Bonet-San-Emeterio, A. González-Calabuig, M. del Valle, Artificial Neural Networks for the Resolution of Dopamine and Serotonin Complex Mixtures Using a Graphene-Modified Carbon Electrode, Electroanalysis. 31 (2019) 390–397. https://doi.org/10.1002/elan.201800525.

[16] G. Hermanson, Bioconjugate Techniques, 2nd Edition, Academic Press, Oxford, 2008.

[17] M. Bonet-San-Emeterio, N. Felipe Montiel, M. del Valle, Graphene for the building of electroanalytical enzyme-based biosensors. Application to the inhibitory detection of emerging pollutants, Nanomaterials. 11 (2021) 2094. https://doi.org/10.3390/nano11082094.

[18] M. Misiti, Y. Misiti, G. Oppenheim, J.-M. Poggi, Wavelet Toolbox: MATLAB ® User's Guide (r2004b), The MathWork, Inc., Natick, MA, 2004.

[19] The MathWorks Inc., Statistics and Machine Learning Toolbox™ Release Notes, Natick, Massachusetts, United States, 2005. www.mathworks.com.

[20] S.G. Mallat, A Theory for Multiresolution Signal Decomposition: The Wavelet Representation, IEEE Transactions on Pattern Analysis and Machine Intelligence. 11 (1989) 674–693. https://doi.org/10.1109/34.192463.

[21] L. Moreno-Barón, R. Cartas, A. Merkoçi, S. Alegret, M. del Valle, L. Leija, P.R. Hernandez, R. Muñoz, Application of the wavelet transform coupled with artificial neural networks for quantification purposes in a voltammetric electronic tongue, Sensors and Actuators, B: Chemical. 113 (2006) 487–499. https://doi.org/10.1016/j.snb.2005.03.063.

[22] X. Cetó, F. Céspedes, M. del Valle, Comparison of methods for the processing of voltammetric electronic tongues data, Microchimica Acta. 180 (2013) 319–330. https://doi.org/10.1007/S00604-012-0938-7/FIGURES/5.

[23] F. Burden, D. Winkler, Bayesian Regularization of Neural Networks, Methods in Molecular Biology. 458 (2008) 23–42. https://doi.org/10.1007/978-1-60327-101-1_3.

[24] M. Haenlein, A.M. Kaplan, A Beginner's Guide to Partial Least Squares Analysis, Understanding Statistics. 3 (2010) 283–297. https://doi.org/10.1207/S15328031US0304_4.

[25] S. de Jong, SIMPLS: An alternative approach to partial least squares regression, Chemometrics and Intelligent Laboratory Systems. 18 (1993) 251–263. https://doi.org/10.1016/0169-7439(93)85002-X.

[26] S. Marco, The need for external validation in machine olfaction: Emphasis on health-related applications, Analytical and Bioanalytical Chemistry. 406 (2014) 3941–3956. https://doi.org/10.1007/s00216-014-7807-7.

[27] D.L. Massart, B.G.M. Vandeginste, L.M.C. Buydens, S. de Jong, P.J. Lewi, J. Smeyers-Verbeke, eds., Handbook of Chemometrics and Qualimetrics: Part A and B, Elsevier, Amsterdam, 1998.

[28] J.N. Miller, J.C. Miller, Statistics and Chemometrics for Analytical Chemistry, Sixth edition, Pearson Eduction Limited, Gosport, 2010. http://197.14.51.10:81/pmb/CHIMIE/0273730428.pdf (accessed January 10, 2018).

[29] A. Legin, D. Kirsanov, M. del Valle, Avoiding nonsense in electronic taste sensing, TrAC - Trends in Analytical Chemistry. 121 (2019) 115675. https://doi.org/10.1016/j.trac.2019.115675.

[30] A. Gutés, D. Calvo, F. Céspedes, M. del Valle, Automatic sequential injection analysis electronic tongue with integrated reference electrode for the determination of ascorbic acid, uric acid and paracetamol, Microchimica Acta. 157 (2007) 1–6. https://doi.org/10.1007/S00604-006-0660-4.

[31] L. Moreno-Barón, R. Cartas, A. Merkoçi, S. Alegret, J.M. Gutiérrez, L. Leija, P.R. Hernandez, R. Muñoz, M. del Valle, Data Compression for a Voltammetric Electronic Tongue Modelled with Artificial Neural Networks, Analytical Letters. 38 (2005) 2189–2206. https://doi.org/10.1080/00032710500259342.

Figures captions

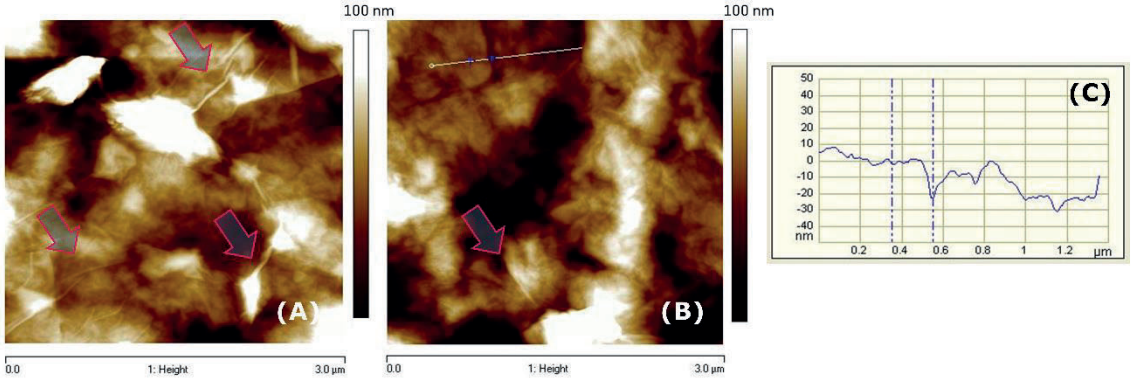

Figure 1. (A and B) AFM topographical study of a 3x3 µm area of commercial GO. (C) Height profile of the image (B), the studied range is marked in the image with a white line and in the graph with two dotted blue lines.

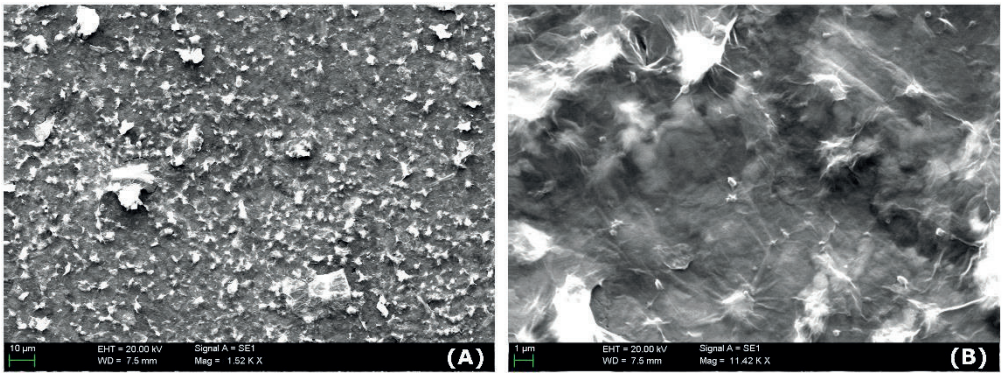

Figure 2. SEM images at different magnifications for ERGO deposited onto a GEC electrode.

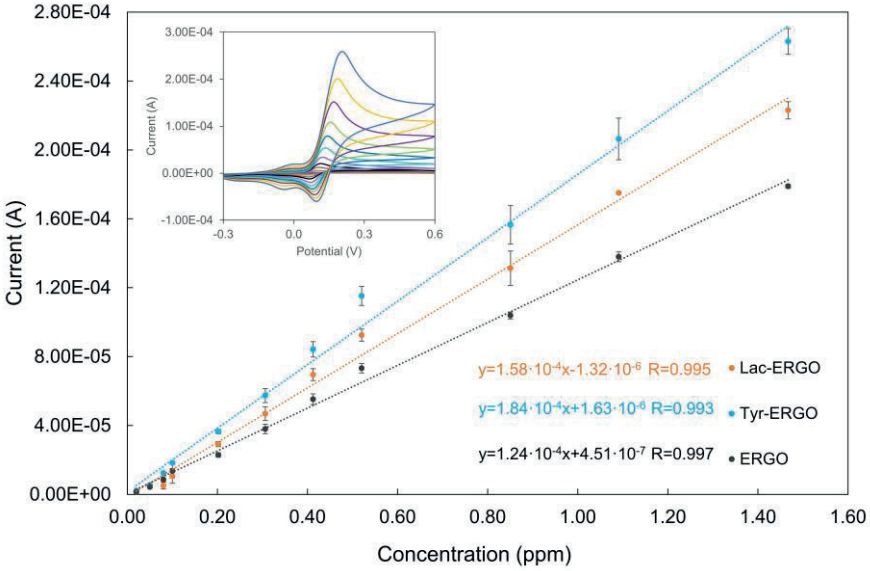

463

464 *Figure 3. Calibration curves for Lac (in yellow), Tyr (in blue), and ERGO (in black) with the corresponding equation of*
465 *the obtained calibration line. The calibrations were carried out for triplicate. Enclosed in the inset are the CV*
466 *voltammograms obtained from the calibration curve for the Tyr-ERGO electrode.*

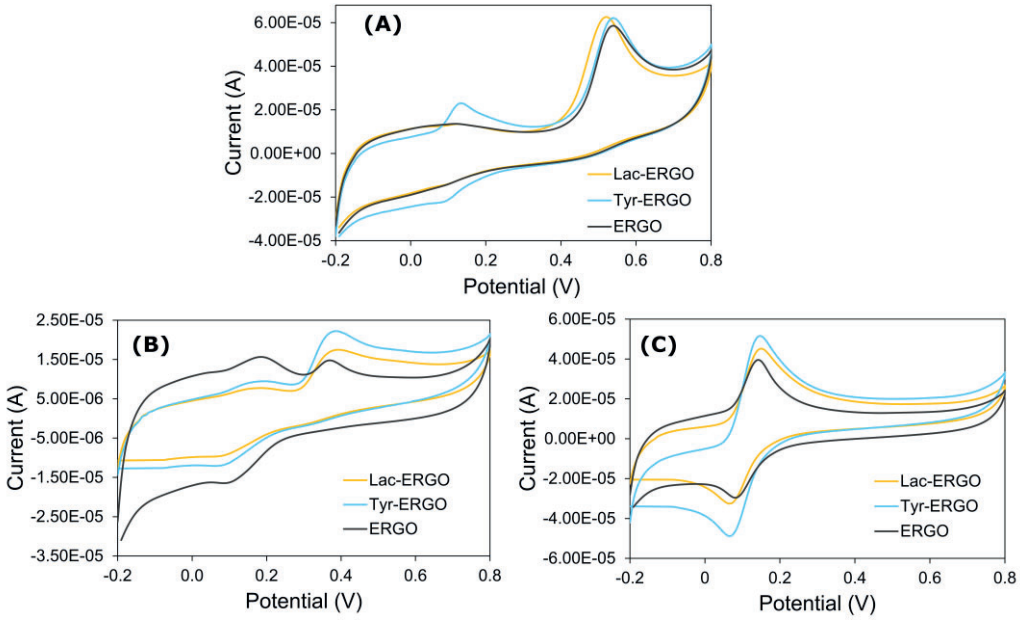

467

468 *Figure 4. Comparison of voltammograms for the sensor array towards 1.5 ppm of (A) 4-EP, (B) 4-EG, and (C) 4-EC.*

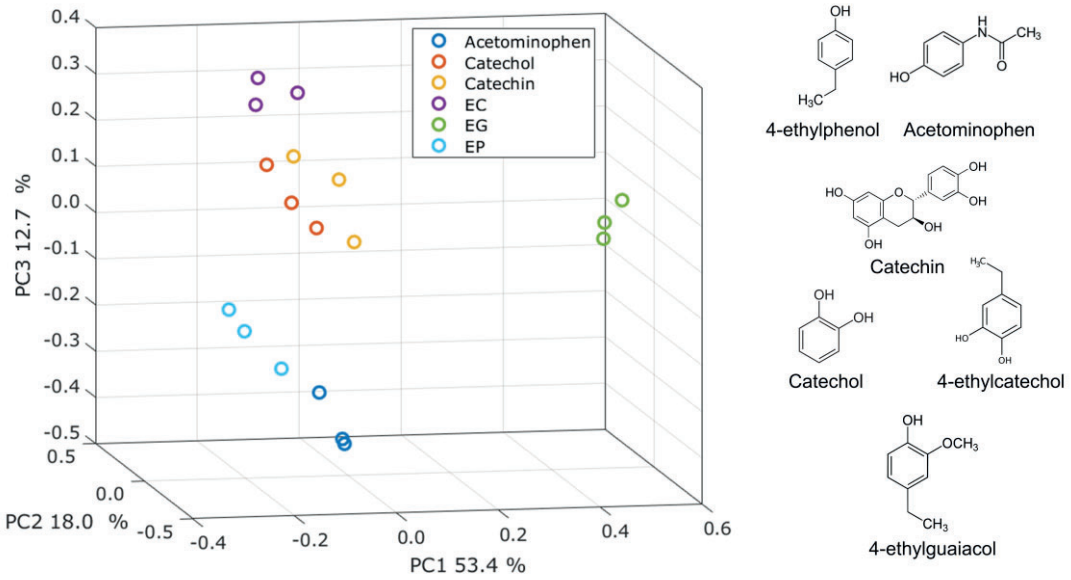

469

470 *Figure 5. Score plot of the first three principal components for ERGO, Tyr-ERGO, and Lac-ERGO electrodes detecting*
471 *the target molecules plus three components with similar structure, catechol, catechin, and acetaminophen (n=3).*

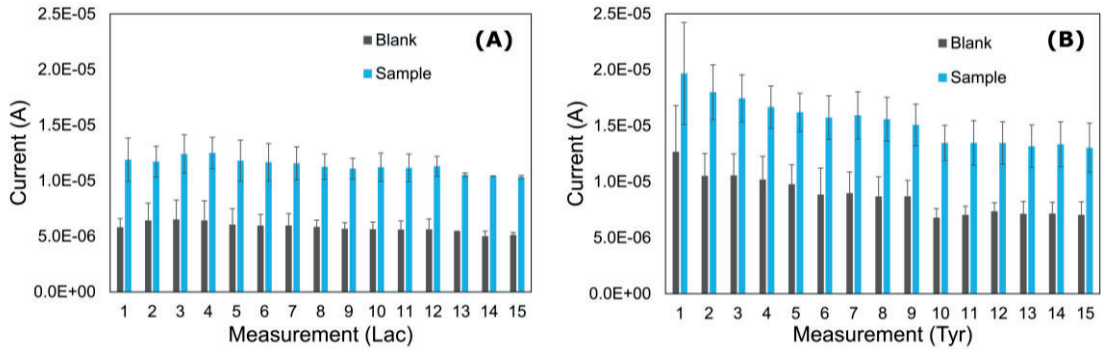

472

473 *Figure 6. Operation stability analysis along 15 alternative measurements of samples of 1 ppm of catechol in phosphate*
474 *buffer and blank for (A) Lac-ERGO electrode, and (B) Tyr-ERGO biosensor. The measurement was performed by*
475 *triplicate.*

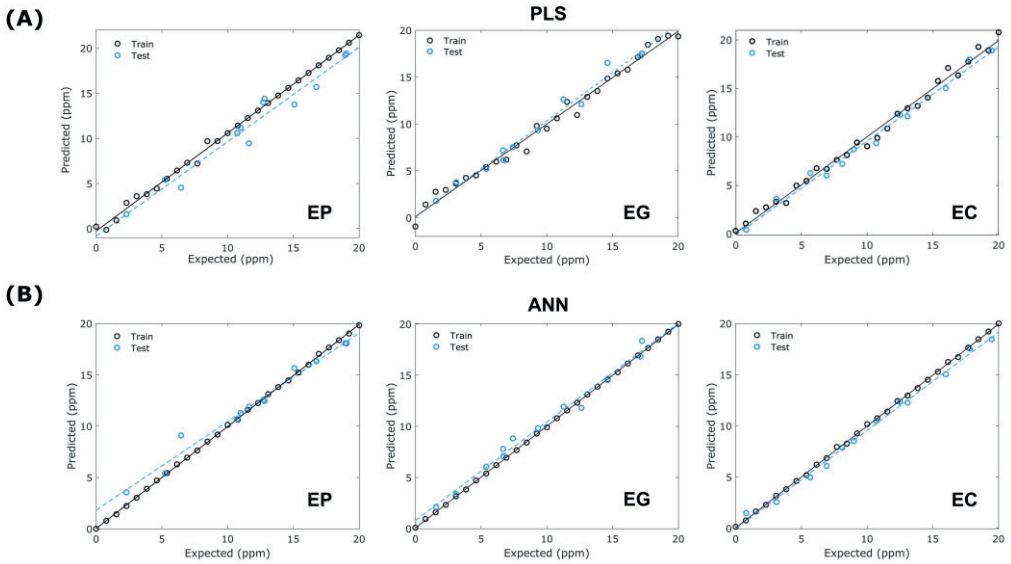

476

477 *Figure 7. Comparison graph of predicted vs. expected concentrations of the three volatile phenols for (A) PLS model,*
478 *and (B) ANN model carried out in phosphate buffer.*

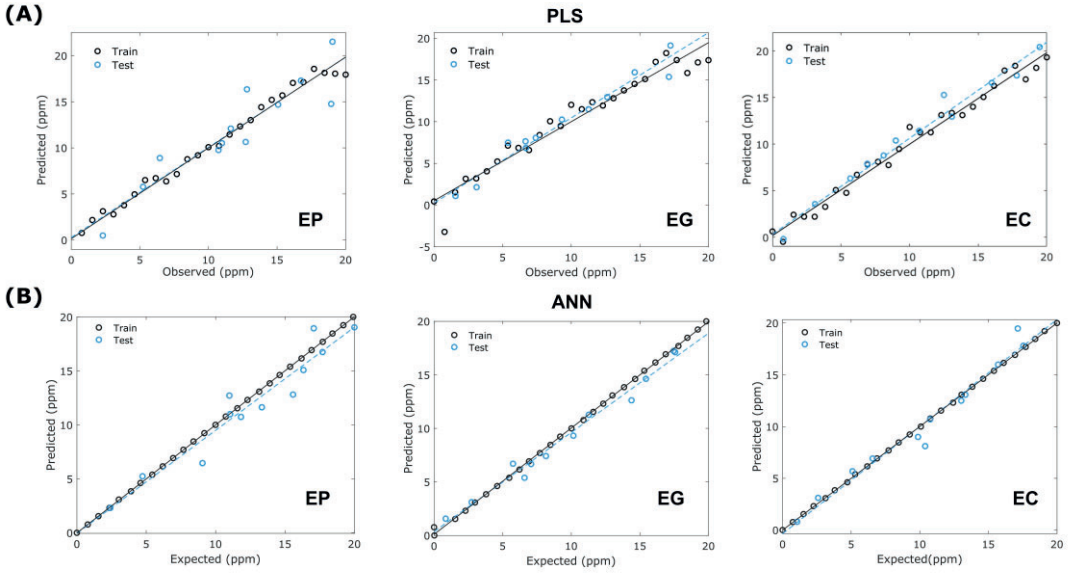

479

480 *Figure 8. Comparison graph of (A) PLS model, and (B) ANN model carried out in wine.*

481

Table 1. Details of the regression lines for the comparison graphs of obtained vs. expected concentrations for PLS and ANN models in phosphate buffer. Uncertainty intervals calculated at the 95% confidence level.

	PLS				
	TRAIN SUBSET				
	Correlation	Slope	Intercept	NRMSE	Total NRMSE
EP	0.997	1.085±0.02	-0.27±0.27	0.043	
EG	0.989	0.988±0.04	0.11±0.51	0.033	0.050
EC	0.992	0.992±0.04	0.08±0.43	0.028	
	TEST SUBSET				
	Correlation	Slope	Intercept	NRMSE	Total NRMSE
EP	0.958	1.046±0.15	-0.84±1.99	0.066	
EG	0.983	1.028±0.09	0.06±1.01	0.040	0.052
EC	0.989	0.970±0.07	-0.14±0.85	0.039	
	ANN				
	TRAIN SUBSET				
	Correlation	Slope	Intercept	NRMSE	Total NRMSE
EP	0.9998	0.994±0.006	0.03±0.07	0.003	
EG	0.9999	0.995±0.003	0.06±0.04	0.005	0.005
EC	0.9996	0.994±0.008	0.04±0.09	0.006	
	TEST SUBSET				
	Correlation	Slope	Intercept	NRMSE	Total NRMSE
EP	0.976	0.864±0.09	1.81±1.16	0.047	
EG	0.984	0.962±0.08	0.81±0.87	0.060	0.040
EC	0.994	0.959±0.05	-0.04±0.58	0.036	

Table 2. Details of the regression lines for the comparison graphs of obtained vs. expected concentrations for PLS and ANN models in wine. Uncertainty intervals calculated at the 95% confidence level.

	PLS				
	TRAIN SUBSET				
	Correlation	Slope	Intercept	NRMSE	Total NRMSE
EP	0.985	0.985±0.051	0.15±0.6	0.069	
EG	0.948	0.948±0.054	0.52±1.1	0.037	0.054
EC	0.982	0.982±0.008	0.18±0.6	0.040	
	TEST SUBSET				
	Correlation	Slope	Intercept	NRMSE	Total NRMSE
EP	0.849	0.977±0.3	0.28±3.3	0.072	
EG	0.958	1.022±0.1	0.24±1.6	0.129	0.077
EC	0.976	1.032±0.1	0.30±1.6	0.062	
	ANN				
	TRAIN SUBSET				
	Correlation	Slope	Intercept	NRMSE	Total NRMSE
EP	0.99996	0.998±0.003	0.03±0.03	0.002	
EG	0.99932	1.006±0.010	-0.08±0.12	0.008	0.005
EC	0.99992	0.999±0.004	0.01±0.04	0.003	

	TEST SUBSET				
	Correlation	Slope	Intercept	NRMSE	Total NRMSE
EP	0.923	0.967±0.19	1.01±2.5	0.092	
EG	0.983	1.060±0.09	-0.21±1.0	0.050	0.060
EC	0.963	0.934±0.12	0.67±1.4	0.065	

Table 3. Comparative table for the recovery values obtained with PLS and ANN prediction models.

	EP				
	Spiked concentration (ppm)	ANN Results (ppm)	PLS Results (ppm)	Recovery yield ANN (%)	Recovery yield PLS (%)
Sample 1	11.82	10.73	9.77	90.8	91.0
Sample 2	4.73	5.23	5.78	110.6	110.4
Sample 3	13.33	11.63	12.10	87.2	104.0
Sample 4	10.99	12.71	10.64	115.7	83.7
	EG				
	Spiked concentration (ppm)	ANN Results (ppm)	PLS Results (ppm)	Recovery yield ANN (%)	Recovery yield PLS (%)
Sample 1	17.45	17.23	19.13	98.7	111.0
Sample 2	15.44	14.62	15.92	94.7	108.9
Sample 3	10.15	9.32	10.25	91.8	110.0
Sample 4	8.15	7.41	8.06	90.9	108.8
	EC				
	Spiked concentration (ppm)	ANN Results (ppm)	PLS Results (ppm)	Recovery yield ANN (%)	Recovery yield PLS (%)
Sample 1	13.02	12.50	15.28	96.0	122.3
Sample 2	6.57	6.91	7.89	105.3	114.1
Sample 3	5.10	5.68	6.31	111.4	111.2
Sample 4	17.55	17.81	17.37	101.5	97.6

Supplementary information

Bioelectronic tongue based on phenol oxidases modified graphene electrodes for the detection of Brettanomyces defect in wine

Marta Bonet-San-Emeterio, Andreu González-Calabuig and Manel del Valle

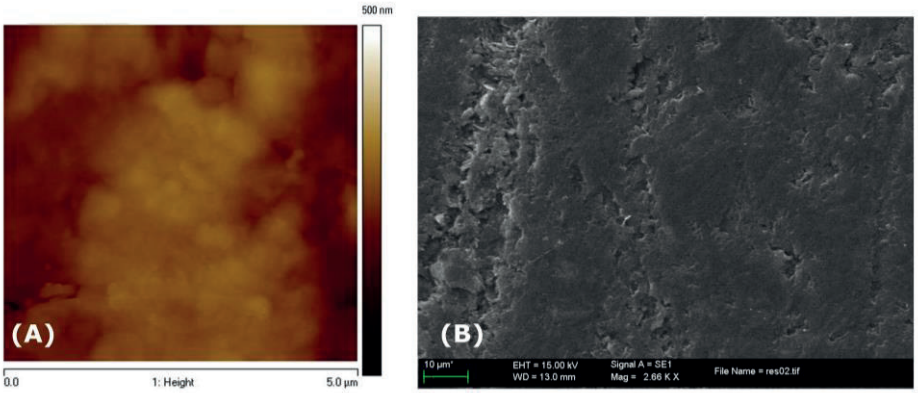

Figure s1. Imaging techniques for a bare GEC electrode, in (A) AFM, and in (B) SEM.

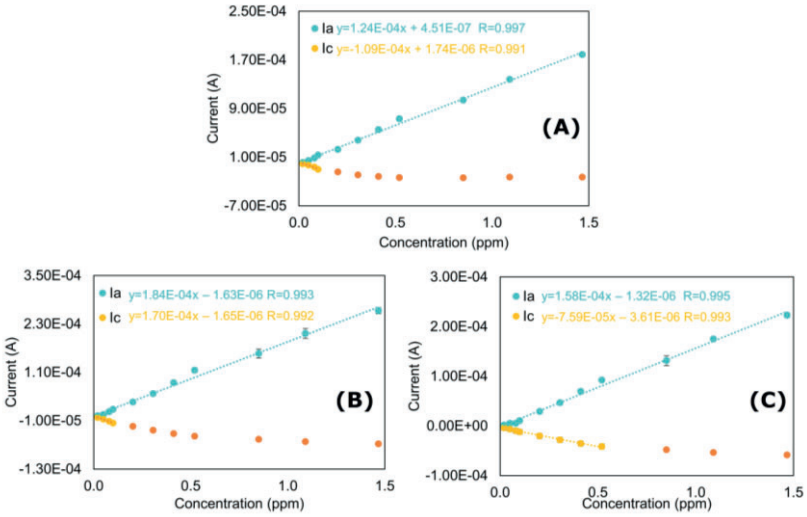

Figure s2. Calibration curves for catechol for (A) ERGO, (B) Tyr, and (C) Lac. In blue analyzed the anodic peak height, and in yellow the cathodic height peak. The darkest part of the Ic curve corresponds to the non-linear zone.

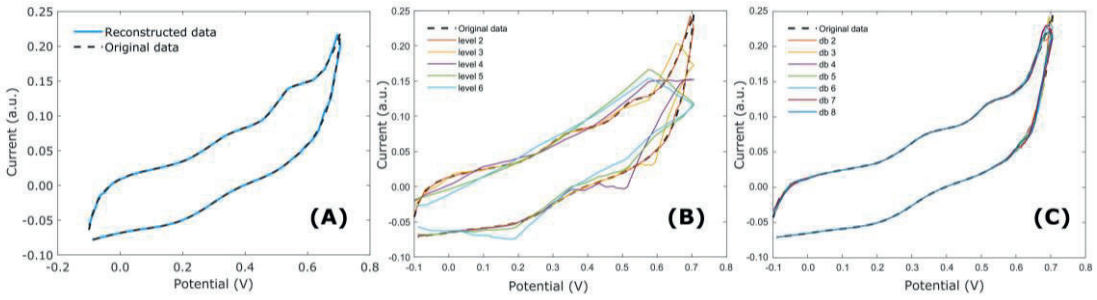

Figure s3. Reconstruction shapes obtained after the application of DWT compression. (A) Final selected compression DWT, db3 and a 2nd level decomposition. The other images depict the caused effects when (B) varied the decomposition level (applied a db3), and (C) when changed the db wavelet. Examples for one of the samples of the bioET measured with Tyr-ERGO biosensor.

Article 4

Modification of electrodes with N-and S-doped carbon dots. Evaluation of the electrochemical response

M. Bonet-San-Emeterio, M. Algarra, M. Petković, M. del Valle

Talanta, 212 (2020) 120806

DOI: 10.1016/j.talanta.2020.120806